國立臺灣大學工學院高分子科學與工程學研究所

博士論文

Institute of Polymer Science and Engineering
College of Engineering
National Taiwan University
Doctoral Dissertation

支鏈效應於予體-受體交替共軛高分子的物理性質以及形態學之研究

Side Chain Effects on the Physical Properties and Morphologies of Donor-Acceptor Alternating Conjugated Polymers

陳建安
Chien-An Chen

指導教授：林唯芳 博士
童世煌 博士

Advisor: Wei-Fang Su, Ph.D.
Shih-Huang Tung, Ph.D.

中華民國 108 年 9 月

September, 2019

doi:10.6342/NTU201904150

國立臺灣大學博士學位論文
口試委員會審定書

論文中文題目：支鏈效應於予體-受體交替共軛高分子的物理性質以及形態學之研究

論文英文題目：Side Chain Effects on the Physical Properties and Morphologies of Donor-Acceptor Alternating Conjugated Polymers

本論文係陳建安君（學號 d02549009）在國立臺灣大學高分子科學與工程學研究所完成之博士學位論文，於民國 108 年 9 月 12 日承下列考試委員審查通過及口試及格，特此證明

口試委員：林唯芳 簽名

（指導教授）

詹益慈 梁世孫

廖文彬

系主任、所長 徐善慈（簽名）

doi:10.6342/NTU201904150

致謝

終於等到寫致謝的這一天，本人非常的感動。六年走來真的很不容易，要感謝的人實在是太多了。首先感謝林唯芳教授辛勤地指導，以及提供大量的研究資源，使我做研究無後顧之憂。再來要感謝童世煌教授不厭其煩地與我討論實驗數據帶領我體會美妙的高分子物理領域，雖然我真的很笨。接著要特別感謝合成組實驗室的學長姊、同學以及學弟妹，俊智學長、唯哲學長、國輝學長、詩翔學長、子恩學姊、祐誠學長、黃蕉蕉學長、蔡奶奶同學、阿牛學弟、子翔學弟、世杰學弟、震華學弟、挺鐘學弟、忠義學弟、博智學弟、鈞皓學弟、子毅學弟、榆凱學弟、家鈺學妹、寶羿學弟、天儷學妹、政錩學弟、姜寧學妹、韻修學妹、coco學妹、紹君學弟以及心寧學妹。感謝實驗室的環境給我的一切喜怒哀樂。感謝大家容忍我的天兵個性。總而言之合成實驗室是很快樂的地方，一個有革命情感的實驗場所。六年中做的合成實驗真的不少，真的感謝高手們的提點跟指導。讓我從一個連萃取都不會的問題兒童，到現在會自行設計實驗，真的很感動。再來要感謝的是元件實驗室的大家，謝謝大家在本人的研究上提供的寶貴意見。我想，如果沒有以上這些人的協助，我的論文應該會很難產。

最後我要感謝我的家人，謝謝父母在博士班六年中提供學費、住宿費以及生活費。雖然平時假日可能忙於實驗，無法回家。但是你們的每一通傳達關心的電話，給予了我莫大的鼓勵。真的非常感謝父母的栽培，我很慶幸我生在一個小康家庭，很感謝父母支持我完成博士學業，希望在未來的有一天都能夠還這份養育之情。

doi:10.6342/NTU201904150

摘要

予體-受體交替共軛高分子被廣泛應用於各種光電元件，諸如高分子太陽能電池、有機場效應電晶體、有機發光二極體。對於這些應用來說，予體-受體交替共軛高分子的電荷遷移率與元件效率表現呈現高度正相關的關係。有兩個關鍵因素影響著電荷遷移率，“奈米微結構的規整度”以及“高分子堆疊方向”。支鏈工程被認為是一種非常有力的技術以創造高度規整奈米微結構的高分子以及調控高分子的堆疊方向。此技術通常涵蓋以下三種參數:(1)支鏈長度(2)支鏈位向(3)支鏈種類。雖然已有大量的支鏈效應的研究對於各種予體-受體交替共軛高分子，但是這些個別的支鏈效應研究是由不同的研究團隊所執行而且難以進行比較。因此，提供一個全面的支鏈效應研究包含上述的三種支鏈參數是非常必要的。在本論文中，我們不僅提供了一個全面的支鏈效應研究還展示了兩種策略透過合理的高分子結構設計利用支鏈工程得到高度規整奈米微結構的高分子以及調控高分子的堆疊方向。

為了執行全面的支鏈效應研究以及創造擁有高度規整奈米微結構的高分子，我們成功合成了八種寡聚噻吩-噻吩并吡咯二酮(3T-TPD)的共軛高分子伴隨著不同的支鏈位向(朝外以及朝內)、支鏈種類(十二碳鏈以及四乙二醇(TEG))、支鏈長度(八碳鏈、六碳鏈、四碳鏈)。這些高分子的光學性質、電化學性質、熱性質以及自組裝行為被系統性地討論。對於這些 3T-TPD 的共軛高分子來說，擁有支鏈朝外的高分子展現較優異的 π-π 堆疊相較於支鏈朝內的高分子，導致支鏈朝外的高分子堆疊形成層板(LAM)結構。然而，支鏈朝內的高分子伴隨著差的主鏈平面性堆疊出極為罕見的六角最密堆積(HEX)結構。對於支鏈種類效應來說，不論是支鏈朝外的高分子以及支鏈朝內的高分子具備 TEG 支鏈展示出較長波長的紫外-可見光吸收光譜以及更高度規整的奈米微結構相較於具備十二碳支鏈的高分子。這些結果指出較為柔軟的 TEG 支鏈可以有效提升高分子的自組裝行為表現。對於支鏈長度效應來說，越長的支鏈越能幫助支鏈朝外的高分子排列成越高度規整的 LAM 結構。相反地，越短的支鏈越適合支鏈朝內的高分子自組裝成越高度規整的 HEX 結構。

更進一步，為了深入研究寡聚醚(OEG)支鏈效應，我們成功合成一系列寡聚噻吩-異靛藍素高分子，P3TI 以及 P4TI，具備不同數量以及位置的 OEG 支鏈。這些高分子的光學性質、熱性質以及自組裝行為被系統性地討論。我們發現 PnTI 的高結晶性是源自於堆疊良好的寡聚噻吩單元。對於僅具備碳鏈支鏈的高分子而言，P3T(R_8)I($R_{b\text{-}16}$) 以及 P4T(R_8)I($R_{b\text{-}16}$)，這些高分子展現出最高的結晶性但是最大的 $d_{\pi\text{-}\pi}$ 相較於其他具備寡聚醚支鏈的高分子。這些高分子的 π-π 堆疊行為是由寡聚噻吩單元所主導，因為在異靛藍素上體積龐大的碳鏈($R_{b\text{-}16}$)阻礙了異靛藍素的緊密堆疊。當這個異靛藍素上體積龐大的碳鏈($R_{b\text{-}16}$)被柔軟且體積小的 OEG 支鏈取代後，例如 P3T(R_8)I(E)、P3T(E)I(E)、P4T(R_8)I(E)以及 P4T(E)I(E)，這些高分子的 π-π 堆疊行為轉變成為異靛藍素單元主導，因為體積小的 OEG 可以使

doi:10.6342/NTU201904150

得異靛藍素堆疊得比寡聚噻吩更緊密，最終犧牲了原本堆疊良好的寡聚噻吩單元。因此，即使這些高分子展現出較小的 $d_{\pi-\pi}$，他們的結晶性也是相對的弱。除此之外，我們發現了 OEG 支鏈的重要功能-藉由調控高分子的結晶性進而調控高分子的堆疊方向。舉列來說，OEG 支鏈成功使得 P3TI 高分子從輕微緣向排列(edge-on oreintation)改變為完全面相排列(face-on oreintation)，此完全面向排列的高分子非常適合應用於太陽能電池。

我們的研究不僅提供了策略以設計具備高度規整奈米微結構的予體-受體交替共軛高分子亦提供了一個方針以調控高分子的堆疊方向，我們期望此研究能對於發展高效能的高分子光電元件有所幫助。

關鍵字: 予體-受體、奈米微結構、堆疊方向、支鏈工程、寡聚醚、自組裝、結晶

doi:10.6342/NTU201904150

Abstract

Donor-acceptor alternating conjugated polymers (D-A CPs) are widely used in optoelectronic devices, such as polymer solar cells (PSCs), organic field-effect transistors (OFETs), and organic light emitting diodes (OLEDs). For those applications, charge mobility of D-A CPs and device performance are in high-positive correlation. There are two critical factors influence the charge mobility, “regularity of nanostructure” and “polymer packing orientation”. Side chain engineering is a powerful technique to create polymers with highly ordered nanostructure and to control the polymer packing orientation. The technique usually involves three parameters: (1) side chain length, (2) side chain location and (3) side chain type. Although there are lots of side chain effect studies in D-A CPs, those studies are carried out from different research groups and each individual side chain effect study is difficult to do comparison. Therefore, to provide a comprehensive side chain effect study including three parameters is necessary. In this dissertation, we not only provided a comprehensive side chain effect study but also demonstrated two strategies to obtain the polymer with highly ordered nanostructure and to control the polymer packing orientation respectively through rational design of polymer using side chain engineering.

In order to do a comprehensive side chain effect study and to create polymers with

doi:10.6342/NTU201904150

highly ordered nanostructure, we successfully synthesized eight oligothiophene-thienopyrroledione (3T-TPD) based CPs with different side chain location (outward and inward), type (dodecyl and tetraethylene glycol (TEG)), and length (octyl, hexyl, and butyl). Those polymer's optical properties, electrochemical properties, thermal properties, and self-assembly behavior had been systematically studied. For 3T-TPD based CPs, outward series polymers show better π-π stacking than inward series polymers, leading to pack into lamellae (LAM) structure. However, inward series polymers with poor coplanarity of backbone pack into rarely found hexagonal (HEX) structure. For side chain type effect, both the outward series polymers and inward series polymers with TEG chains show longer wavelength of λ_{max} of UV-Vis absorption and higher order of the nanostructure than the polymers with dodecyl chains. These results reveal that the more flexible TEG chain can enhance the self-assembly behavior of the polymers. For side chain length effect, the outward series polymers have higher order of LAM with longer side chain. On the contrary, shorter side chain is more suitable for inward series polymers to self-assemble into higher order of HEX.

Furthermore, in order to investigate oligo(ethylene glycol) (OEG) side chain effect in depth, we successfully synthesized a series of oligothiophene-isoindigo based polymers, P3TI and P4TI, by varying amount and location of OEG side chain. Their

doi:10.6342/NTU201904150

optical properties, thermal properties, and morphologies are systematically studied. High crystallization capability of PnTI polymers is mainly contributed from the stable stacking of oligothiophene unit. For the polymers with all alkyl side chains, P3T(R_8)I($R_{b\text{-}16}$) and P4T(R_8)I($R_{b\text{-}16}$), they show the highest crystallinity but the largest $d_{\pi\text{-}\pi}$ among each series polymers. Their π-π stacking behavior is dominated by oligothiophene unit because the bulky alkyl side chains ($R_{b\text{-}16}$) on isoindigo unit prohibit close packing of isoindigo unit. As the bulky $R_{b\text{-}16}$ side chains on isoindigo unit are replaced by linear and flexible OEG side chains, i.e. P3T(R_8)I(E), P3T(E)I(E), P4T(R_8)I(E), and P4T(E)I(E), their π-π stacking behavior is dominated by isoindigo unit because isoindigo unit with small size of OEG side chains can stack more closely than oligothiophene unit, resulting in a sacrifice for stable stacking of oligothiophene unit. Therefore, even though they show relatively short $d_{\pi\text{-}\pi}$, their crystallinity is relatively low. In addition, OEG side chains are capable of controlling the packing orientation of the polymers by adjusting the crystallinity of the polymers. For instance, OEG side chains change the packing orientation of P3TI polymers from slightly edge-on orientation of P3T(R_8)I($R_{b\text{-}16}$) to fully face-on orientation of P3T(R_8)I(E) and P3T(E)I(E) which is suitable for polymer solar cell application.

Our studies not only provide a strategy to design a D-A CPs with highly ordered nanostructure but also provide a guide to control the polymer packing orientation for

doi:10.6342/NTU201904150

potential application in high performance optoelectronic devices.

Keywords: donor-acceptor, nanostructure, packing orientation, side chain engineering, oligo(ethylene glycol), self-assembly, crystallization

doi:10.6342/NTU201904150

Table of Content

doi:10.6342/NTU201904150

doi:10.6342/NTU201904150

List of Figures

doi:10.6342/NTU201904150

doi:10.6342/NTU201904150

doi:10.6342/NTU201904150

doi:10.6342/NTU201904150

doi:10.6342/NTU201904150

doi:10.6342/NTU201904150

doi:10.6342/NTU201904150

doi:10.6342/NTU201904150

List of Tables

doi:10.6342/NTU201904150

Chapter 1 Introduction

1.1 Development of Donor-Acceptor Alternating Conjugated Polymer

Donor-acceptor alternating conjugated polymers (D-A CPs) have been widely used in polymer solar cell (PSC)[1-5], organic field-effect transistor (OFET)[6-10], organic light emitting diode (OLED)[11-14], gas sensor[15-17], cancer thermo-chemotherapy[18-19] and so on. The D-A CPs are constructed from alternating copolymerization of electron-rich unit (donor) and electron-deficient unit (acceptor). According to the molecular orbital theory, as donor and acceptor are bonded together, a new highest occupied molecular orbital (HOMO) and a new lowest unoccupied molecular orbital (LUMO) will be generated to form low bandgap polymer. **Figure 1.1** shows that the new HOMO of donor-acceptor is close to the original HOMO of donor, and the new LUMO of donor-acceptor is close to the original LUMO of acceptor. Therefore, the HOMO, the LUMO, and the bandgap of D-A CPs are tunable through selecting different donor and acceptor units. Hence, the D-A CPs can be rationally designed to absorb ultraviolet–visible (UV-Vis) light for the application of PSC and OLED. Besides, the difference between the strength of electron donating ability of the donor unit and the strength of electron accepting ability of the acceptor unit determine that D-A CPs are hole transporting (p-type) materials[20-25], electron transporting (n-type) materials[6, 26-29] or ambipolar materials[10, 30-33]. For examples, strong donor such as oligothiophene

doi:10.6342/NTU201904150

(nT) and weak acceptor such as isoindigo (I) can construct classic p-type material, PnTI (**Figure 1.2**)[25, 34]. In terms of gas sensor application, our lab reported recently that the PnTI can be fabricated into OFET, and we found that the mobility of PnTI varied as ammonia gas (NH_3) attached to PnTI [15]. In cancer thermo-chemotherapy application, Yang et al. used isoindigo derivative-bithiophene based conjugated polymer, PBIBDF-BT, to fabricate a photothermal transducer (**Figure 1.3**)[19]. They mixed the PBIBDF-BT, the anti-cancer medicine (DOX), thermal sensitive polymer (mPEG-*b*-PHEP) to create special micelles. The core of the micelle contains PBIBDF-BT polymers and the shell of the micelle consists of thermal sensitive polymers. The anti-cancer medicines are trapped between the core and the shell. As the micelles are under near-infrared (NIR) light illumination, PBIBDF can absorb NIR, then convert the light to heat to induce the micelles to release the anti-cancer medicines.

doi:10.6342/NTU201904150

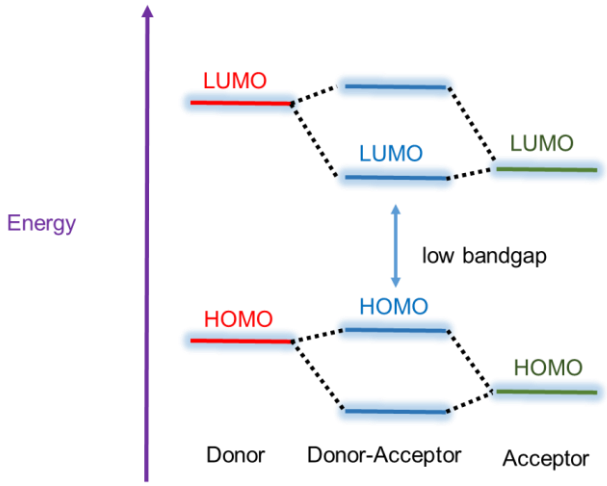

Figure 1.1. Schematic diagram of molecular orbital theory

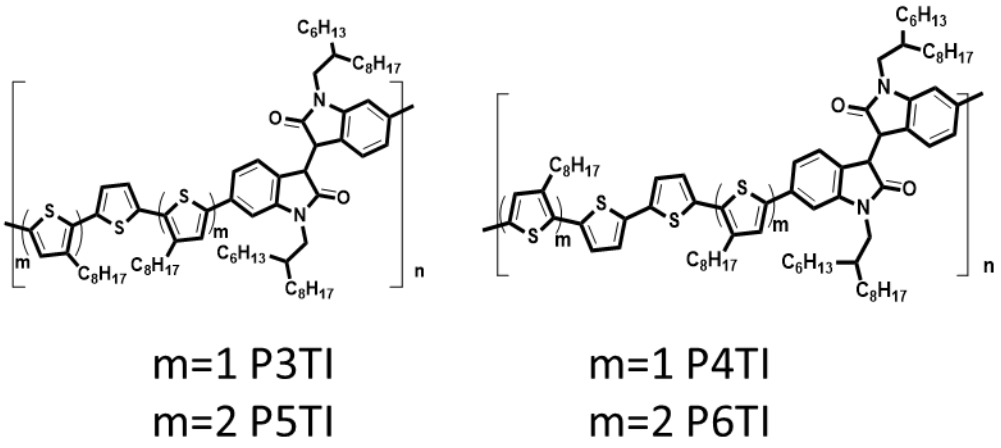

Figure 1.2. Chemical structure of PnTI (n=3, 4, 5, and 6)

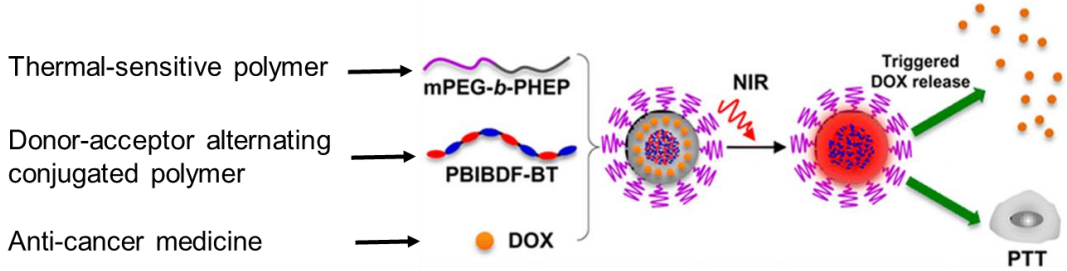

Figure 1.3. Schematic diagram to illustrate cancer thermo-chemotherapy by using a donor-acceptor alternating conjugated polymer, PBIBDF-BT.

doi:10.6342/NTU201904150

Figure 1.4 summarizes commonly used donors and acceptors and their energy levels. In general, donor units usually are constructed from thiophene, benzene, and fused thiophene-benzene rings, such as oligothiphene[35-37], benzodithiophene[38-40], cyclopentadithiophene (CPDT)[41-43], selenophene[44-46], carbazole[47-49], and so on. On the other hand, acceptors are constructed from benzene, pyridine, and pyrrole, such as benzothiadiazole[50-52], isoindigo[25, 53-56], pyrrolo[3,4-c]pyrrole-1,4- dione (DPP)[57-59], thieno[3,4-c]pyrrole-4,6-dione (TPD)[60-64], triazole[65-67]. All donors and acceptors have their own merits. In this dissertation, we choose oligothiophene-TPD (P3TTPD series) and oligothiophene-isoindigo based (P3TI & P4TI series) conjugated polymers (**Figure 1.5**) as model polymers to study "side chain effect". The oligothiophene is a common donor and has been widely employed for constructing high mobility polymers because of high crystallinity of oligothiophene. The TPD molecule is a common acceptor and it can be easily synthesized in large scale. The TPD-based conjugated polymers also show good device performance (OFET: μ_h ~1 $cm^2/(V.\ s)$; PSC: power conversion efficiency ~ 8%)[68-70]. On the other hand, isoindigo is also a common acceptor and it can be easily synthesized. In addition, the isoindigo is a nature dye and can be extracted from plants, such as Strobilanthes formosanus Moore (台灣馬藍) (**Figure 1.6(a)**). Two thousand years ago, a special blue-dye technique had been developed through using isoindigo dye in China (**Figure 1.6(b)**).

doi:10.6342/NTU201904150

Interestingly, the isoindigo-based polymers also show good device performance (OFET: μ_h ~1 $cm^2/(V.\ s)$; PSC: power conversion efficiency ~ 8%)[25, 53, 71].

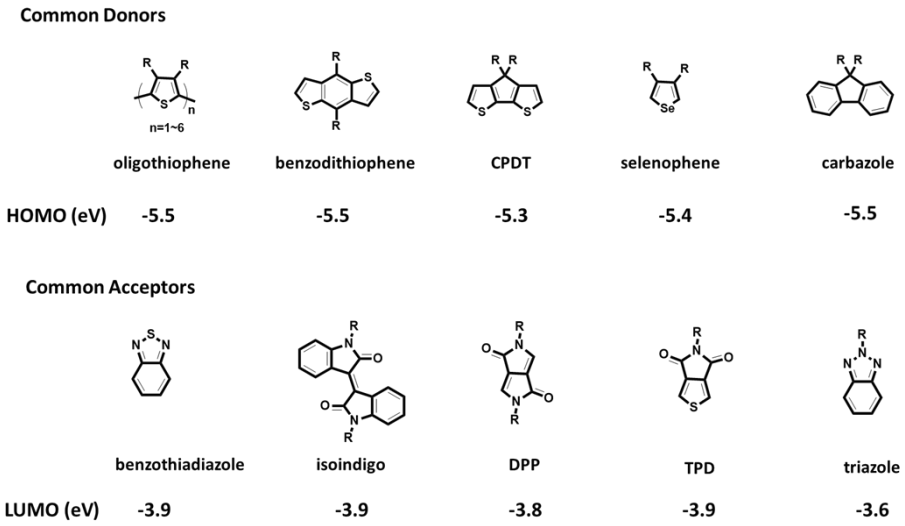

Figure 1.4. Chemical structures, HOMO, and LUMO of common donors and acceptors

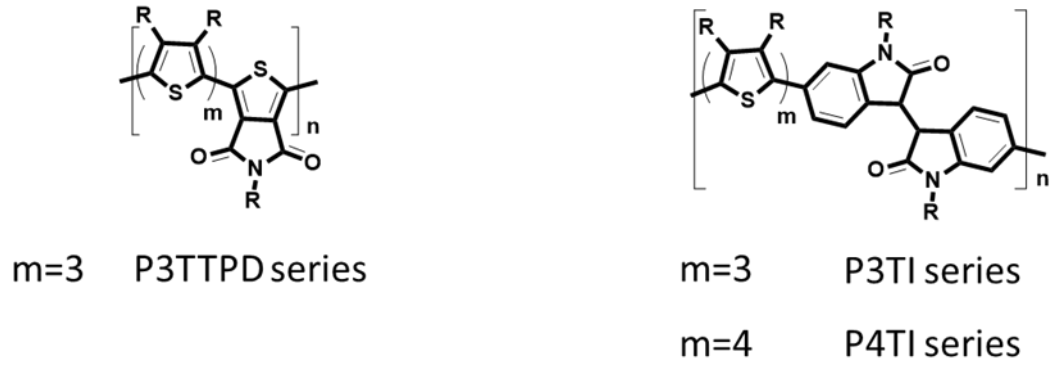

Figure 1.5. Chemical structure of oligothiophene-TPD based conjugated polymers (P3TTPD series), and oligothiophene-isoindigo based conjugated polymers (P3TI, and P4TI series).

doi:10.6342/NTU201904150

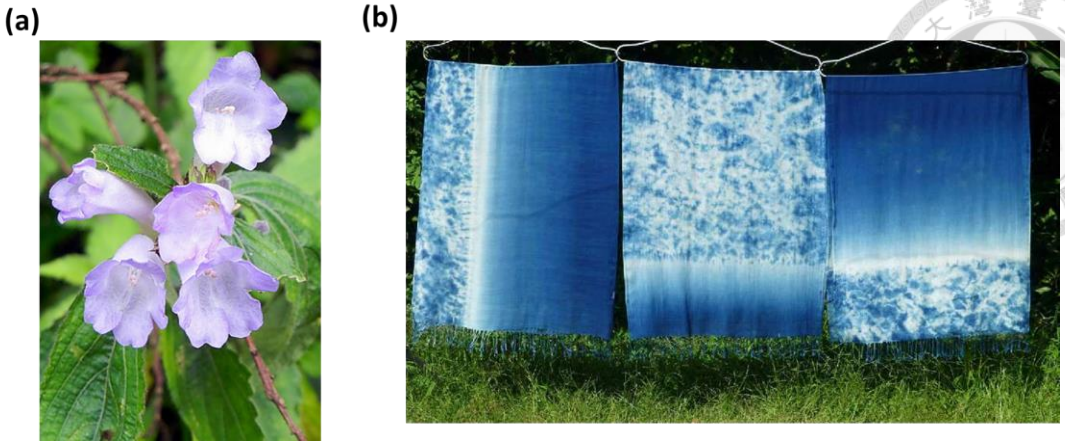

Figure 1.6. Isoindigo dye, (a) from Strobilanthes formosanus Moore (台灣馬藍) and (b) products fabricated by blue-dye technique.

1.2 Relationship between Morphology of Donor-acceptor Alternating Conjugated Polymer and Device Performance

In order to realize how the morphologies of D-A CPs influence the device performance, the chemical structure of D-A CPs must be understood. The chemical structure of D-A CPs can be divided into main chain and side chain (**Figure 1.7**). The main chain is made of stiff π-conjugated bond and the side chain is usually built on flexible non-conjugated bond. The main chain has the active functions of light absorption and charge transportation. On the other hand, the side chain enables the polymer to dissolve and disperse in organic solvent and enhance the organization and crystallization of polymer. **Figure 1.8** shows a schematic diagram of self-assembly of D-A CPs. The process contains two stages.[72] In stage I, as one polymer chain

doi:10.6342/NTU201904150

approaches to another polymer chain, the main chain of each polymer will be stacked up (π-π stacking) through strong π-π interaction to form a 2D laminate. In stage II, lots of laminates self-assemble into 3D lamellae structure. Many studies show that the regularity of lamellae structure influence the efficiency of charge transportation, leading to affect the device performance[73-75]. In general, more ordered lamellae structure provides preferable three-dimension framework to facilitate the charge transportation (**Figure 1.9(a)**) to improve the device performance. Therefore "regularity of nanostructure" is one of critical factors for device performance.

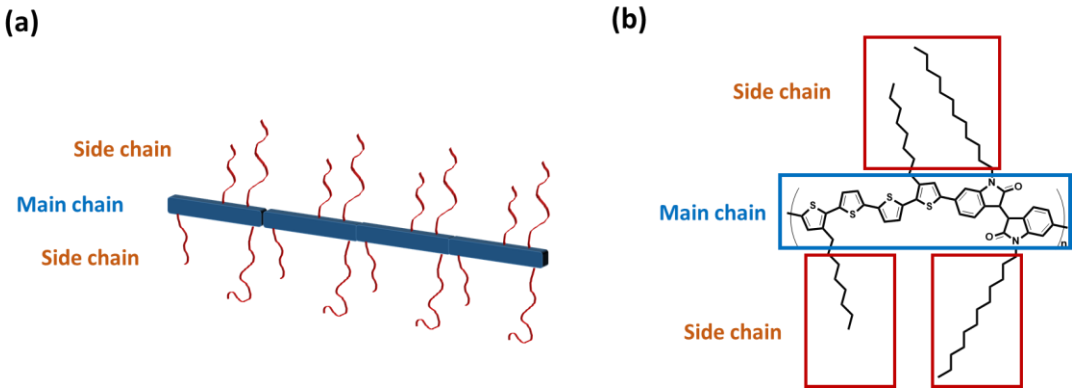

Figure 1.7. Polymer chain structure, (a) schematic diagram and (b) an example of P4TI

doi:10.6342/NTU201904150

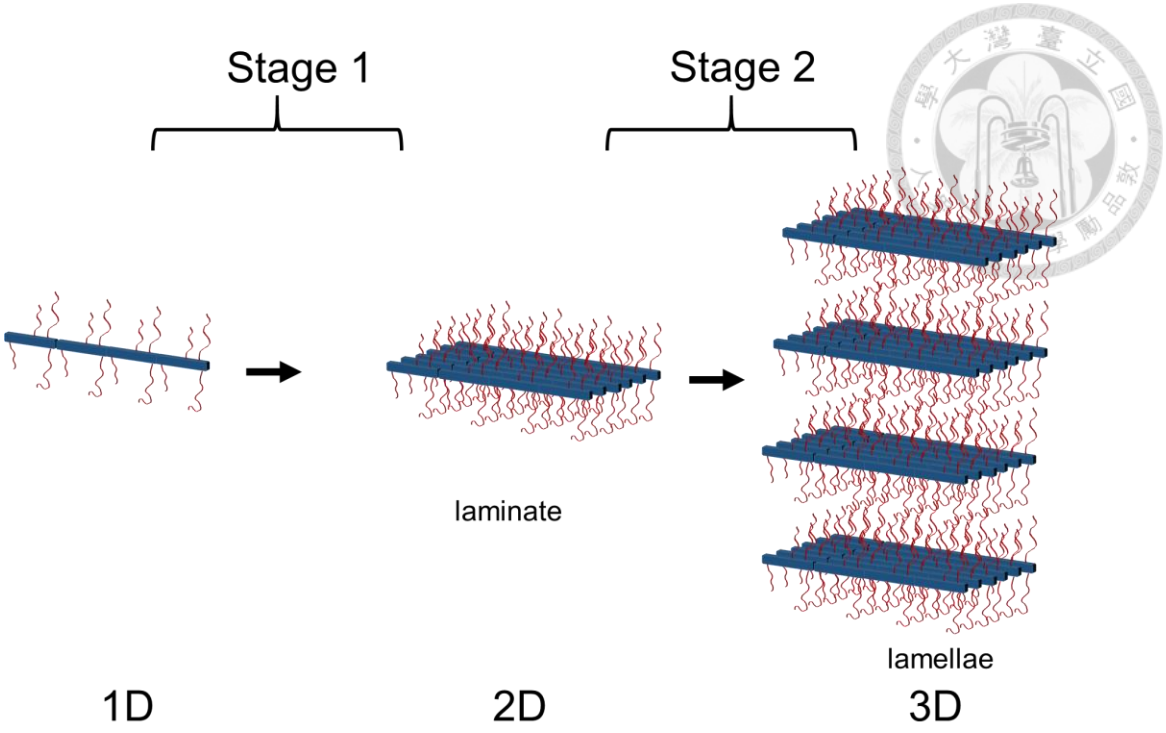

Figure 1.8. Schematic diagram to illustrate the self-assembly of D-A CPs.

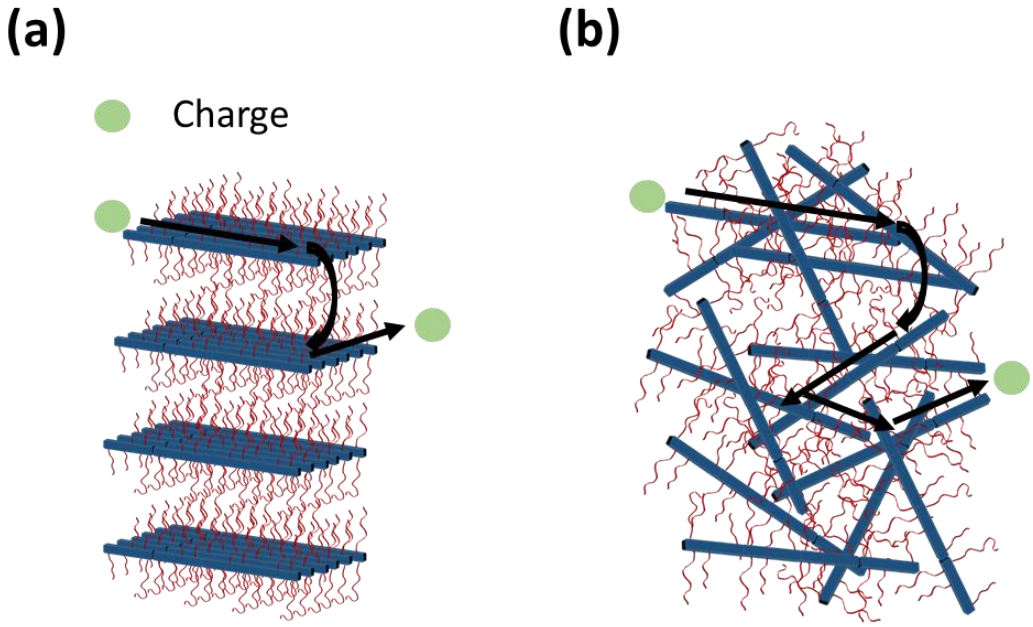

Figure 1.9. Schematic diagrams to illustrate the ease of charge transportation, (a) short pathway in ordered lamella and (b) long pathway in disordered structure.

doi:10.6342/NTU201904150

Another critical factor is “packing orientation of polymer chains”. **Figure 1.10** reveals three charge transportation routes: (1) along the main chain of polymer (2) along the 2D laminate (3) along the 3D lamellae structure. The rate of charge transportation in route 1 (R_{route1}) is fastest due to the continuous 1D π-conjugated bond without charge hopping. In route 2 and route 3, charges must hop from one main chain of polymer to another main chain of polymer. Hence the distance between main chains and the rate of charge transportation are in inverse proportion. So the rate of charge transportation in route 2 (R_{route2}) is faster than the rate of charge transportation in route 3 (R_{route3}) due to the closer π-π stacking. For every D-A CP containing continuous π-conjugated system, R_{route1} is similar that can be ignored, then R_{route2} becomes the rate determination step. Therefore, the direction of route 2 (direction of π-π stacking) strongly influence the device performance. Researchers devoted their efforts to understanding the relationship between packing orientation of polymer chains and device performance, and a term of “packing orientation” was clearly defined in the literature.[72] The organization of main chain and side chain of polymer can be defined as the “face” and the “edge” of the 2D laminate, respectively. For the face of 2D laminate lies on the substrate, leading to that the direction of π-π stacking is perpendicular to the substrate, the packing orientation is called “face-on orientation” (**Figure 1.11(a)**). For the edge of the 2D laminate stands on the substrate,

doi:10.6342/NTU201904150

leading to that the direction of π-π stacking is parallel to the substrate, the packing orientation is called “edge-on orientation” (**Figure 1.11(b)**). In PSC and OLED, cathode and anode are located at top and bottom of the device, and the polymer is sandwiched in between two electrodes (**Figure 1.12(a)**). Therefore, the “face-on orientation” is favorable for PSC and OLED because the direction of π-π stacking is vertically in line with the electrodes. On the other hand, in OFETs, the electrodes of source and drain are located at left and right side of the devices, and the polymer is sandwiched in between two electrodes (**Figure 1.12(b)**). Therefore, the “edge-on orientation” is favorable for OFETs because the direction of π-π stacking is horizontally in line with electrodes.

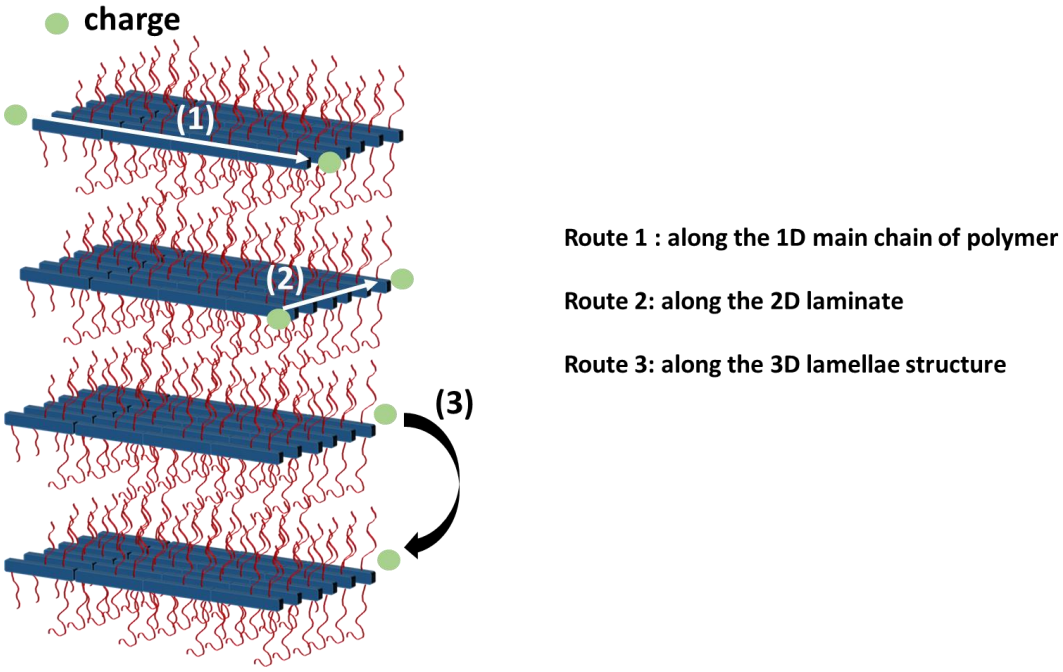

Figure 1.10. Schematic diagram of three charge transportation routes.

doi:10.6342/NTU201904150

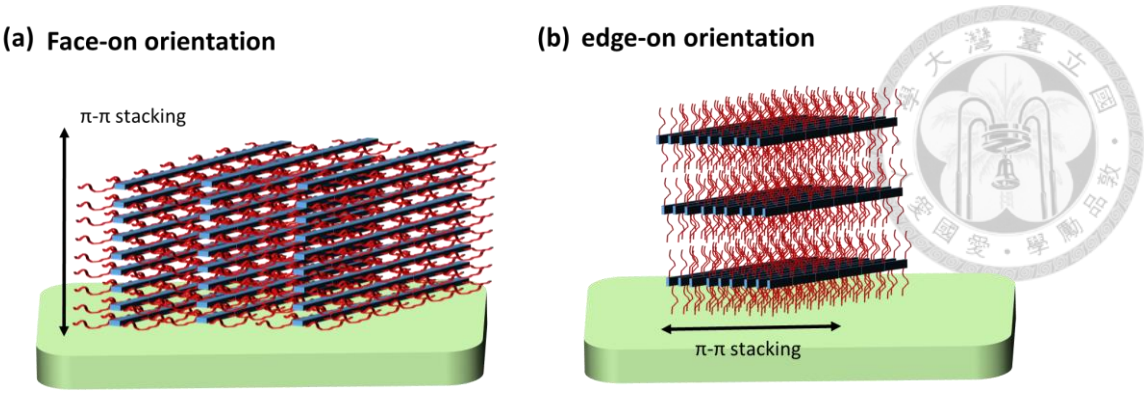

Figure 1.11. Schematic diagrams of 3D lamellae structure with different packing orientation of polymer chains, (a) face-on orientation and (b) edge-on orientation.

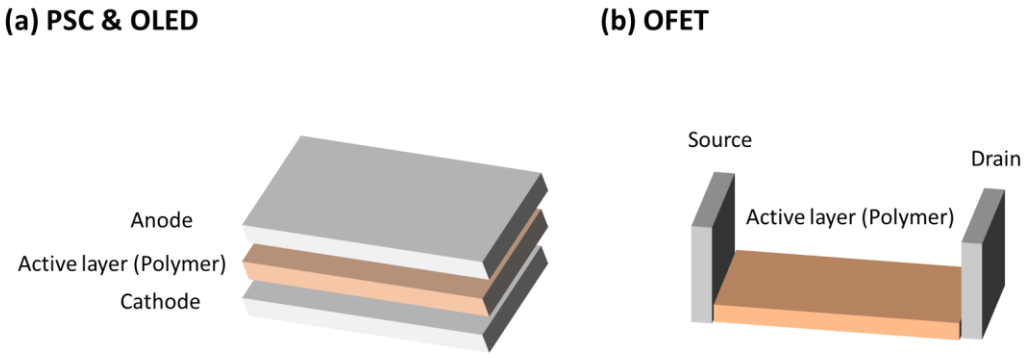

Figure 1.12. Schematic diagrams of device structures, (a) PSC, OLED and (b) OFET

The previous investigations show that the morphologies of D-A CPs are influenced by (1) processing solvent[74, 76] (2) heat[77-78] (3) molecular weight[79-80] (4) side chain[81-84] (5) main chain curvature[85-86] and so on. Among these parameters, the side chain effect is most significant. The term of "side chain engineering" is thus derived from that the technique can tune the morphologies of polymers to improve the device performance. The details of side chain engineering are discussed in the next section.

doi:10.6342/NTU201904150

1.3 Side Chain Engineering

In this section, we discuss side chain effect on not only D-A CPs but also other conjugated polymers, such as conjugated homopolymers, conjugated random copolymers, etc. As above section mentioned (**Chapter 1.2**), the "side chain engineering" is a technique to tune the chemical and physical properties and to improve the device performance of conjugated polymer. The technique usually involves three parameters: (1) side chain length[87-89], (2) side chain location[69, 90-91] and (3) side chain type[92-94], and those parameters are discussed below.

(1) Side chain length effect

In 1986, the first organic field-effect transistor was fabricated based on polythiophene without any side chain prepared by electrochemical polymerization[95]. The hole mobility of the device was very low as 10^{-5} cm^2 V^{-1} s^{-1} attributed to the low-quality thin film. In order to improve the quality of thin film, solution processing must be applied to fabricate uniform film, so linear alkyl side chains need to be installed on the polythiophene to let the polymer dissolve in solvents. The first question researchers met was "How long the side chain should be chosen?". In general, side chain is a double-edged sword. The longer side chain provides polymer with superior chain mobility to pack into more ordered nanostructure that is favorable for charge transporting, but the longer side chain reduced the charge transportation

doi:10.6342/NTU201904150

rate at the same time due to its intrinsic insulated property. Therefore, researchers devoted their efforts to finding the optimized side chain length for conjugated polymers. In 2005, Jenekhe et al. had synthesized a series of poly(3-alkylthiophene) with different side chain length (butyl, hexyl, octyl, decyl, and dodecyl) and systematically studied side chain length effect on the device performance (**Figure 1.13.**)[96]. They found that "hexyl" is optimized side chain length for polythiophene. For D-A CPs or other conjugated polymers with more rigid main chain than polythiophene, longer side chain than hexyl must be introduced. The most commonly used long and bulky side chain was branched alkyl side chain such as 2-ethylhexyl (-C_2C_6), 2-hexyldecyl (-C_6C_{10}), 2-octyldodecyl (-C_8C_{12}), and 2-decyltetradecyl (-$C_{10}C_{14}$). Numerous side chain length effects have been systematically studied in D-A CPs by introducing branched alkyl chain[60, 87, 89].

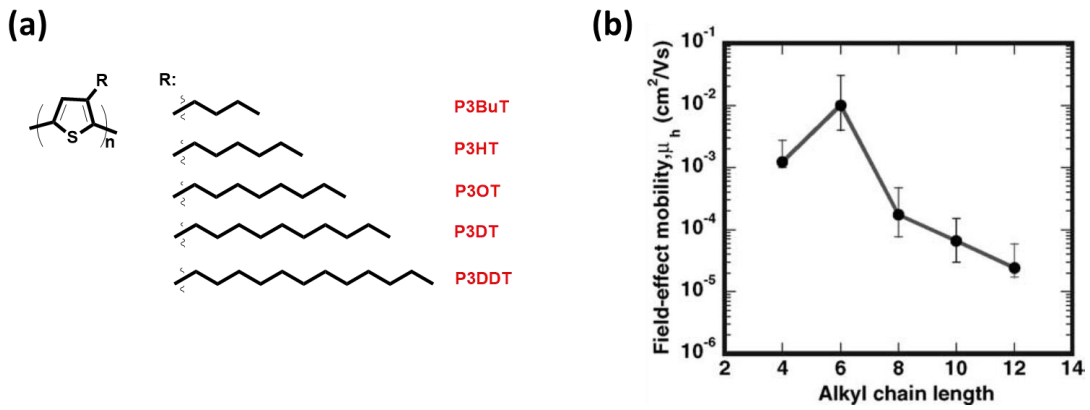

Figure 1.13. Poly(3-alkylthiophene) with different side chain length, (a) chemical structures and (b) the relationship between side chain length and device performance.

doi:10.6342/NTU201904150

(2) Side chain location effect

The side chain location effect was first found in poly(3-alkylthiophene) system. In the early stages of developing poly(3-alkylthiophene), the regioregularity of polymer is low due to the poor synthesis technique, implying that some alkyl side chains are on the opposite location on the thiophene as shown in **Figure 1.14(a)**. Because those side chains on the opposite location produce steric hindrance, the main chain of polymer must be twisted to reduce the steric hindrance. Due to the twisted main chain, the polymer is difficult to self-assemble into ordered nanostructure, leading to poor device performance (hole mobility ~10^{-6} cm^2 V^{-1} s^{-1})[97]. In 1992, regioregular poly(3-alkylthiophene) had been synthesized successfully by McCulloughh et al[98]. All alkyl side chains are on the same location on the thiophene without steric hindrance as shown in **Figure 1.14(b)**, so the polymer main chain keeps good coplanarity, resulting in good device performance (~10^{-2} cm^2 V^{-1} s^{-1})[97]. Therefore, researchers realized that side chain location strongly influence the main chain coplanarity to sway the device performance. Many side chain location effects have been systematically studied in D-A CPs by rational design of side chain location[69, 90-91]. For example, in 2015, Marks et al. systematically studied side chain location effect on the properties of 3T-TPD based conjugated polymers (the same oligothiophene-TPD based conjugated polymers we studied)[69]. The results show that the location of side chain can significantly

doi:10.6342/NTU201904150

influence the coplanarity and the crystallinity of the polymers, leading to affect the performance of the devices.

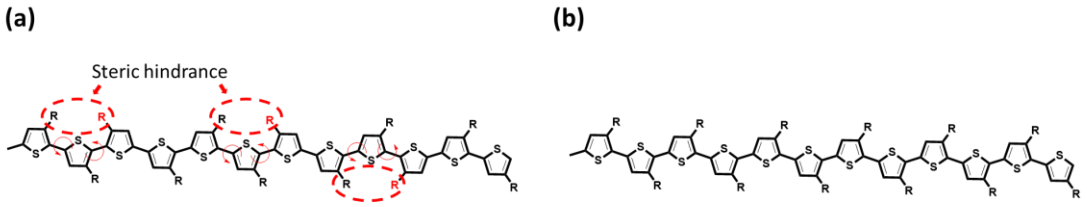

Figure 1.14. Chemical structures of poly(3-alkylthiophene) with (a) poor regioregularity and (b) good regioregularity.

(3) Side chain type effect

Multiple side chains, such as hybrid side chains[99-100], ionic side chains[101-102], oligoether side chains[92-93], fluoroalkyl side chains[103], and latent reactive side chains[104], have been developed to replace alkyl side chains due to their interesting properties (**Figure 1.15**). For examples, hybrid side chains such as alkoxy (-OR), and alkylamino (-NHR) utilized intramolecular interactions (e.g., S(thienyl)—O(alkoxy) interaction or hydrogen bonding) to lock the main chain into a coplanar structure, resulting in good device performance. Like the hybrid side chains, either oligoether side chains or fluoroalkyl side chains can enhance the intramolecular interaction due to strong affinity between each side chains, leading to more ordered nanostructure. However, ionic side chains and latent reactive side chains cannot enhance

doi:10.6342/NTU201904150

intramolecular interaction, but those functional side chain let conjugated polymers have some interesting application, such as to modify the work function of electrode[102], and to become cross-linked conjugated polymers by post-treatment using UV light[104]. Among these side chains, oligoether side chains attracts our attention due to the following advantages: (1) the most flexible side chain (2) good solubility in non-toxic polar solvent (water, acetone, methanol, tetrahydrofurane, etc) (3) able to complex with metal. Therefore, in this dissertation, we used oligoether(oilgoethylene glycol) side chain to study side chain type effect on the properties of D-A CPs.

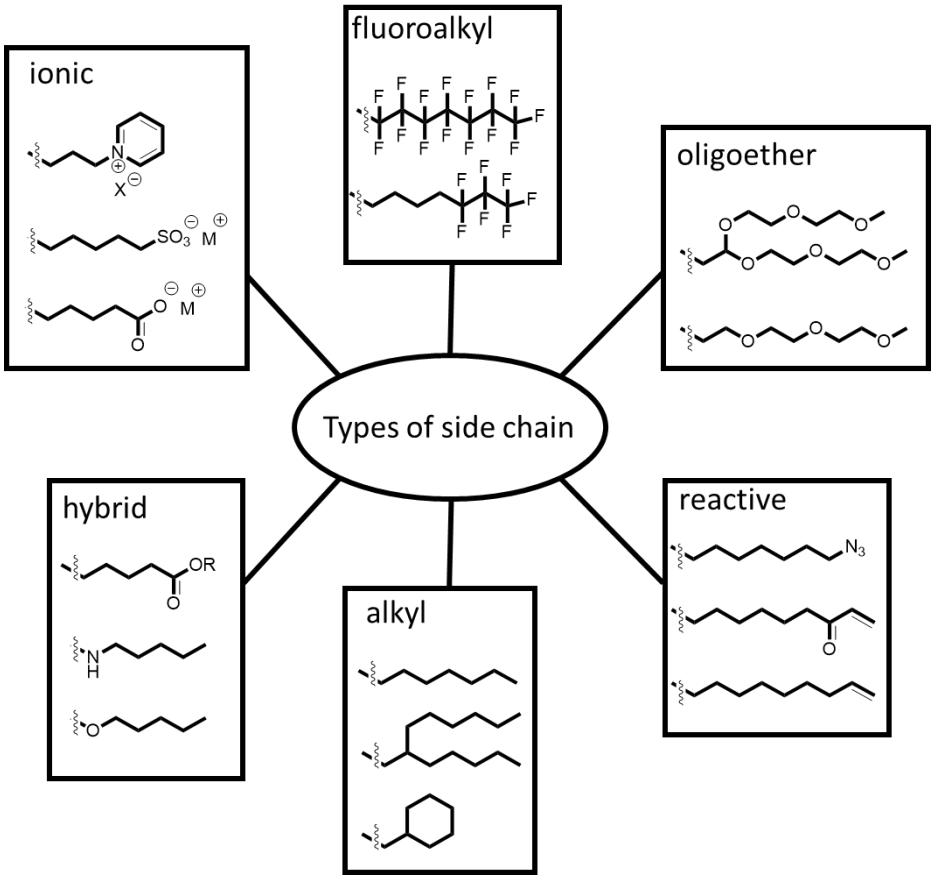

Figure 1.15. Types of side chain.

doi:10.6342/NTU201904150

1.4 Motivation and Objective

Although there are lots of side chain effect studies in D-A CPs, those studies are carried out from different research groups and each individual side chain effect study is difficult to do comparison. Thus we propose to do a systematic and comprehensive side chain effect study including location, length, and type of side chains. In addition, the oilgoethylene glycol (OEG) side chain effect on the properties of D-A CPs has not been extensive studied and sometimes the results are controversial. Some studies indicate that OEG shortens the distance of π-π stacking ($d_{\pi-\pi}$) of polymers, thus enhances the crystallinity of polymer and improves the device performance by replacing bulky alkyl side chain with OEG.[93, 105-107] However, Mei and You et al. indicate that although OEG reduce the $d_{\pi-\pi}$ of polymers, it deteriorates the crystallinity of polymers and device performance.[108-109] These studies encouraged us to investigate an insight of OEG effect. Therefore, we used oligothiophene-TPD based polymers and oligothiophene-isoindigo based polymers to do a comprehensive side chain effect study and a complete OEG side chain effect study, respectively.

(1) Comprehensive side chain effect study

We designed eight oligothiophene-TPD based conjugated polymers, P3TTPD, with two side chains on the 3T unit by varying their location (outward, and inward), types on the TPD unit (dodecyl and tetraethylene glycol (TEG)), and three different lengths on the 3T unit (octyl, hexyl, and butyl). The detailed chemical structure, synthesis,

doi:10.6342/NTU201904150

characterization and self-assembly of the polymers are discussed in the following sections.

(2) Complete OEG side chain effect study

We chose two oligothiophene-isoindigo based conjugated polymers (PnTI), P3TI and P4TI, as model polymers to systematically study the OEG side chain effect. For P3TI and P4TI model polymers, octyl side chains are installed on oligothiophene unit, and 2-hexyldecyl side chains are placed on isoindigo unit. We gradually replaced alkyl side chains with OEG side chains and systematically studied the changes of physical properties of the polymers. The 2-hexyldecyl side chains on isoindigo unit are replaced by OEG side chains at first. Then, the octyl side chains on oligothiophene unit are also replaced by the OEG side chains. The detailed chemical structure, synthesis, characterization and self-assembly of the polymers are discussed in the following sections.

doi:10.6342/NTU201904150

Chapter 2 Results and Discussion

This chapter is divided into two parts. The results of oligothiophene-TPD based conjugated polymers are discussed in **Chaper 2.1**. The results of oligothiophene-isoindigo based conjugated polymers are discussed in **Chapter 2.2**.

2.1 Oligothiophene-TPD based Conjugated Polymers

The names and chemical structure of polymers are shown in **Figure 2.1**. They are named P3T(R_{in})TPD(R), P3T(R_{in})TPD(E), P3T(R_{on})TPD(R), and P3T(R_{on})TPD(E), where "R" is alkyl side chain, "E" is oligoether side chain, "i" represents the two R located at 3,3" position of 3T (inward), "o" represents the two R located at 4,4" position of 3T (outward), and "n" is the length of R. The characterization and self-assembly of the polymers are discussed in the following sections. To avoid the molecular weight effect in this study, we synthesized the polymers with similar molecular weight in the range of 3KDa~7KDa (**Table 5.4**). Please to note that when we discuss the side chain location effect, we compare P3T(R_{o8})TPD(R) and P3T(R_{i8})TPD(R). Both polymers consist of octyl group on 3T unit and dodecyl on TPD unit. As we discuss the side chain type effect, we do two individual comparisons: (1) P3T(R_{o8})TPD(R) vs P3T(R_{o8})TPD(E), (2) P3T(R_{i8})TPD(R) vs P3T(R_{i8})TPD(E). For these polymers, the side chains on 3T unit are fixed as octyl. When we discuss the

doi:10.6342/NTU201904150

side chain length effect, we do two individual comparisons: (1) P3T(R_{o8})TPD(E) vs P3T(R_{o6})TPD(E) vs P3T(R_{o4})TPD(E), (2) P3T(R_{i8})TPD(E) vs P3T(R_{i8})TPD(E) vs P3T(R_{i4})TPD(E). For these polymers, the side chains on TPD unit are fixed as TEG.

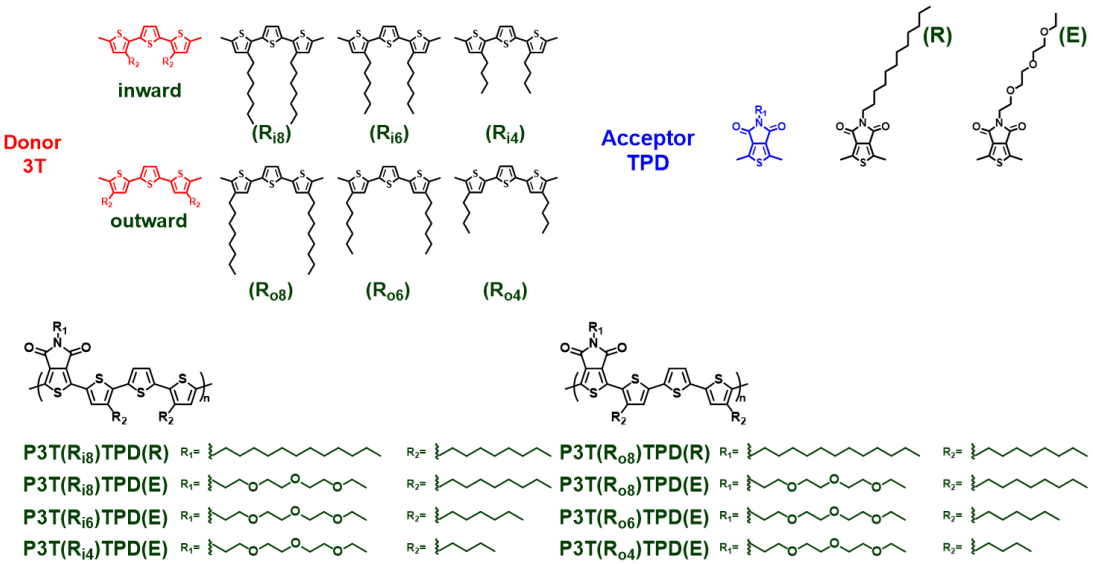

Figure 2.1. Chemical structures of P3TTPD polymers

2.1.1 Molecular Orbital Computation

The coplanarity of polymer backbone (main chain) is a critical factor for polymer packing (π-π stacking). In general, the polymer backbone with good coplanarity is favorable for π-π stacking. Molecular orbital computation is powerful tool to help us realizing the coplanarity of polymer backbone. The results of computation are shown in **Figure 2.2**. The torsion angles between aromatic rings are summarized in **Table 2.1**. In addition, the size of polymer also can be estimated. The width of polymer chain (W)

doi:10.6342/NTU201904150

was calculated from the following formula:

$$\mathrm{W}\ (\text{Å}) = l_1 * cos\theta_1 + 4.6 + l_2 * cos\theta_2$$

Where 4.6 Å is the width of polymer backbone, l_1 is chain length of octyl, hexyl, or butyl, l_2 is chain length of TEG or dodecyl, θ_1 is angle between the side chain (l_1) and backbone plan, and θ_2 is angle between the side chain (l_2) and backbone plan, as shown in **Figure 2.3**. All parameters and the width of polymer chain are shown in **Table 2.2**.

doi:10.6342/NTU201904150

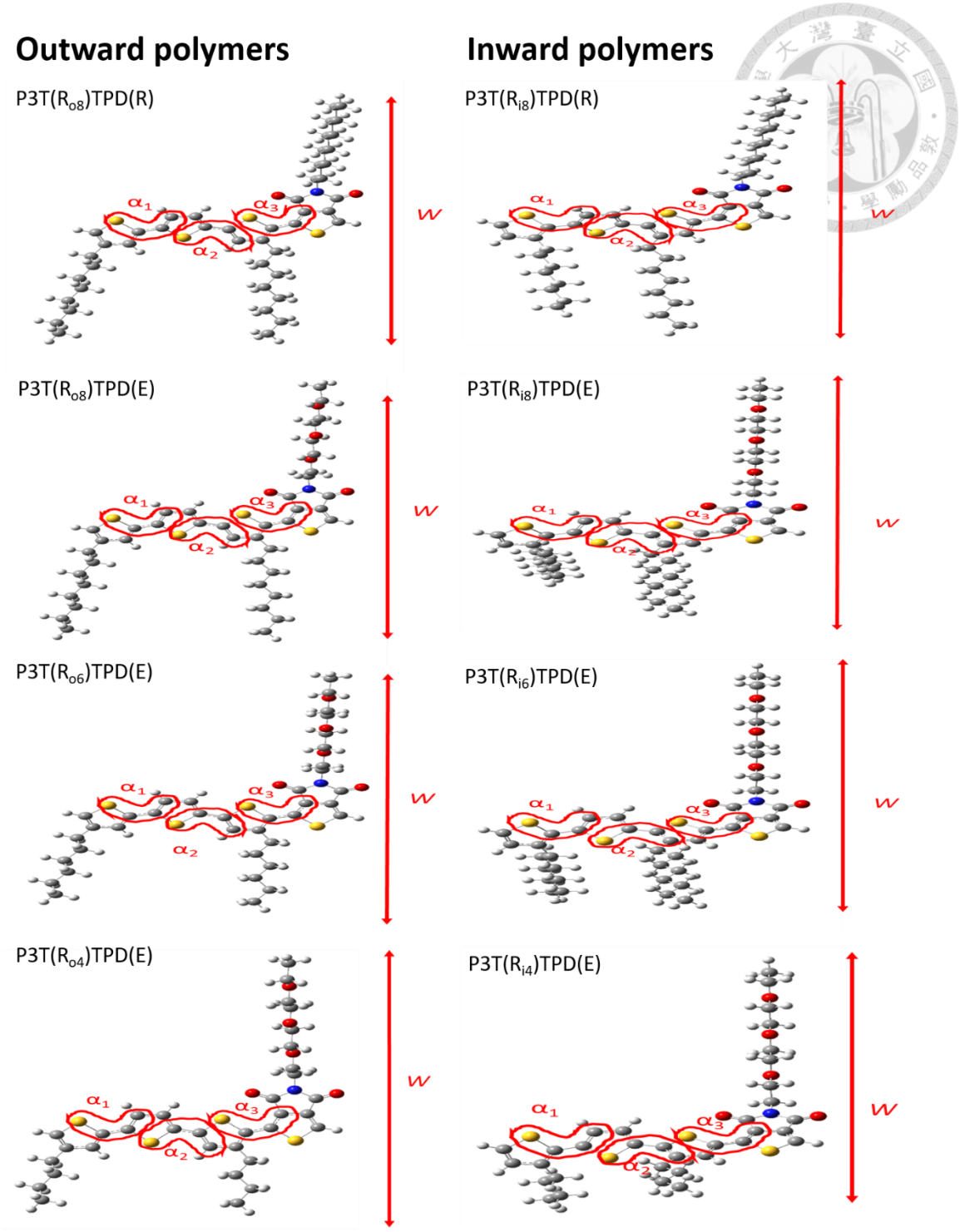

Figure 2.2. Molecular simulation results, including front view of molecular plan, of outward and inward series of 3T-TPD based conjugated polymers.

doi:10.6342/NTU201904150

Table 2.1. Summary of molecular simulation parameters of 3T-TPD based CPs

Polymer	α_1 (^{o})	α_2 (^{o})	α_3 (^{o})
P3T(R_{o8})TPD(R)	16	-10	2
P3T(R_{o8})TPD(E)	-17	2	3
P3T(R_{o6})TPD(E)	-17	2	0
P3T(R_{o4})TPD(E)	-17	2	0
P3T(R_{i8})TPD(R)	41	-24	3
P3T(R_{i8})TPD(E)	-42	-30	2
P3T(R_{i6})TPD(E)	-41	-25	3
P3T(R_{i4})TPD(E)	-41	-29	2

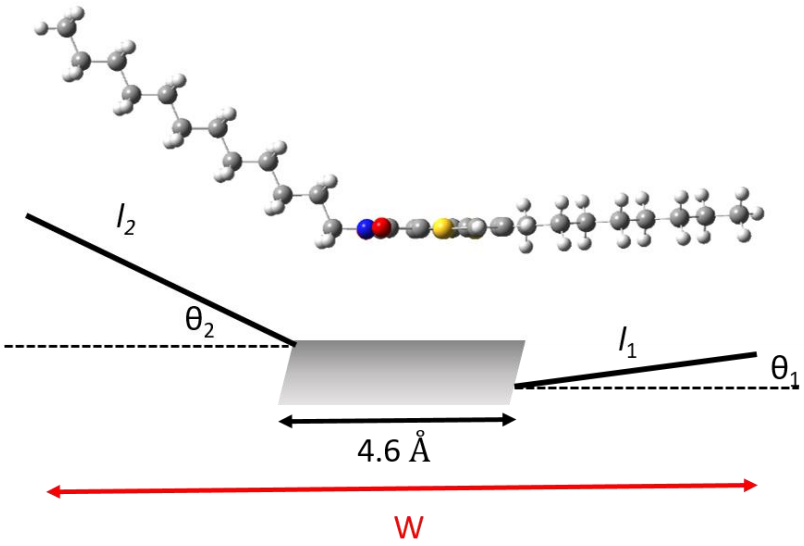

Figure 2.3. Schematic diagram to explain how to calculate the width of polymer chain.

doi:10.6342/NTU201904150

Table 2.2. Calculation parameters and width of polymer chain

Polymer	l_1 (Å)	θ_1 (°)	l_2 (Å)	θ_2 (°)	W (Å)
P3T(R_{o8})TPD(R)	10.3	2	15.3	39	26.8
P3T(R_{o8})TPD(E)	10.3	6	13.1	30	25.2
P3T(R_{o6})TPD(E)	7.7	1	13.1	8	25.3
P3T(R_{o4})TPD(E)	5.1	1	13.1	9	21.7
P3T(R_{i8})TPD(R)	10.3	20	15.3	39	26.1
P3T(R_{i8})TPD(E)	10.3	26	13.1	29	25.3
P3T(R_{i6})TPD(E)	7.7	21	13.1	29	23.3
P3T(R_{i4})TPD(E)	5.1	26	13.1	28	20.8

The results of molecular orbital computation reveal that the outward series polymers have better coplanarity than the inward series polymers due to smaller torsion angles between aromatic rings.

2.1.2 Optical Properties

Figure 2.4 shows the film absorption spectra of 3T-TPD based CPs. The λ_{max}, $\lambda_{shoulder}$ and bandgap of the films are summarized in **Table 2.3**. For side chain location effect, the polymer with outward side chains (P3T(R_{o8})TPD(R)) shows a red-shift of λ_{max} (529 nm vs 507 nm) and a higher absorption of $\lambda_{shoulder}$ than the polymer with inward side chains (P3T(R_{i8})TPD(R)). The results signify that P3T(R_{o8})TPD(R) have better polymer packing than P3T(R_{i8})TPD(R). For the side chain type effect (TEG vs. dodecyl), the polymer with oligoether side chain shows longer wavelength of λ_{max}

doi:10.6342/NTU201904150

than the polymer with alkyl side chain. For outward series polymers, the P3T(R_{o8})TPD(E) shows a longer wavelength of λ_{max} (573nm vs 529nm, red-shift: 44nm) as compared with P3T(R_{o8})TPD(R). For inward series polymers, P3T(R_{i8})TPD(E) also shows larger red-shift λ_{max} (510nm vs 507nm, red-shift: 3nm) than P3T(R_{i8})TPD(R). In comparison, the red-shifted amount of λ_{max} is more significant in outward series polymers (44 nm) than in inward series polymers (3 nm). All above results indicate that the oligoether side chain is more effective on the packing of polymers than the alkyl side chain due to the presence of oxygen atom having more spatial space for self-assembly[109].

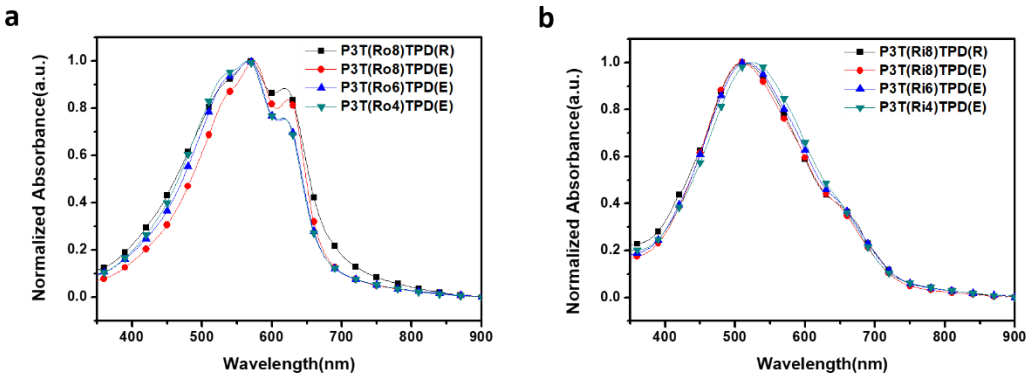

Figure 2.4. Optical absorption spectra of (a) outward series polymer (P3T(R_{on})TPD(R,E)) films and (b) inward series polymer (P3T(R_{in})TPD(R,E)) films spun-cast from 10 mg/ml chloroform solutions.

doi:10.6342/NTU201904150

Table 2.3. Summary of optical property of 3T-TPD based CPs

Polymer	λ_{max} (nm)[a]	$\lambda_{shoulder}$ (nm)[a]	E_g^{opt} (eV)[b]
P3T(R_{o8})TPD(R)	529	618	1.86
P3T(R_{o8})TPD(E)	573	671	1.85
P3T(R_{o6})TPD(E)	567	671	1.85
P3T(R_{o4})TPD(E)	562	667	1.86
P3T(R_{i8})TPD(R)	507	-	1.72
P3T(R_{i8})TPD(E)	510	-	1.72
P3T(R_{i6})TPD(E)	513	-	1.71
P3T(R_{i4})TPD(E)	517	-	1.72

[a] UV-Vis absorption spectra of films were measured using spun-cast film from 10 mg/ml chloroform solutions. [b] Optical bandgap of each film was calculated from its absorption edge (onset of the peak) of UV-Vis spectrum

The side chain length effect was investigated by reducing from octyl to hexyl and butyl side chains on 3T unit. For outward series polymers, the polymer with longest side chain (P3T(R_{o8})TPD(E)) shows the longest wavelength of λ_{max} (573 nm), indicates that the molecular packing and self-assembly of polymer is advanced with

doi:10.6342/NTU201904150

increasing side chain length. On the contrary, for the inward series polymers, the polymer with the shortest side chain (P3T(R_{i4})TPD(E)) shows the longest wavelength of λ_{max} (517 nm). That reveals the self-assembly behavior of polymer is improved with decreasing side chain length. The more detailed discussions on the structural formation mechanism using model will be present in the later section to explain the differences of self-assembly behaviors among the 3T-TPD based CPs.

The optical bandgaps of the polymers are calculated by the following formula, $1240/\lambda_{onset}$, where λ_{onset} is the onset of absorption peak with longest wavelength. For the polymer with the outward side chains, the polymers have similar bandgap of 1.85~1.86 eV (**Table 2.3**). In comparison, the inward series polymers have lower band gap of 1.71~1.72 eV than the outward series polymers. In addition, the type and length of side chain do not significantly influence the bandgap of the polymers. In general, the polymer with better packing, the bandgap of the polymer is smaller.[25] However, we observed that the inward series polymers, known to have poor packing, exhibit smaller bandgap than the outward series polymers. This interesting result may be related to the extended conjugating length of inward series polymers. The detailed discussions will be presented in the later section of morphology.

doi:10.6342/NTU201904150

2.1.3 Electrochemical Properties

Figure 2.5 shows cyclic voltammetry spectra and schematic diagram of energy level of 3T-TPD based CPs. Every polymer shows clear oxidation peak at oxidation condition (0 V→1.4 V→0 V). However, no significant peak is observed for each polymer at reduction condition (0 V→-1.4 V→0 V). The results indicate every polymer is p-type. The HOMO and LUMO energy level of each polymer were calculated using the following formula:

$$\mathbf{HOMO} = -\{E_{oxi} - E_{Fc/Fc^+} + \mathbf{5.13}\}eV$$

$$\mathbf{LUMO} = -\mathbf{HOMO} + E_g^{opt}$$

Where E_{oxi} and E_{Fc/Fc^+}, and E_g^{opt} are oxidation potential of the polymer, oxidation potential of the ferrocene as standard, and bandgap value is obtained from UV-Vis spectrum of the polymer, respectively. For side chain location effect, the outward series polymer, P3T(R_{o8})TPD(R), shows higher energy level (HOMO: -5.48 eV vs. -5.56 eV, LUMO: -3.62 eV vs. -3.84 eV) than the polymers with inward side chains, P3T(R_{i8})TPD(R). The results are due to better coplanarity of backbone of P3T(R_{o8})TPD(R) than that of P3T(R_{i8})TPD(R), which promoting electrons to be delocalized easily. By comparing TEG (E) chain with dodecyl (R) chain, for outward series polymers, P3T(R_{o8})TPD(E) shows higher energy level (HOMO: -5.24 eV vs. -5.48 eV, LUMO: -3.39 eV vs. -3.62 eV) than that of P3T(R_{o8})TPD(R). The same

doi:10.6342/NTU201904150

trend is also found in inward series polymers. These results are attributed to the stronger electron donating ability of TEG chain than that of dodecyl chain. Furthermore, the side chain length (octyl vs. hexyl vs. butyl) on the 3T moeity marginally affects the energy level of the polymers as shown in **Figure 2.5(b)**. The difference on the electron donating ability of different length of alkyl chains are not significant.[88]

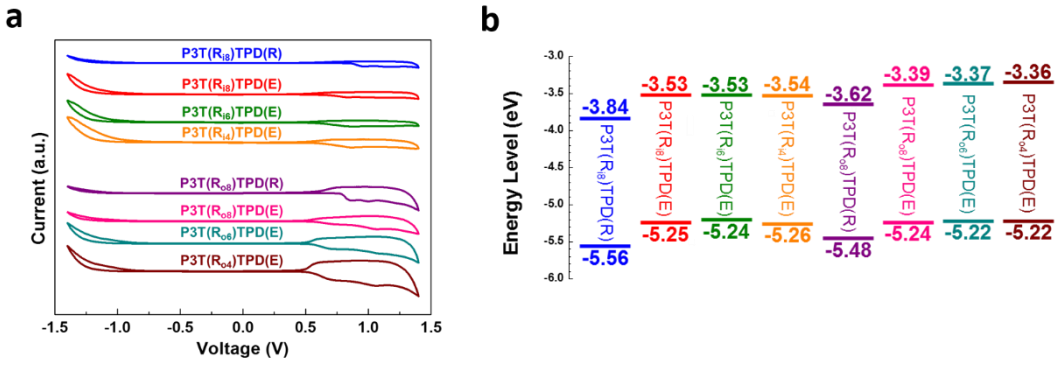

Figure 2.5. 3T-TPD based CPs' (a) cyclic voltammetry spectra and (b) energy levels.

doi:10.6342/NTU201904150

2.1.4 Thermal Properties

TGA profiles of 3T-TPD based CPs are shown in **Figure 2.6**. The TGA data are summarized in **Table 2.4**. The outward series polymer, P3T(R_{o8})TPD(R) shows T_d of 416°C. The T_d is decreased to 393°C by replacing dodecyl chain with TEG chain. The inward series polymers also show the same trend (436 °C → 383 °C). These results are due to that reactive oxygen radicals induce the polymer to be dissociated easily. There is no significant trend by varying the side chain length from octyl to hexyl and butyl. Even though TEG chain reduces the thermal stability of the polymers, all 3T-TPD based CPs still show high T_d over 350 °C. The DSC profiles of 3T-TPD based CPs are shown in **Figure 2.7** and relevant data are summarized in **Table 2.4**. The outward series polymers show obvious melting peaks. However, no significant peak is observed in inward series polymers. These results indicate that outward series polymers have better π-π stacking than inward series polymers due to the higher degree of coplanarity. The outward series polymer, P3T(R_{o8})TPD(R) shows 239°C of T_m. The T_m is increased to 296°C by replacing dodecyl chain with TEG chain. These results indicate that the more flexible TEG chain helps the outward series polymer to pack into highly ordered nanostructure. Furthermore, the T_m is decreased from 296°C to 266°C to 247°C by changing the octyl to hexyl to butyl. This result reveals that the outward series polymers pack into highly ordered nanostructure with increased side

doi:10.6342/NTU201904150

chain length. The longer side chain provides more mobility than the shorter side chain during the self-assembly process. All results of DSC are in agreement with the results of UV-Vis spectra.

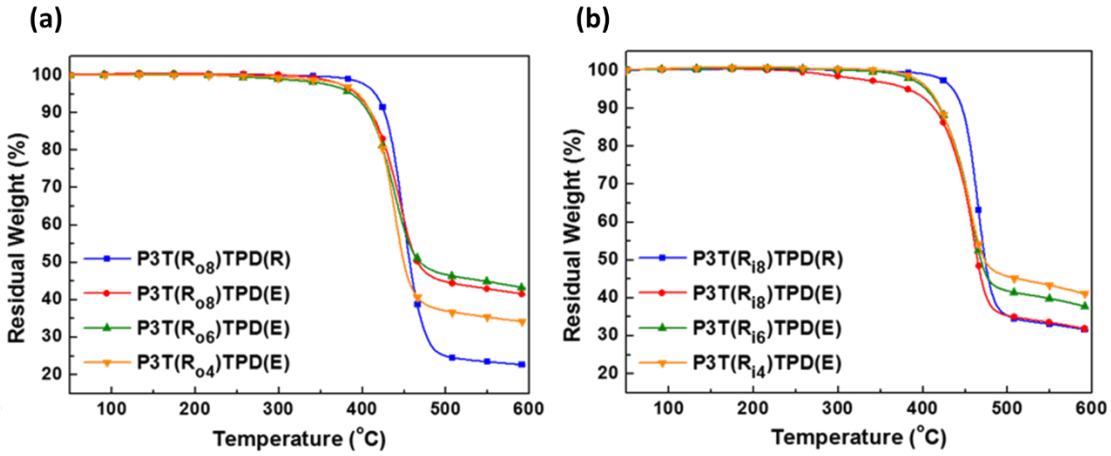

Figure 2.6. TGA profiles of (a) outward series and (b) inward series of 3T-TPD based CPs.

doi:10.6342/NTU201904150

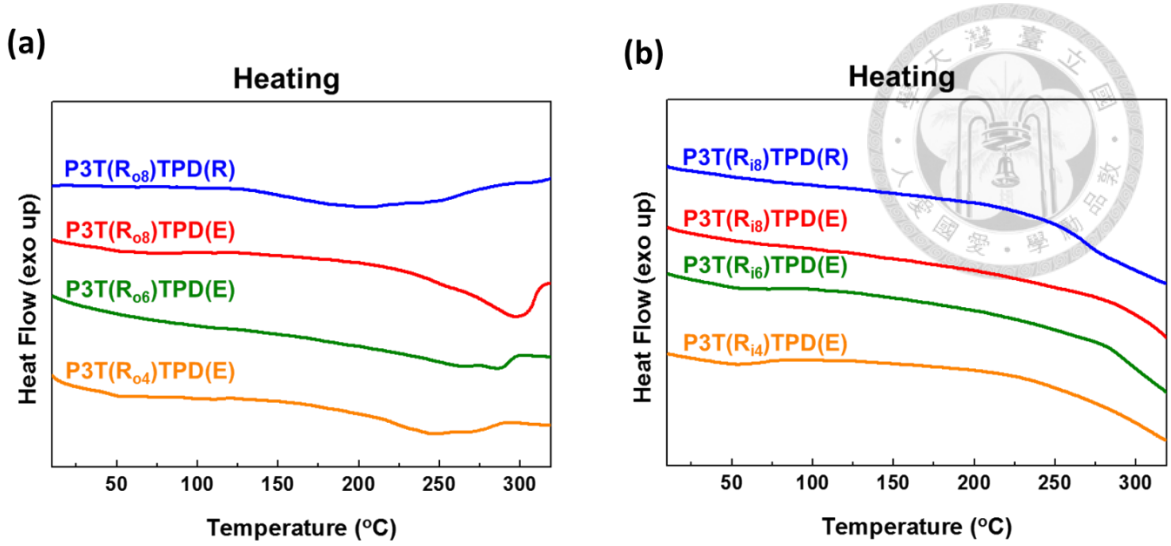

Figure 2.7. DSC profiles of (a) outward series and (b) inward series of 3T-TPD based conjugated polymers.

Table 2.4. Thermal properties of 3T-TPD based CPs

Polymer	T_d (°C)	T_m (°C)
P3T(R_{o8})TPD(R)	416	239
P3T(R_{o8})TPD(E)	393	296
P3T(R_{o6})TPD(E)	388	266
P3T(R_{o4})TPD(E)	395	247
P3T(R_{i8})TPD(R)	436	-
P3T(R_{i8})TPD(E)	383	-
P3T(R_{i6})TPD(E)	405	-
P3T(R_{i4})TPD(E)	407	-

doi:10.6342/NTU201904150

2.1.5 Morphology Study

Figure 2.8 shows 2D patterns of grazing-incidence wide angle x-ray scattering (GIWAXS) of the film of 3T-TPD based CPs. The outward series polymer, P3T(R_{o8})TPD(R), shows random orientation. By replacing the dodecyl (R) chain with TEG (E) chain, P3T(R_{o8})TPD(E) shows edge-on orientation. The orientation remains by varying the side chain length. However, inward series polymers show random orientation. In order to investigate the nanostructures of polymers, the line cut data of GIWAXS are shown in **Figure 2.9**. The relevant data are summarized in **Table 2.5.**

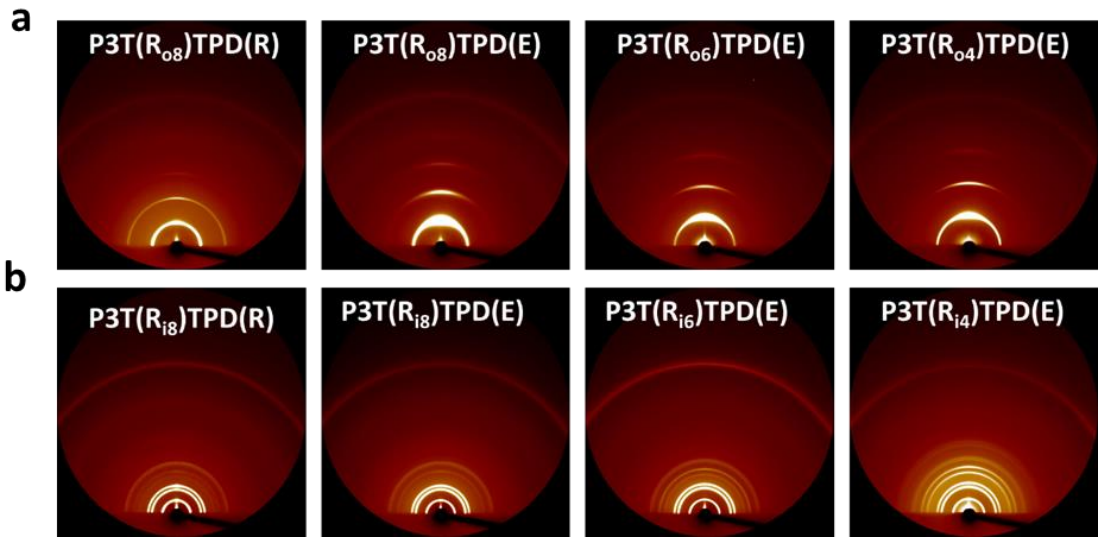

Figure 2.8. 2D patterns of GIWAXS of (a) outward series polymers and of (b) inward series polymers

doi:10.6342/NTU201904150

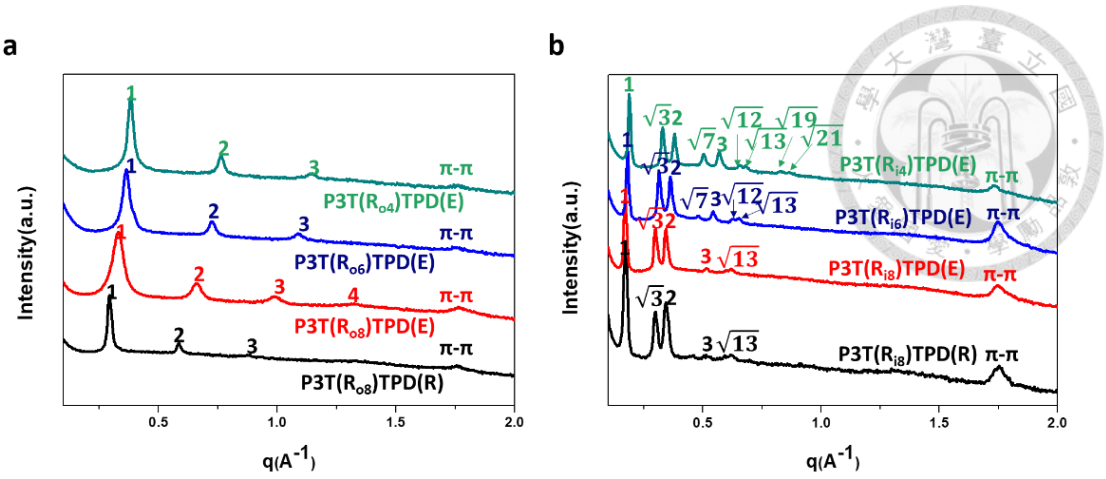

Figure 2.9. Line cut data of GIWAXS of (a) outward series polymers and of (b) inward series polymers

Table 2.5. Summary of GIWAXS parameters of the polymer films

Polymer	d-spacing (A)	$d_{\pi-\pi}$ (A)	peak ratio	structure
P3T(R_{o8})TPD(R)	21.4	3.6	1:2:3	LAM
P3T(R_{o8})TPD(E)	19.0	3.6	1:2:3:4	LAM
P3T(R_{o6})TPD(E)	17.3	3.6	1:2:3	LAM
P3T(R_{o4})TPD(E)	16.4	3.6	1:2:3	LAM
P3T(R_{i8})TPD(R)	36.7	3.6	$1:\sqrt{3}:2:3:\sqrt{13}$	HEX
P3T(R_{i8})TPD(E)	36.7	3.6	$1:\sqrt{3}:2:3:\sqrt{13}$	HEX
P3T(R_{i6})TPD(E)	34.9	3.6	$1:\sqrt{3}:\sqrt{7}:2:3:\sqrt{12}:\sqrt{13}$	HEX
P3T(R_{i4})TPD(E)	33.4	3.6	$1:\sqrt{3}:2:\sqrt{7}:3:\sqrt{12}:\sqrt{13}:\sqrt{19}:\sqrt{21}$	HEX

doi:10.6342/NTU201904150

In outward series polymers (**Figure 2.9(a)**), P3T(R_{o8})TPD(R) shows multiple scattering peaks in the ratio of 1:2:3, typical scattering pattern for ordered lamellae (LAM) structure, and one peak in high q region (q> 1.5 $Å^{-1}$) which presents π-π stacking. The d-spacing and $d_{π-π}$ is 21.4 Å and 3.6 Å, respectively. For the side chain type effect (TEG vs. dodecyl), P3T(R_{o8})TPD(E) shows more scattering peaks in the ratio of 1:2:3:4 than P3T(R_{o8})TPD(R). The result indicates that P3T(R_{o8})TPD(E) can self-assemble into higher order LAM structure than P3T(R_{o8})TPD(R) because E is more flexible than R. For P3T(R_{o8})TPD(E), the d-spacing and $d_{π-π}$ is 19.0 Å and 3.6 Å, respectively. The d-spacing of the polymer decreased by 2.4 Å as replacing alkyl chain with TEG chain, signifying that TEG chain occupies smaller spacing than alkyl chain even though the amount of atoms in the chain is similar (TEG: 11 atoms, alkyl chain: 12 atoms). These results suggest that the flexible TEG chain having larger spatial space in outward series polymers can dramatically improve the self-assembly behavior and change orientation from random to edge-on. Furthermore, by decreasing from octyl to hexyl to butyl, the d-spacing of the polymer becomes smaller from 19.0 Å to 17.3 Å to 16.4 Å, but the regularity of its nanostructure is reduced. Therefore, in outward series polymers, P3T(R_{o8})TPD(E), shows the highest order of LAM structure.

In inward series polymers (**Figure 2.9(b)**), P3T(R_{i8})TPD(R) shows multiple

doi:10.6342/NTU201904150

scattering peaks in the ratio of $1:\sqrt{3}:2:3:\sqrt{13}$, typical scattering pattern for ordered hexagonal (HEX) structure, and one peak in high q region. The d-spacing and $d_{\pi\text{-}\pi}$ are 36.7 Å and 3.6 Å, respectively. This special HEX structure is rarely found in donor-acceptor alternating CPs. The formation mechanism will be discussed later using model. For the side chain type effect (TEG vs. dodecyl), in the inward polymers, both side chains show similar order of HEX structure, so the effect is not obvious. However, the effect of side chain length on the self-assembly behavior of inward polymers is quite large (octyl vs. hexyl vs. butyl), the regularity of HEX is dramatically enhanced with decreased side chain length. Hence, the shortest side chain inward polymer, P3T(R_{i4})TPD(E) shows the highest order of HEX structure with scattering peaks in the ratio of $1:\sqrt{3}:2:\sqrt{7}:3:\sqrt{12}:\sqrt{13}:\sqrt{19}:\sqrt{21}$.

In general, the $d_{\pi\text{-}\pi}$ (distance of backbone packing) of conducting polymer is influenced by the steric effect from the size of the side chain. It is interesting to note that, the $d_{\pi\text{-}\pi}$ does not change at all among the synthesized polymers. This result indicates that the $d_{\pi\text{-}\pi}$ is determined by the large side chain on the "TPD" unit (TEG or dodecyl) rather than the small side chains on 3T unit (octyl, hexyl or butyl). Even though TEG occupied smaller space than dodecyl, the size difference in one atom between them does not provide enough steric effect to affect $d_{\pi\text{-}\pi}$. Therefore, all synthesized polymers with TEG or dodecyl on TPD acceptor show the same value of

doi:10.6342/NTU201904150

$d_{\pi\text{-}\pi}$ regardless the side chain length on 3T donor.

In a short summary, the outward series polymers self-assemble into LAM, and inward series polymers having curvature structure, self-assemble into HEX. The polymers with TEG chain show higher order of nanostructure than the polymers with dodecyl chain because the TEG chain is more flexible than the alkyl chain. Thus, the TEG chain is more effective to assist the self-assembly of the outward series polymers than that of the inward series polymers. In outward series polymers, the highest order of LAM can be achieved with longest side chain. On the contrary, in inward series polymers, the polymer with shortest side chain shows the highest order of HEX. Both data of GIWAXS and UV-Vis provide the information of molecular packing and they are in good agreement. The contradict results of side chain length effect between inward series polymers and outward series polymer will be discussed later using model.

Two polymers: P3T(R_{o8})TPD(E) and P3T(R_{i4})TPD(E) exhibit highest order of LAM and HEX, respectively among 3T-TPD based CPs. **Figure 2.10** shows their AFM images. According to the results of 2D-GIWAXS, P3T(R_{o8})TPD(E) shows edge-on orientation, so the arrangement of lamellar layer is parallel to the substrate. Hence, the surface morphology of P3T(R_{o8})TPD(E) is flat with less feature as shown in **Figure 2.10(a)**. The AFM image of P3T(R_{i4})TPD(E) exhibits alternating bright and

doi:10.6342/NTU201904150

dark straps which indicate hard segments and soft segments respectively as shown in **Figure 2.10(b)**. This pattern is a kind of HEX pattern. Furthermore, these straps are straight and their length is over 500 nm. The length of each polymer chain is about 1nm estimated from its molecular weight. We speculated the strap is made from polymer bundles. Every polymer bundle is resulted from self-assembled polymer backbone about 1 nm, estimated from its molecular weight. Such long and straight straps reveal that conjugated length of the polymer is extended by well attached polymer bundles as shown in **Figure 2.11**. Thus, the extended conjugating length of inward series polymers exhibit smaller bandgap as compared with outward series polymers. Other AFM images of the films of synthesized polymers are shown in **Figure 2.12**.

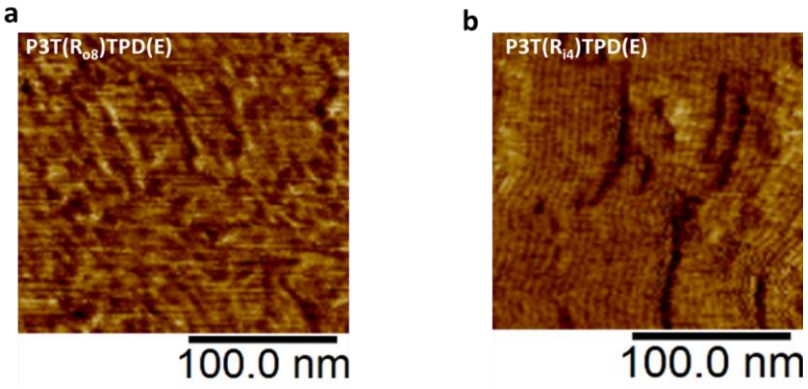

Figure 2.10. Two representative phase images of (a) P3T(R_{o8})TPD(E) and of (b) P3T(R_{i4})TPD(E) with the most ordered LAM and HEX respectively among 3T-TPD based CPs.

doi:10.6342/NTU201904150

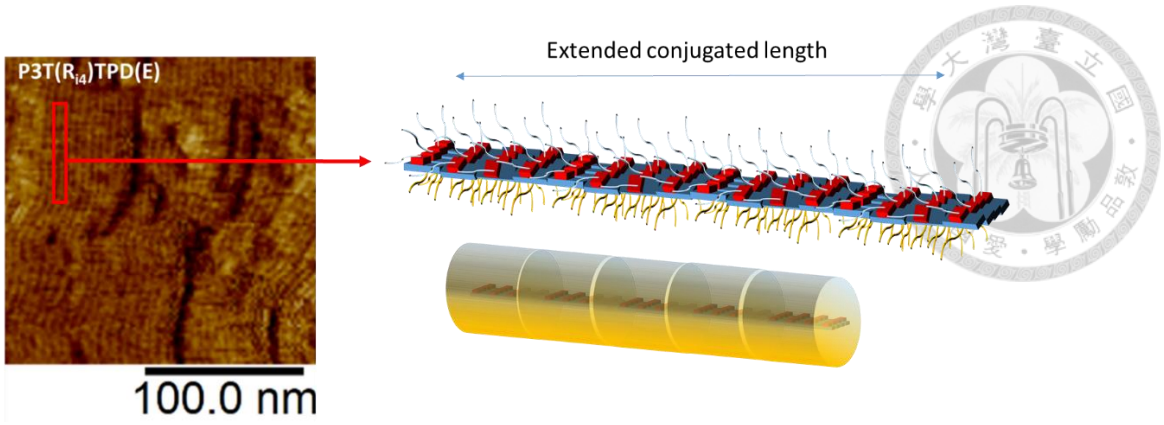

Figure 2.11. Schematic diagram to explain how the conjugated length of P3T(R_{i4})TPD(E) is extended by well attached polymer bundles.

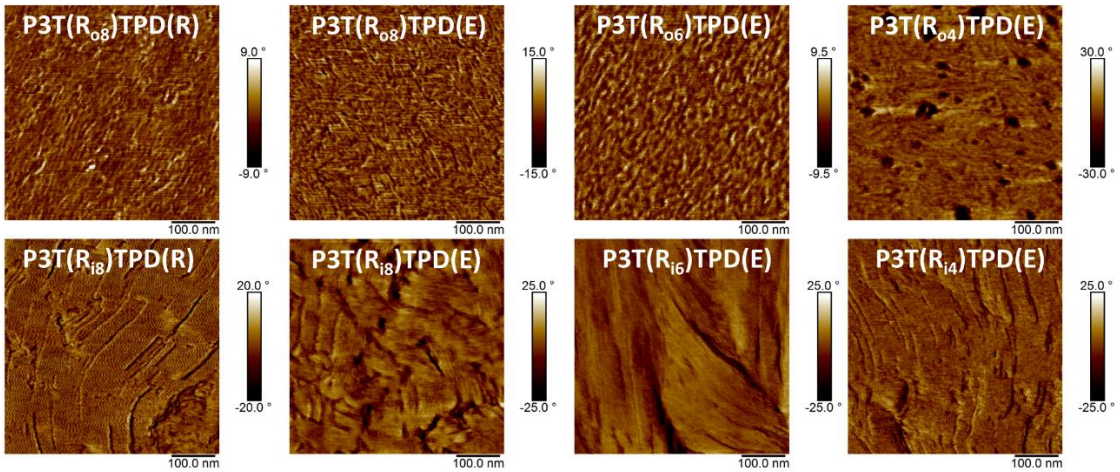

Figure 2.12. AFM phase images of films of 3T-TPD based CPs.

doi:10.6342/NTU201904150

2.1.6 Model for Self-assembly Behavior

We propose two models to explain the formation lamella structure (LAM) from P3T(R_{o8})TPD(E) and hexagonal structure (HEX) from P3T(R_{i4})TPD(E) respectively as shown in **Figure 2.13**. One usually expects the formation of lamella structure from conducting polymers due to their rigid rod characteristics.[25] From above discussion, we can conclude that the outward series polymers have better coplanarity in the backbone and better π-π stacking as compared with inward series polymers. Many backbones of the polymers can pack into a long-range lamellar layer with side chains sticking out straight and further self-assemble into lamellar structure. Therefore, the longer side chains provide better chain mobility of polymer to form higher ordered laminates as compared with shorter side chains (**Figure 2.13(a)**). The far right sketch of **Figure 2.13(a)** is a proposed cross-sectional view of the LAM accordingly to this model. According to the molecular simulation of P3T(R_{o8})TPD(E), the calculated width of single molecule is 25.2Å (**Table 2.2**). Then the calculated d-spacing should be 25.2Å as well if all of the side chains are fully extended. The measured datum of 19.0Å from GIWAXS indicates that the side chains are interdigitated in the lamellae layer. The formation curvature HEX for conducting polymer is rather unusual. Then, why do we observe it in the inward series polymers? For inward series polymers with poor coplanarity in the backbone, so only few backbones of the polymers can pack

doi:10.6342/NTU201904150

into a short-range lamellar layer. In addition, because of their twisted backbone, the hydrophilic TEG side chains and hydrophobic dodecyl side chains around the polymer backbones are segregated and self-assembled into cylinder and further into hexagonal structure (**Figure 2.13(b)**). The far right sketch of **Figure 2.13(b)** is a proposed cross-sectional view of according to this model. According to the molecular simulation of P3T(R_{i4})TPD(E), the width of single molecule is 20.8Å. Then the calculated d-spacing is 36.0Å which is within the range of measured datum of 33.4Å from GIWAXS. Furthermore, all of side chains on the inward series polymers are compressed in the cylinders with little room for them to sticking out. Thus, the shorter alkyl side chains provide larger free volume to form highly ordered hexagonal structure as compared with longer alkyl side chain.

doi:10.6342/NTU201904150

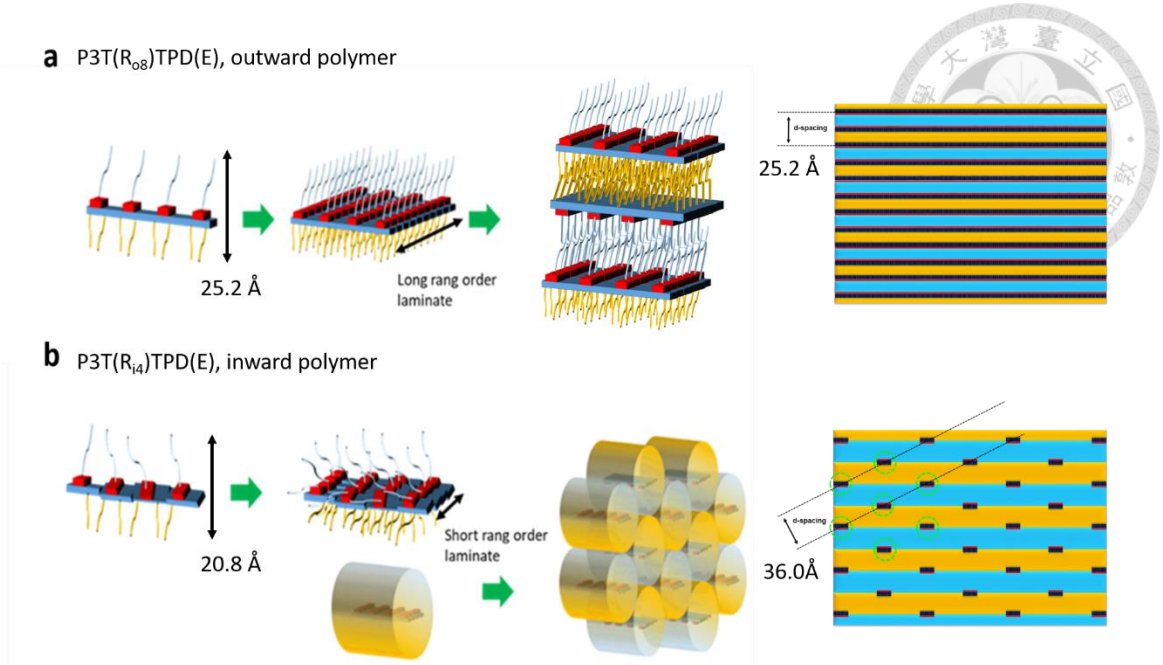

Figure 2.13. Structure formation mechanisms of self-assembly of P3TTPDs, (a) P3T(R_{o8})TPD(E) and (b) P3T(R_{i4})TPD(E) with lamellae structure and hexagonal structure respectively. Where blue line, yellow line, red box and blue box represent TEG chain, alkyl chain, imide group on TPD unit, and thiophene unit, respectively. The d-spacing is calculated from the width of polymer chain based on this model.

2.1.7 Summary

We successfully synthesize eight 3T-TPD based CPs with different side chain location (outward and inward), type (dodecyl and TEG), and length (octyl, hexyl, and butyl). Their optical properties, electrochemical properties, thermal properties, and self-assembly behavior had been systematically studied. For side chain location effect, the outward series polymers show longer wavelength of λ_{max} of UV-Vis absorption

doi:10.6342/NTU201904150

and obvious melting behavior than the inward series polymers. These results indicate that the outward series polymers pack better than inward series polymers and display self-assembled LAM. However, interestingly, the inward series polymers self-assemble into high order of HEX which is rarely found in D-A CPs. For side chain type effect, both the outward series polymers and inward series polymers with TEG chains show longer wavelength of λ_{max} of UV-Vis absorption and higher order of the nanostructure than the polymers with dodecyl chains. These results reveal that the more flexible TEG chain can enhance the self-assembly behavior of the polymers. For side chain length effect, the outward series polymers have higher order of LAM with longer side chain. On the contrary, shorter side chain is more suitable for inward series polymers to self-assemble into higher order of HEX. Finally, we purposed two models to explain the formation mechanism of LAM and HEX respectively. This study provides a new strategy to design new D-A CPs with highly ordered nanostructure for potential application in optoelectronic devices or sensors.

doi:10.6342/NTU201904150

2.2 Oligothiophene-isoindigo based Conjugated Polymers

The names and chemical structure of polymers are shown in **Figure 2.14**. They are named as P3T(R_8)I($R_{b\text{-}16}$), P3T(R_8)I(E), P3T(E)I(E), P4T(R_8)I($R_{b\text{-}16}$), P4T(R_8)I(E), and P4T(E)I(E), where R_8, $R_{b\text{-}16}$, and E represent octyl, branched 2-hexyldecyl, and OEG, respectively. Note that the OEG introduced in this work, i.e. tetraethylene glycol (TEG), cannot attach on the oligothiophene unit directly and the use of thiophene-3-ylmethanol to react with TEG is necessary. Therefore, the OEG on oligothiophene unit has one OCH_2 unit longer than the OEG on isoindigo unit. The methoxy-TEG is expected to have similar properties as TEG in terms of flexibility, hydrophobicity, and so on. To simplify the discussion, the OEG is used to represent either methoxy-TEG or TEG. The characterization and self-assembly of the polymers are discussed in the following sections. To avoid the molecular weight effect in this study, we synthesized the polymers with similar molecular weight in the range of 12 KDa~20 KDa (**Table 5.6**).

doi:10.6342/NTU201904150

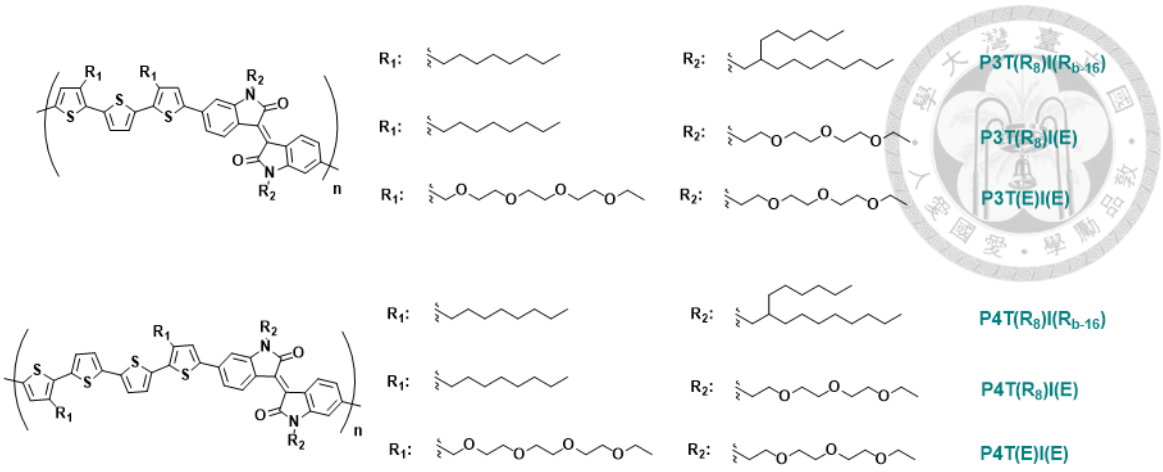

Figure 2.14. Chemical structures of PnTI polymers.

2.2.1 Optical Properties

Figure 2.15 displays the absorption spectra of annealed PnTI films. All of the polymers show broad dual band absorption between 300 ~ 850 nm. The λ_{max} between 600 ~ 700 nm and $\lambda_{shoulder}$ between 700 ~ 800 nm are contributed from intramolecular charge transfer (ICT) and intermolecular π-π stacking, respectively. The intensity of $\lambda_{shoulder}$ is related to the packing of polymer molecule and closely correlated to the crystallinity[110]. The values of λ_{max}, $\lambda_{shoulder}$, and the calculated optical bandgap are listed in **Table 2.6**. For P3TI polymers, P3T(R_8)I($R_{b\text{-}16}$) shows a clear $\lambda_{shoulder}$, implying that P3T(R_8)I($R_{b\text{-}16}$) has a high extent of π-π stacking and high crystallinity. As $R_{b\text{-}16}$ was replaced by OEG on isoindigo unit, i.e. P3T(R_8)I(E), the λ_{max} red-shifts from 660 nm to 678 nm, but no clear $\lambda_{shoulder}$ is observed. The results indicate that flexible and linear OEG on isoindigo unit may shorten the distance of π-π stacking of

doi:10.6342/NTU201904150

the polymer to have a red-shift of λ_{max}. However, the crystallinity of the polymer is decreased. Further replacing R_8 on oligothiophene unit with OEG, i.e. P3T(E)I(E), the $\lambda_{shoulder}$ disappears and the λ_{max} is blue-shift from 678 nm to 639 nm. The results show OEG on oligothiophene unit further decreases the crystallinity of polymer. Similar results can also be found in P4TI polymers. The crystallinity of the polymer affected by the OEG side chains plays a critical role in the packing orientation of the polymer chains, which will be discussed later.

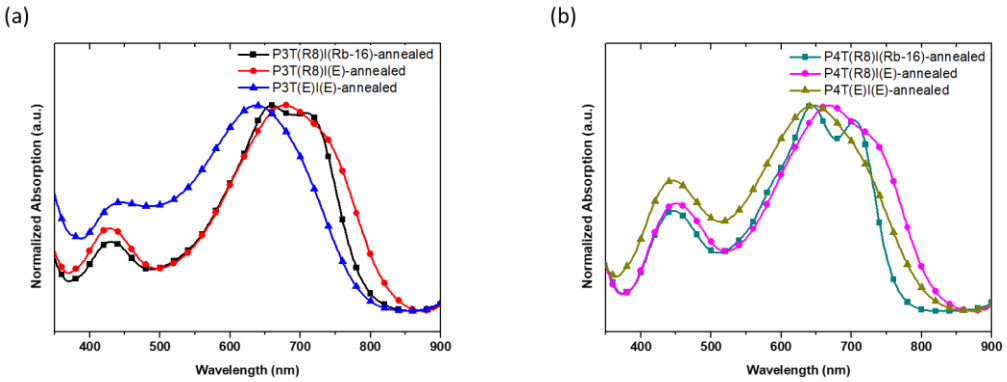

Figure 2.15. UV-Vis absorption spectra of (a) P3TI and (b) P4TI thin films spun-cast from 10 mg/ml chloroform solutions then annealed at 200 ºC for 1 h.

doi:10.6342/NTU201904150

Table 2.6. Summary of optical property for oligothiophene-isoindigo based CPs

Polymer	λ_1 (nm)[a]	λ_{max} (nm)[a]	$\lambda_{shoulder}$ (nm)[a]	E_g^{opt} (eV)[b]
P3T(R_8)I($R_{b\text{-}16}$)	430	660	710	1.54
P3T(R_8)I(E)	430	678	733	1.48
P3T(E)I(E)	439	639	-	1.56
P4T(R_8)I($R_{b\text{-}16}$)	448	644	705	1.61
P4T(R_8)I(E)	452	669	720	1.51
P4T(E)I(E)	447	646	-	1.54

[a] UV-Vis absorption spectra of films were measured using spun-cast film from 10 mg/ml chloroform solutions. [b] Optical bandgap of each film was calculated from its absorption edge (onset of the peak) of UV-Vis spectrum

2.2.2 Thermal Properties

Figure 2.16 shows the TGA and DSC profiles of PnTI polymers. The degradation temperature T_d and the melting temperature T_m are summarized in **Table 2.7**. TGA profiles reveal that the polymers with all alkyl side chains, P3T(R_8)I($R_{b\text{-}16}$) and P4T(R_8)I($R_{b\text{-}16}$), exhibit the highest T_d in their respective series of polymers. For the replacement of $R_{b\text{-}16}$ with OEG on isoindigo unit, the T_d of P3T(R_8)I(E) and P4T(R_8)I(E) are slightly reduced by 5 ~ 9 °C. However, for the further replacement of

doi:10.6342/NTU201904150

R_8 with OEG on oligothiophene unit, the T_d of P3T(E)I(E) and P4T(E)I(E) are greatly reduced by 101 ~ 115 °C as compared with their alkyl analogues. The large decrease in the thermal stability is because the oxygen atoms on OEG tend to form oxygen radicals at high temperature and promote radical chain decomposition reaction.

The DSC profiles reveal the crystallization behavior of the polymers. For P3TI polymers, only P3T(R_8)I($R_{b\text{-}16}$) shows a sharp melting peak at 268 °C and no melting peak is observed for the polymers with OEG side chains before thermal degradation. For P4TI polymers, as compared P4TI(R_8)I($R_{b\text{-}16}$) with P4T(R_8)I(E), P4T(R_8)I($R_{b\text{-}16}$) shows a sharper melting peak at higher temperature of 307 °C while the melting peak of P4T(R_8)I(E) is broader and at lower temperature of 299 °C. The melting peak is absent for P4T(E)I(E) before degradation. These results indicate that the OEG side chains inhibit the crystallization of the PnTI polymers, consistent with the UV-Vis absorption spectra shown in **Figure 2.15**. In the case of the higher crystallinity polymers, P3T(R_8)I($R_{b\text{-}16}$) and P4T(R_8)I($R_{b\text{-}16}$), considering that the bulky branched side chains ($R_{b\text{-}16}$) can prohibit the close packing of the isoindigo unit, the crystallization of the polymer should be dominantly driven by the oligothiophene unit with smaller side chains (R_8). This can also be supported by the fact that the T_m of P4T(R_8)I($R_{b\text{-}16}$) with more thiophene units is higher than that of P3T(R_8)I($R_{b\text{-}16}$) even though they have the same isoindigo unit.[111] The decrease in crystallinity upon

doi:10.6342/NTU201904150

replacing the alkyl side chains on isoindigo with OEG is because the small size of linear OEG side chains allow the isoindigo unit to be more closely packed, which may slightly shift the relative positions of the polymer backbones and in turn sacrifice the original stable packing of the oligothiophene unit. This argument can be verified by the change of π-π d-spacing upon the incorporation of OEG chains as shown in the GIWAXS study which will be discussed below.

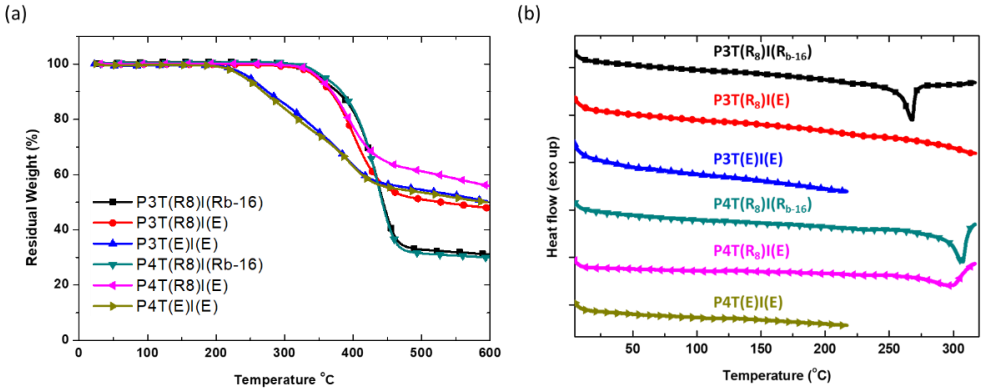

Figure 2.16. (a) TGA profiles and (b) DSC profiles of PnTI polymers.

doi:10.6342/NTU201904150

Table 2.7. Thermal properties of PnTI polymers

Polymer	T_d (°C)	T_m (°C)
P3T(R_8)I($R_{b\text{-}16}$)	352	268
P3T(R_8)I(E)	347	-
P3T(E)I(E)	251	-
P4T(R_8)I($R_{b\text{-}16}$)	359	307
P4T(R_8)I(E)	350	299
P4T(E)I(E)	244	-

2.2.3 Morphology Study

Figure 2.17 shows the 2D-GIWAXS patterns of the PnTI thin films. The polymer films were annealed at 200 °C for 1 h to ensure that the morphology of the polymer films are thermodynamically stable. All of the P4TI polymers show highly ordered lamellae structure with clear multiple scattering peaks at a q ratio of 1:2:3. The scattering peak contributed from π-π stacking can also be observed. In contrast, the P3TI polymers only show a clear first-order scattering peak from lamellae and a π-π stacking scattering. The results are attributed to the shape and coplanarity of polymer chains. The molecular conformation of D-A unit of polymer was simulated using Gaussian 9.0 software as shown in **Figure 2.18** and **Table 2.8**. The linear and planar

doi:10.6342/NTU201904150

backbones of P4TI polymers can stack into a more ordered lamellar structure. On the contrary, the S-shaped and twisted backbones of P3TI polymers are not suitable for lamellar stacking.

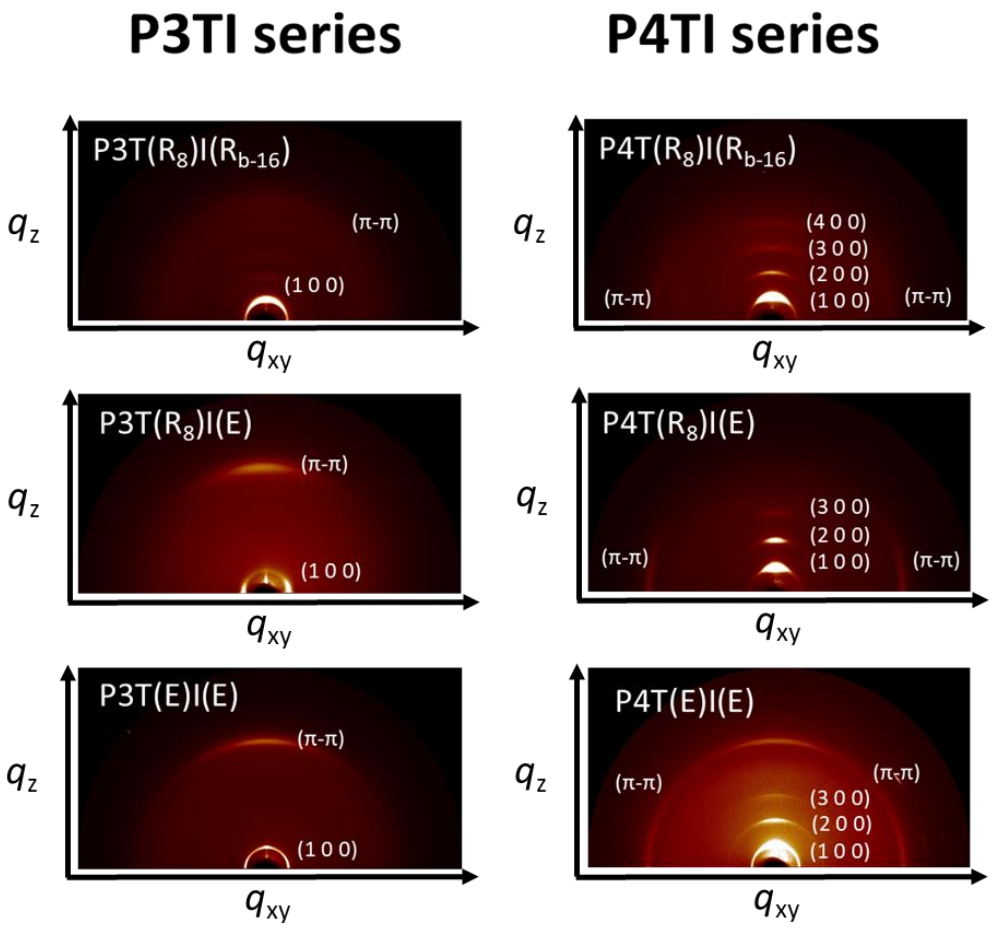

Figure 2.17. 2D-GIWAXS patterns of annealed PnTI films which were drop-cast from 10 mg/ml chloroform solutions then annealed at 200 °C for 1 h.

doi:10.6342/NTU201904150

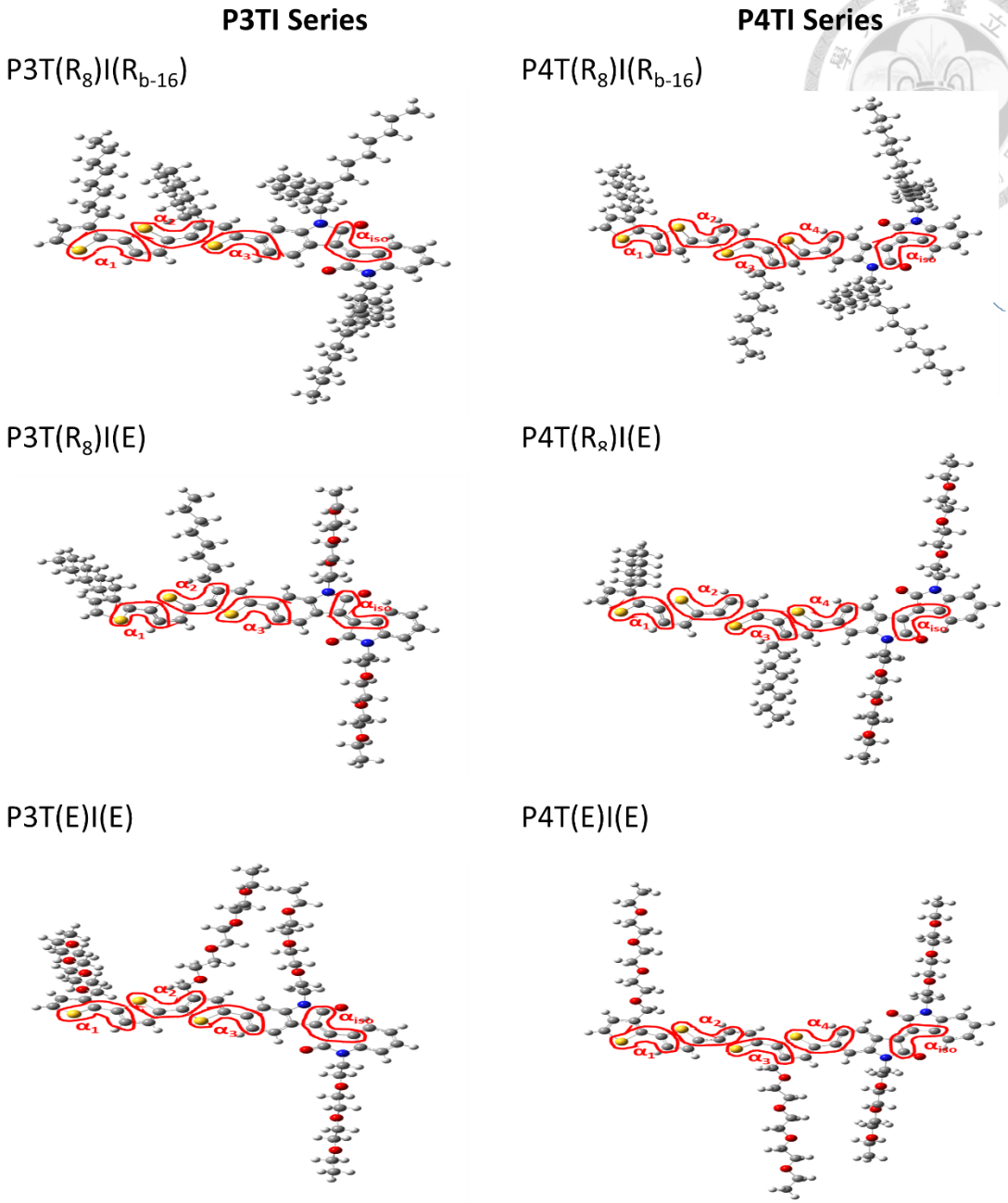

Figure 2.18. Molecular simulation results, including front view of molecular plan, of PnTI polymers.

doi:10.6342/NTU201904150

Table 2.8. Summary of molecular simulation of PnTI polymers

Polymer	α_1 (°)	α_2 (°)	α_3 (°)	α_4 (°)	α_{iso} (°)	α_{total}(°)	curvature
P3T(R_8)I($R_{b\text{-}16}$)	-33	-34	24	-	-12	-55	S-shaped
P3T(R_8)I(E)	47	-25	21	-	-12	31	S-shaped
P3T(E)I(E)	32	31	-20	-	-12	31	S-shaped
P4T(R_8)I($R_{b\text{-}16}$)	44	-17	16	-21	-12	10	linear
P4T(R_8)I(E)	45	-15	26	-21	-12	23	linear
P4T(E)I(E)	-33	-11	25	17	-12	9	linear

Figure 2.19a and **2.19b** show the line cut data along q_z-axis and q_{xy}-axis, from which the d-spacing of the lamellar stacking d_L and the π-π stacking $d_{\pi\text{-}\pi}$ can be estimated. The calculated d_L and $d_{\pi\text{-}\pi}$ are listed in **Table 2.9**. The d_L of P3TI polymers (19.4 Å ~ 20.9 Å) are larger than those of P4TI polymers (16.2 Å ~ 18.0 Å), which is attributed to the radially wider S-shaped P3TI backbone. For both P3TI and P4TI polymers, the replacement of $R_{b\text{-}16}$ with OEG on isoindigo reduces d_L, from 20.9 Å to 19.4 Å and from 18.0 Å to 16.2 Å for P3TI and P4TI respectively. The OEG side chain with smaller volume may need to interdigitate between backbones to have close packing. Further replacing the R_8 with OEG on oligothiophene increases d_L to 20.3 Å and 18.0 Å respectively, due to the longer length of the OEG chains compared to R_8

doi:10.6342/NTU201904150

chains.

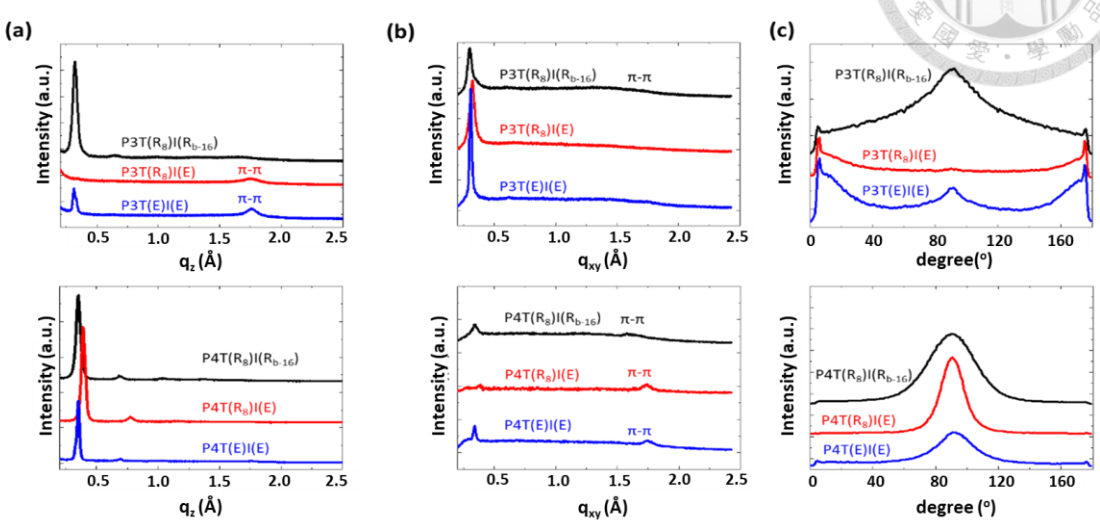

Figure 2.19. (a) Line cut data of z-axis, (b) line cut data of xy-axis, and (c) pole figures of the primary peak (100) extracted from the 2D-GIWAXS patterns.

Table 2.9. Summary of the GIWAXS parameters of annealed PnTI films

Polymer	Peak ratio	d_L (Å)	$d_{\pi-\pi}$ (Å)	Orientation
P3T(R_8)I(R_{b-16})	1	20.9	3.92	slightly edge-on
P3T(R_8)I(E)	1	19.4	3.57	face-on
P3T(E)I(E)	1	20.3	3.57	face-on
P4T(R_8)I(R_{b-16})	1:2:3:4	18.0	3.92	edge-on
P4T(R_8)I(E)	1:2:3	16.2	3.61	edge-on
P4T(E)I(E)	1:2:3	18.0	3.61	mixed

doi:10.6342/NTU201904150

The effect of OEG on $d_{\pi-\pi}$ is similar for both P3TI and P4TI polymers, and the change is intriguing. We have shown that the crystallinity of both P3TI and P4TI polymers decreases when more OEG chains are incorporated into PnTIs by DSC study (**Figure 2.16b**), but surprisingly, the scattering peaks of the π-π stacking become sharper and $d_{\pi-\pi}$ decreases when OEG chains are attached on the isoindigo unit (**Figure 2.19a** and 2**.19b**). For P3TI polymers, $d_{\pi-\pi}$ is reduced from 3.92 Å of P3T(R_8)I(R_{b-16}) to 3.57 Å of P3T(R_8)I(E) and P3T(E)I(E). For P4TI polymers, $d_{\pi-\pi}$ is reduced from 3.92 Å to 3.61 Å. As mentioned earlier, in the case of P3T(R_8)I(R_{b-16}) and P4T(R_8)I(R_{b-16}), isoindigo unit cannot closely pack due to the large steric hindrance of the bulky branched R_{b-16}. The packing of P3T(R_8)I(R_{b-16}) and P4T(R_8)I(R_{b-16}) chains is therefore dominated by oligothiophene unit and the spacing $d_{\pi-\pi}$ of 3.92 Å happens to be close to the $d_{\pi-\pi}$ of 3.87 Å of poly(3-alkylthiophene)[112]. Once the isoindigo unit are grafted with linear OEG, the packing of the isoindigo unit becomes dominant regardless of the type of side chains on the oligothiophenes, which thus gives a $d_{\pi-\pi}$ of 3.57 ~ 3.61 Å close to the $d_{\pi-\pi}$ of 3.65 Å of isoindigo oligomers[113]. Note that although the isoindigo unit with linear OEG chains can control the packing of PnTI polymers, they are unable to cause the crystallization of the polymer chains. Instead, their close packing deteriorates the crystallization of oligothiophene unit, as shown by the DSC profiles in **Figure 2.16b**. In other words, the crystallization of

doi:10.6342/NTU201904150

PnTI is driven by the oligothiophene unit, not the isoindigo unit.

The orientation of the PnTI packing can be determined from the 2D-GIWAXS as shown in **Figure 2.17**. **Figure 2.19** illustrates line cut data and the pole figures based on the intensity of the first-order (100) scattering as a function of the azimuthal angle. A stronger (100) peak on q_z-axis than on q_{xy}-axis in **Figure 2.19a** and 2**.19b** and a stronger (100) intensity around 90^o in the pole figures of **Figure 2.19c** indicate a preference for edge-on orientation, which can also be determined from a stronger π-π stacking peak on q_{xy}-axis than on q_z-axis. The opposite results indicate a preference for face-on orientation. For P3TI polymers, the replacement of alkyl side chains with OEG dramatically transforms the slightly edge-on orientation of P3T(R_8)I($R_{b\text{-}16}$) to the highly face-on orientation of P3T(R_8)I(E) and P3T(E)I(E) where a clear scattering of π-π stacking appears in the q_z direction. For P4TI polymers, the effect of OEG side chain is not as pronounced as in P3TI polymers. The orientation is from the highly ordered edge-on arrangement of P4T(R_8)I($R_{b\text{-}16}$) and P4T(R_8)I(E) changed to a mixed arrangement of P4T(E)I(E) where some face-on structure appears. The orientations of the films are summarized in **Table 2.9**.

In thin films, the conjugated polymers with strong intermolecular interactions, especially the backbone π-π interactions, generally show high crystallinity and tend to arrange in the edge-on fashion to extend the range of ordered packing in the in-plane

doi:10.6342/NTU201904150

direction.[114] Another critical factor influences the packing orientation of polymer is the backbone conformation. It has been shown that in order to closely contact the substrate, the polymers with S-shape backbones prefer to pack with the face-on orientation while the polymers with linear backbones favor the edge-on orientation.[114] By combining these two factors, we can explain the orientation of P3TI and P4TI thin films as follows. The backbones of P3TI polymers are S-shaped and the face-on orientation is naturally favorable. However, the high crystallinity of P3T(R_8)I($R_{b\text{-}16}$) implies a significant intermolecular interactions that may dominate the packing, and thus edge-on orientation is slightly preferred in this case. For P3T(R_8)I(E) and P3T(E)I(E), the introduction of OEG side chain decreases the crystallinity and therefore the S-shaped backbones cause the polymers to adopt the face-on orientation. The backbones of P4TI polymers are linear so that the edge-on orientation is inherently favorable. Along with the high crystallinity, P4T(R_8)I($R_{b\text{-}16}$) and P4T(R_8)I(E) thin films are as expectedly highly edge-on oriented while the lower crystallinity allows P4T(E)I(E) to reveal some face-on feature. These results indicate that OEG side chains are capable of controlling the packing orientation of PnTI polymers in thin films by altering the intermolecular interactions.

doi:10.6342/NTU201904150

2.2.4 Summary

We successfully synthesized a series of P3TI and P4TI polymers by varying amount and location of oligo(ethylene glycol) (OEG) side chain. Their optical properties, thermal properties, and morphologies are systematically studied. High crystallization capability of PnTI polymers is mainly contributed from the stable stacking of oligothiophene unit. For the polymers with all alkyl side chains, P3T(R_8)I($R_{b\text{-}16}$) and P4T(R_8)I($R_{b\text{-}16}$), they show the highest crystallinity but the largest $d_{\pi\text{-}\pi}$ among each series polymers. Their π-π stacking behavior is dominated by oligothiophene unit because the bulky alkyl side chains ($R_{b\text{-}16}$) on isoindigo unit prohibit close packing of isoindigo unit. As the bulky $R_{b\text{-}16}$ side chains on isoindigo unit are replaced by linear and flexible OEG side chains, i.e. P3T(R_8)I(E), P3T(E)I(E), P4T(R_8)I(E), and P4T(E)I(E), their π-π stacking behavior is dominated by isoindigo unit because isoindigo unit with small size of OEG side chains can stack more closely than oligothiophene unit, resulting in a sacrifice for stable stacking of oligothiophene unit. Therefore, even though they show relatively short $d_{\pi\text{-}\pi}$, their crystallinity is relatively low. In our opinions, OEG side chains can alter the π-π stacking behavior of the polymer chains to influence the crystallinity of the polymers, especially for donor-acceptor conjugated polymers. In addition, OEG side chains are capable of controlling the packing orientation of the polymers by adjusting the crystallinity of the

doi:10.6342/NTU201904150

polymers. For instance, OEG side chains change the packing orientation of P3TI polymers from slightly edge-on orientation of P3T(R_8)I($R_{b\text{-}16}$) to fully face-on orientation of P3T(R_8)I(E) and P3T(E)I(E) which is suitable for polymer solar cell application.

doi:10.6342/NTU201904150

Chapter 3 Conclusions

In order to do a comprehensive side chain effect study, we successfully synthesize eight 3T-TPD based CPs with different side chain location (outward and inward), type (dodecyl and TEG), and length (octyl, hexyl, and butyl). Those polymer's optical properties, electrochemical properties, thermal properties, and self-assembly behavior had been systematically studied. For 3T-TPD based CPs, outward series polymers show better π-π stacking than inward series polymers, leading to pack into LAM structure. However, inward series polymers with poor coplanarity of backbone pack into rarely found HEX structure. For side chain type effect, both the outward series polymers and inward series polymers with TEG chains show longer wavelength of λ_{max} of UV-Vis absorption and higher order of the nanostructure than the polymers with dodecyl chains. These results reveal that the more flexible TEG chain can enhance the self-assembly behavior of the polymers. For side chain length effect, the outward series polymers have higher order of LAM with longer side chain. On the contrary, shorter side chain is more suitable for inward series polymers to self-assemble into higher order of HEX.

To investigate oligo(ethylene glycol) (OEG) side chain effect in depth, we successfully synthesized a series of P3TI and P4TI polymers by varying amount and location of OEG side chain. Their optical properties, thermal properties, and

doi:10.6342/NTU201904150

morphologies are systematically studied. High crystallization capability of PnTI polymers is mainly contributed from the stable stacking of oligothiophene unit. For the polymers with all alkyl side chains, P3T(R_8)I($R_{b\text{-}16}$) and P4T(R_8)I($R_{b\text{-}16}$), they show the highest crystallinity but the largest $d_{\pi\text{-}\pi}$ among each series polymers. Their π-π stacking behavior is dominated by oligothiophene unit because the bulky alkyl side chains ($R_{b\text{-}16}$) on isoindigo unit prohibit close packing of isoindigo unit. As the bulky $R_{b\text{-}16}$ side chains on isoindigo unit are replaced by linear and flexible OEG side chains, i.e. P3T(R_8)I(E), P3T(E)I(E), P4T(R_8)I(E), and P4T(E)I(E), their π-π stacking behavior is dominated by isoindigo unit because isoindigo unit with small size of OEG side chains can stack more closely than oligothiophene unit, resulting in a sacrifice for stable stacking of oligothiophene unit. Therefore, even though they show relatively short $d_{\pi\text{-}\pi}$, their crystallinity is relatively low. In addition, OEG side chains are capable of controlling the packing orientation of the polymers by adjusting the crystallinity of the polymers. For instance, OEG side chains change the packing orientation of P3TI polymers from slightly edge-on orientation of P3T(R_8)I($R_{b\text{-}16}$) to fully face-on orientation of P3T(R_8)I(E) and P3T(E)I(E) which is suitable for polymer solar cell application.

Our studies not only provide a strategy to design a D-A conjugated polymer with highly ordered nanostructure but also give a guide to control the polymer packing

doi:10.6342/NTU201904150

orientation for potential application in optoelectronic devices or sensors.

doi:10.6342/NTU201904150

Chapter 4 Recommendations

(1) Introduce fluoroalkyl side chain into the polymers with OEG side chains

Our studies have proved that OEG can improve the self-assembly behavior and control the packing orientation of polymers. However, the polymers with OEG side chains show relative low thermal stability. Besides, OEG side chains are hydrophilic, which let the polymers absorb lots of moisture. Considering that optoelectronic devices should be used under tough condition, high temperature and high humidity, the devices of the polymers with OEG side chains cannot be used for a long time. In order to enhance the thermal stability and hydrophobicity of the polymers with OEG side chains, we can introduce fluoroalkyl side chains into the polymers. Therefore, we designed a series of oligothiophene-TPD based polymers and oligothiophene-isoindigo based polymers containing fluoroalkyl side chains and OEG side chains as shown in **Figure 4.1** and **Figure 4.2**. The synthesis and characterization of these new series polymers should be carried out to observe the effect of fluoroalkyl side chain on the physical properties and morphologies of polymers.

doi:10.6342/NTU201904150

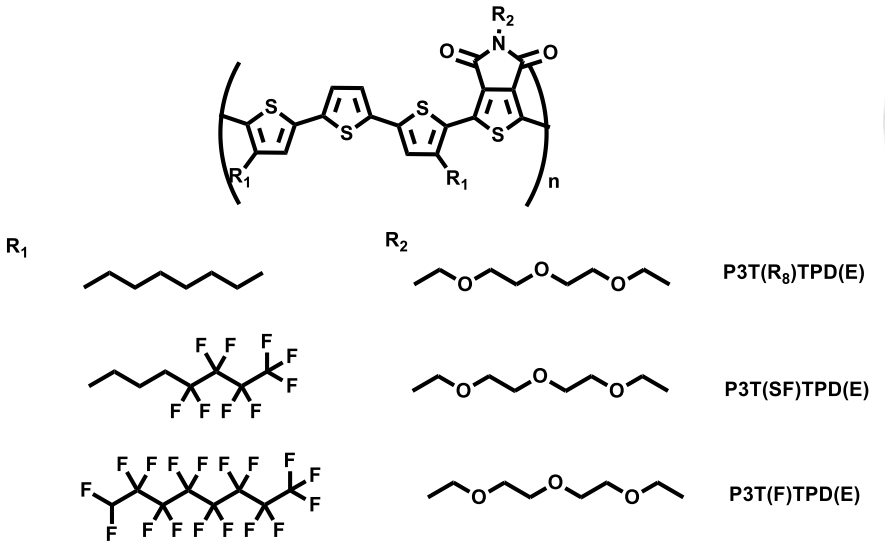

Figure 4.1. Chemical structure of oligothiophene-TPD based polymers

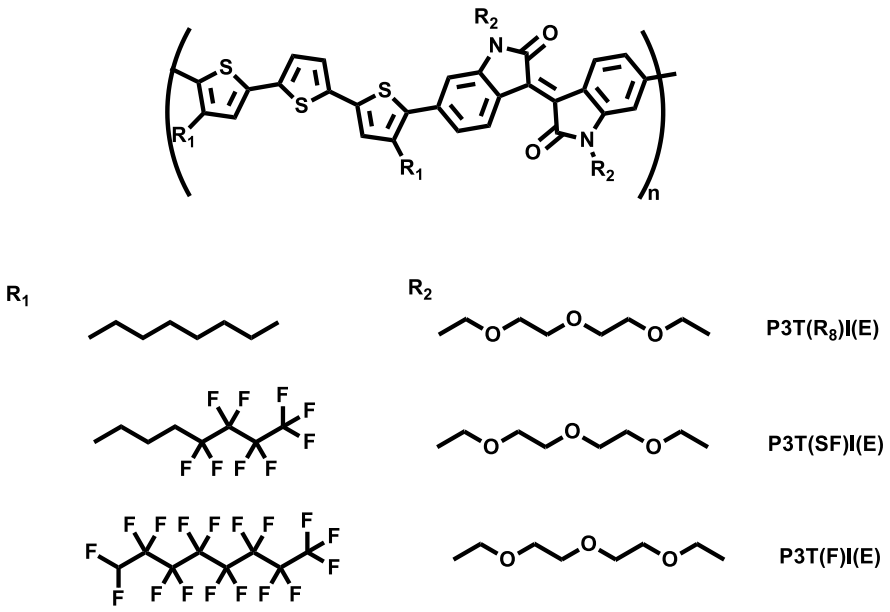

Figure 4.2. Chemical structure of oligothiophene-isoindigo based polymers

(2) Add salt into the polymers with OEG side chains

Hayward et al. had successfully synthesized a kind of diblock copolymer, P3HT-b-P3TEGT, as shown in **Figure 4.3**[115]. This polymer contains nonpolar

doi:10.6342/NTU201904150

(hexyl) and polar (TEG) side chains. After adding salt, potassium iodide, into the polymer, the polymer and the salt self-assemble into superhelical structure via strong interaction between OEG and potassium ion as shown in **Figure 4.3**. This wonderful work inspired us to study the variation of morphologies of D-A CPs containing OEG side chains after adding salt.

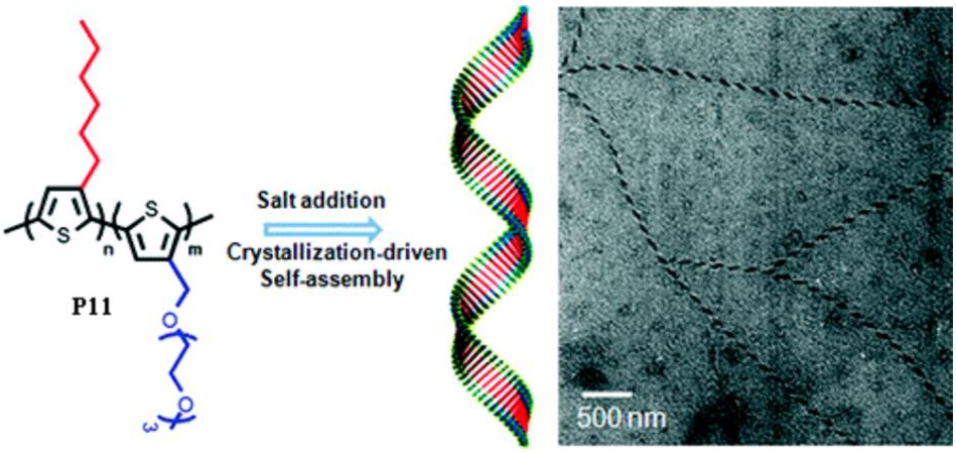

Figure 4.3. Schematic diagram to illustrate how the P3HT-b-P3TEGT and salt (KI) self-assemble into superhelical structure.

(3) Fabricate highly-aligned hexagonal-cylinder array of P3T(R_{in})TPD(R,E)

It is interesting to find that P3T(R_{in})TPD(R,E) polymers pack into special hexagonal-cylinder nanostrure, but these cylinders are in anisotropic alignment. Therefore, we would like to fabricate higly-aligned hexagonal-cylinder array. Yager et al. had susccefully used Soft-Shear Laser Zone Annealing (SS-LZA) technique to fabricate highly-aligned hexagonal array of block copolymer as shown in **Figure**

doi:10.6342/NTU201904150

4.4[116]. Therefore, we could use similar pathway-engineering to fabricate highly-aligned hexagonal of P3T(R_{in})TPD(R,E) polymers. Hence, this kind of study will be very valuable, because highly-aligned hexagonal array of D-A CPs can be a nanopattern with an interval of <5nm between two cylinders and may have outstanding device performance due to highly-aligned cylinders.

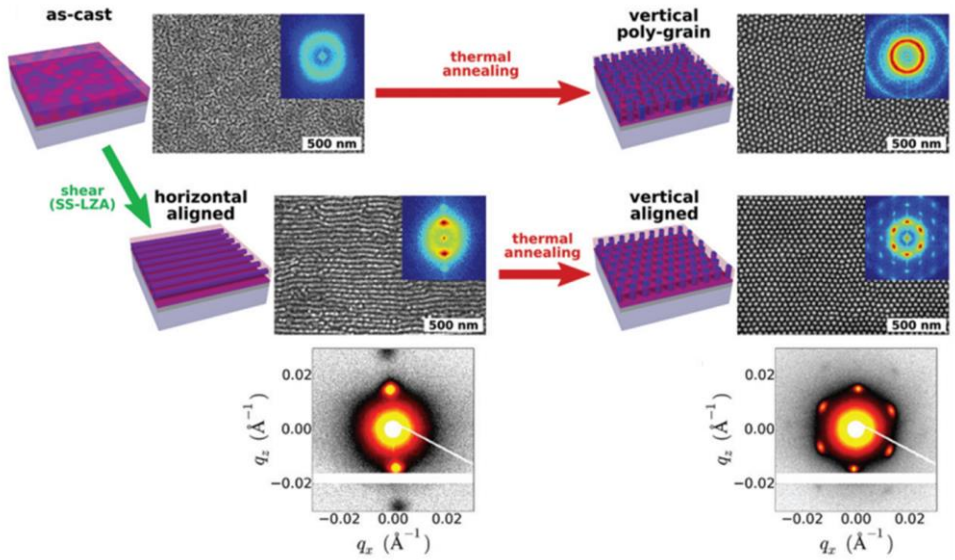

Figure 4.4 Schematic diagram to illustrate how to fabricate highly-aligned hexagonal-cylinder array of block copolymers

(4) Fabricate optoelectronic devices

We can use two series polymers, P3TTPDs and PnTIs, to fabricate optoelectronic devices and systematically study the relationship between their physical properties and device performance. Then we can prove that OEG improves device performance.

doi:10.6342/NTU201904150

Chapter 5 Experimental Section

5.1 Chemical and Instrument

Table 5.1 lists the chemicals that were used in this dissertation. They were used as received without further purifications. **Table 5.2** lists the instruments in this dissertation.

Table 5.1. List of chemicals

Chemicals	Purity	Supplier
acetic acid	>99%	Fisher Scientific
acetic anhydride	99%	ACROS ORGANICS
acetone	>99.5%	MACRON FINE CHEMICALS
acetonitrile	99%	ACROS ORGANICS
anhydrous magnesium sulfate	97%	ACROS ORGANICS
[1,3-Bis(diphenylphosphino)propane]dichloronickel(II)	99%	ACROS ORGANICS
2,5-bis(trimethylstannyl)thiophene	97%	ALDRICH Materials Science
2,2'-bithiophene	97%	Matrix SCIENTIFIC
1-bromo-2,5-pyrrolidinedione	99%	ACROS ORGANICS
1-bromobutane	99%	ACROS ORGANICS
1-bromododecane	98%	ACROS ORGANICS

doi:10.6342/NTU201904150

Chemicals	Purity	Supplier
1-bromohexane	99%	ACROS ORGANICS
6-bromoisatin	97%	Matrix Scientific
1-bromooctane	99%	ACROS ORGANICS
6-bromooxindole	97%	Matrix Scientific
3-bromothiophene	97%	Matrix Scientific
celite	-	ACROS ORGANICS
chloroform	99.5%	MACRON Fine Chemicals
D-acetone	>99%	ACROS ORGANICS
D-chloroform	99.8%	Merck Millipore
D-dimethyl sulfoxide	>99%	ACROS ORGANICS
dichloromethane	99.5%	MACRON Fine Chemicals
dimethylformamide	99.8%	ACROS ORGANICS
ether	>99%	J.T.Baker
2-(2-(2-ethoxyethoxy)ethoxy)ethanol	95%	Aldrich Materials Science
ethyl acetate	>99.5%	MACRON Fine Chemicals
ferrocene	98%	ACROS ORGANICS
hexane	99%	MACRON Fine Chemicals
2-hexyl-1-decanol	97%	Aldrich Materials Science

doi:10.6342/NTU201904150

Chemicals	Purity	Supplier
hydrazine hydrate (64 wt% in water)	-	ACROS ORGANICS
hydrochloric acid	-	Scharlau
hydrogen bromide (48 wt% in water)	-	ACROS ORGANICS
magnesium	99.9%	ACROS ORGANICS
methanol	>99.5%	MACRON FINE CHEMICALS
n-butyllithium(2.5M in hexane)	-	Rockwood Lithium
phosphorus tribromide	99%	ACROS ORGANICS
potassium 1,3-dioxoisoindolin-2-ide	99%	ACROS ORGANICS
potassium hydroxide	>87%	Fisher Scientific
silica gel	-	SILICYCLE
sodium	99%	ACROS ORGANICS
sodium bicarbonate	> 99%	ACROS ORGANICS
sodium hydride (60 wt% in mineral oil)	-	ACROS ORGANICS
sulfuric acid	-	Fisher Scientific
tetrabromomethane	99%	ACROS ORGANICS
tetrabutylammonium perchlorate	99%	ACROS ORGANICS
tetrahydrofuran	>99.5%	MACRON FINE CHEMICALS
thiophene	>99%	ACROS ORGANICS

doi:10.6342/NTU201904150

Chemicals	Purity	Supplier
thiophene-3,4-dicarboxylic acid	98%	Matrix Scientific
thiophene-3-ylmethanol	97%	Acros Organics
trifluoroacetic acid	99%	Acros Organics
trimethyltin chloride (1M in tetrahydrofuran)	-	Acros Organics
triphenylphosphine	99%	Alfa Aesar
tris(dibenzylideneacetone)dipalladium(0)	97%	Acros Organics
tris(*o*-tolyl)phosphine	99%	Acros Organics

Preparation of anhydrous solvents

Dichloromethane and dimethylformamide are dried over 4A molecular sieve overnight.

Ether and tetrahydrofurane are refluxed over sodium in the presence of benzophenone until the purple color appears from the formation of sodium-benzo complex.

doi:10.6342/NTU201904150

Table 5.2. List of instruments

Instruments (abbreviations)	Producer	Model	Location
atomic force microscopy (AFM)	BRUKER	AS-12VLR	NTUPhy[1] R300
cyclic voltammetry (CV)	[H]	CHI611E	NTUCB[2] R503
differential scanning calorimetry (DSC)	TA Instruments	Q200	NTUCE[3] R3
gel permeation chromatography (GPC)	Viscotek	GPCMax/ TDA305	NTUCB R503
glass oven (annealer)	BUCHI	B-585	NTUCB R503
grazing incident wide-angle x-ray scattering (GIWAXS)	--	Mar 345 Imaging Plate Area Detector	NSRRC[4] 17A1
microwave reactor	CEM	Benchmate	NTUCB R502
nuclear magnetic resonance (NMR)	BRUKER	DPX-400	NTUChem[5] A525
spin coater	Laurell Technologies Corporation	WS-400A	NTUPhy R215
thermogravimetric analysis (TGA)	TA Instruments	Q50	NTUCB R503
ultraviolet-visible absorption spectroscopy (UV-vis)	PerkinElmer	Lambda 35	NTUPhy R215

[1] Building No. 2, Department of Physics, National Taiwan University (NTU)

[2] Center of Biotechnology, NTU

[3] College of Engineering Building, NTU

[4] National Synchrotron Radiation Research Center

[5] Integrated Chemistry Building, Department of Chemistry, NTU

doi:10.6342/NTU201904150

5.2 Material Preparation

This section includes the synthesis schemes, procedures of intermediates, monomers, and polymers. ^{1}H NMR profiles for all intermediates and monomers.

5.2.1 Oligothiophene-TPD based Conjugated Polymers

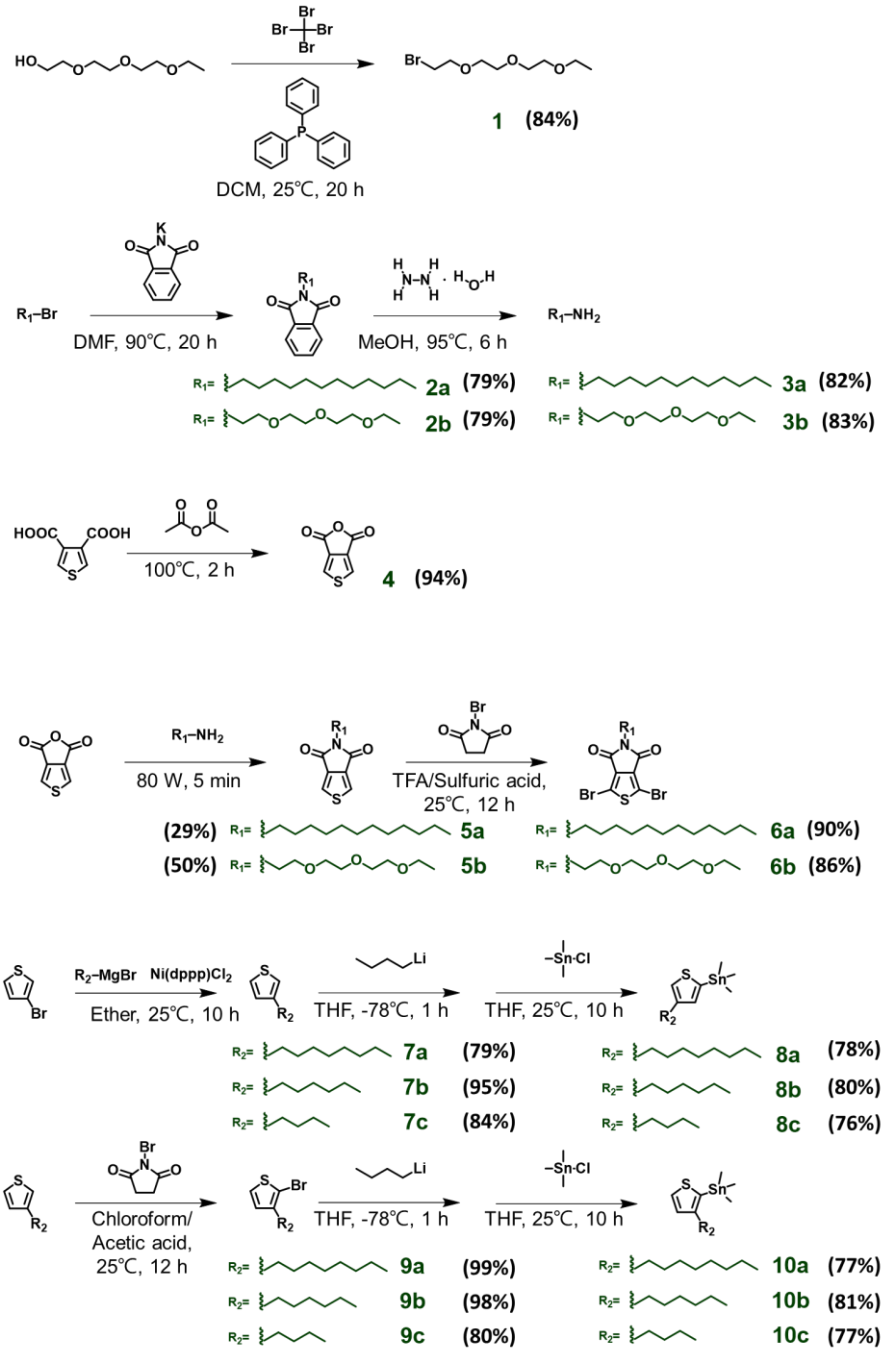

Figure 5.1. Synthetic scheme of compound 1~compound 10

doi:10.6342/NTU201904150

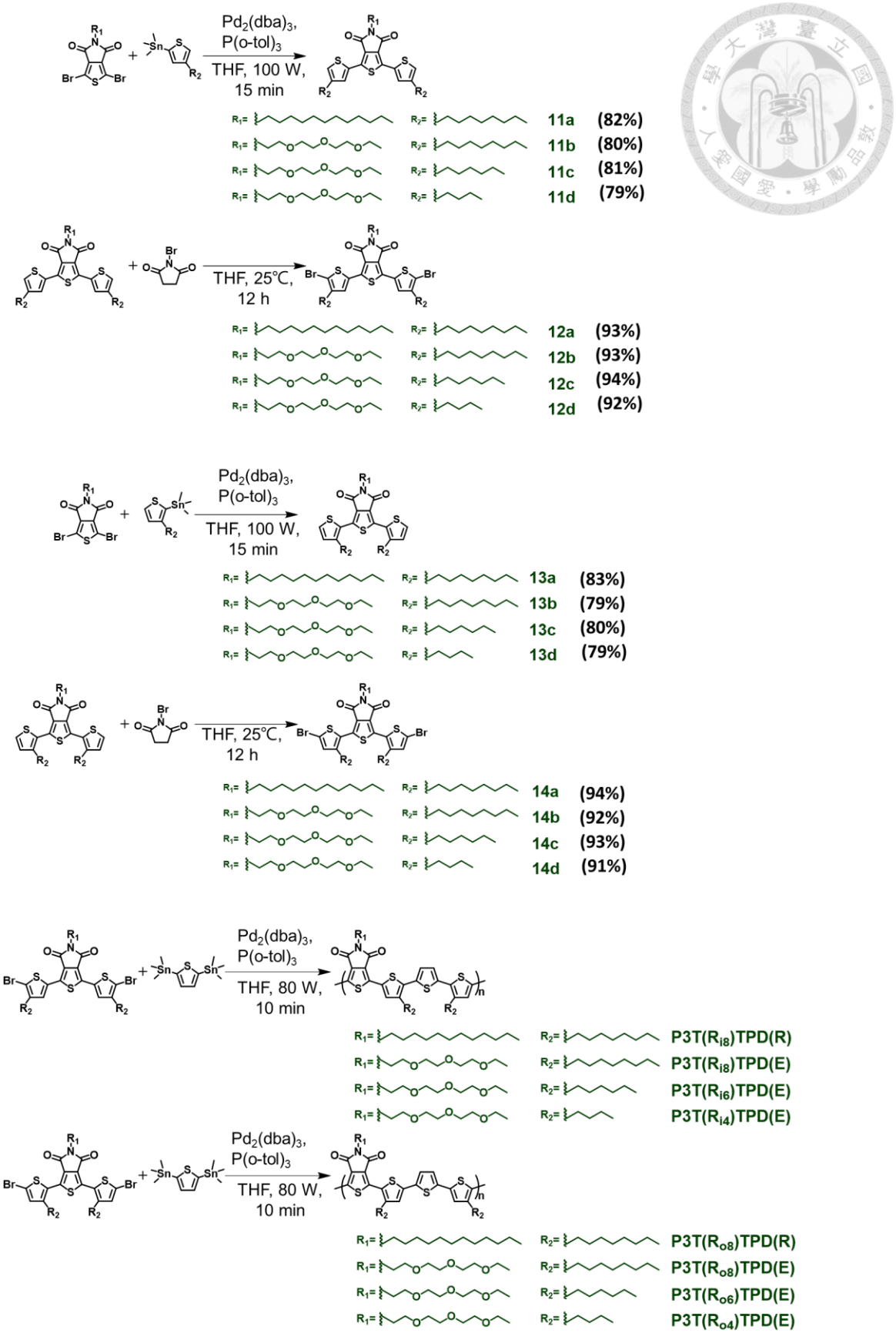

Figure 5.2. Synthetic scheme of compound 11~compound 14 and P3TTPD polymers

doi:10.6342/NTU201904150

Synthesis of compound 1

1, 1-bromo-2-(2-(2-ethoxyethoxy)ethoxy)ethane

2-(2-(2-ethoxyethoxy)ethoxy)ethanol (10.00 g, 56.11 mmole) and tetrabromomethane (24.19 g, 72.94 mmole) were placed in a 500 ml round bottom flask (flask A) and triphenylphosphine (17.66 g, 67.33 mmole) was placed in a 250 ml round bottom flask (flask B). The two flasks were evacuated by vacuum for few minutes and refilled them with nitrogen. Then 100 ml and 200 ml of anhydrous dichloromethane were added into the flask A and B, respectively. The flask A was put in a 0 ^{o}C ice bath and the flask B solution was transferred to flask A slowly. The mixture was stirred at room temperature for 20 hours and then the dichloromethane was removed by rotary evaporator. Then 300 ml of ether was added into the flask and the solution was filtered by filter paper. The filtrate was collected and the ether was removed by rotary evaporator. Finally, the condensed mixture was further purified by distillation under reduced pressure (100 ^{o}C, 0.08 torr) to obtain colorless oil, compound 1 (11.36 g, 84%). ^{1}H NMR (400 MHz, $CDCl_3$) δ 3.81 (t, *J* = 6.4 Hz, 2H), 3.70 – 3.63 (m, 6H), 3.59 (m, 2H), 3.52 (q, *J* = 7.0 Hz, 2H), 3.47 (t, *J* = 6.4 Hz, 2H), 1.21 (t, *J* = 7.0 Hz, 3H).

doi:10.6342/NTU201904150

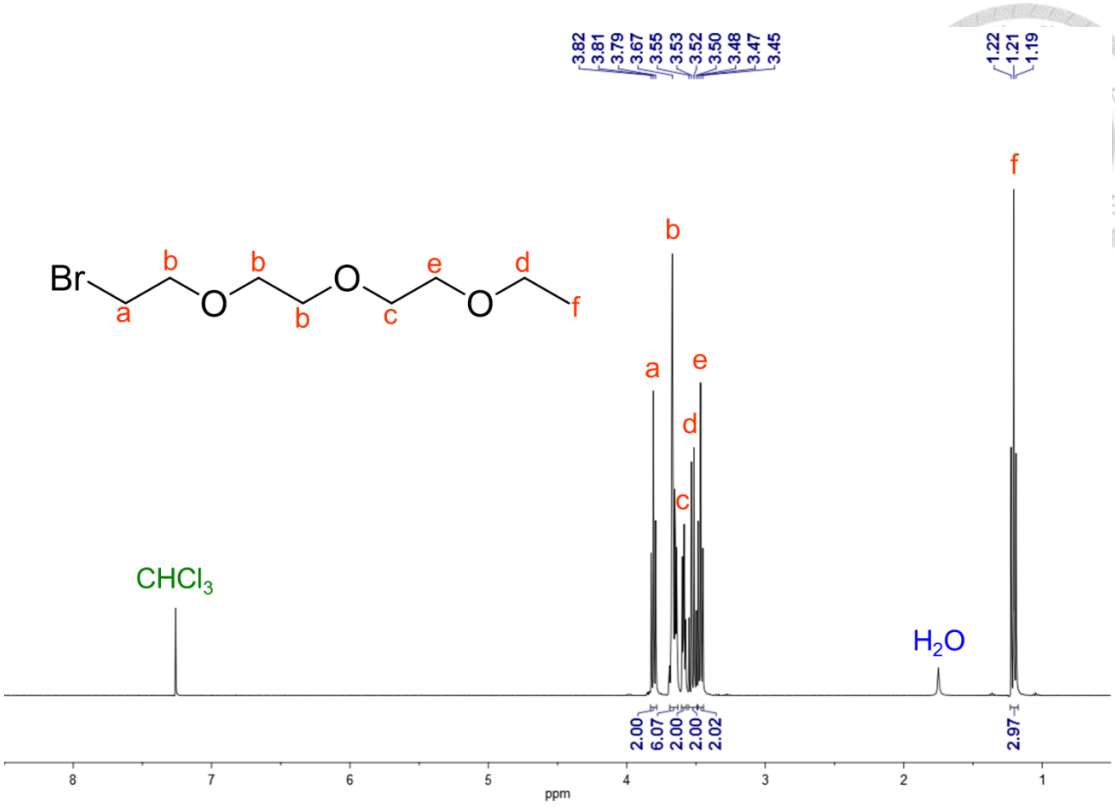

Figure 5.3. ^{1}H NMR of compound 1

Synthesis of compound 2a

2-dodecylisoindoline-1,3-dione

Potassium 1,3-dioxoisoindolin-2-ide (8.17 g, 44.13 mmole) was placed in a 500 ml round bottom flask (flask A) and 1-bromododecane (10.00 g, 40.12 mmole) was placed in a 250 ml round bottom flask (flask B). The two flasks were evacuated by vacuum for few minutes and refilled them with nitrogen. Then, 200 ml of dimethylformamide was added into the flask B and the solution was transferred into the flask A slowly. The solution was heated to 90 ^{o}C through oil bath and stirred for 20 hours. The mixture was extracted by using dichloromethane and distilled water and

doi:10.6342/NTU201904150

then the organic layer was collected, dried by anhydrous magnesium sulfate, and filtered by filter paper. The filtrate was collected and the dichloromethane was removed by rotary evaporator. The condensed mixture was further purified by column chromatography (dichloromethane as eluent, silica gel) to obtain white solid, compound 2a (10.00 g, 79%). ^{1}H NMR (400 MHz, $CDCl_3$) δ 7.83 (dd, *J* = 5.4, 3.0 Hz, 2H), 7.70 (dd, *J* = 5.4, 3.0 Hz, 2H), 3.67 (t, *J* = 7.2 Hz, 2H), 1.70 – 1.62 (quintet, *J* = 5.4, 2H), 1.36 – 1.19 (m, 18H), 0.87 (t, *J* = 6.9 Hz, 3H).

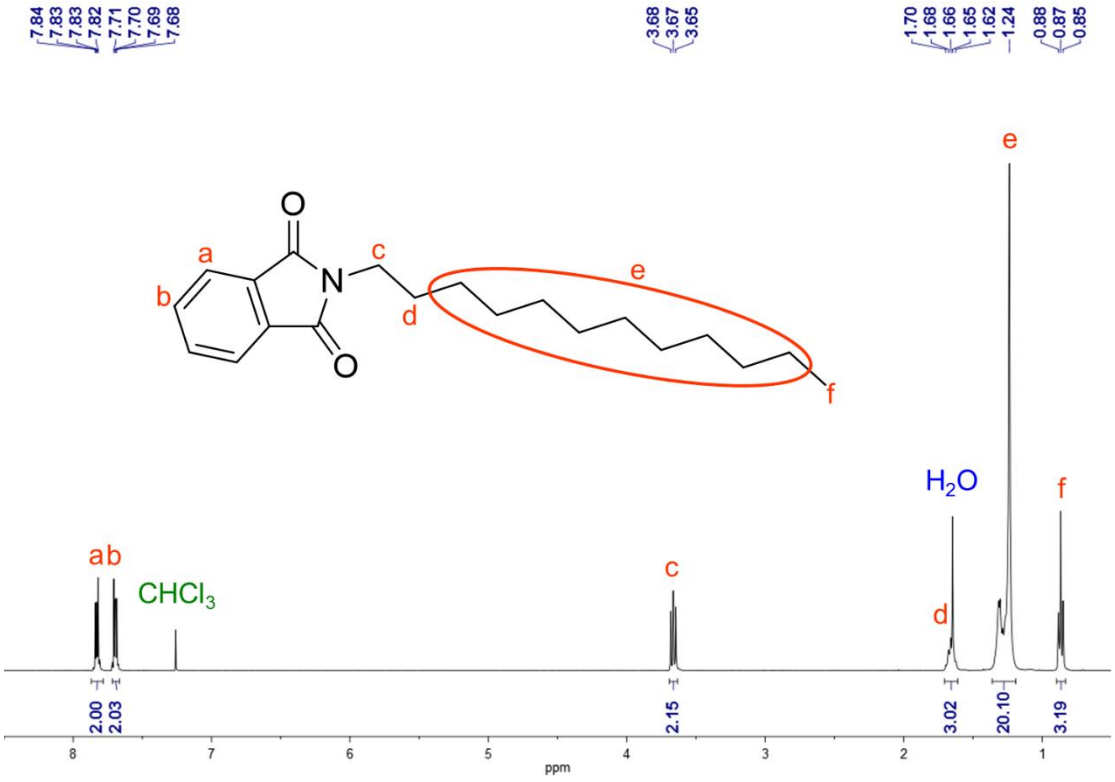

Figure 5.4. ^{1}H NMR of compound 2a

doi:10.6342/NTU201904150

Synthesis of compound 2b

2-(2-(2-(2-ethoxyethoxy)ethoxy)ethyl)isoindoline-1,3-dione

Potassium 1,3-dioxoisoindolin-2-ide (8.45 g, 45.62 mmole) was placed in a 500 ml round bottom flask (flask A) and compound 1 (10.00 g, 41.47 mmole) was placed in a 250 ml round bottom flask (flask B). Following the same synthetic procedure of compound 2a, one obtained pale yellow oil, compound 2b (10.07 g, 79%). ^{1}H NMR (400 MHz, $CDCl_3$) δ 7.83 (dd, *J* = 5.4, 3.1 Hz, 2H), 7.70 (dd, *J* = 5.4, 3.1 Hz, 2H), 3.89 (t, *J* = 5.8 Hz, 2H), 3.73 (t, *J* = 5.8 Hz, 2H), 3.66 – 3.55 (m, 6H), 3.53 – 3.44 (m, 4H), 1.17 (t, *J* = 7.0 Hz, 3H).

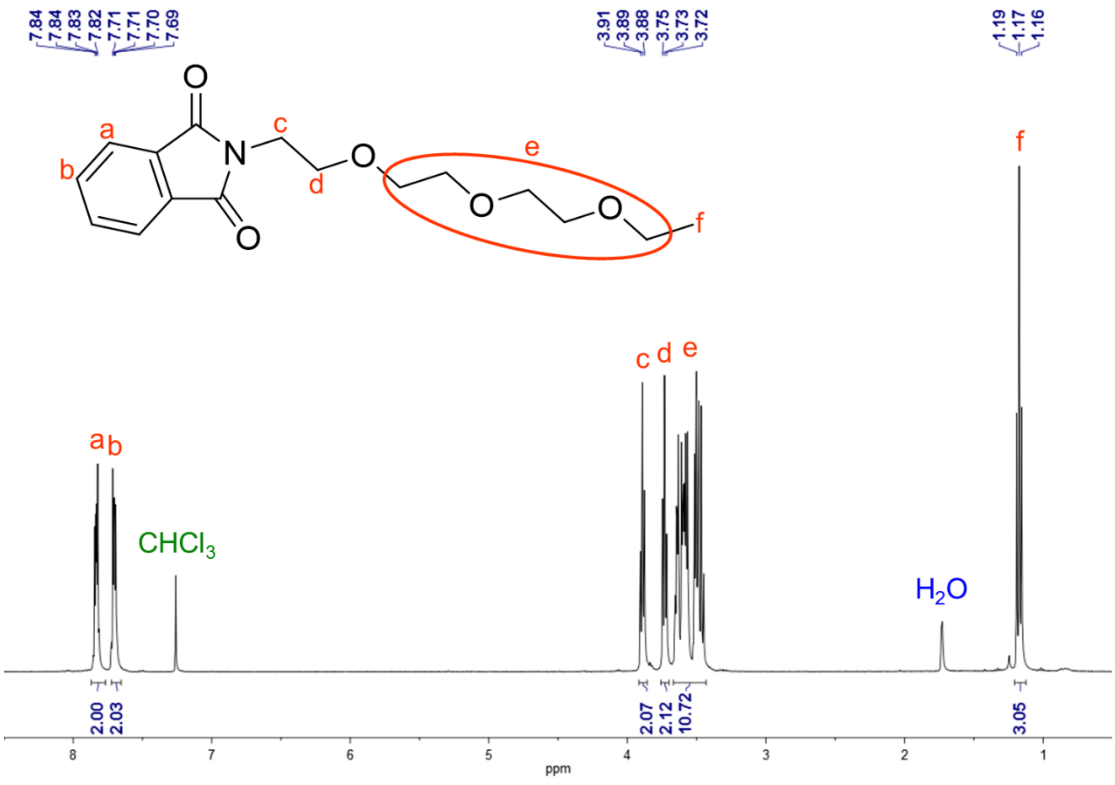

Figure 5.5. ^{1}H NMR of compound 2b

doi:10.6342/NTU201904150

Synthesis of compound 3a

dodecan-1-amine

Compound 2a (10 g, 31.70 mmole) and 400 ml methanol was placed in a 500 ml round bottom flask and then hydrazine hydrate (64 wt% in distilled water, 3.08 ml, 87.84 mmole) was added into the flask through syringe. The mixture was heated to 95 ^{o}C through oil bath and stirred for 6 hours. The methanol was removed by rotary evaporator and the condensed mixture was extracted by using dichloromethane and 10 wt% potassium hydroxide aqueous solution. The organic layer was collected, dried over anhydrous magnesium sulfate, and filtered by filter paper. The filtrate was collected and the dichloromethane was removed by rotary evaporator to obtain pale yellow oil, compound 3a (4.82 g, 82%) without further purification. ^{1}H NMR (400 MHz, $CDCl_3$) δ 2.67 (t, *J* = 7.0 Hz, 2H), 1.48 – 1.38 (m, 4H), 1.33 – 1.20 (m, 18H), 0.87 (t, *J* = 6.8 Hz, 3H).

doi:10.6342/NTU201904150

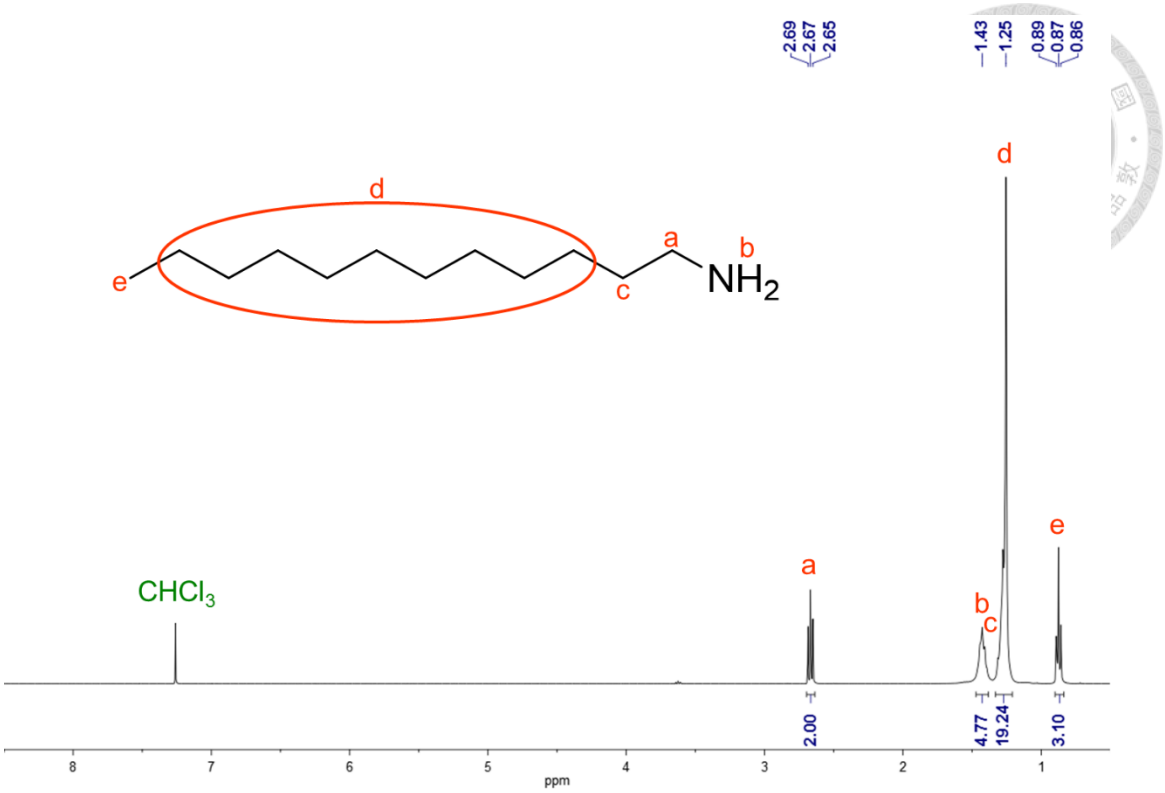

Figure 5.6. ^{1}H NMR of compound 3a

Synthesis of compound 3b

2-(2-(2-ethoxyethoxy)ethoxy)ethanamine

Compound 2b (9.74 g, 31.70 mmole) and 400 ml methanol was placed in a 500 ml round bottom flask and then hydrazine hydrate (64 wt% in distilled water, 3.08 ml, 87.84 mmole) was added into the flask through syringe. Following the synthetic procedure of compound 3a, one obtained pale yellow oil, compound 3b (4.79 g, 83%). ^{1}H NMR (400 MHz, $CDCl_3$) δ 3.69 – 3.46 (m, 12H), 2.86 (t, *J* = 5.2 Hz, 2H), 1.29 (s, 2H), 1.21 (t, *J* = 7.0 Hz, 3H).

doi:10.6342/NTU201904150

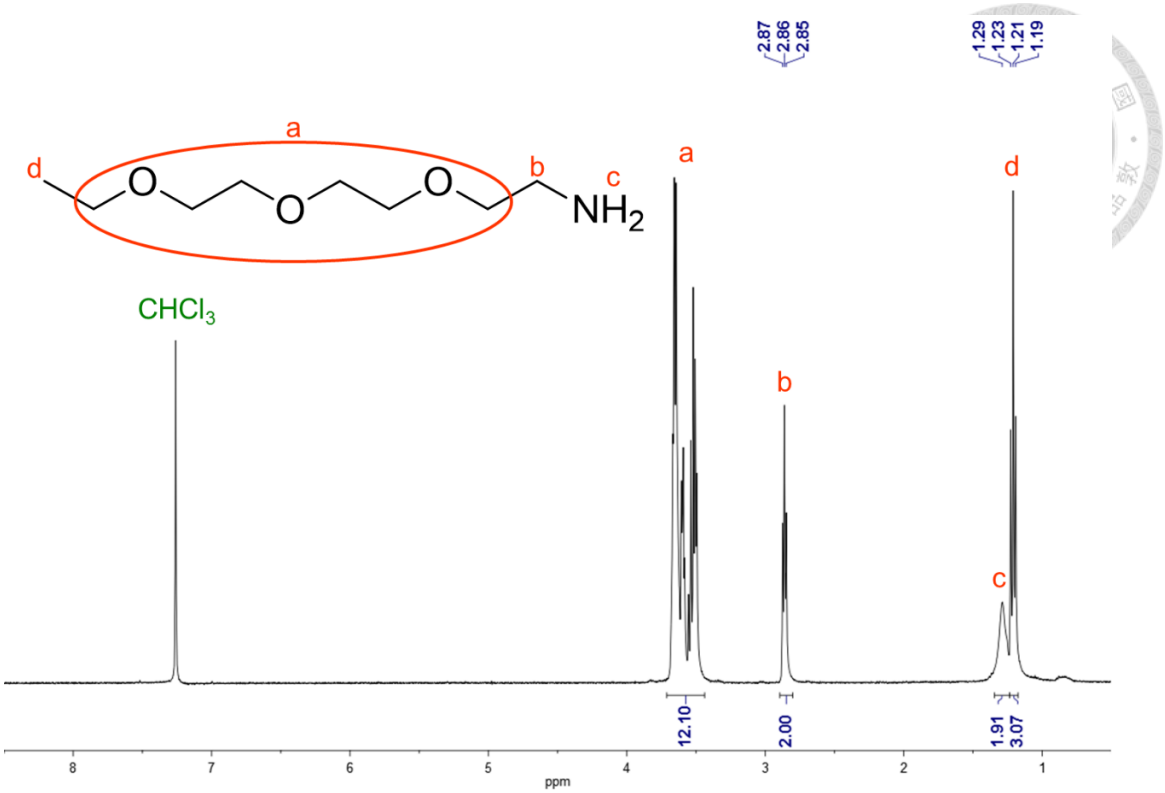

Figure 5.7. ^{1}H NMR of compound 3b

Synthesis of compound 4

Thieno[3,4-c]furan-1,3-dione

Thiophene-3,4-dicarboxylic acid (10.00 g, 58.10 mmole) and acetic anhydride (40 ml) were placed in a 250 ml round bottom flask, heated to 100 ^{o}C, and the mixture were stirred for 2 hours. Then, the acetic anhydride was removed by distillation under reduced pressure (60 ^{o}C, 0.08 torr). The mixture was recrystallized by using tetrahydrofuran (THF) and hexane (THF: hexane=1: 10) three times to obtain brown needle solid, compound 4 (4.79 g, 94%). ^{1}H NMR (400 MHz, $CDCl_3$) δ 8.09 (s, 2H).

doi:10.6342/NTU201904150

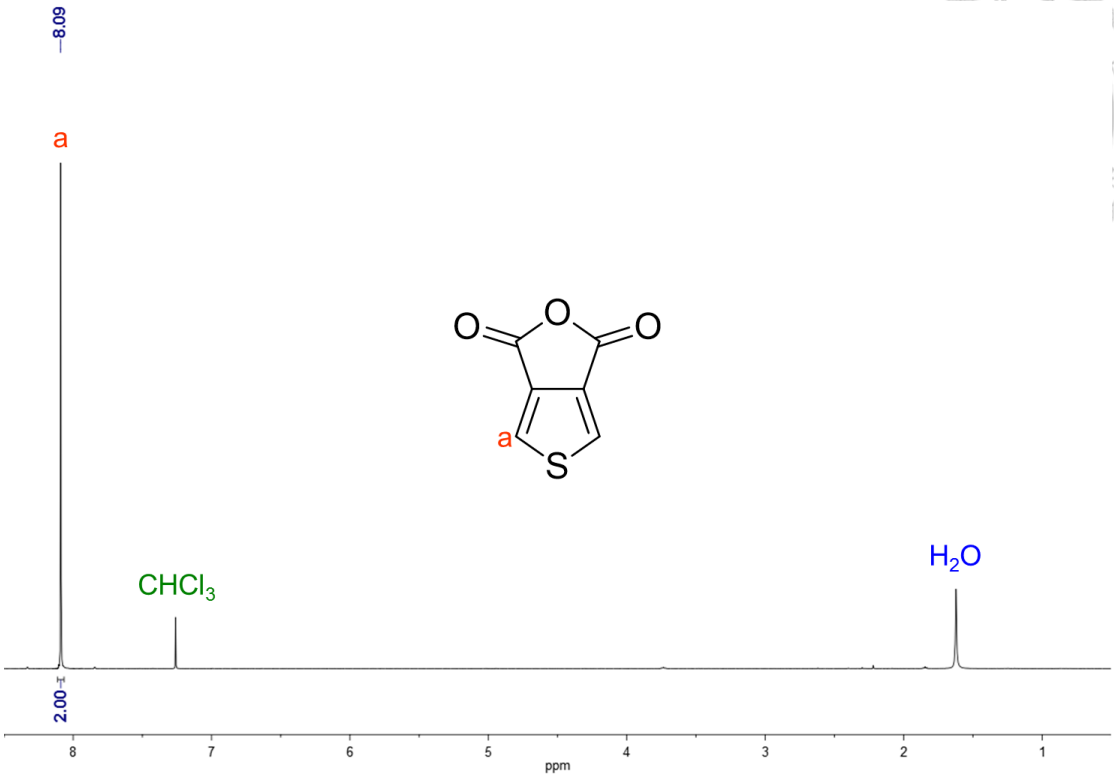

Figure 5.8. ^{1}H NMR of compound 4

Synthesis of compound 5a

5-dodecyl-4H-thieno[3,4-c]pyrrole-4,6(5H)-dione

Compound 4 (1.00 g, 5.81 mmole) and compound 3a (1.08g, 5.81 mmole) were placed in a 10ml microwave vessel then the vessel was put in the microwave reactor (CEM Benchmate), and parameters for the reaction were set at 150 ^{o}C, 80 W, and 5 min. Then, the mixture was purified through column chromatography (ether as eluent, silica gel) to obtain pale yellow oil, compound 5a (0.60 g, 29%). ^{1}H NMR (400 MHz, $CDCl_3$) δ 7.80 (s, 2H), 3.60 (t, *J* = 7.4 Hz, 2H), 1.61 (quintet, *J* = 7.2 Hz, 2H), 1.35 – 1.20 (m, 18H), 0.87 (t, *J* = 6.8 Hz, 3H).

doi:10.6342/NTU201904150

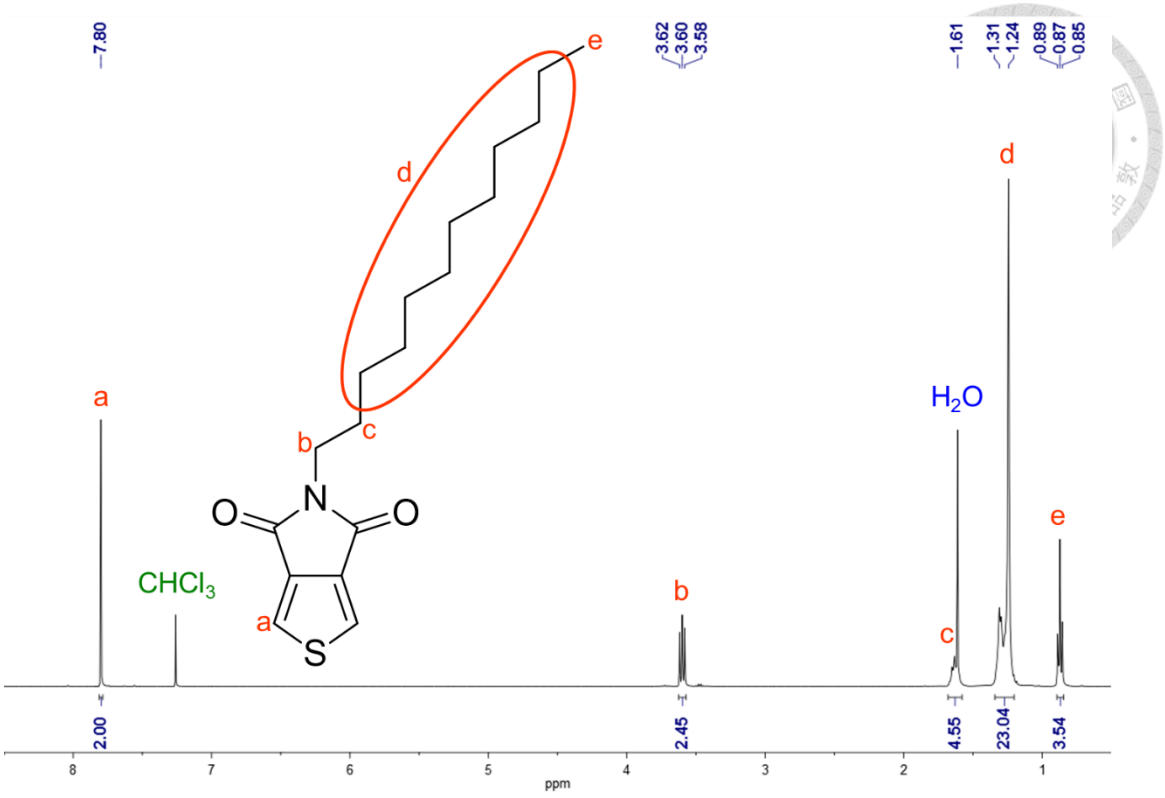

Figure 5.9. ^{1}H NMR of compound 5a

Synthesis of compound 5b

5-(2-(2-(2-ethoxyethoxy)ethoxy)ethyl)-4H-thieno[3,4-c]pyrrole-4,6(5H)- dione

Compound 4 (1.00 g, 5.81 mmole) and compound 3b (1.03g, 5.81 mmole) were placed in a 10ml microwave vessel then the vessel was put in the microwave reactor (CEM Benchmate), and parameters for the reaction were set at 150 ^{o}C, 80 W, and 5 min. Then, the mixture was purified through column chromatography (ether as eluent, silica gel) to obtain pale yellow oil, compound 5b (1.02 g, 50%). ^{1}H NMR (400 MHz, $CDCl_3$) δ 7.81 (s, 2H), 3.83 (t, *J* = 5.8 Hz, 2H), 3.71 (t, *J* = 5.8 Hz, 2H), 3.66 – 3.63 (m, 2H), 3.62 – 3.58 (m, 4H), 3.55 – 3.46 (m, 4H), 1.19 (t, *J* = 7.0 Hz, 3H).

doi:10.6342/NTU201904150

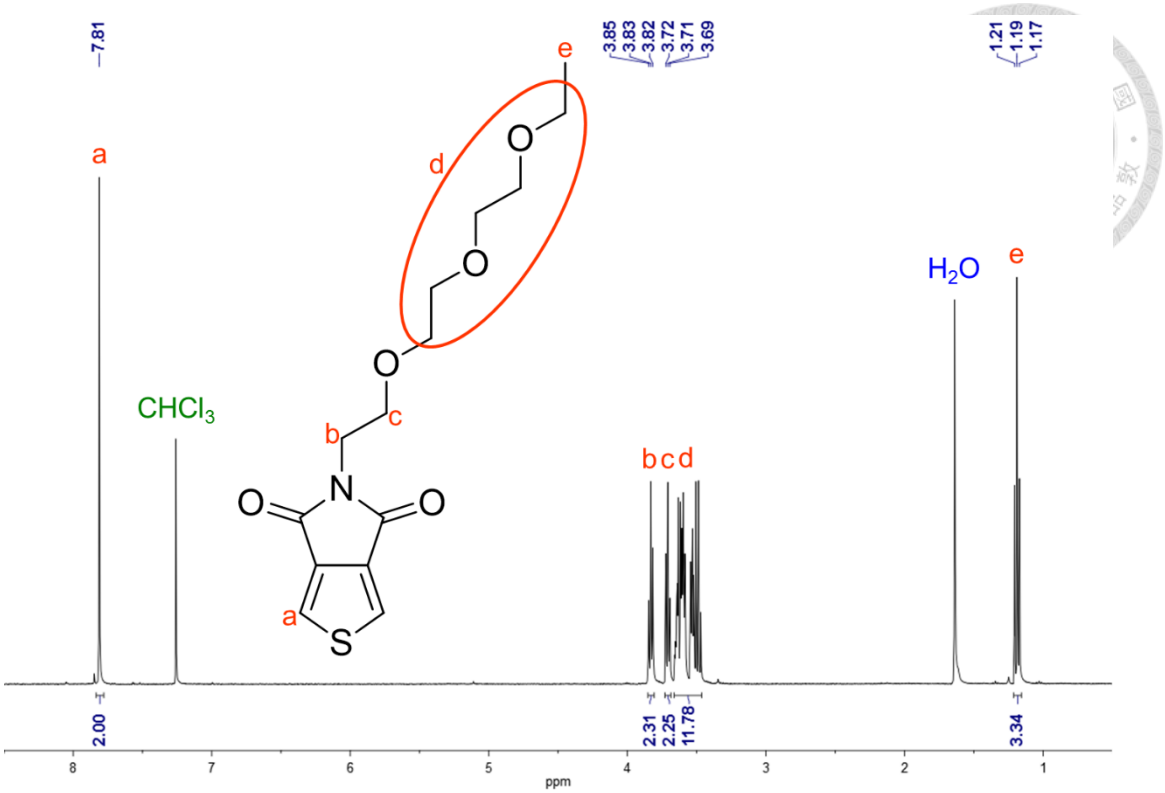

Figure 5.10. [1]H NMR of compound 5b

Synthesis of compound 6a

1,3-dibromo-5-dodecyl-4H-thieno[3,4-c]pyrrole-4,6(5H)-dione

Compound 5a (1.00 g, 3.11 mmole), 15 ml trifluoroacetic acid, 5 ml concentrated sulfuric acid were placed in a 50 ml round bottom flask, and then 1-bromo-2,5-pyrrolidinedione (1.38 g, 7.78 mmole) was added into the flask slowly in 2 hours. The mixture was stirred at room temperature for 12 hours and then extracted by ether and distilled water. The organic layer was collected, dried over anhydrous magnesium sulfate, and filtered by filter paper. The filtrate was collected and the ether was removed by rotary evaporator. The condensed mixture was further purified by

doi:10.6342/NTU201904150

column chromatography (ether as eluent, silica gel) to obtain white solid, compound 5a (1.34 g, 90%). ^{1}H NMR (400 MHz, $CDCl_3$) δ 3.59 (t, J = 7.2 Hz, 2H), 1.63 (quintet, J = 7.2 Hz, 2H), 1.34 – 1.20 (m , 18H), 0.88 (t, J = 6.9 Hz, 3H).

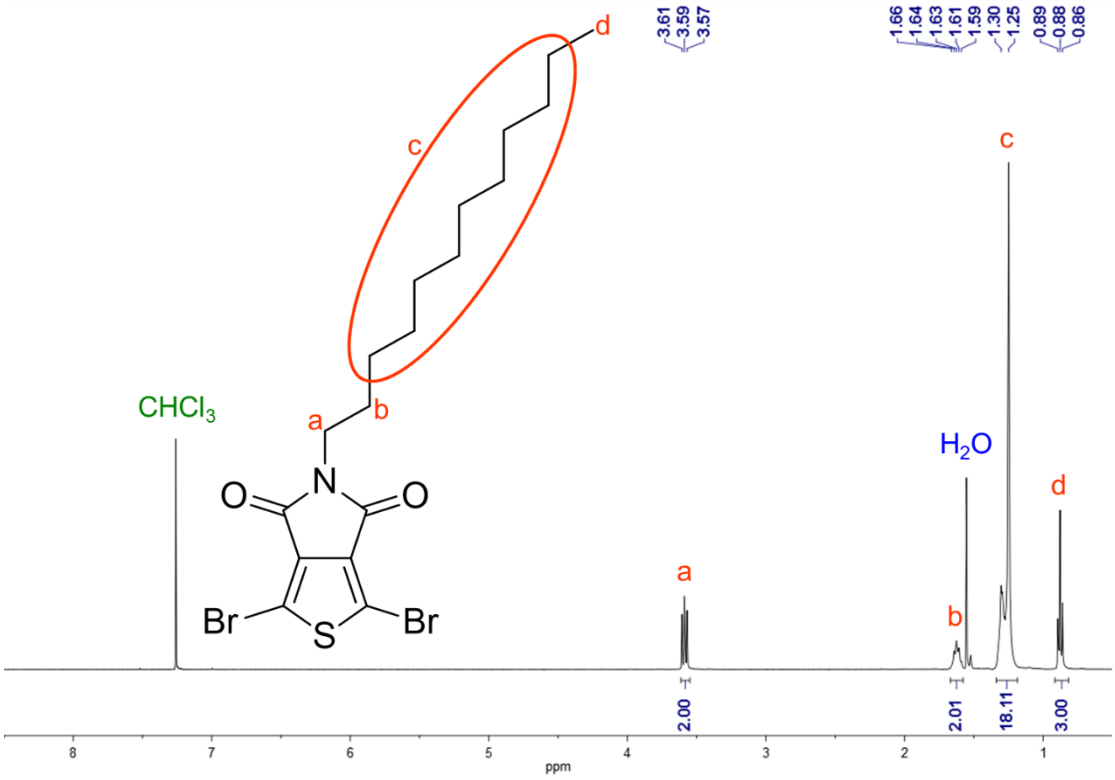

Figure 5.11. ^{1}H NMR of compound 6a

Synthesis of compound 6b

1,3-dibromo-5-(2-(2-(2-ethoxyethoxy)ethoxy)ethyl)-4H-thieno[3,4-c]pyrrole-4,6(5 H)-dione

Compound 5b (1.00 g, 3.19 mmole), 15 ml trifluoroacetic acid, and 5 ml concentrated sulfuric acid were placed in 50 ml round bottom flask, and then

doi:10.6342/NTU201904150

1-bromo-2,5-pyrrolidinedione (1.42 g, 7.98 mmole) was added into the flask slowly in 2 hours. Following the synthetic procedure of compound 6a, one obtained white solid, compound 6b (1.50 g, 86%). ^{1}H NMR (400 MHz, $CDCl_3$) δ 3.81 (t, *J* = 5.6 Hz, 2H), 3.70 (t, *J* = 5.7 Hz, 2H), 3.66 – 3.59 (m, 6H), 3.57 – 3.47 (m, 4H), 1.20 (t, *J* = 7.0 Hz, 3H).

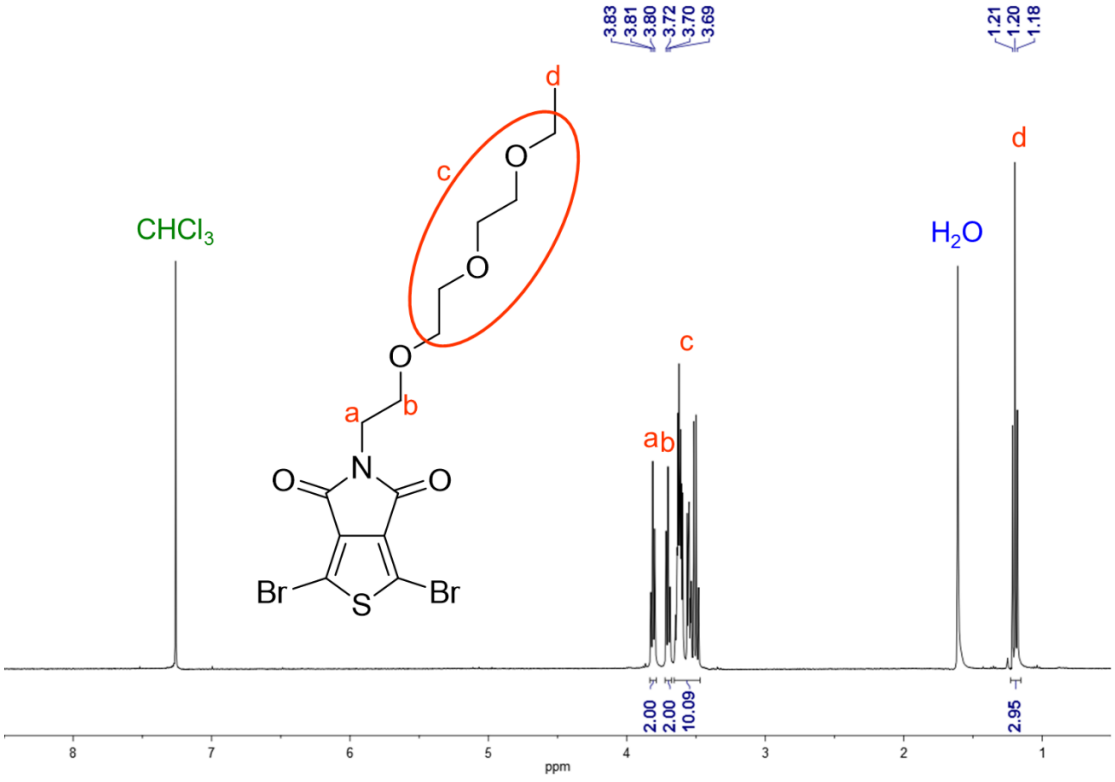

Figure 5.12. ^{1}H NMR of compound 6b

doi:10.6342/NTU201904150

Synthesis of compound 7a

3-octylthiophene

A 500 ml round bottom flask (flask A) and a 1000 ml round bottom flask (flask B) were evacuated by vacuum system and refilled the nitrogen to remove the moisture in the flask. Then, magnesium (8.95 g, 0.37 mole) and 300 ml anhydrous ether were placed in the flask A, and 3-bromothiophene (30.00 g, 0.18 mole), [1,3-Bis(diphenylphosphino)propane]dichloronickel(II) (200.00 mg, 0.37 mmole), and 300 ml anhydrous ether were placed in the flask B. Then the flask A was put in 0 ^{o}C ice bath and 1-bromooctane (53.30 g, 0.28 mole) was added into the flask A through syringe slowly in 2 hours. After complete adding 1-bromooctane, the mixture was stirred under room temperature for 2 hours. Then, the solution in the flask A was transferred in the flask B. After that, the mixture was stirred under room temperature for 10 hours. Then, 200 ml 1M hydrochloric acid was added into the flask B to terminate the reaction and the solution was extracted by using ether and distilled water. The organic layer was collected, dried over anhydrous magnesium sulfate, and filtered by filter paper. The filtrate was collected and the ether was removed by rotary evaporator. Finally, the condensed mixture can be further purified by distillation under reduced pressure (60 ^{o}C, 0.08 torr) to obtain colorless oil, compound 7a (28.54 g, 79%). ^{1}H NMR (400 MHz, $CDCl_3$) δ 7.23 (dd, *J* = 4.9, 2.9 Hz, 1H), 6.93 (dd, *J* =

doi:10.6342/NTU201904150

6.6, 3.9 Hz, 2H), 2.62 (t, *J* = 7.8 Hz, 2H), 1.68 – 1.57 (m, 2H), 1.35 – 1.22 (m, 10H), 0.88 (t, *J* = 6.8 Hz, 3H).

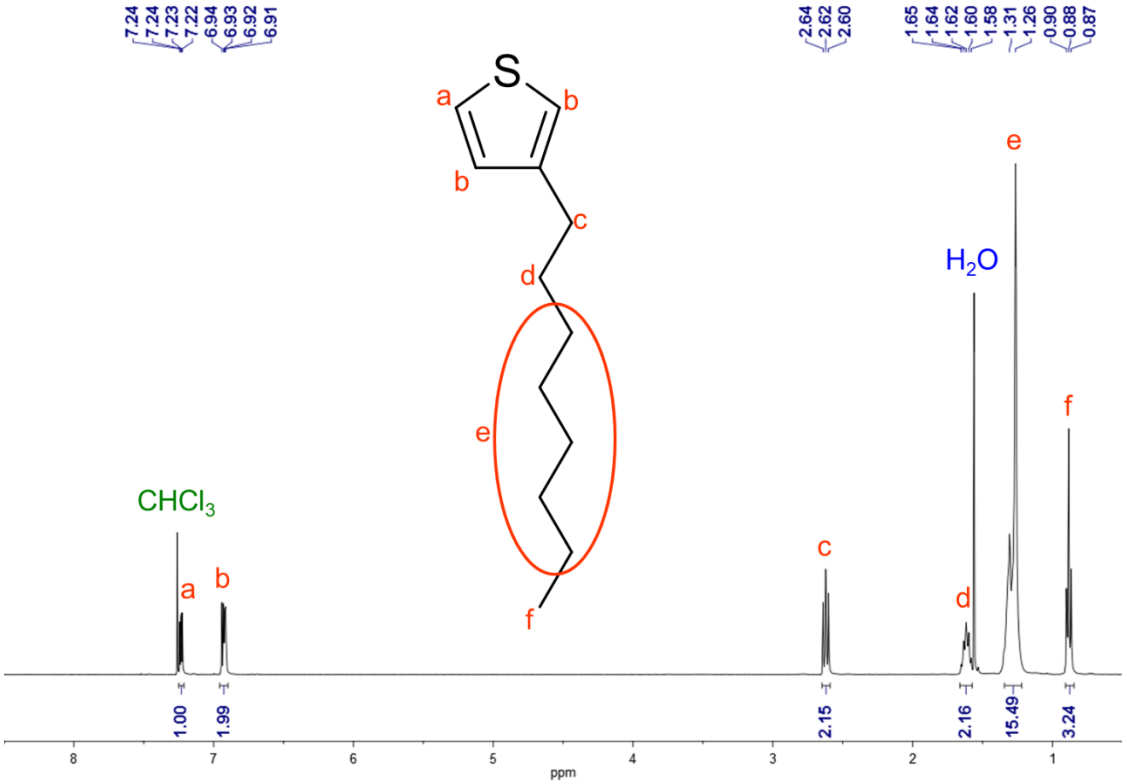

Figure 5.13. ^{1}H NMR of compound 7a

Synthesis of compound 7b

3-hexylthiophene

Magnesium (8.95 g, 0.37 mole), 3-bromothiophene (30.00 g, 0.18 mole), [1,3-Bis(diphenylphosphino)propane]dichloronickel(II) (200 mg, 0.37 mmole), and 1-bromohexane (45.55 g, 0.28 mole) were used to do the reaction. Following the synthetic procedure of compound 7a, one obtained colorless oil, compound 7b (29.42

doi:10.6342/NTU201904150

g, 95%). ^{1}H NMR (400 MHz, $CDCl_3$) δ 7.23 (dd, *J* = 4.9, 2.9 Hz, 1H), 6.93 (dd, *J* = 6.6, 3.9 Hz, 2H), 2.62 (t, *J* = 7.8 Hz, 2H), 1.68 – 1.57 (m, 2H), 1.35 – 1.22 (m, 6H), 0.88 (t, *J* = 6.8 Hz, 3H).

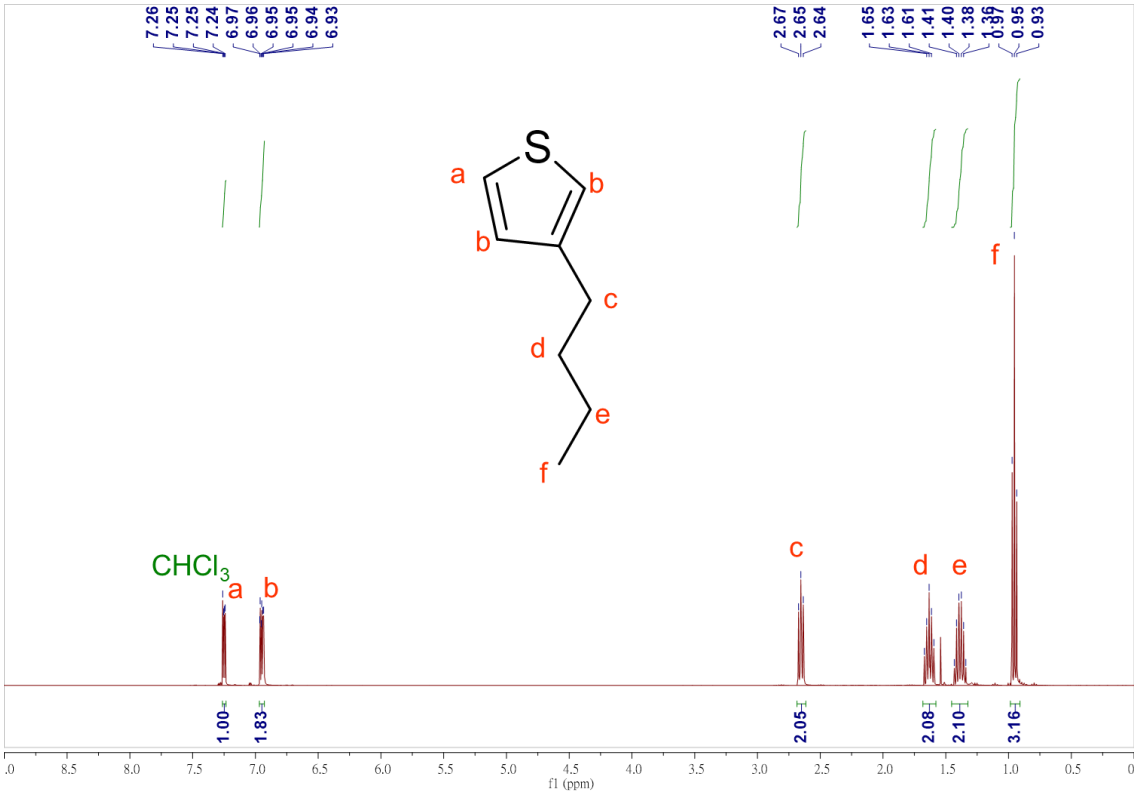

Figure 5.14. ^{1}H NMR of compound 7b

Synthesis of compound 7c

3-butylthiophene

Magnesium (8.95 g, 0.37 mole), 3-bromothiophene (30.00 g, 0.18 mole), [1,3-Bis(diphenylphosphino)propane]dichloronickel(II) (200 mg, 0.37 mmole), and 1-bromobutane (37.82 g, 0.28 mole) were used to do the reaction. Following the

doi:10.6342/NTU201904150

synthetic procedure of compound 7a, one obtained colorless oil, compound 7c (21.68 g, 84%). ^{1}H NMR (400 MHz, $CDCl_3$) δ 7.23 (dd, *J* = 4.9, 2.9 Hz, 1H), 6.93 (dd, *J* = 6.6, 3.9 Hz, 2H), 2.62 (t, *J* = 7.8 Hz, 2H), 1.68 – 1.57 (m, 2H), 1.35 – 1.22 (m, 2H), 0.88 (t, *J* = 6.8 Hz, 3H).

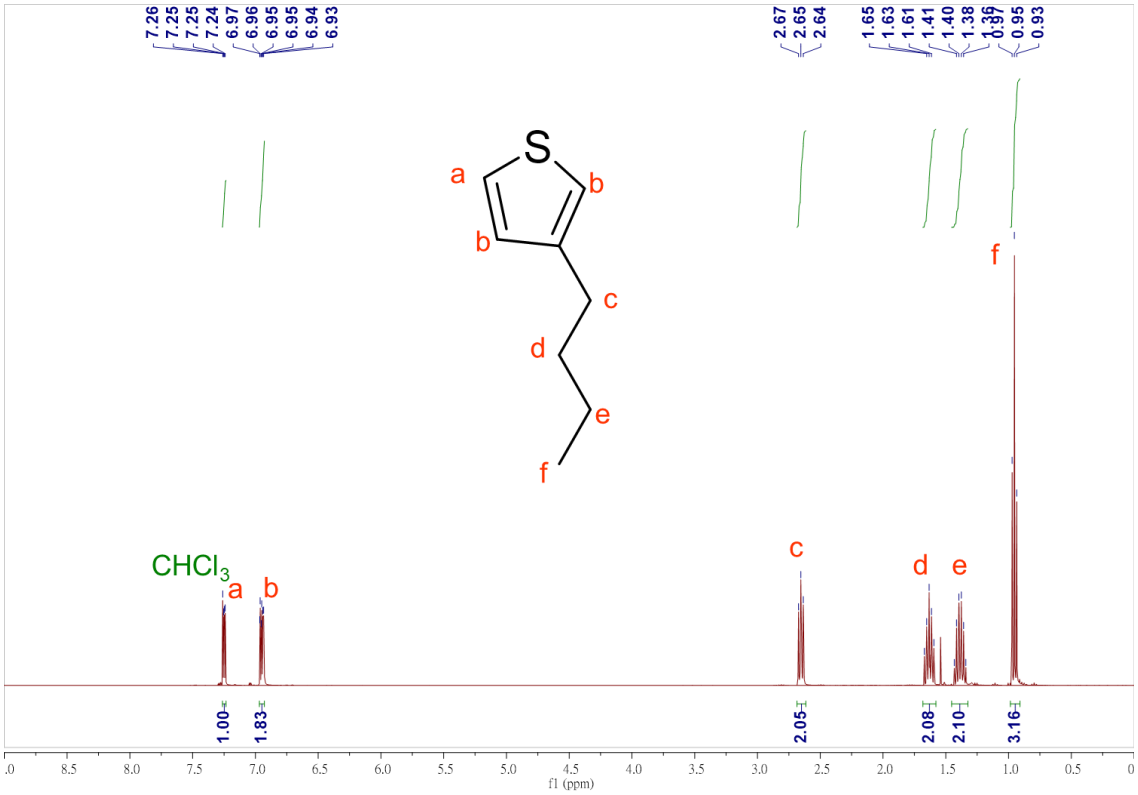

Figure 5.15. ^{1}H NMR of compound 7c

Synthesis of compound 8a

trimethyl(4-octylthiophene-2-yl)stannane

A 150 ml round bottom flask was evacuated by vacuum system and refilled the nitrogen to remove the moisture in the flask. Next, compound 7a (4.91 g, 25 mmole) and 50 ml anhydrous tetrahydrofuran were placed in the flask. After that, the flask

doi:10.6342/NTU201904150

was put in -78°C dry ice bath. Then, 10 ml 2.5M n-butyllithium in hexane solution (25 mmole) was added into the flask and the solution was stirred for 2 hours. The -78°C dry ice bath was removed and the solution was stirred at room temperature for 1 hour. Then the flask was put in -78°C dry ice bath again and 25 ml 1M trimethyltin chloride in tetrahydrofuran solution (25 mmole) was added into the flask. After complete adding the trimethyltin chloride solution, the -78°C dry ice bath was removed and the solution was stirred at room temperature for 12 hours. The mixture was extracted by hexane and distilled water. The organic layer was collected, dried over anhydrous magnesium sulfate, and filtered by filter paper. The filtrate was collected and the hexane was removed by rotary evaporator. Finally, the condensed mixture can be further purified by column chromatography (hexane as eluent, celite gel) to obtain pale yellow oil, compound 8a (7.03 g, 78%). ^{1}H NMR (400 MHz, $CDCl_3$) δ 7.19 (d, *J* = 0.8 Hz, 1H), 7.01 (s, 1H), 2.65 (t, *J* = 7.8 Hz, 2H), 1.63 (quintet, *J* = 7.5 Hz, 2H), 1.29 (d, *J* = 21.8 Hz, 10H), 0.88 (t, *J* = 6.8 Hz, 3H), 0.35 (s, 9H).

doi:10.6342/NTU201904150

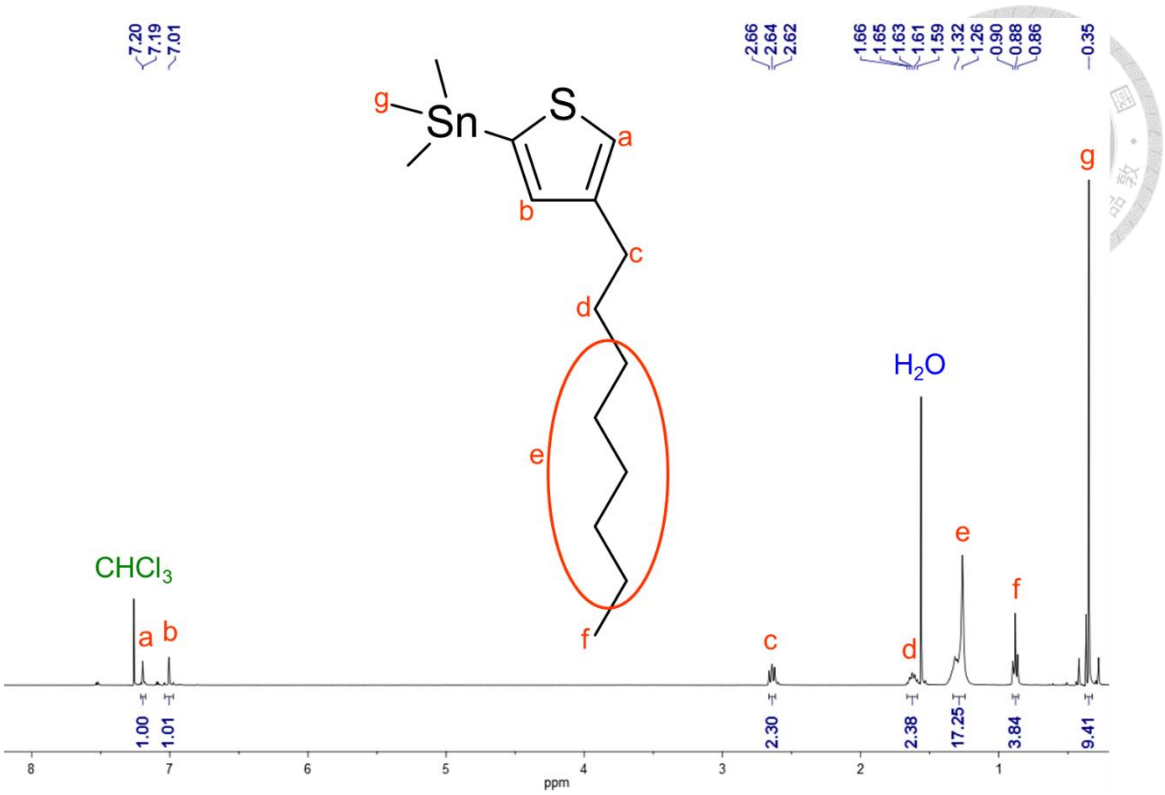

Figure 5.16. ^{1}H NMR of compound 8a

Synthesis of compound 8b

(4-hexylthiophene-2-yl)trimethylstannane

Compound 7b (4.21 g, 25 mmole), 10 ml 2.5M n-butyllithium in hexane solution (25 mmole), and 25 ml 1M trimethyltin chloride in tetrahydrofuran solution (25 mmole) were used to do the reaction. Following the synthetic procedure of compound 8a, one obtained pale yellow oil, compound 8b (6.64 g, 80%). ^{1}H NMR (400 MHz, $CDCl_3$) δ 7.19 (d, *J* = 0.8 Hz, 1H), 7.01 (s, 1H), 2.65 (t, *J* = 7.8 Hz, 2H), 1.63 (quintet, *J* = 7.5 Hz, 2H), 1.29 (d, *J* = 21.8 Hz, 6H), 0.88 (t, *J* = 6.8 Hz, 3H), 0.35 (s, 9H).

doi:10.6342/NTU201904150

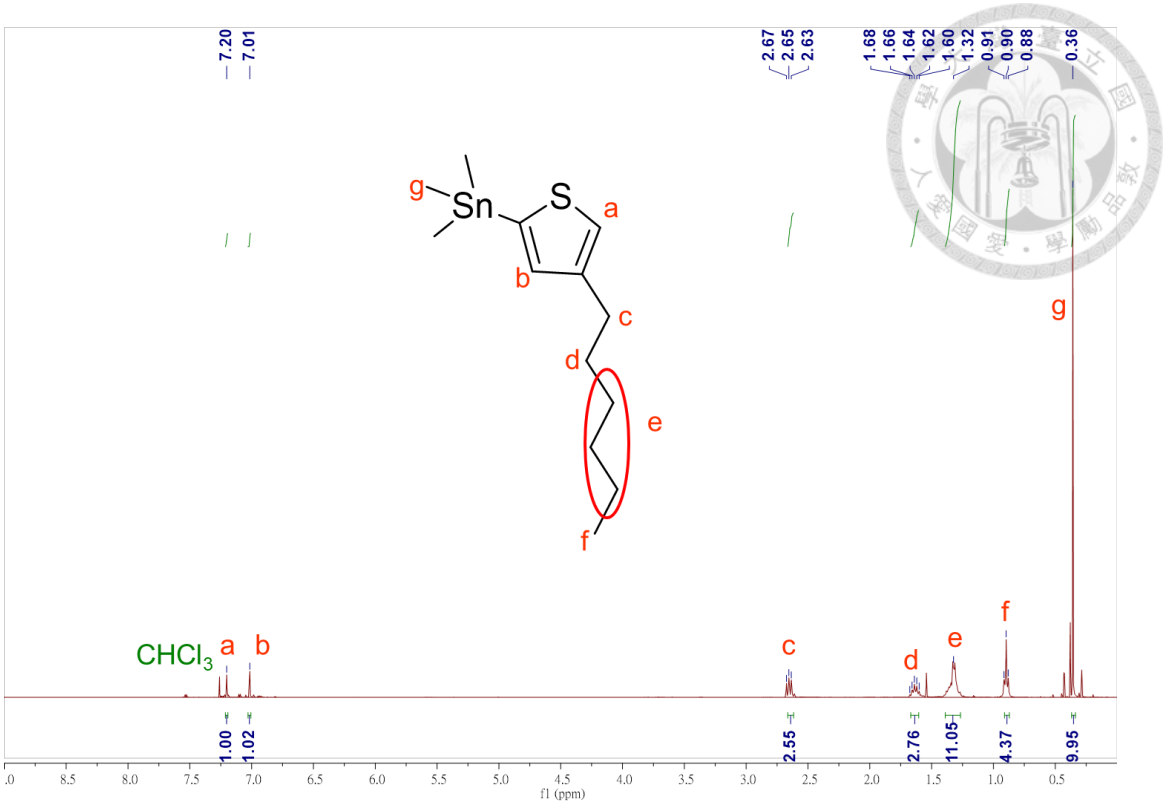

Figure 5.17. ^{1}H NMR of compound 8b

Synthesis of compound 8c

(4-butylthiophene-2-yl)trimethylstannane

Compound 7c (3.51 g, 25 mmole), 10 ml 2.5M n-butyllithium in hexane solution (25 mmole), and 25 ml 1M trimethyltin chloride in tetrahydrofuran solution (25 mmole) were used to do the reaction. Following the synthetic procedure of compound 8a, one obtained pale yellow oil, compound 8c (5.78 g, 76%).

doi:10.6342/NTU201904150

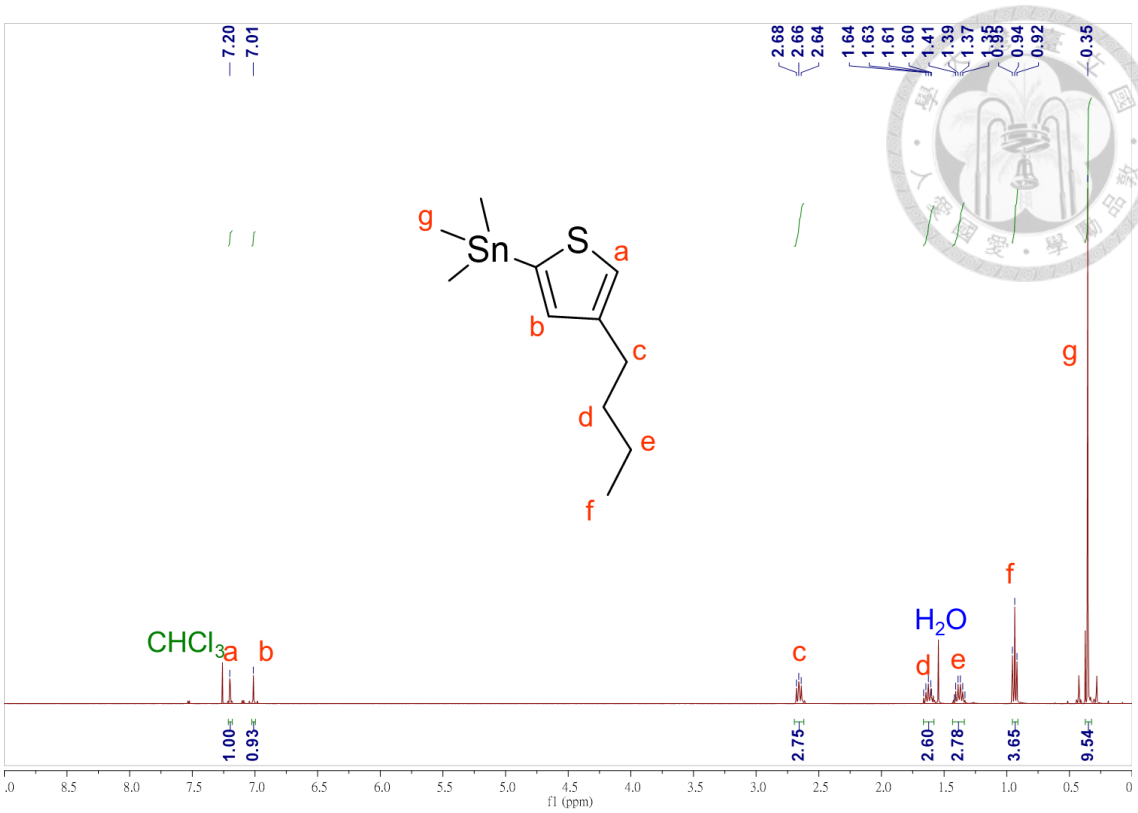

Figure 5.18. ^{1}H NMR of compound 8c

Synthesis of compound 9a

2-bromo-3-octylthiophene

Compound 7a (10.00 g, 0.51 mole), 135 ml chloroform, and 135 ml acetic acid were placed in a 500 ml round bottom flask and then 1-bromo-2,5-pyrrolidinedione (9.06 g, 0.51 mole) was added into the flask slowly in 2 hours. The mixture was stirred at room temperature for 12 hours and then extracted by chloroform and 10 wt% potassium hydroxide aqueous solution. The organic layer was collected, dried by anhydrous magnesium sulfate, and filtered by filter paper. The filtrate was collected and the chloroform was removed by rotary evaporator. The condensed mixture was

doi:10.6342/NTU201904150

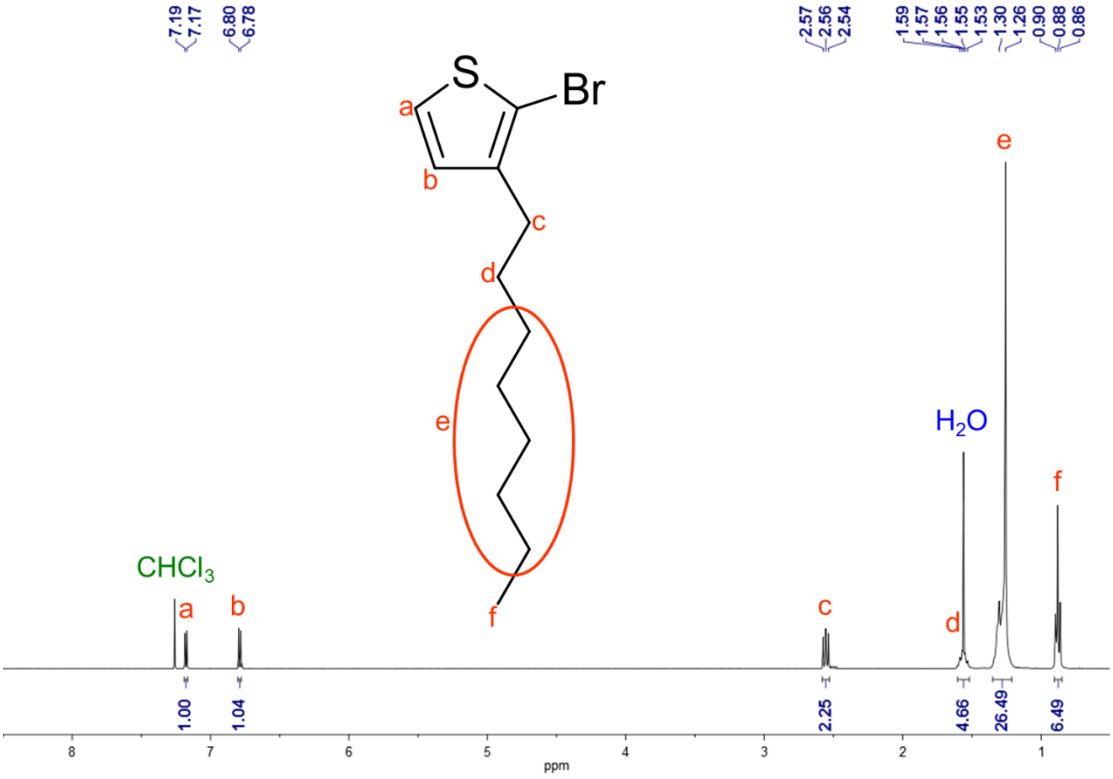

Figure 5.19. ^{1}H NMR of compound 9a

Synthesis of compound 9b

2-bromo-3-hexylthiophene

Compound 7b (8.58 g, 0.51 mole), 135 ml chloroform,135 ml acetic acid, and 1-bromo-2,5-pyrrolidinedione (9.06 g, 0.51 mole) were used to do the reaction.

doi:10.6342/NTU201904150

Following the synthetic procedure of compound 9a, the condensed mixture was further purified by distillation under reduced pressure (90 °C, 0.08 torr) to obtain colorless oil, compound 9b (12.34 g, 98%). ^{1}H NMR (400 MHz, $CDCl_3$) δ 7.18 (d, J = 5.6 Hz, 1H), 6.79 (d, J = 5.6 Hz, 1H), 2.58 – 2.53 (m, 2H), 1.60 – 1.52 (m, 2H), 1.28 (d, J = 18.7 Hz, 6H), 0.88 (t, J = 6.8 Hz, 3H).

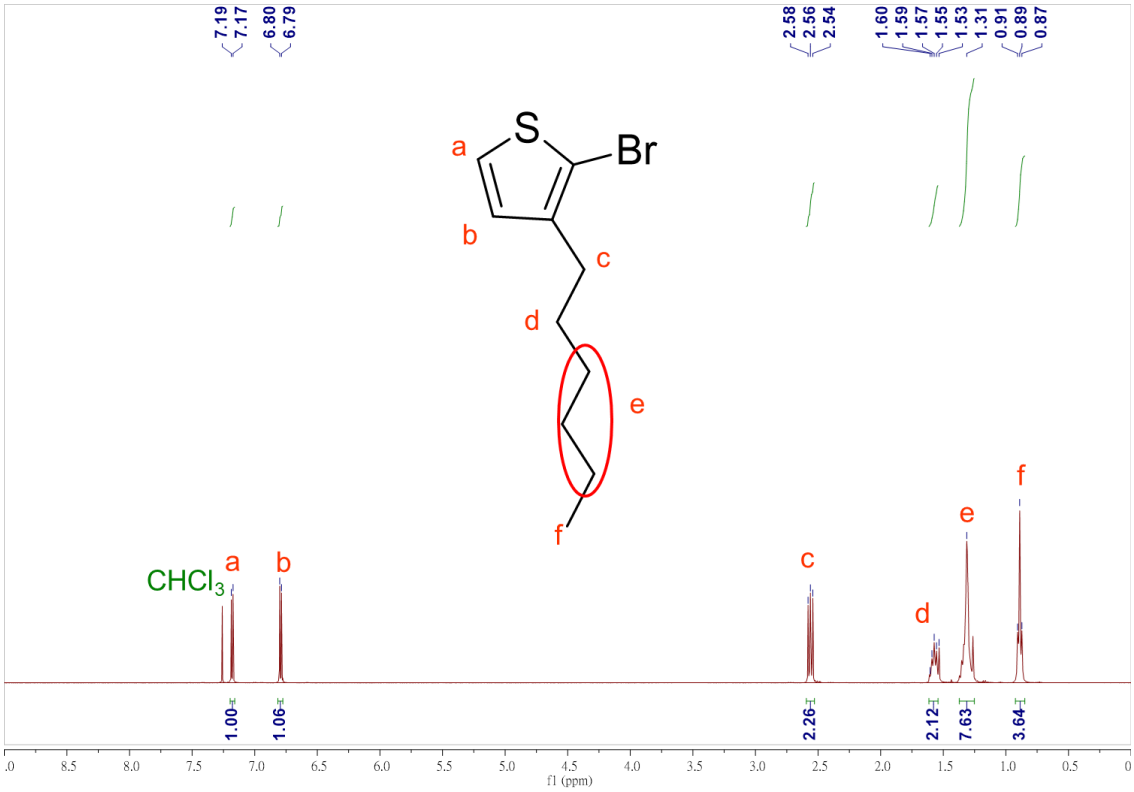

Figure 5.20. ^{1}H NMR of compound 9b

doi:10.6342/NTU201904150

Synthesis of compound 9c

2-bromo-3-butylthiophene

Compound 7c (7.15 g, 0.51 mole), 135 ml chloroform,135 ml acetic acid, and 1-bromo-2,5-pyrrolidinedione (9.06 g, 0.51 mole) were used to do the reaction. Following the synthetic procedure of compound 9a, the condensed mixture was further purified by distillation under reduced pressure (60 ^{o}C, 0.08 torr) to obtain colorless oil, compound 9c (8.93 g, 80%). ^{1}H NMR (400 MHz, $CDCl_3$) δ 7.18 (d, J = 5.6 Hz, 1H), 6.79 (d, J = 5.6 Hz, 1H), 2.58 – 2.53 (m, 2H), 1.60 – 1.52 (m, 2H), 1.28 (d, J = 18.7 Hz, 2H), 0.88 (t, J = 6.8 Hz, 3H).

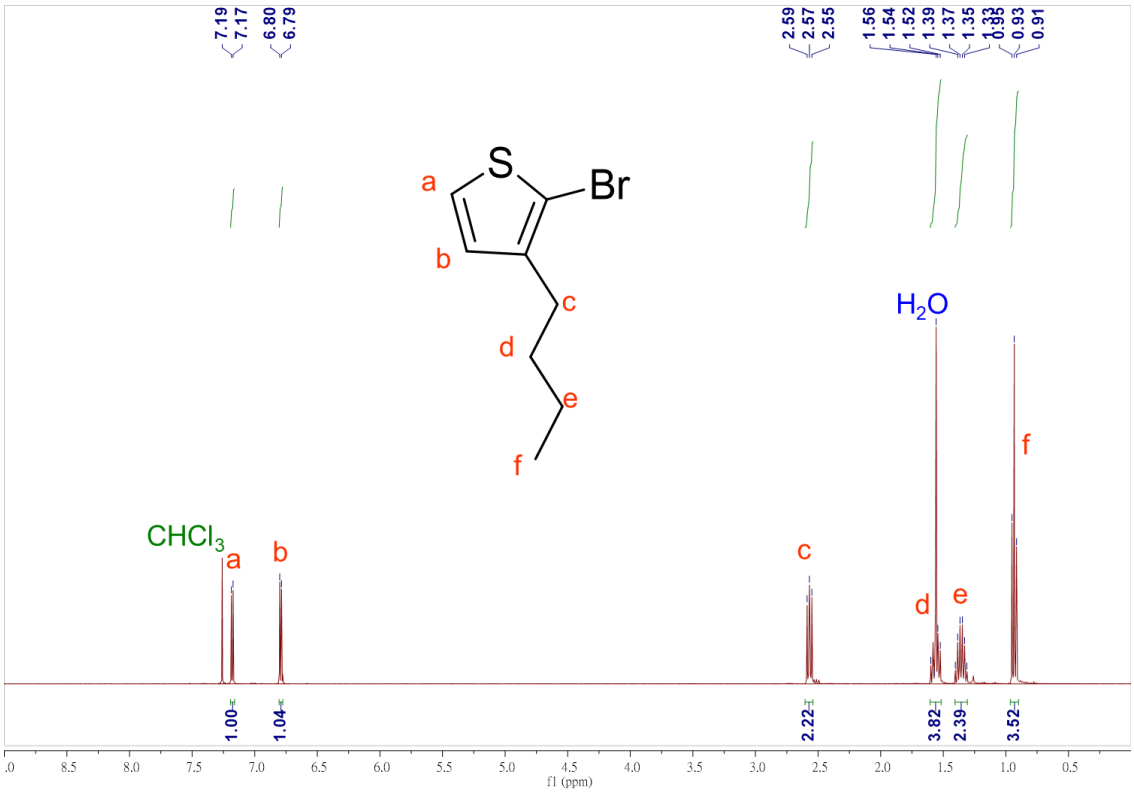

Figure 5.21. ^{1}H NMR of compound 9c

doi:10.6342/NTU201904150

Synthesis of compound 10a

trimethyl(3-octylthiophene-2-yl)stannane

A 150 ml round bottom flask was evacuated by vacuum system and refilled the nitrogen to remove the moisture in the flask. Then, compound 9a (6.89 g, 25 mmole) and 50 ml anhydrous tetrahydrofuran were placed in the flask. The flask was put in -78 ^{o}C dry ice bath. Then, 10 ml 2.5M n-butyllithium in hexane solution (25 mmole) was added into the flask and the solution was stirred for 2 hours. Next, the -78 ^{o}C dry ice bath was removed and the solution was stirred at room temperature for 1 hour. Then the flask was put in -78 ^{o}C dry ice bath again and 25 ml 1M trimethyltin chloride in tetrahydrofuran solution (25 mmole) was added into the flask. After complete adding the trimethyltin chloride solution, the -78 ^{o}C dry ice bath was removed and the solution was stirred at room temperature for 12 hours. Then, the mixture was extracted by hexane and distilled water. The organic layer was collected, dried by anhydrous magnesium sulfate, and filtered by filter paper. The filtrate was collected and the hexane was removed by rotary evaporator. Finally, the condensed mixture can be further purified by column chromatography (hexane as eluent, celite gel) to obtain pale yellow oil, compound 10a (6.94 g, 77%). ^{1}H NMR (400 MHz, $CDCl_3$) δ 7.53 (d, J = 4.7 Hz, 1H), 7.09 (d, J = 4.6 Hz, 1H), 2.64 – 2.59 (m, 2H), 1.62 – 1.51 (m, 2H), 1.28 (d, J = 18.8 Hz, 10H), 0.88 (t, J = 6.3 Hz, 3H), 0.37 (s, 9H).

doi:10.6342/NTU201904150

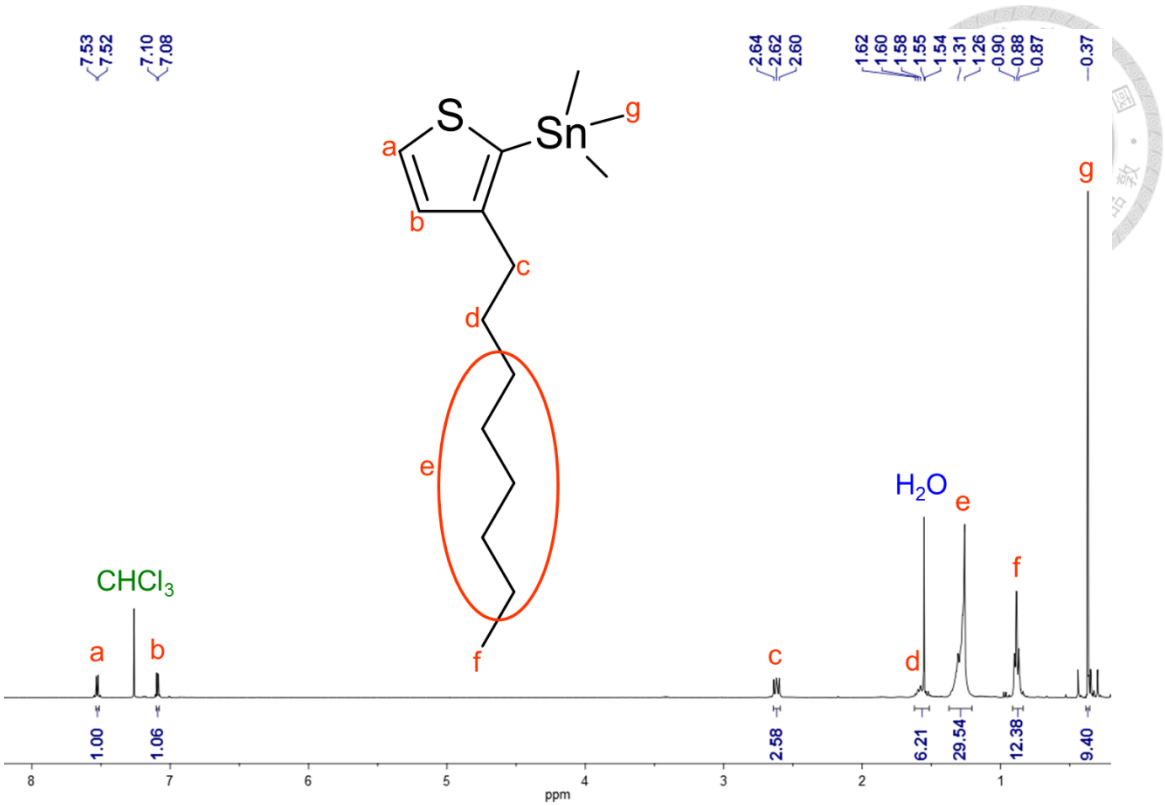

Figure 5.22. ^{1}H NMR of compound 10a

Synthesis of compound 10b

(3-hexylthiophene-2-yl)trimethylstannane

Compound 9b (6.18 g, 25 mmole), 10 ml 2.5M n-butyllithium in hexane solution (25 mmole), and 25 ml 1M trimethyltin chloride in tetrahydrofuran solution (25 mmole) were used to do the reaction. Following the synthetic procedure of compound 10a, one obtained pale yellow oil, compound 10b (6.72 g, 81%). ^{1}H NMR (400 MHz, $CDCl_3$) δ 7.53 (d, J = 4.7 Hz, 1H), 7.09 (d, J = 4.6 Hz, 1H), 2.64 – 2.59 (m, 2H), 1.62 – 1.51 (m, 2H), 1.28 (d, J = 18.8 Hz, 6H), 0.88 (t, J = 6.3 Hz, 3H), 0.37 (s, 9H).

doi:10.6342/NTU201904150

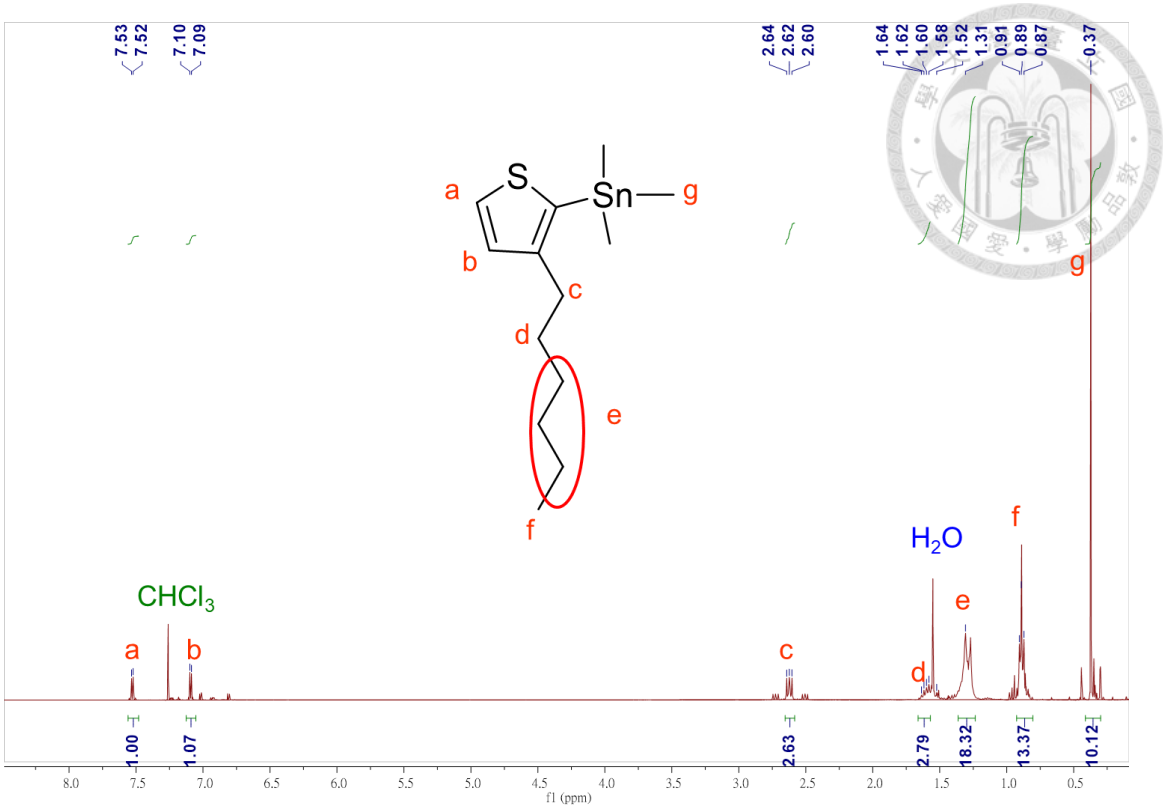

Figure 5.23. ^{1}H NMR of compound 10b

Synthesis of compound 10c

(3-butylthiophene-2-yl)trimethylstannane

Compound 9c (5.48 g, 25 mmole), 10 ml 2.5M n-butyllithium in hexane solution (25 mmole), and 25 ml 1M trimethyltin chloride in tetrahydrofuran solution (25 mmole) were used to do the reaction. Following the synthetic procedure of compound 10a, one obtained pale yellow oil, compound 10c (5.86 g, 77%). ^{1}H NMR (400 MHz, $CDCl_3$) δ 7.53 (d, J = 4.7 Hz, 1H), 7.09 (d, J = 4.6 Hz, 1H), 2.64 – 2.59 (m, 2H), 1.62 – 1.51 (m, 2H), 1.28 (d, J = 18.8 Hz, 2H), 0.88 (t, J = 6.3 Hz, 3H), 0.37 (s, 9H).

doi:10.6342/NTU201904150

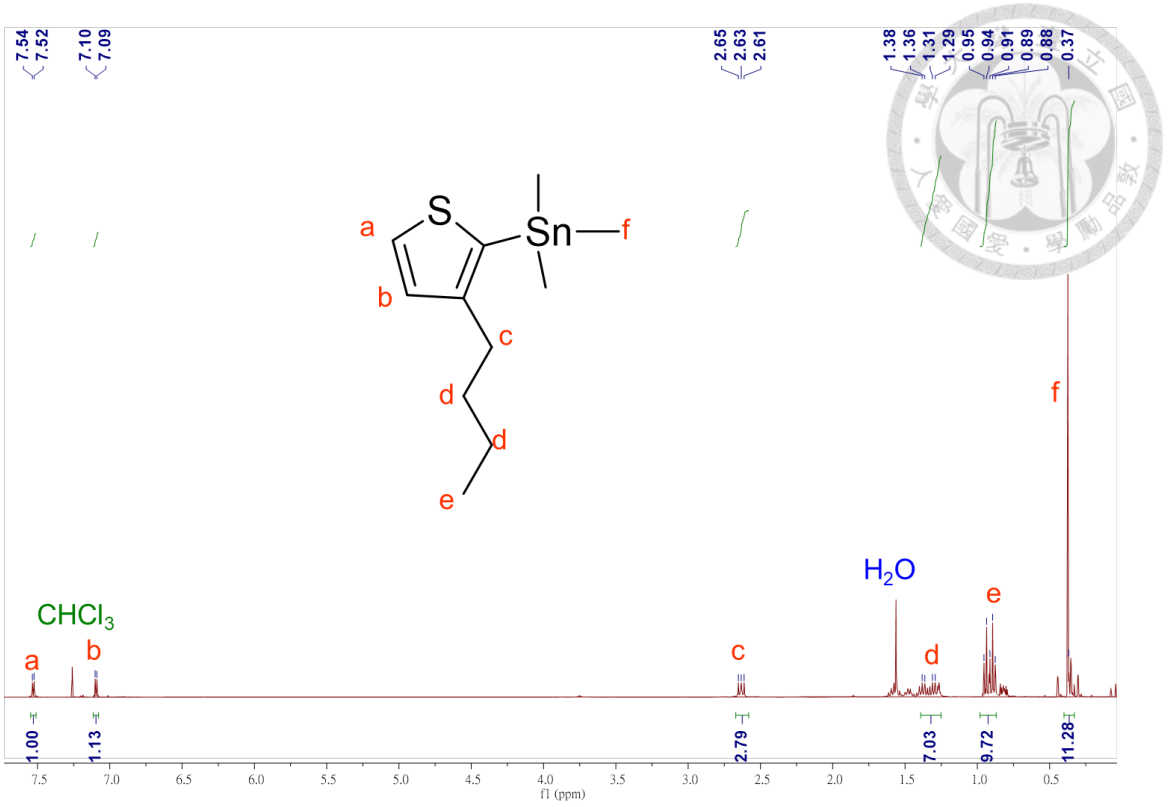

Figure 5.24. ^{1}H NMR of compound 10c

Synthesis of compound 11a

5-dodecyl-1,3-bis(4-octylthiophene-2-yl)-4H-thieno[3,4-c]pyrrole-4,6(5H)-dione

Compound 6a (1.00 g, 2.09 mmole), compound 8a (2.25 g, 6.27mmole), tris(dibenzylideneacetone)dipalladium(0) (91.6 mg, 0.10 mmole), **tris(*o*-tolyl)phosphine** (60.9 mg, 0.20 mmole), and 4 ml degassed tetrahydrofuran were placed in a 10ml microwave vessel then the vessel was put in the microwave reactor, and parameters for the reaction were set at 100 °C, 100 W, and 15 min. The mixture was purified through column chromatography (dichloromethane/hexane=2/3 as eluent, silica gel) to obtain yellow solid, compound 11a (1.22 g, 82%). ^{1}H NMR

doi:10.6342/NTU201904150

(400 MHz, $CDCl_3$) δ 7.87 (s, 2H), 7.02 (s, 2H), 3.65 (t, *J* = 7.4 Hz, 4H), 2.62 (t, *J* = 7.6 Hz, 4H), 1.71 – 1.60 (m, 6H), 1.38 – 1.22 (m, 38H), 0.91 – 0.84 (m, 9H).

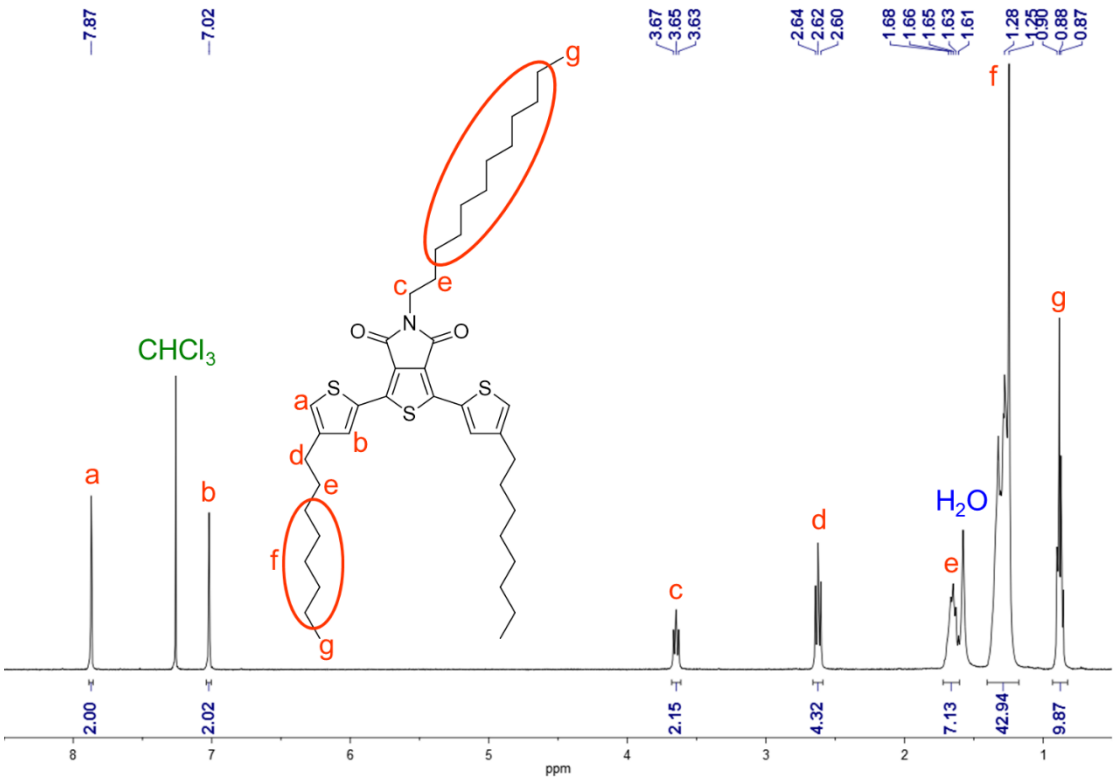

Figure 5.25. ^{1}H NMR of compound 11a

Synthesis of compound 11b

5-(2-(2-(2-ethoxyethoxy)ethoxy)ethyl)-1,3-bis(4-octylthiophene-2-yl)-4H-thieno[3, 4-c]pyrrole-4,6(5H)-dione

Compound 6b (0.98 g, 2.09 mmole), compound 8a (2.25 g, 6.27mmole), tris(dibenzylideneacetone)dipalladium(0) (91.6 mg, 0.10 mmole), **tris(*o*-tolyl)phosphine** (60.9 mg, 0.20 mmole), and 4 ml degassed tetrahydrofuran

doi:10.6342/NTU201904150

were placed in a 10ml microwave vessel then the vessel was put in the microwave reactor, and parameters for the reaction were set at 100 °C, 100 W, and 15 min. After that, the mixture was purified through column chromatography (ether/hexane=1/3 as eluent, silica gel) to obtain yellow oil, compound 11b (1.19 g, 80%). ^{1}H NMR (400 MHz, $CDCl_3$) δ 7.85 (s, 2H), 7.02 (s, 2H), 3.88 (t, *J* = 6.0 Hz, 2H), 3.75 (t, *J* = 5.9 Hz, 2H), 3.69 – 3.58 (m, 6H), 3.53 – 3.42 (m, 4H), 2.63 (t, *J* = 7.8 Hz, 4H), 1.65 (quintet, *J* = 7.3 Hz, 4H), 1.39 – 1.21 (m, 20H), 1.16 (t, *J* = 7.0 Hz, 3H), 0.88 (t, *J* = 6.8 Hz, 6H).

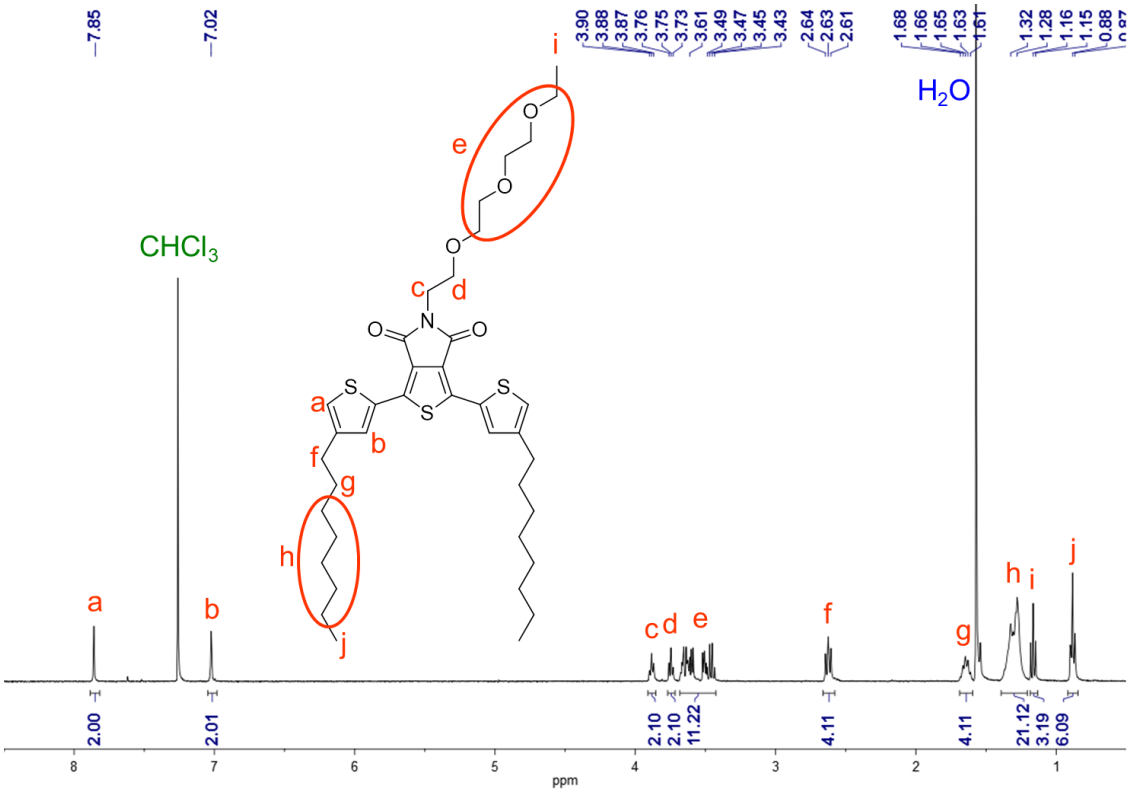

Figure 5.26. ^{1}H NMR of compound 11b

doi:10.6342/NTU201904150

Synthesis of compound 11c

5-(2-(2-(2-ethoxyethoxy)ethoxy)ethyl)-1,3-bis(4-hexylthiophene-2-yl)-4H-thieno[3,4-c]pyrrole-4,6(5H)-dione

Compound 6b (0.98 g, 2.09 mmole), compound 8b (2.08 g, 6.27mmole), tris(dibenzylideneacetone)dipalladium(0) (91.6 mg, 0.10 mmole), **tris(*o*-tolyl)phosphine** (60.9 mg, 0.20 mmole), and 4 ml degassed tetrahydrofuran were placed in a 10ml microwave vessel then the vessel was put in the microwave reactor, and parameters for the reaction were set at 100 ^{o}C, 100 W, and 15 min. After that, the mixture was purified through column chromatography (ether/hexane=1/3 as eluent, silica gel) to obtain yellow oil, compound 11c (1.11 g, 81%). ^{1}H NMR (400 MHz, $CDCl_3$) δ 7.85 (s, 2H), 7.02 (s, 2H), 3.88 (t, *J* = 6.0 Hz, 2H), 3.75 (t, *J* = 5.9 Hz, 2H), 3.69 – 3.58 (m, 6H), 3.53 – 3.42 (m, 4H), 2.63 (t, *J* = 7.8 Hz, 4H), 1.65 (quintet, *J* = 7.3 Hz, 4H), 1.39 – 1.21 (m, 12H), 1.16 (t, *J* = 7.0 Hz, 3H), 0.88 (t, *J* = 6.8 Hz, 6H).

doi:10.6342/NTU201904150

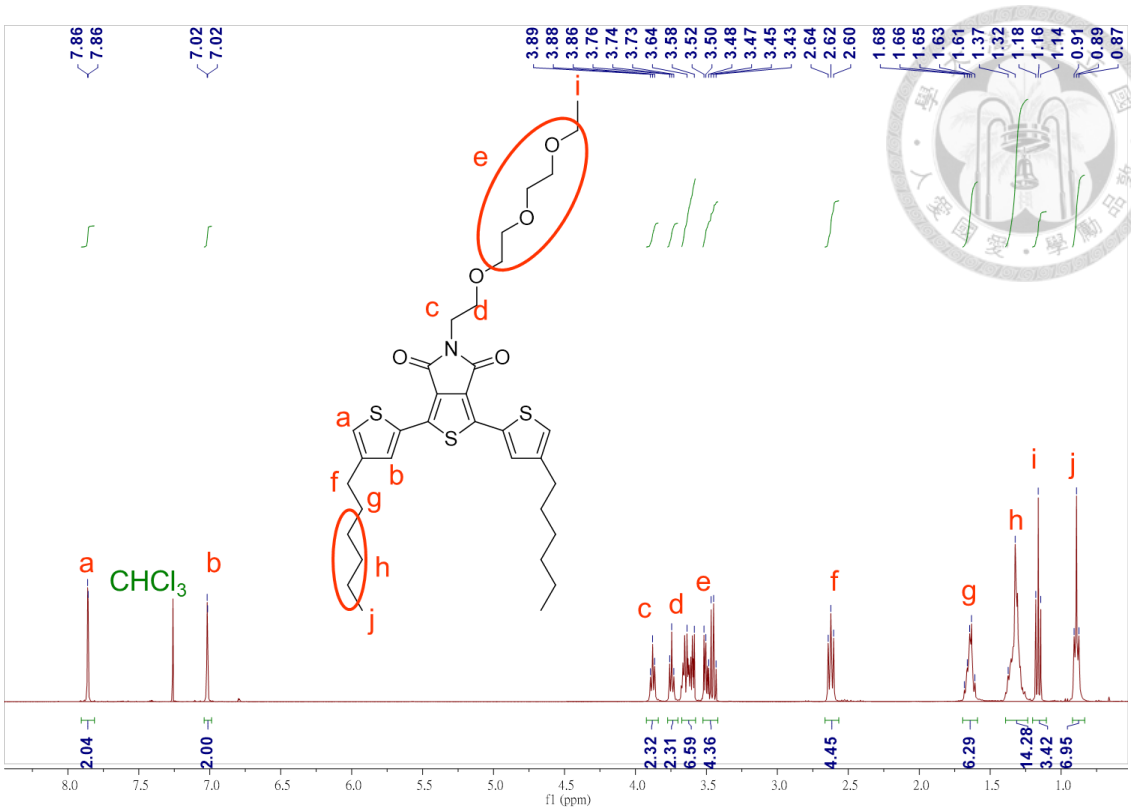

Figure 5.27. ^{1}H NMR of compound 11c

Synthesis of compound 11d

1,3-bis(4-butylthiophene-2-yl)-5-(2-(2-(2-ethoxyethoxy)ethoxy)ethyl)-4H-thieno[3,4-c]pyrrole-4,6(5H)-dione

Compound 6b (0.98 g, 2.09 mmole), compound 8c (1.91 g, 6.27mmole), tris(dibenzylideneacetone)dipalladium(0) (91.6 mg, 0.10 mmole), **tris(*o*-tolyl)phosphine** (60.9 mg, 0.20 mmole), and 4 ml degassed tetrahydrofuran were placed in a 10ml microwave vessel then the vessel was put in the microwave reactor, and parameters for the reaction were set at 100 ºC, 100 W, and 15 min. After that, the mixture was purified through column chromatography (ether/hexane=1/3 as

doi:10.6342/NTU201904150

eluent, silica gel) to obtain yellow oil, compound 11d (0.99 g, 79%). ^{1}H NMR (400 MHz, $CDCl_3$) δ 7.85 (s, 2H), 7.02 (s, 2H), 3.88 (t, *J* = 6.0 Hz, 2H), 3.75 (t, *J* = 5.9 Hz, 2H), 3.69 – 3.58 (m, 6H), 3.53 – 3.42 (m, 4H), 2.63 (t, *J* = 7.8 Hz, 4H), 1.65 (quintet, *J* = 7.3 Hz, 4H), 1.39 – 1.21 (m, 4H), 1.16 (t, *J* = 7.0 Hz, 3H), 0.88 (t, *J* = 6.8 Hz, 6H).

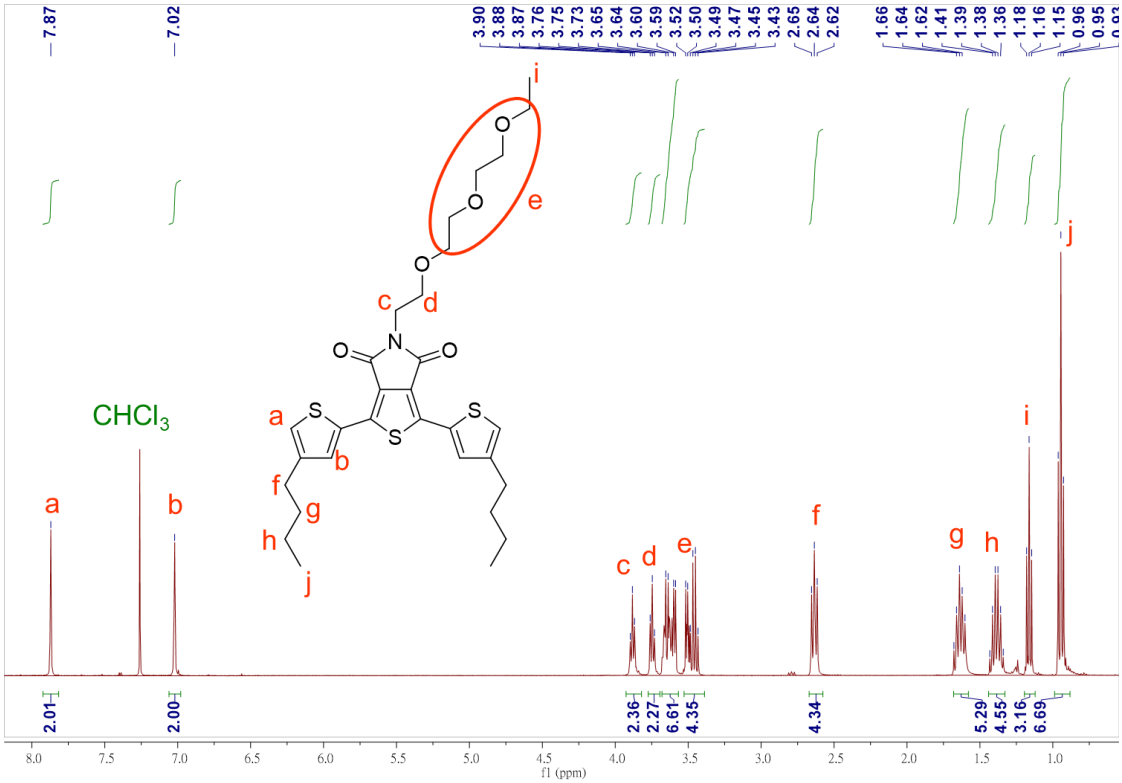

Figure 5.28. ^{1}H NMR of compound 11d

doi:10.6342/NTU201904150

Synthesis of compound 12a

1,3-bis(5-bromo-4-octylthiophene-2-yl)-5-dodecyl-4H-thieno[3,4-c]pyrrole-4,6(5H)-dione

Compound 11a (1 g, 1.41 mmole), and 50 ml tetrahydrofuran were placed in 150ml round bottom flask and then 1-bromo-2,5-pyrrolidinedione (527 mg , 2.96 mmole) was added into the flask. The mixture was stirred at room temperature for 12 hours. After reaction, the tetrahydrofuran was removed by rotary evaporator and the condensed mixture was further purified by column chromatography (ether as eluent) to obtain yellow solid, compound 12a (1.14 g, 93%). ^{1}H NMR (400 MHz, $CDCl_3$) δ 7.62 (s, 2H), 3.64 (t, *J* = 7.4Hz, 2H), 2.58 (t, *J* = 7.8Hz, 4H), 1.70 – 1.59 (m, 6H), 1.39 – 1.20 (m, 38H), 0.88 (s, 9H).

doi:10.6342/NTU201904150

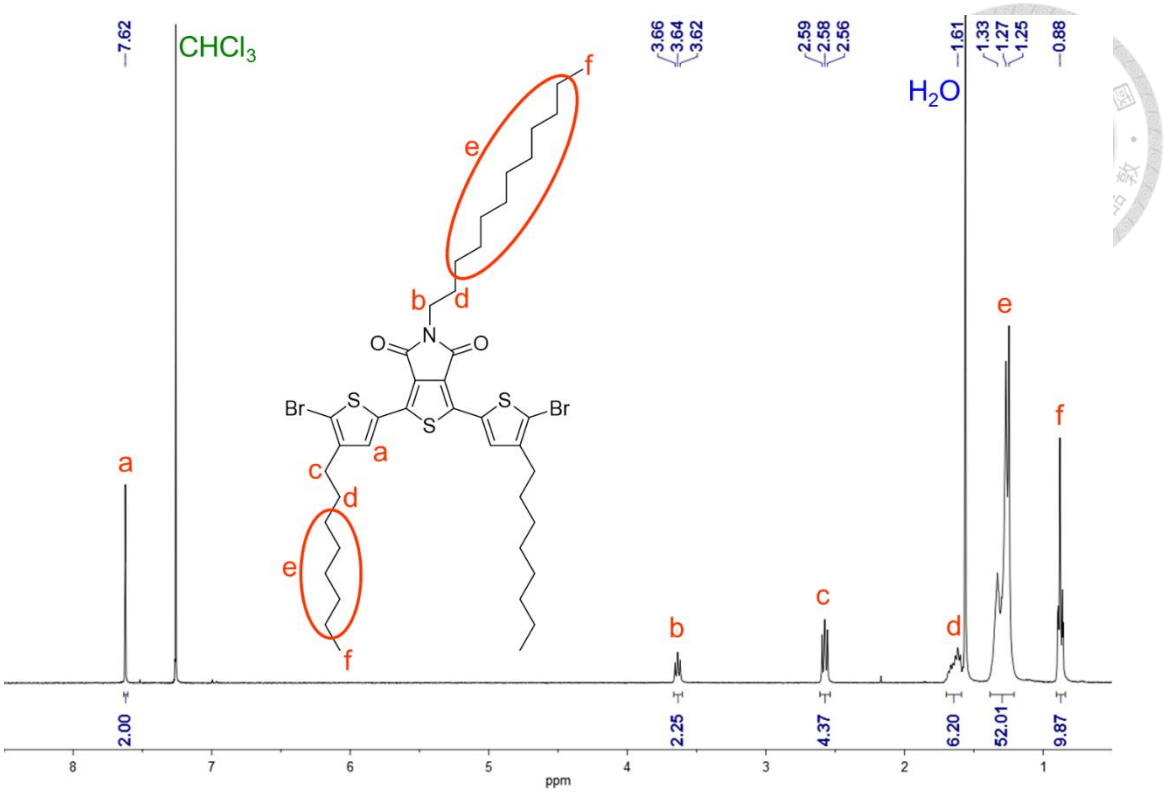

Figure 5.29. ^{1}H NMR of compound 12a

Synthesis of compound 12b

1,3-bis(5-bromo-4-octylthiophene-2-yl)-5-(2-(2-(2-ethoxyethoxy)ethoxy)ethyl)-4H -thieno[3,4-c]pyrrole-4,6(5H)-dione

Compound 11b (0.99 g, 1.41 mmole), and 50 ml tetrahydrofuran were placed in 150ml round bottom flask and then 1-bromo-2,5-pyrrolidinedione (527 mg, 2.96 mmole) was added into the flask. The mixture was stirred at room temperature for 12 hours. After reaction, the tetrahydrofuran was removed by rotary evaporator and the condensed mixture was further purified by column chromatography (ether as eluent) to obtain yellow solid, compound 12b (1.14 g, 93%). ^{1}H NMR (400 MHz, $CDCl_3$) δ

doi:10.6342/NTU201904150

7.62 (s, 2H), 3.87 (t, *J* = 5.9 Hz, 2H), 3.74 (t, *J* = 5.8 Hz, 2H), 3.68 – 3.58 (m, 6H), 3.53 – 3.43 (m, 4H), 2.58 (t, *J* = 6.9 Hz, 4H), 1.66 – 1.58 (m, 4H), 1.38 – 1.22 (m, 20H), 1.17 (t, *J* = 7.0 Hz, 3H), 0.88 (t, *J* = 6.9 Hz, 6H).

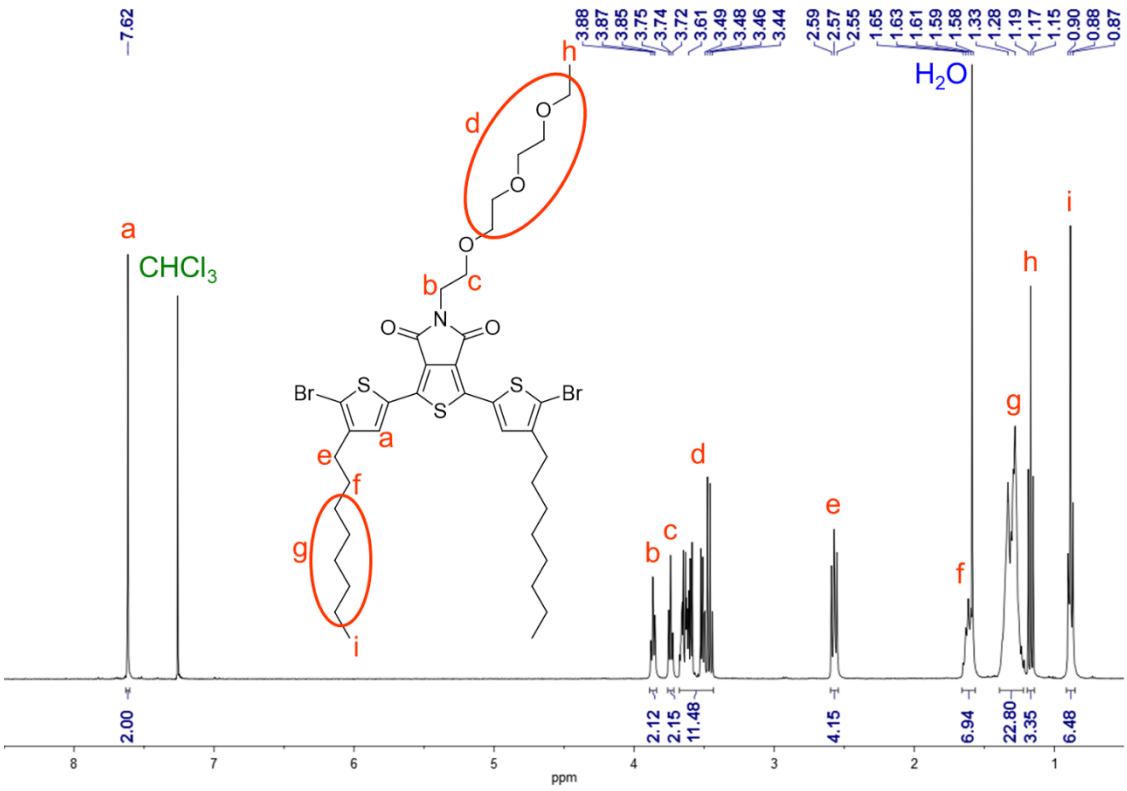

Figure 5.30. ^{1}H NMR of compound 12b

Synthesis of compound 12c

1,3-bis(5-bromo-4-hexylthiophene-2-yl)-5-(2-(2-(2-ethoxyethoxy)ethoxy)ethyl)-4 H-thieno[3,4-c]pyrrole-4,6(5H)-dione

Compound 11c (0.91 g, 1.41 mmole), and 50 ml tetrahydrofuran were placed in 150ml round bottom flask and then 1-bromo-2,5-pyrrolidinedione (527 mg , 2.96

doi:10.6342/NTU201904150

mmole) was added into the flask. The mixture was stirred at room temperature for 12 hours. After reaction, the tetrahydrofuran was removed by rotary evaporator and the condensed mixture was further purified by column chromatography (ether as eluent) to obtain yellow solid, compound 12c (1.17 g, 94%). ^{1}H NMR (400 MHz, $CDCl_3$) δ 7.62 (s, 2H), 3.87 (t, *J* = 5.9 Hz, 2H), 3.74 (t, *J* = 5.8 Hz, 2H), 3.68 – 3.58 (m, 6H), 3.53 – 3.43 (m, 4H), 2.58 (t, *J* = 6.9 Hz, 4H), 1.66 – 1.58 (m, 4H), 1.38 – 1.22 (m, 12H), 1.17 (t, *J* = 7.0 Hz, 3H), 0.88 (t, *J* = 6.9 Hz, 6H).

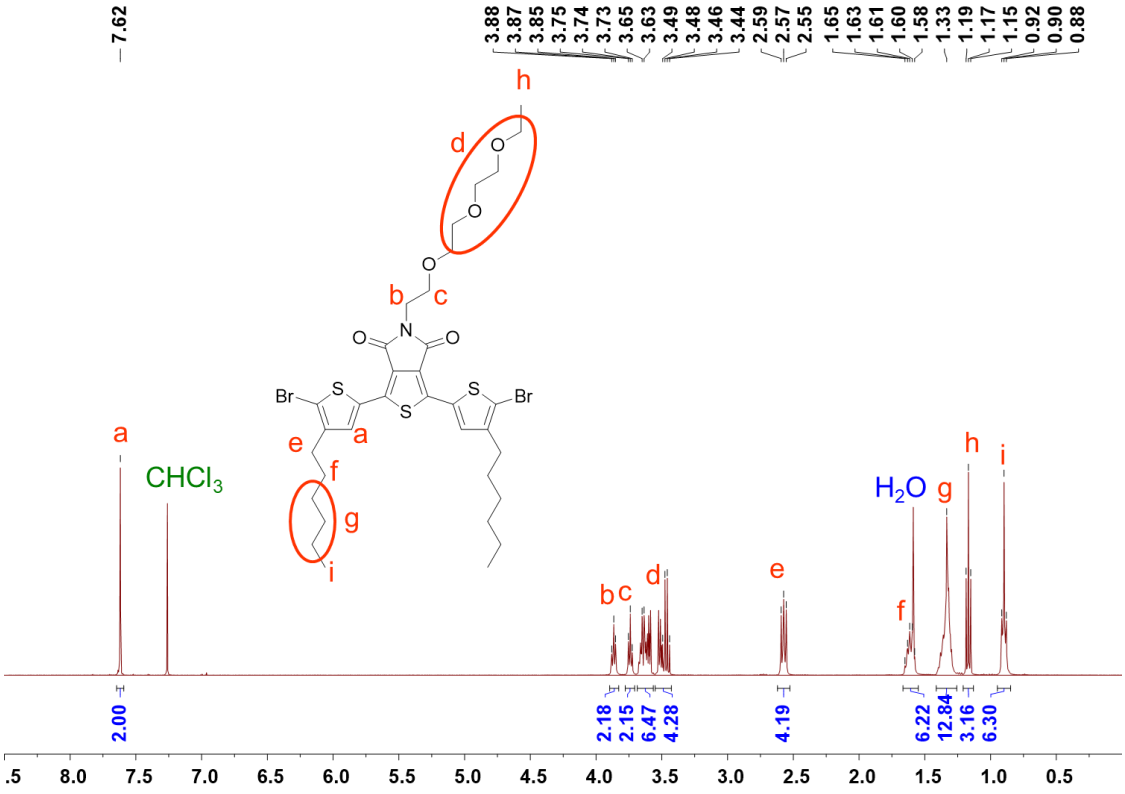

Figure 5.31. ^{1}H NMR of compound 12c

doi:10.6342/NTU201904150

Synthesis of compound 12d

1,3-bis(5-bromo-4-butylthiophene-2-yl)-5-(2-(2-(2-ethoxyethoxy)ethoxy)ethyl)-4H-thieno[3,4-c]pyrrole-4,6(5H)-dione

Compound 11d (0.83 g, 1.41 mmole), and 50 ml tetrahydrofuran were placed in 150ml round bottom flask and then 1-bromo-2,5-pyrrolidinedione (527 mg , 2.96 mmole) was added into the flask. The mixture was stirred at room temperature for 12 hours. After reaction, the tetrahydrofuran was removed by rotary evaporator and the condensed mixture was further purified by column chromatography (ether as eluent) to obtain yellow solid, compound 12d (1.17 g, 92%). ^{1}H NMR (400 MHz, $CDCl_3$) δ 7.62 (s, 2H), 3.87 (t, *J* = 5.9 Hz, 2H), 3.74 (t, *J* = 5.8 Hz, 2H), 3.68 – 3.58 (m, 6H), 3.53 – 3.43 (m, 4H), 2.58 (t, *J* = 6.9 Hz, 4H), 1.66 – 1.58 (m, 4H), 1.38 – 1.22 (m, 4H), 1.17 (t, *J* = 7.0 Hz, 3H), 0.88 (t, *J* = 6.9 Hz, 6H).

doi:10.6342/NTU201904150

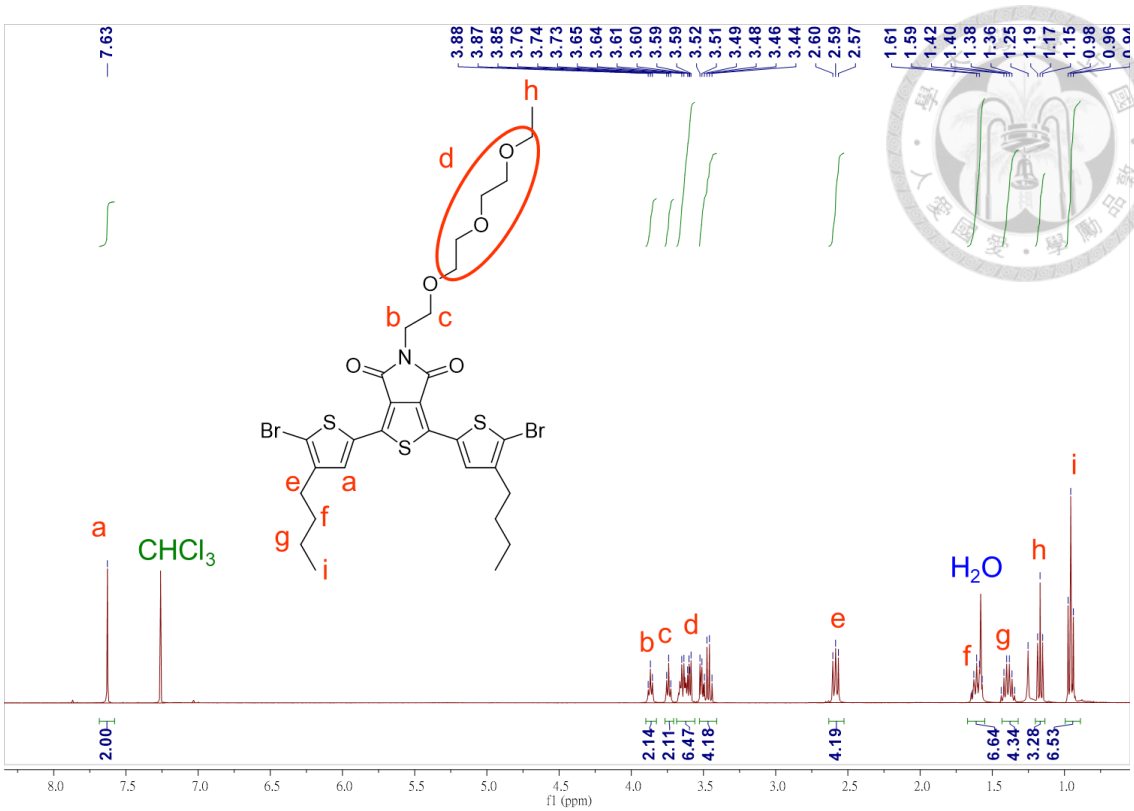

Figure 5.32. ^{1}H NMR of compound 12d

Synthesis of compound 13a

5-dodecyl-1,3-bis(3-octylthiophene-2-yl)-4H-thieno[3,4-c]pyrrole-4,6(5H)-dione

Compound 6a (1.00 g, 2.09 mmole), compound 10a (2.25 g, 6.27 mmole), tris(dibenzylideneacetone)dipalladium(0) (91.6 mg, 0.10 mmole), **tris(*o*-tolyl)phosphine** (60.9 mg, 0.20 mmole), and 4 ml degassed tetrahydrofuran were placed in a 10ml microwave vessel then the vessel was put in the microwave reactor, and parameters for the reaction were set at 100 ºC, 100 W, and 15 min. After that, the mixture was purified through column chromatography (dichloromethane/hexane=2/3 as eluent, silica gel) to obtain yellow oil, compound

doi:10.6342/NTU201904150

13a (1.25 g, 83%). ^{1}H NMR (400 MHz, $CDCl_3$) δ 7.41 (d, J = 5.2 Hz, 2H), 7.01 (d, J = 5.2 Hz, 2H), 3.63 – 3.58 (m, 2H), 2.82 – 2.76 (m, 4H), 1.68 – 1.60 (m, 6H), 1.37 – 1.19 (m, 38H), 0.86 (q, J = 6.9 Hz, 9H).

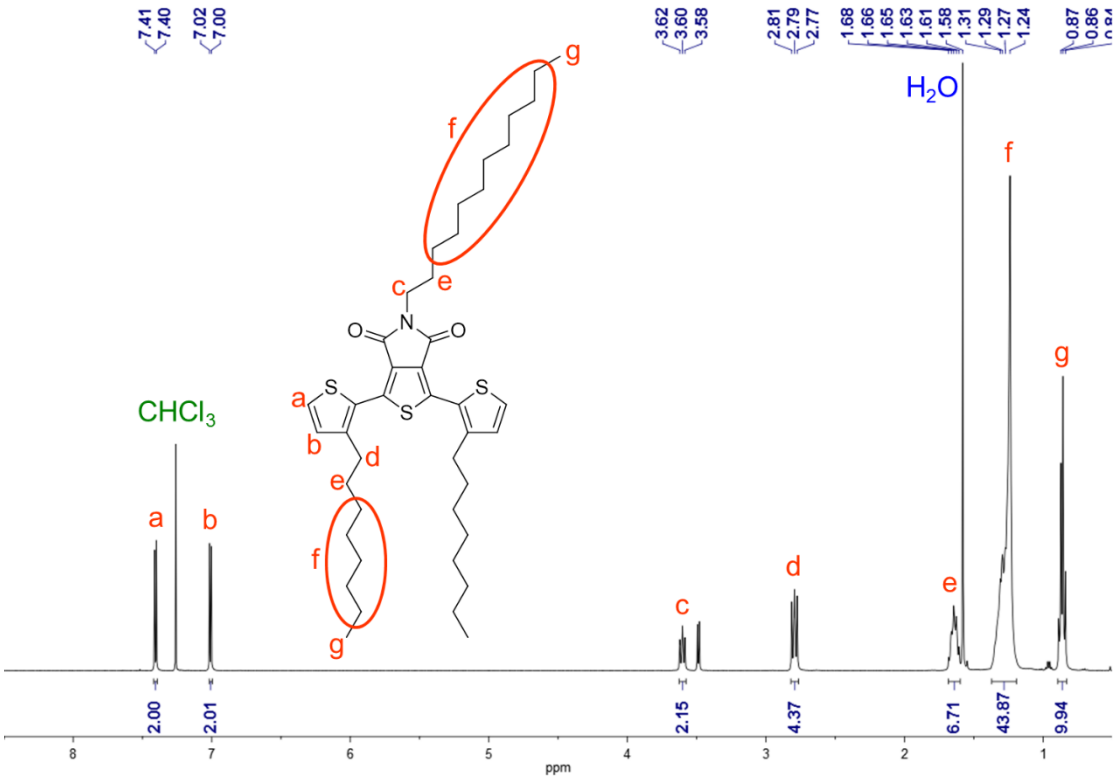

Figure 5.33. ^{1}H NMR of compound 13a

doi:10.6342/NTU201904150

Synthesis of compound 13b

5-(2-(2-(2-ethoxyethoxy)ethoxy)ethyl)-1-(3-hexylthiophene-2-yl)-3-(3-octylthiophene-2-yl)-4H-thieno[3,4-c]pyrrole-4,6(5H)-dione

Compound 6b (0.98 g, 2.09 mmole), compound 10a (2.25 g, 6.27mmole), tris(dibenzylideneacetone)dipalladium(0) (91.6 mg, 0.10 mmole), **tris(*o*-tolyl)phosphine** (60.9 mg, 0.20 mmole), and 4 ml degassed tetrahydrofuran were placed in a 10ml microwave vessel then the vessel was put in the microwave reactor, and parameters for the reaction were set at 100 ^{o}C, 100 W, and 15 min. After that, the mixture was purified through column chromatography (ether/hexane=1/3 as eluent, silica gel) to obtain yellow oil, compound 13b (1.18 g, 79%). ^{1}H NMR (400 MHz, $CDCl_3$) δ 7.41 (d, J = 5.2 Hz, 2H), 7.01 (d, J = 5.2 Hz, 2H), 3.83 (t, J = 6.0 Hz, 2H), 3.71 (t, J = 5.9 Hz, 2H), 3.53 (ddd, J = 26.1, 21.0, 9.8 Hz, 10H), 2.82 – 2.77 (m, 4H), 1.68 – 1.60 (m, 4H), 1.25 (d, J = 3.9 Hz, 20H), 1.18 (t, J = 7.0 Hz, 3H), 0.86 (t, J = 6.9 Hz, 6H).

doi:10.6342/NTU201904150

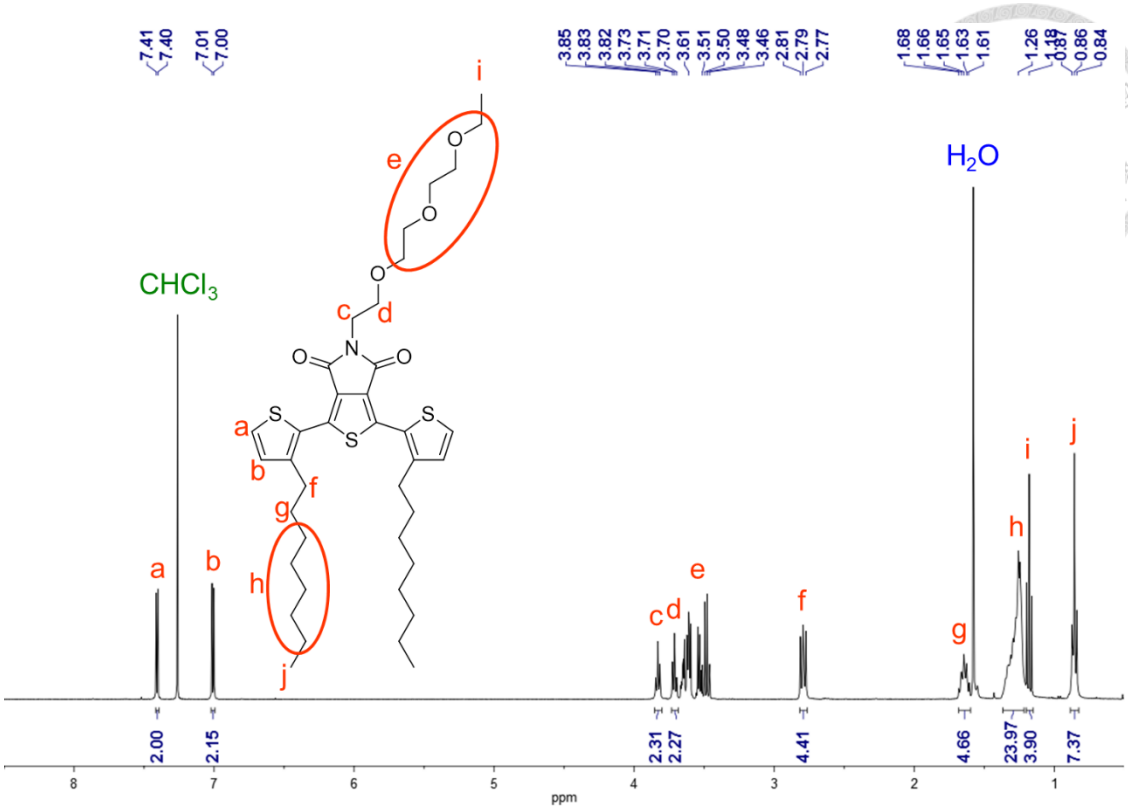

Figure 5.34. [1]H NMR of compound 13b

Synthesis of compound 13c

5-(2-(2-(2-ethoxyethoxy)ethoxy)ethyl)-1,3-bis(3-hexylthiophene-2-yl)-4H-thieno[3,4-c]pyrrole-4,6(5H)-dione

Compound 6b (0.98 g, 2.09 mmole), compound 10b (2.08 g, 6.27mmole), tris(dibenzylideneacetone)dipalladium(0) (91.6 mg, 0.10 mmole), **tris(*o*-tolyl)phosphine** (60.9 mg, 0.20 mmole), and 4 ml degassed tetrahydrofuran were placed in a 10ml microwave vessel then the vessel was put in the microwave reactor, and parameters for the reaction were set at 100 °C, 100 W, and 15 min. After that, the mixture was purified through column chromatography (ether/hexane=1/3 as

doi:10.6342/NTU201904150

eluent, silica gel) to obtain yellow oil, compound 13c (1.10 g, 80%). ^{1}H NMR (400 MHz, $CDCl_3$) δ 7.41 (d, J = 5.2 Hz, 2H), 7.01 (d, J = 5.2 Hz, 2H), 3.83 (t, J = 6.0 Hz, 2H), 3.71 (t, J = 5.9 Hz, 2H), 3.53 (ddd, J = 26.1, 21.0, 9.8 Hz, 10H), 2.82 – 2.77 (m, 4H), 1.68 – 1.60 (m, 4H), 1.25 (d, J = 3.9 Hz, 12H), 1.18 (t, J = 7.0 Hz, 3H), 0.86 (t, J = 6.9 Hz, 6H).

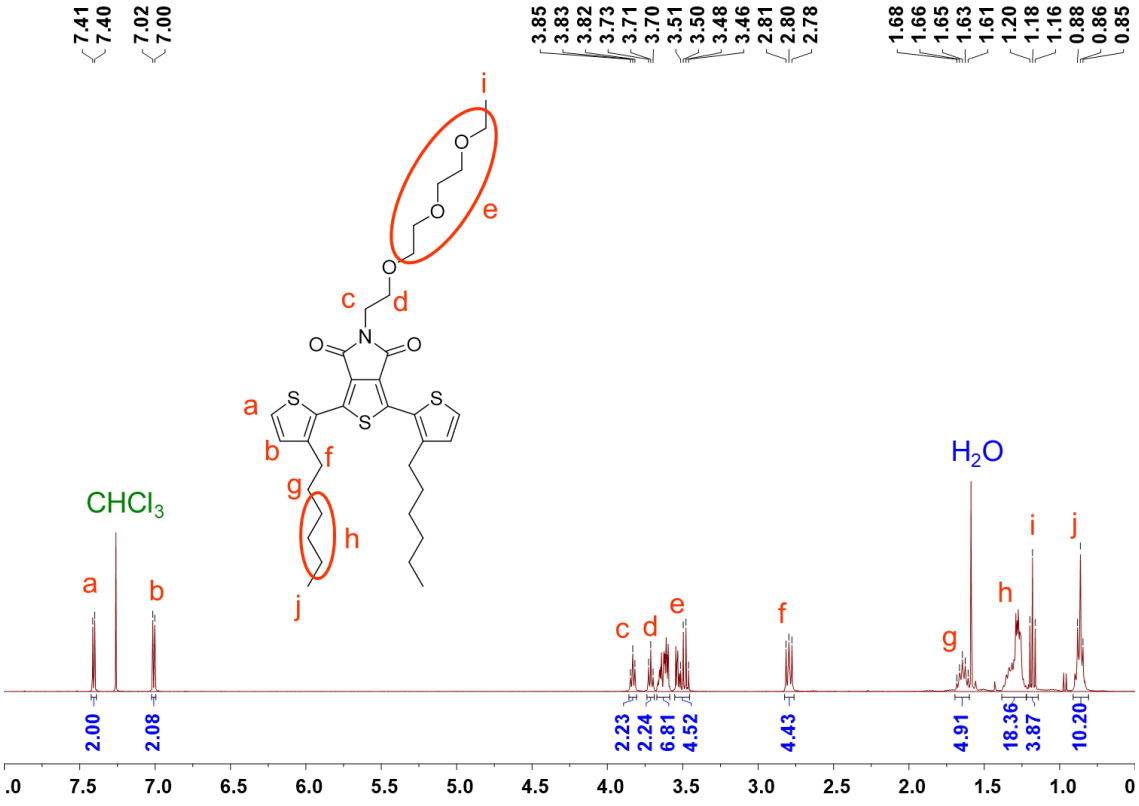

Figure 5.35. ^{1}H NMR of compound 13c

doi:10.6342/NTU201904150

Synthesis of compound 13d

1,3-bis(3-butylthiophene-2-yl)-5-(2-(2-(2-ethoxyethoxy)ethoxy)ethyl)-4H-thieno[3,4-c]pyrrole-4,6(5H)-dione

Compound 6b (0.98 g, 2.09 mmole), compound 10c (1.91 g, 6.27mmole), tris(dibenzylideneacetone)dipalladium(0) (91.6 mg, 0.10 mmole), **tris(*o*-tolyl)phosphine** (60.9 mg, 0.20 mmole), and 4 ml degassed tetrahydrofuran were placed in a 10ml microwave vessel then the vessel was put in the microwave reactor, and parameters for the reaction were set at 100 ºC, 100 W, and 15 min. After that, the mixture was purified through column chromatography (ether/hexane=1/3 as eluent, silica gel) to obtain yellow oil, compound 13d (0.99 g, 79%). ^{1}H NMR (400 MHz, $CDCl_3$) δ 7.41 (d, J = 5.2 Hz, 2H), 7.01 (d, J = 5.2 Hz, 2H), 3.83 (t, J = 6.0 Hz, 2H), 3.71 (t, J = 5.9 Hz, 2H), 3.53 (ddd, J = 26.1, 21.0, 9.8 Hz, 10H), 2.82 – 2.77 (m, 4H), 1.68 – 1.60 (m, 4H), 1.25 (d, J = 3.9 Hz, 4H), 1.18 (t, J = 7.0 Hz, 3H), 0.86 (t, J = 6.9 Hz, 6H).

doi:10.6342/NTU201904150

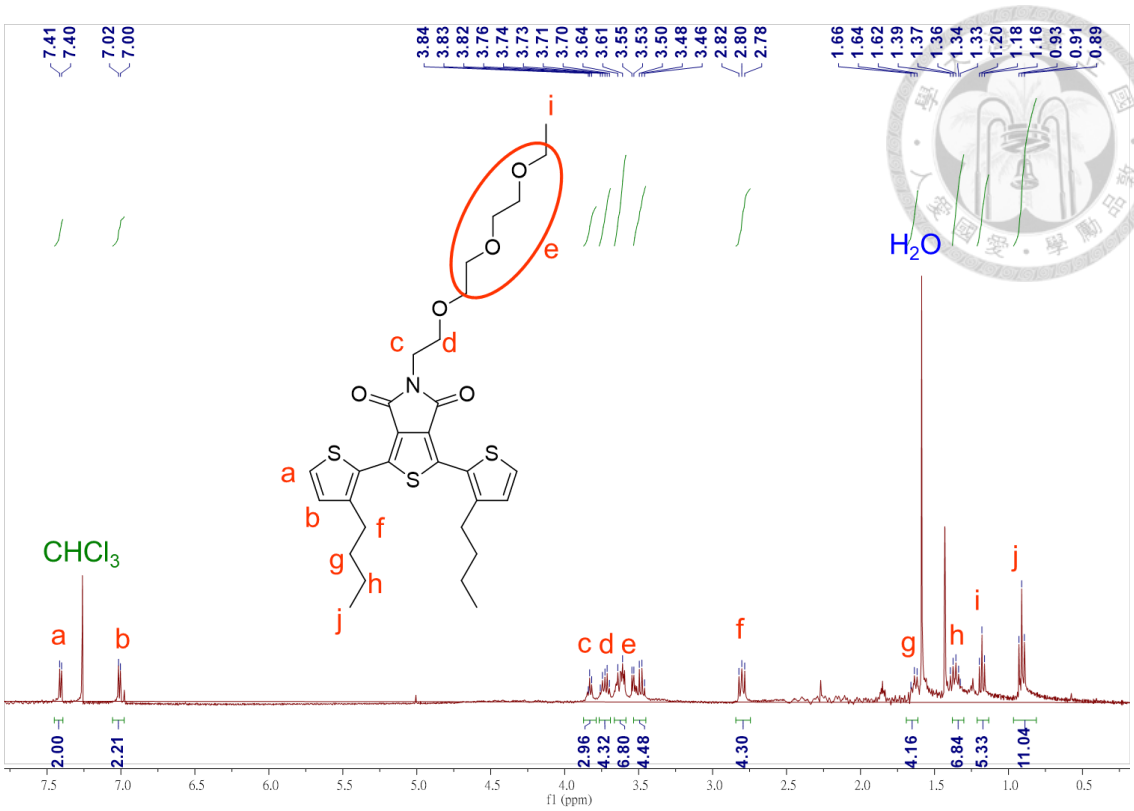

Figure 5.36. ^{1}H NMR of compound 13d

Synthesis of compound 14a

1,3-bis(5-bromo-3-octylthiophene-2-yl)-5-dodecyl-4H-thieno[3,4-c]pyrrole-4,6(5H)-dione

Compound 13a (1.00 g, 1.41 mmole), and 50 ml tetrahydrofuran were placed in 150ml round bottom flask and then 1-bromo-2,5-pyrrolidinedione (527 mg , 2.96 mmole) was added into the flask. The mixture was stirred at room temperature for 12 hours. After reaction, the tetrahydrofuran was removed by rotary evaporator and the condensed mixture was further purified by column chromatography (ether as eluent) to obtain yellow solid, compound 14a (1.15 g, 94%). ^{1}H NMR (400 MHz, $CDCl_3$) δ

doi:10.6342/NTU201904150

6.97 (s, 2H), 3.60 (t, J = 7.3 Hz, 2H), 2.76 – 2.69 (m, 4H), 1.62 (dd, J = 14.5, 7.4 Hz, 6H), 1.37 – 1.16 (m, 38H), 0.87 (td, J = 6.7, 3.7 Hz, 9H).

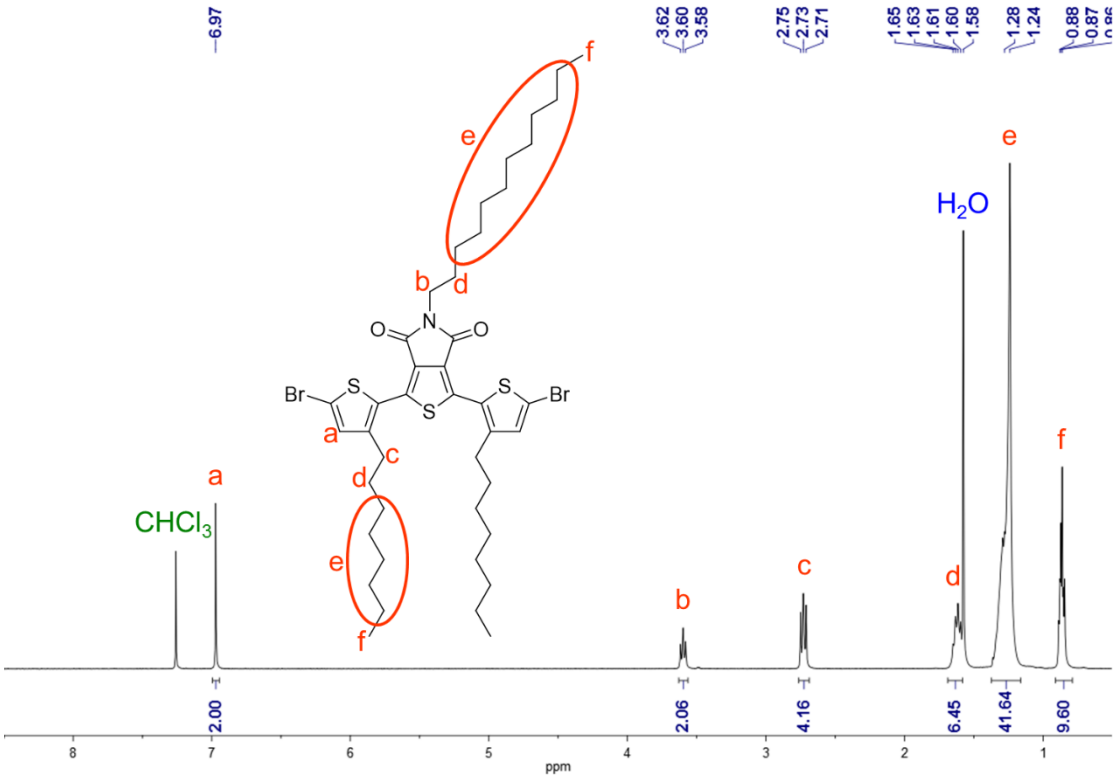

Figure 5.37. ^{1}H NMR of compound 14a

Synthesis of compound 14b

1,3-bis(5-bromo-3-octylthiophene-2-yl)-5-(2-(2-(2-ethoxyethoxy)ethoxy)ethyl)-4H-thieno[3,4-c]pyrrole-4,6(5H)-dione

Compound 13b (0.99 g, 1.41 mmole), and 50 ml tetrahydrofuran were placed in 150ml round bottom flask and then 1-bromo-2,5-pyrrolidinedione (527 mg, 2.96 mmole) was added into the flask. The mixture was stirred at room temperature for 12

doi:10.6342/NTU201904150

hours. After reaction, the tetrahydrofuran was removed by rotary evaporator and the condensed mixture was further purified by column chromatography (ether as eluent) to obtain yellow solid, compound 14b (1.13 g, 92%). ^{1}H NMR(400 MHz, $CDCl_3$) δ 6.97 (s, 2H), 3.83 (t, J = 5.8 Hz, 2H), 3.71 (t, J = 5.8 Hz, 2H), 3.67 – 3.46 (m, 10H), 2.76 – 2.69 (m, 4H), 1.66 – 1.57 (m, 4H), 1.25 (s, 20H), 1.18 (t, J = 7.0 Hz, 3H), 0.86 (t, J = 6.9 Hz, 6H).

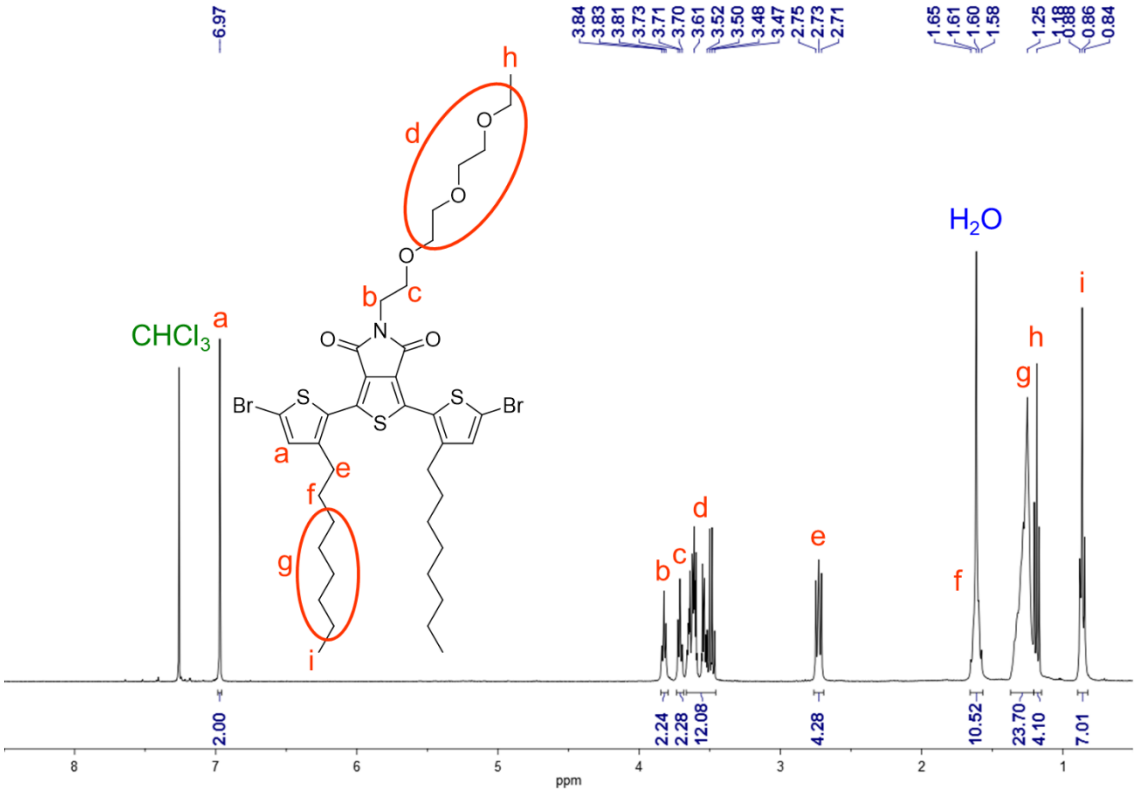

Figure 5.38. ^{1}H NMR of compound 14b

doi:10.6342/NTU201904150

Synthesis of compound 14c

1,3-bis(5-bromo-3-hexylthiophene-2-yl)-5-(2-(2-(2-ethoxyethoxy)ethoxy)ethyl)-4 H-thieno[3,4-c]pyrrole-4,6(5H)-dione

Compound 13c (0.91 g, 1.41 mmole), and 50 ml tetrahydrofuran were placed in 150ml round bottom flask and then 1-Bromo-2,5-pyrrolidinedione (527 mg, 2.96 mmole) was added into the flask. The mixture was stirred at room temperature for 12 hours. After reaction, the tetrahydrofuran was removed by rotary evaporator and the condensed mixture was further purified by column chromatography (ether as eluent) to obtain yellow solid, compound 14c (1.16 g, 93%). ^{1}H NMR(400 MHz, $CDCl_3$) δ 6.97 (s, 2H), 3.83 (t, J = 5.8 Hz, 2H), 3.71 (t, J = 5.8 Hz, 2H), 3.67 – 3.46 (m, 10H), 2.76 – 2.69 (m, 4H), 1.66 – 1.57 (m, 4H), 1.25 (s, 12H), 1.18 (t, J = 7.0 Hz, 3H), 0.86 (t, J = 6.9 Hz, 6H).

doi:10.6342/NTU201904150

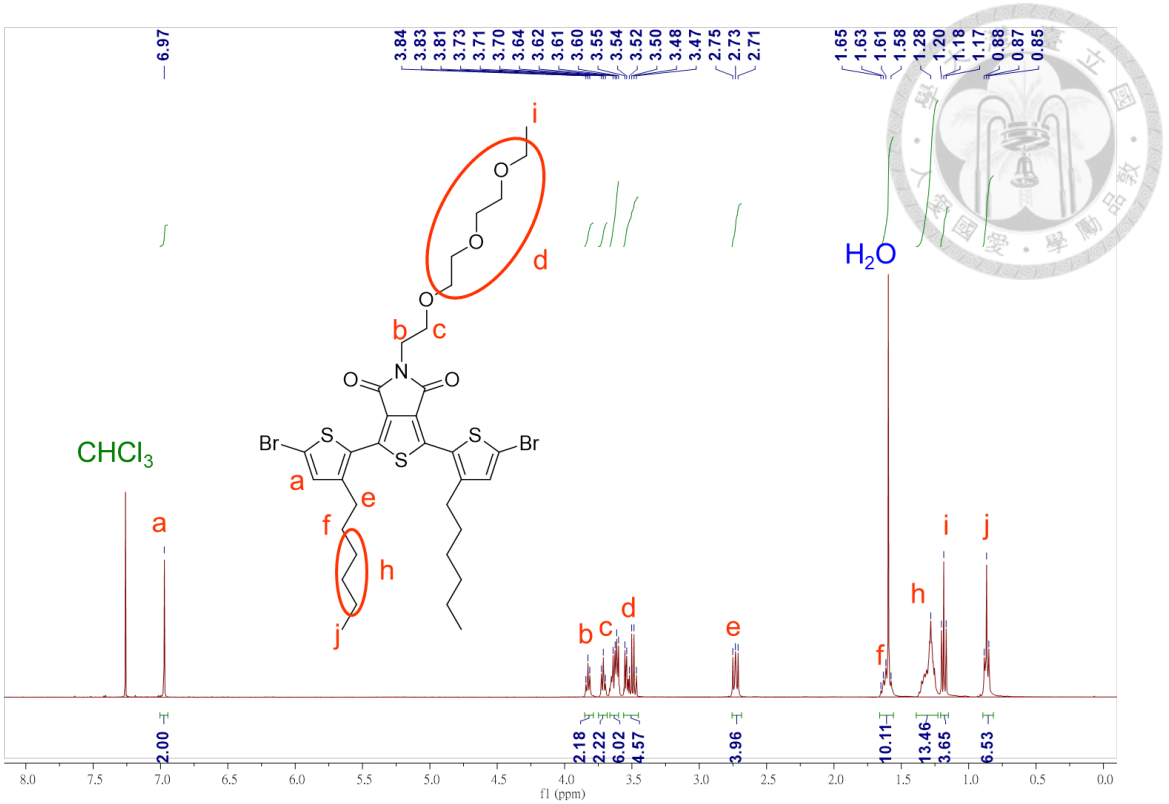

Figure 5.39. ^{1}H NMR of compound 14c

Synthesis of compound 14d

1,3-bis(5-bromo-3-butylthiophene-2-yl)-5-(2-(2-(2-ethoxyethoxy)ethoxy)ethyl)-4H -thieno[3,4-c]pyrrole-4,6(5H)-dione

Compound 13d (0.83 g, 1.41 mmole), and 50 ml tetrahydrofuran were placed in 150ml round bottom flask and then 1-bromo-2,5-pyrrolidinedione (527 mg, 2.96 mmole) was added into the flask. The mixture was stirred under room temperature for 12 hours. After reaction, the tetrahydrofuran was removed by rotary evaporator and the condensed mixture was further purified by column chromatography (ether as eluent) to obtain yellow solid, compound 14d (1.15 g, 91%). ^{1}H NMR(400 MHz,

doi:10.6342/NTU201904150

$CDCl_3$) δ 6.97 (s, 2H), 3.83 (t, J = 5.8 Hz, 2H), 3.71 (t, J = 5.8 Hz, 2H), 3.67 – 3.46 (m, 10H), 2.76 – 2.69 (m, 4H), 1.66 – 1.57 (m, 4H), 1.25 (s, 4H), 1.18 (t, J = 7.0 Hz, 3H), 0.86 (t, J = 6.9 Hz, 6H).

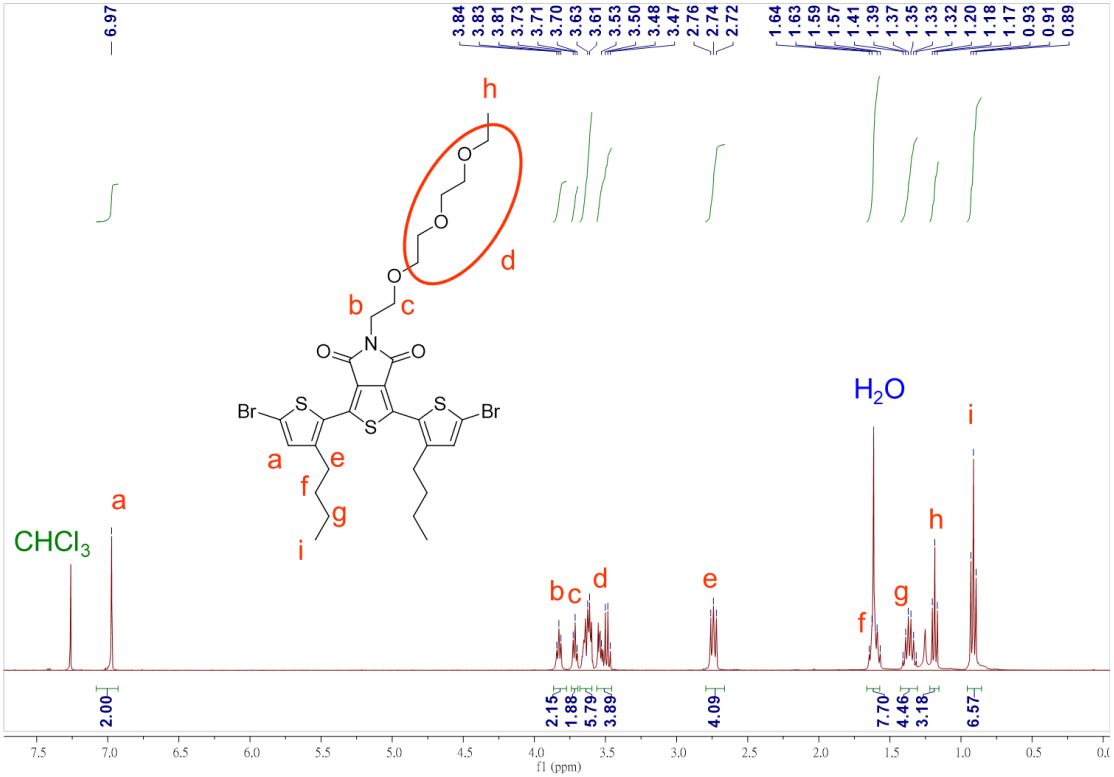

Figure 5.40. ^{1}H NMR of compound 14d

doi:10.6342/NTU201904150

General procedure for polymerization of oligothiophene-TPD based CPs.

The two monomers (0.2 mmole each), tris(dibenzylideneacetone)dipalladium(0) (10 mg, 0.01 mmole), **tris(*o*-tolyl)phosphine** (15 mg, 0.05 mmole) and 4 ml degassed tetrahydrofuran were placed in a 10ml microwave vessel to do the Still coupling polymerization by microwave reactor. The parameters for the reaction were set at 100 ^{o}C, 100 W, and 15 min. After polymerization, the polymers were precipitated in methanol then subjected to purification via Soxhlet extractions using a specific solvent sequence, methanol→acetone→hexane→tetrahydrofuran→chloroform. Then we collected the chloroform solutions, removed the chloroform by rotary evaporator, and finally acquired pure polymers. The information of the monomers used in polymerization and the yield is shown in **Table 5.3.** The molecular weights of these polymers are measured by gel permeation chromatography (GPC) vs. polystyrene standards using chloroform as eluent. The molecular weight information of all synthesized TPD-based CPs is shown in **Table 5.4**.

doi:10.6342/NTU201904150

Table 5.3. Monomers used in polymerization and polymer yield

Polymers	Monomer 1	Monomer 2	Yield
P3T(R_{o8})TPD(R)	14a		33%
P3T(R_{o8})TPD(E)	14b		39%
P3T(R_{o6})TPD(E)	14c		26%
P3T(R_{o4})TPD(E)	14d	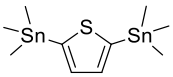	29%
P3T(R_{i8})TPD(R)	12a		71%
P3T(R_{i8})TPD(E)	12b		80%
P3T(R_{i6})TPD(E)	12c		76%
P3T(R_{i4})TPD(E)	12d		68%

doi:10.6342/NTU201904150

Table 5.4. Summary of molecular weight of 3T-TPD based CPs

Polymers	Mn(KDa)	Mw(KDa)	PDI
P3T(R_{o8})TPD(R)	3.65	5.73	1.57
P3T(R_{o8})TPD(E)	7.06	14.82	2.10
P3T(R_{o6})TPD(E)	4.69	9.56	2.04
P3T(R_{o4})TPD(E)	4.23	7.69	1.82
P3T(R_{i8})TPD(R)	4.07	4.69	1.15
P3T(R_{i8})TPD(E)	6.09	6.87	1.13
P3T(R_{i6})TPD(E)	4.08	4.79	1.17
P3T(R_{i4})TPD(E)	3.11	3.74	1.20

doi:10.6342/NTU201904150

5.2.2 Oligothiophene-isoindigo based Conjugated Polymers

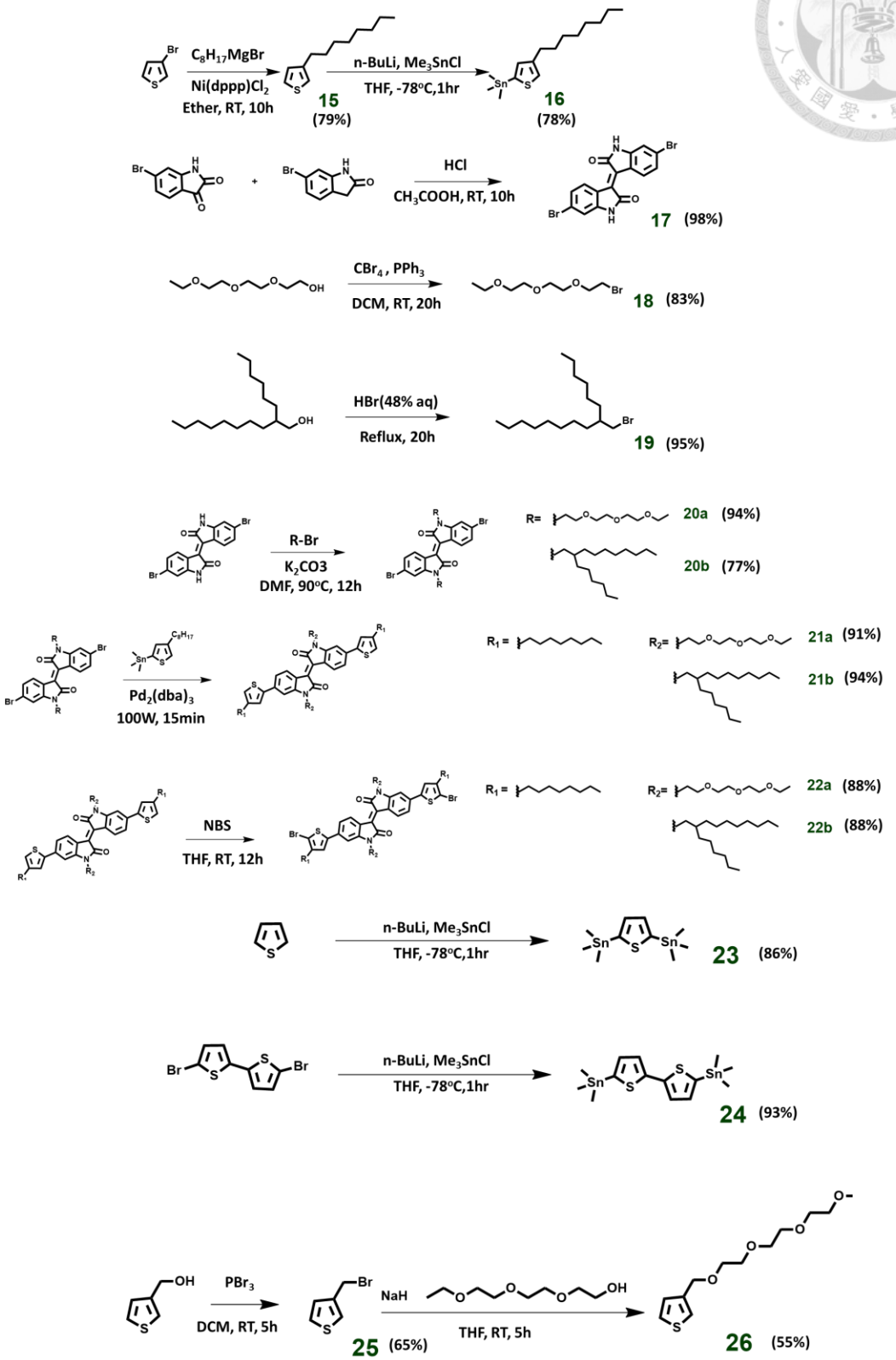

Figure 5.41. Synthetic scheme of compound 15~ compound 26

doi:10.6342/NTU201904150

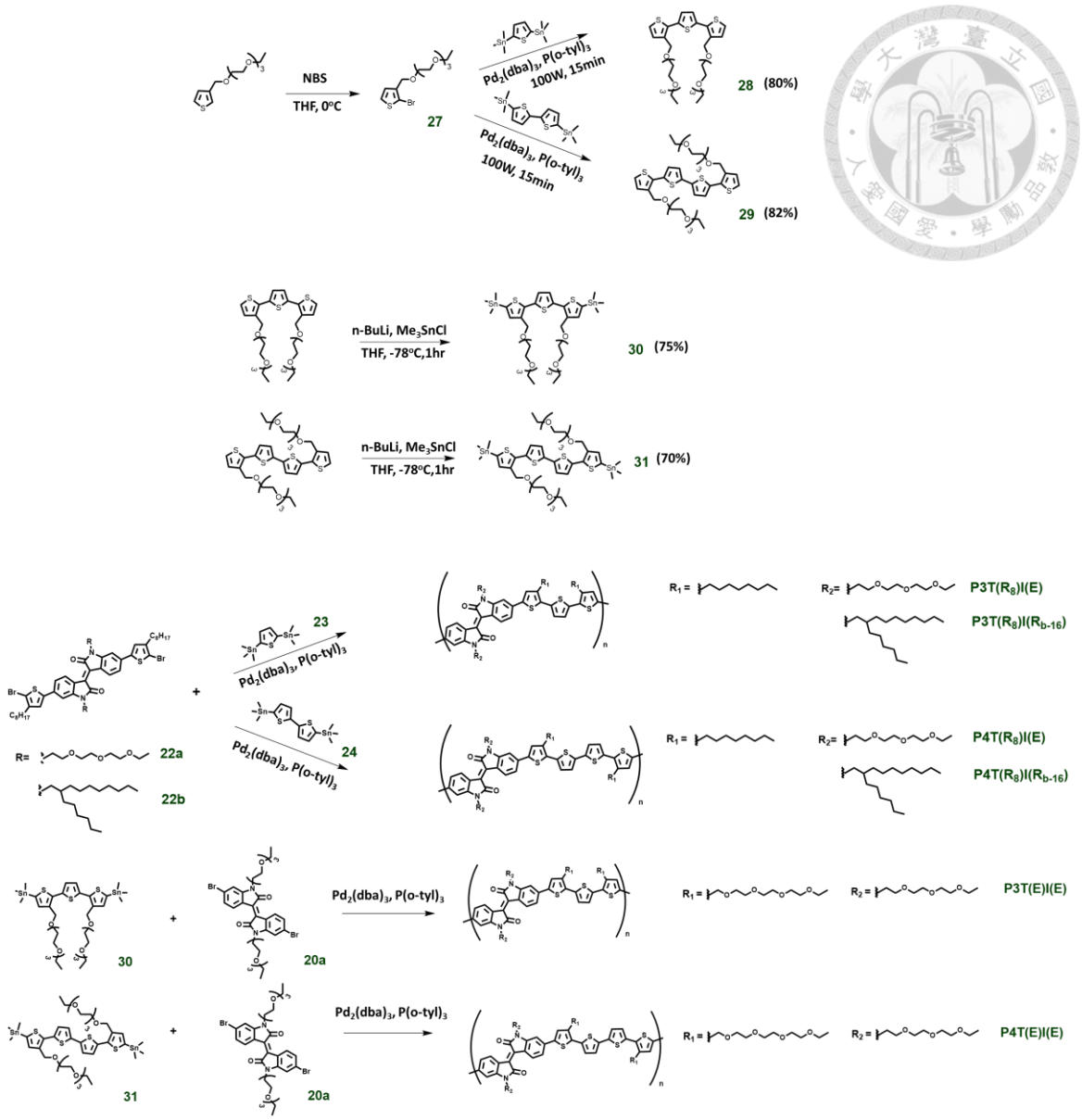

Figure 5.42. Synthetic scheme of compound 27 ~ compound 31 and PnTI polymers

doi:10.6342/NTU201904150

Synthesis of compound 15

3-octylthiophene

A 500 ml round bottom flask (flask A) and a 1000 ml round bottom flask (flask B) were evacuated by vacuum system and refilled the nitrogen to remove the moisture in the flask. Then, magnesium (8.95 g, 0.37 mole) and 300 ml anhydrous ether were placed in the flask A, and 3-bromothiophene (30.00 g, 0.18 mole), [1,3-Bis(diphenylphosphino)propane]dichloronickel(II) (200 mg, 0.37 mmole), and 300 ml anhydrous ether were placed in the flask B. Then the flask A was put in 0 ^{o}C ice bath and 1-bromooctane (53.30 g, 0.28 mole) was added into the flask A through syringe slowly in 2 hours. After complete adding 1-bromooctane, the mixture was stirred under room temperature for 2 hours. Then, the solution in the flask A was transferred in the flask B. After that, the mixture was stirred under room temperature for 10 hours. Then, 200 ml 1M hydrochloric acid was added into the flask B to terminate the reaction and the solution was extracted by using ether and distilled water. The organic layer was collected, dried over anhydrous magnesium sulfate, and filtered by filter paper. The filtrate was collected and the ether was removed by rotary evaporator. Finally, the condensed mixture can be further purified by distillation under reduced pressure (60 ^{o}C, 0.08 torr) to obtain colorless oil, compound 15 (28.54 g, 79%). ^{1}H NMR (400 MHz, $CDCl_3$) δ 7.23 (dd, J = 4.9, 2.9 Hz, 1H), 6.93 (dd, J = 6.6,

doi:10.6342/NTU201904150

3.9 Hz, 2H), 2.62 (t, *J* = 7.8 Hz, 2H), 1.68 – 1.57 (m, 2H), 1.35 – 1.22 (m, 10H), 0.88 (t, *J* = 6.8 Hz, 3H). ^{13}C NMR (100 MHz, $CDCl_3$, δ): 143.63, 128.64, 125.36, 120.10, 32.24, 30.92, 30.65, 30.06, 29.71, 23.02, 14.45.

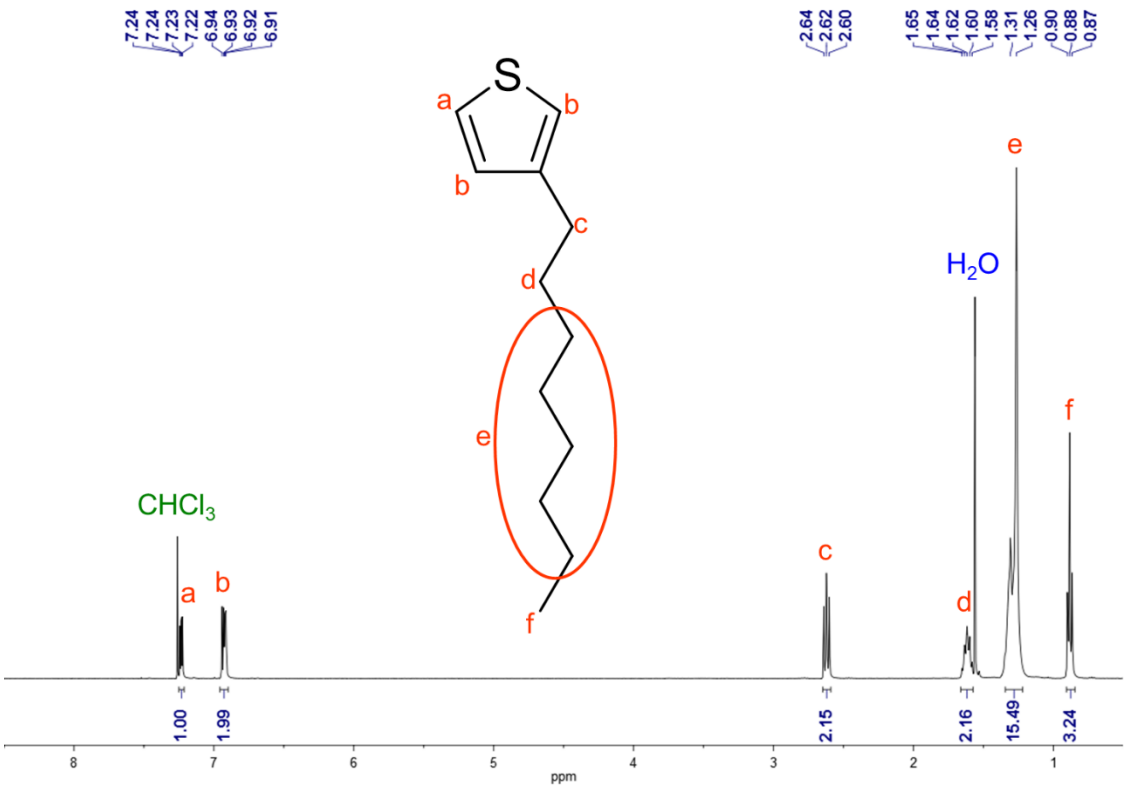

Figure 5.43. ^{1}H NMR of compound 15

Synthesis of compound 16

trimethyl(4-octylthiophene-2-yl)stannane

A 150 ml round bottom flask was evacuated by vacuum system and refilled the nitrogen to remove the moisture in the flask. Next, compound 15 (4.91 g, 25 mmole) and 50 ml anhydrous tetrahydrofuran were placed in the flask. After that, the flask

doi:10.6342/NTU201904150

was put in -78°C dry ice bath. Then, 10 ml 2.5M n-butyllithium in hexane solution (25 mmole) was added into the flask and the solution was stirred for 2 hours. The -78°C dry ice bath was removed and the solution was stirred at room temperature for 1 hour. Then the flask was put in -78°C dry ice bath again and 25 ml 1M trimethyltin chloride in tetrahydrofuran solution (25 mmole) was added into the flask. After complete adding the trimethyltin chloride solution, the -78°C dry ice bath was removed and the solution was stirred at room temperature for 12 hours. The mixture was extracted by hexane and distilled water. The organic layer was collected, dried over anhydrous magnesium sulfate, and filtered by filter paper. The filtrate was collected and the hexane was removed by rotary evaporator. Finally, the condensed mixture can be further purified by column chromatography (hexane as eluent, celite gel) to obtain pale yellow oil, compound 16 (7.03 g, 78%). ^{1}H NMR (400 MHz, $CDCl_3$) δ 7.19 (d, *J* = 0.8 Hz, 1H), 7.01 (s, 1H), 2.65 (t, *J* = 7.8 Hz, 2H), 1.63 (quintet, *J* = 7.5 Hz, 2H), 1.29 (d, *J* = 21.8 Hz, 10H), 0.88 (t, *J* = 6.8 Hz, 3H), 0.35 (s, 9H). ^{13}C NMR (100 MHz, $CDCl_3$, δ): 144.97,137.00, 125.99, 33.25, 31.11, 30.34, 30.06, 29.86, 29.90, 29.62, 23.03, 14.46, -7.94.

doi:10.6342/NTU201904150

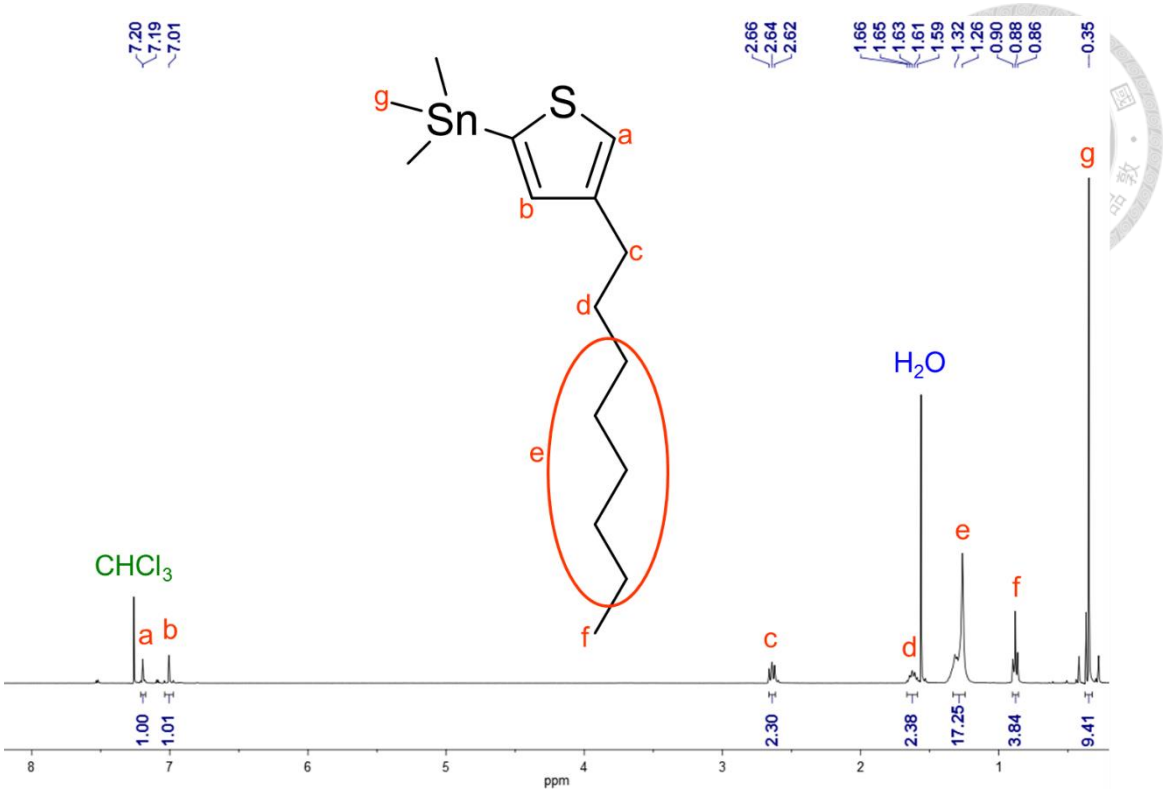

Figure 5.44. ^{1}H NMR of compound 16

Synthesis of compound 17

(E)-6,6'-dibromo-[3,3'-biindolinylidene]-2,2'-dione

6-bromooxindole (23.45g, 0.11mole), 6-bromoisatin (25.00g, 0.11mole), 750 ml acetic acid, and 5 ml hydrochloric acid were placed in a 1000 ml flask. The mixture was heated to reflux for 24 hours. Then the mixture was filtered by filter paper and washed by methanol several times until the filtrate was neutral. Finally, the solid was collected and dried to obtain dark red solid, compound 17 (45.53g, 98%). ^{1}H NMR (400MHz, D_6-DMSO) δ 11.11(s, 2H), 9.03(d, *J*=8.6Hz, 2H), 7.22(d, *J*=8.7Hz, 2H), 7.03(s, 2H). ^{13}C NMR (100 MHz, $CDCl_3$, δ): 168.14, 146.22, 132.46, 131.02, 126.53,

doi:10.6342/NTU201904150

125.12, 120.23, 111.54.

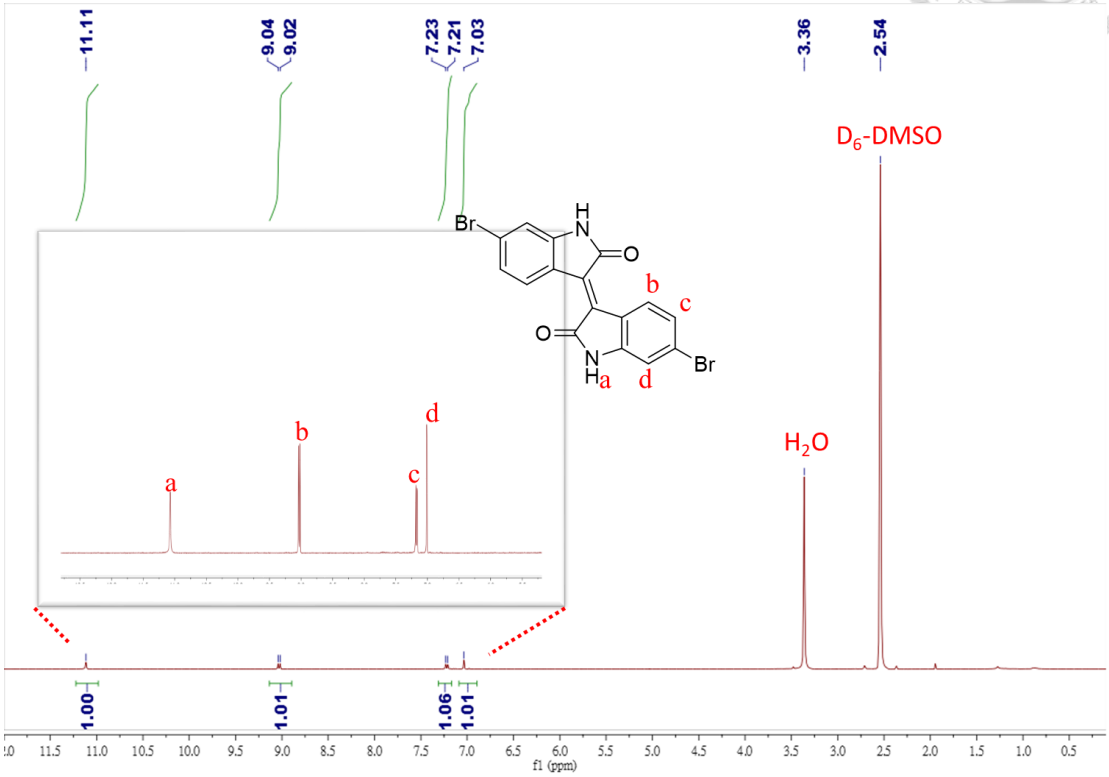

Figure 5.45. ^{1}H NMR of compound 17

Synthesis of compound 18

1-bromo-2-(2-(2-ethoxyethoxy)ethoxy)ethane

2-(2-(2-ethoxyethoxy)ethoxy)ethanol (10.00 g, 56.11 mmole) and tetrabromomethane (24.19 g, 72.94 mmole) were dissolved in 100 ml of anhydrous dichloromethane and then the solution was cooled to 0℃ in ice bath. A solution of triphenylphosphine (17.66 g, 67.33 mmole) in 100 ml of anhydrous dichloromethane was slowly transferred into the aforementioned low temperature solution. After the transfer was

doi:10.6342/NTU201904150

finished, ice bath was removed and the solution was reacted at ambient temperature under stirring for 20 hours. Then, the dichloromethane was removed by rotary evaporator. The sticky yellow solid was obtained and it was washed several times by ether. The combined ether solution was concentrated, and then distilled under vacuum (100 ^{o}C, 0.08 torr) to obtain colorless oil, compound 18 (11.21 g, 83 %). ^{1}H NMR (400 MHz, $CDCl_3$) δ 3.81 (t, *J* = 6.4 Hz, 2H), 3.70 – 3.63 (m, 6H), 3.59 (m, 2H), 3.52 (q, *J* = 7.0 Hz, 2H), 3.47 (t, *J* = 6.4 Hz, 2H), 1.21 (t, *J* = 7.0 Hz, 3H). ^{13}C NMR (100 MHz, $CDCl_3$, δ): 71.24, 70.25, 66.21, 41.00, 15.25.

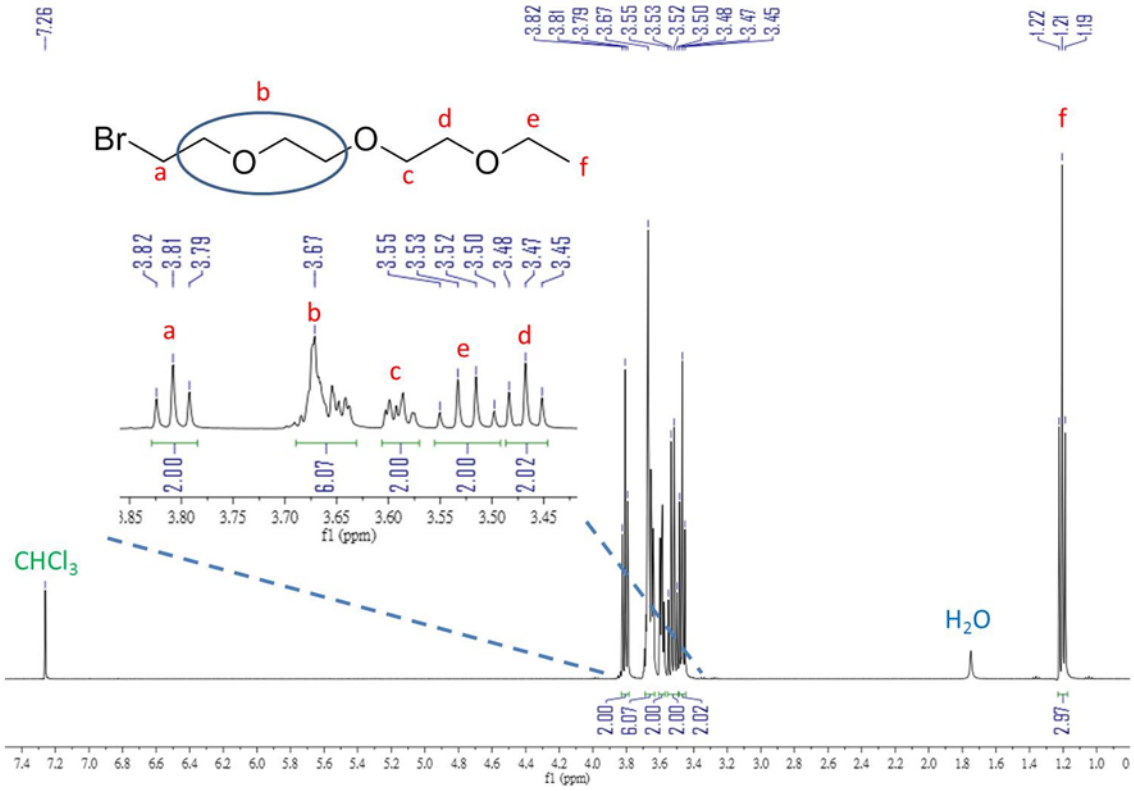

Figure 5.46. ^{1}H NMR of compound 18

doi:10.6342/NTU201904150

Synthesis of compound 19

7-(bromomethyl)pentadecane

2-hexyl-1-decanol (40.00 g, 0.17 mole) and 48wt% hydrogen bromide aqueous solution (100.00 g, 0.49 mole) were placed in a 250 ml flask. The mixture was heated to reflux for 10 hours. The mixture was extracted by hexane and distilled water. The organic layer was collected, dried over anhydrous magnesium sulfate, and filtered by filter paper. The filtrate was collected and the hexane was removed by rotary evaporator. The condensed mixture was further purified by column chromatography (toluene as eluent) to obtain colorless oil, compound 19 (47.86g, 95%). ^{1}H NMR (400MHz, $CDCl_3$) δ 3.45(d, *J*=4.8Hz, 2H), 1.63-1.55(m, 1H), 1.45-1.17(m, 24H), 0.93-0.81(m, 6H). ^{13}C NMR (100 MHz, $CDCl_3$, δ): 40.07, 39.88, 32.93, 32.24, 32.16, 30.14, 29.90, 29.81, 29.65, 26.89, 23.03, 14.45.

doi:10.6342/NTU201904150

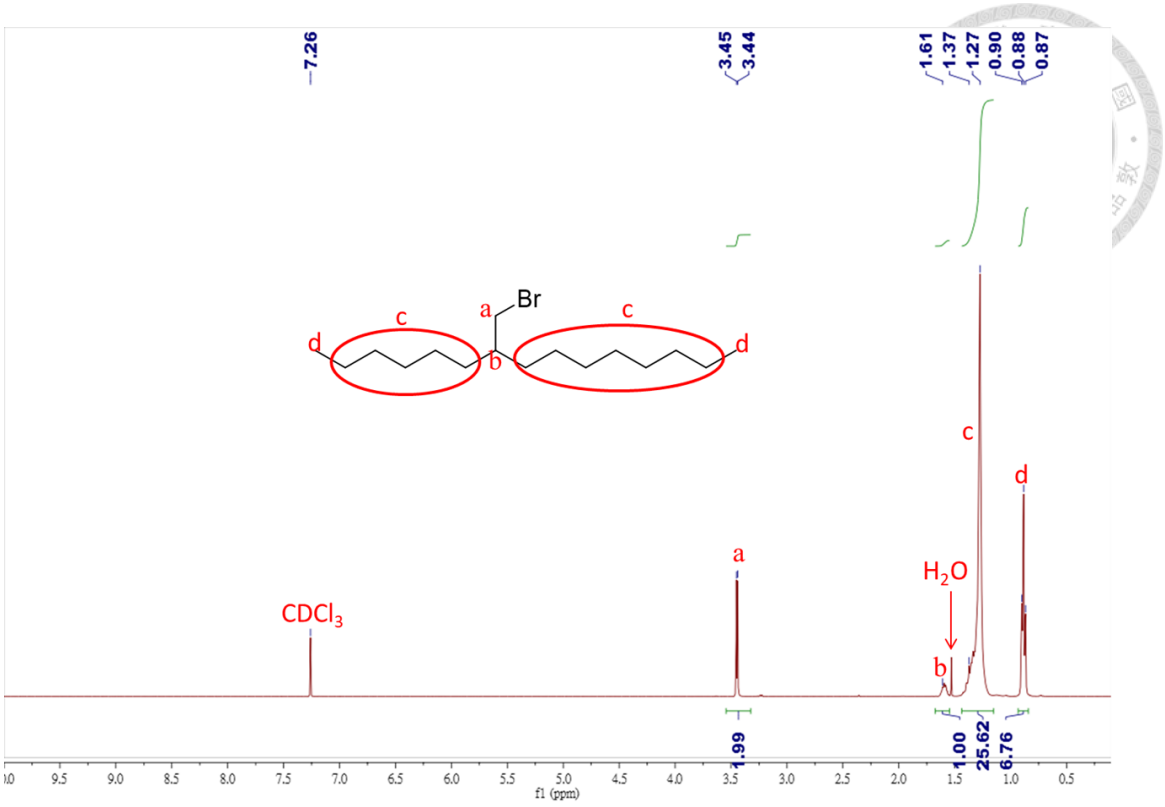

Figure 5.47. ^{1}H NMR of compound 19

Synthesis of compound 20a

(E)-6,6'-dibromo-1,1'-bis(2-(2-(2-ethoxyethoxy)ethoxy)ethyl)-[3,3'-biindolinylidene]-2,2'-dione

Compound 17 (5.00 g, 11.90 mmole), compound 18 (6.76 g, 29.76 mmole) and anhydrous potassium carbonate (8.22 g, 59.5 mmole) were placed in a round bottom flask. 100 ml of anhydrous dimethylformamide was added and the mixture was reacted at 90 ^{o}C for 12 hours under stirring. After the solution was cooled to ambient temperature, the mixture was extracted with ether and distilled water several times. The combined organic layers were dried over anhydrous magnesium sulfate and the

doi:10.6342/NTU201904150

solution was filtered. Ether was removed by rotary evaporator, and the solid product was purified by silica gel column chromatography with ether as eluent. After removal of ether, the product was recrystallized from cold hexane. The red solid was collected by filtration, compound 20a (8.28 g, 94%). ^{1}H NMR (400 MHz, acetone) δ 9.14 (d, J = 8.6 Hz, 2H), 7.33 (d, J = 1.9 Hz, 2H), 7.19 (dd, J = 8.6, 1.9 Hz, 2H), 4.02 (t, J = 5.4 Hz, 4H), 3.78 (t, J = 5.4 Hz, 4H), 3.61 – 3.36 (m, 20H), 1.08 (t, J = 7.0 Hz, 6H). ^{13}C NMR (100 MHz, $(CD_3)_2CO$, δ): 168.49, 147.67, 133.22, 131.89, 127.13, 125.41, 121.29, 113.49, 71.46, 70.68, 66.84, 41.22, 15.65.

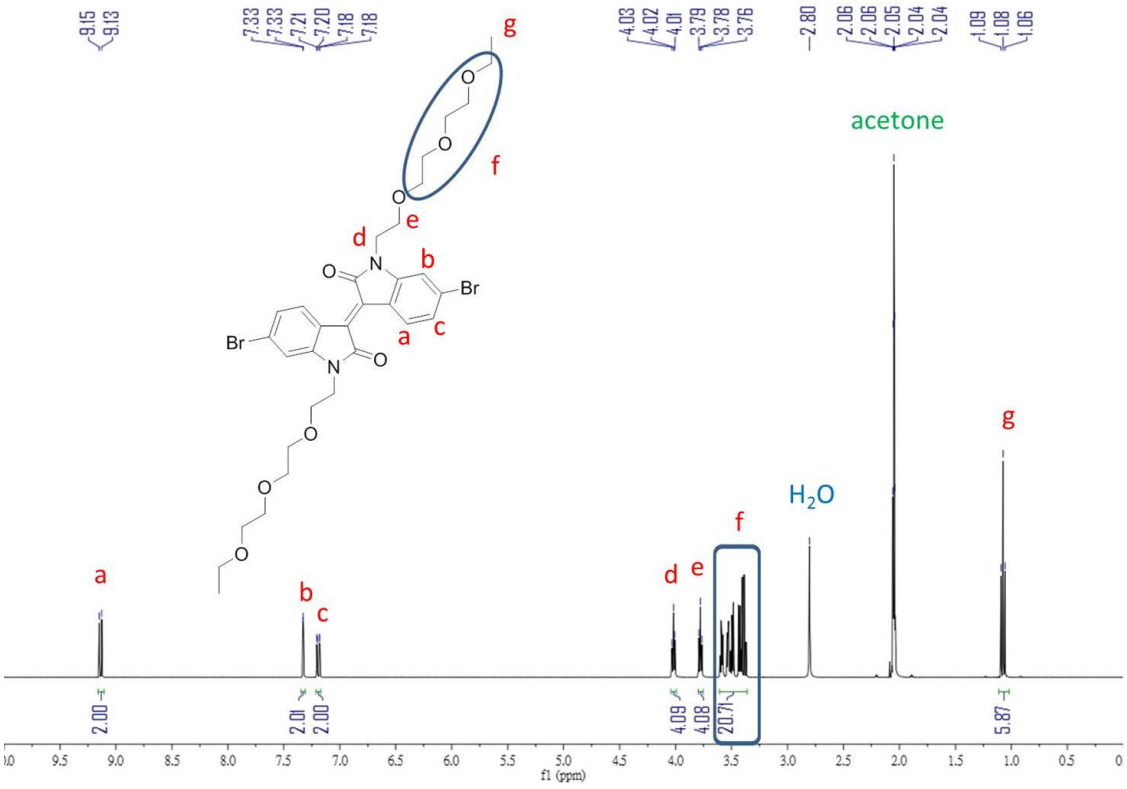

Figure 5.48. ^{1}H NMR of compound 20a

doi:10.6342/NTU201904150

Synthesis of compound 20b

(E)-6,6'-dibromo-1,1'-bis(2-hexyldecyl)-[3,3'-biindolinylidene]-2,2'-dione

Compound 17 (5.00 g, 11.90 mmole), compound 19 (9.08 g, 29.76 mmole) and anhydrous potassium carbonate (8.22 g, 59.5 mmole) were used to do the reaction. Following the synthetic procedure of compound 20a, (5.86 g, 77%), and the solid product was purified by silica gel column chromatography with solvent mixture hexane: dichloromethane = 2: 1 (v/v) as eluent. After removal of the solvents, the product was recrystallized from methanol. The reddish solid was collected by filtration, compound 20b (9.82 g, 95%). ^{1}H NMR (400 MHz, $CDCl_3$) δ 9.06 (d, *J* = 8.6 Hz, 2H), 7.15 (dd, *J* = 8.6, 1.8 Hz, 2H), 6.88 (d, *J* = 1.7 Hz, 2H), 3.61 (d, *J* = 7.5 Hz, 4H), 1.91-1.83 (m, 2H), 1.39 – 1.20 (m, 24H), 0.86 (m, *J* = 6.8 Hz, 6H). ^{13}C NMR (100 MHz, $CDCl_3$, δ): 168.34, 146.49, 132.78, 131.41, 126.97, 125.36, 120.69, 111.78, 44.98, 36.42, 32.21, 32.15, 31.94, 31.85, 30.32, 29.99, 29.89, 29.64, 26.71, 23.00, 14.40.

doi:10.6342/NTU201904150

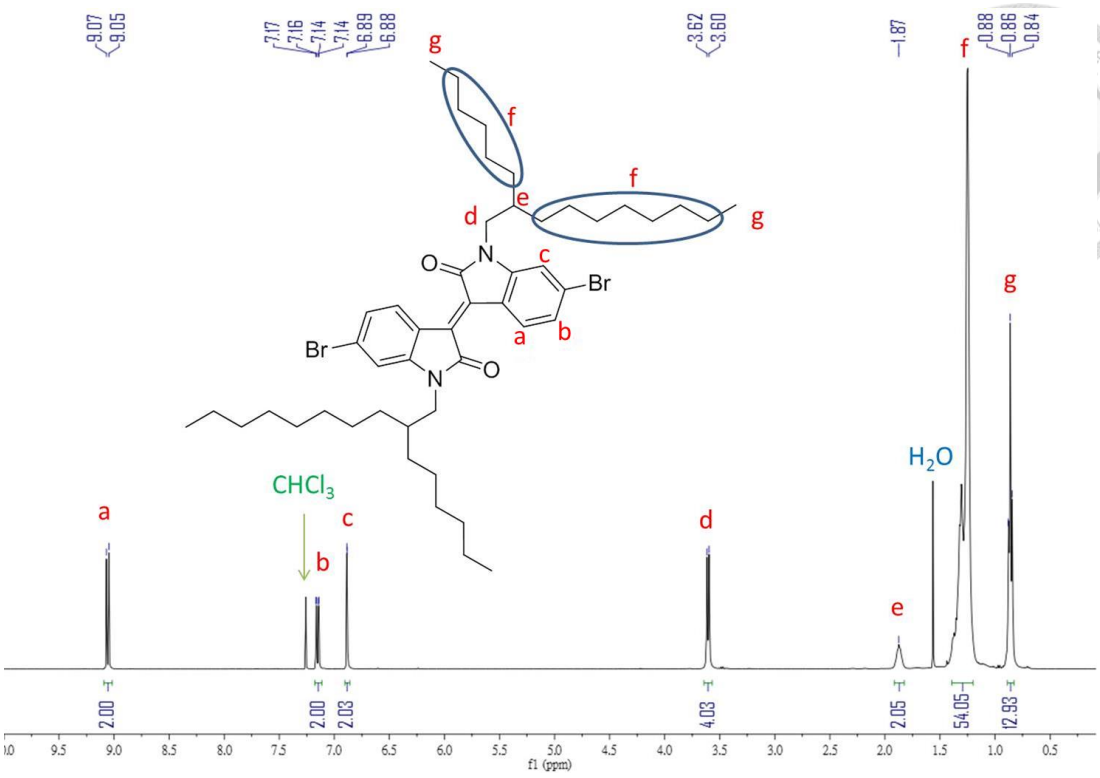

Figure 5.49. ^{1}H NMR of compound 20b

Synthesis of compound 21a

(E)-1,1'-bis(2-(2-(2-ethoxyethoxy)ethoxy)ethyl)-6,6'-bis(4-octylthiophene-2-yl)-[3, 3'-biindolinylidene]-2,2'-dione

Compound 20a (1.50 g, 2.03 mmole), compound 16 (2.19 g, 6.09 mmole), tris(dibenzylideneacetone)dipalladium(0) (92.7 mg, 0.10 mmole), and tri(o-tolyl)phosphine (61.8 mg , 0.20 mmole) were added to a 10 ml microwave tube. After being capped with Teflon septum, the tube was vacuumed and refilled with nitrogen three times. Anhydrous tetrahydrofurane (3 ml) was added to the tube via syringe. The parameter of microwave was set to be 90 ºC, 100 W and 15 minutes

doi:10.6342/NTU201904150

under standard mode. After the tube was cooled down, the mixture was concentrated and then purified by silica gel column chromatography with ether as eluent. Ether was then removed under reduced pressure, and the residual sticky product was recrystallized in cold hexane to obtain dark red solid, compound 21a (1.79 g, 91 %). ^{1}H NMR (400 MHz, $CDCl_3$) δ 9.13 (d, *J* = 8.4 Hz, 2H), 7.28 (dd, *J* = 4.2, 1.5 Hz, 3H), 7.25 (d, *J* = 1.9 Hz, 1H), 7.16 (d, *J* = 1.7 Hz, 2H), 6.94 (d, *J* = 1.1 Hz, 2H), 4.05 (t, *J* = 5.8 Hz, 4H), 3.79 (t, *J* = 5.7 Hz, 4H), 3.67 – 3.63 (m, 4H), 3.62 – 3.59 (m, 4H), 3.56 – 3.52 (m, 4H), 3.48 – 3.42 (m, 8H), 2.65 – 2.61 (m, 4H), 1.67 (quintet, *J* = 7.5 Hz,4H), 1.42 – 1.24 (m, 6H), 1.16 (t, *J* = 7.0 Hz, 6H), 0.89 (t, *J* = 6.9 Hz, 6H). ^{13}C NMR (100 MHz, $CDCl_3$, δ): 168.49, 147.67, 145.04, 144.06, 138.31, 133.22, 131.89, 127.13, 125.41, 121.29, 113.49, 71.46, 70.68, 66.84, 41.22, 32.24, 30.83, 30.02, 29.75, 15.65.

doi:10.6342/NTU201904150

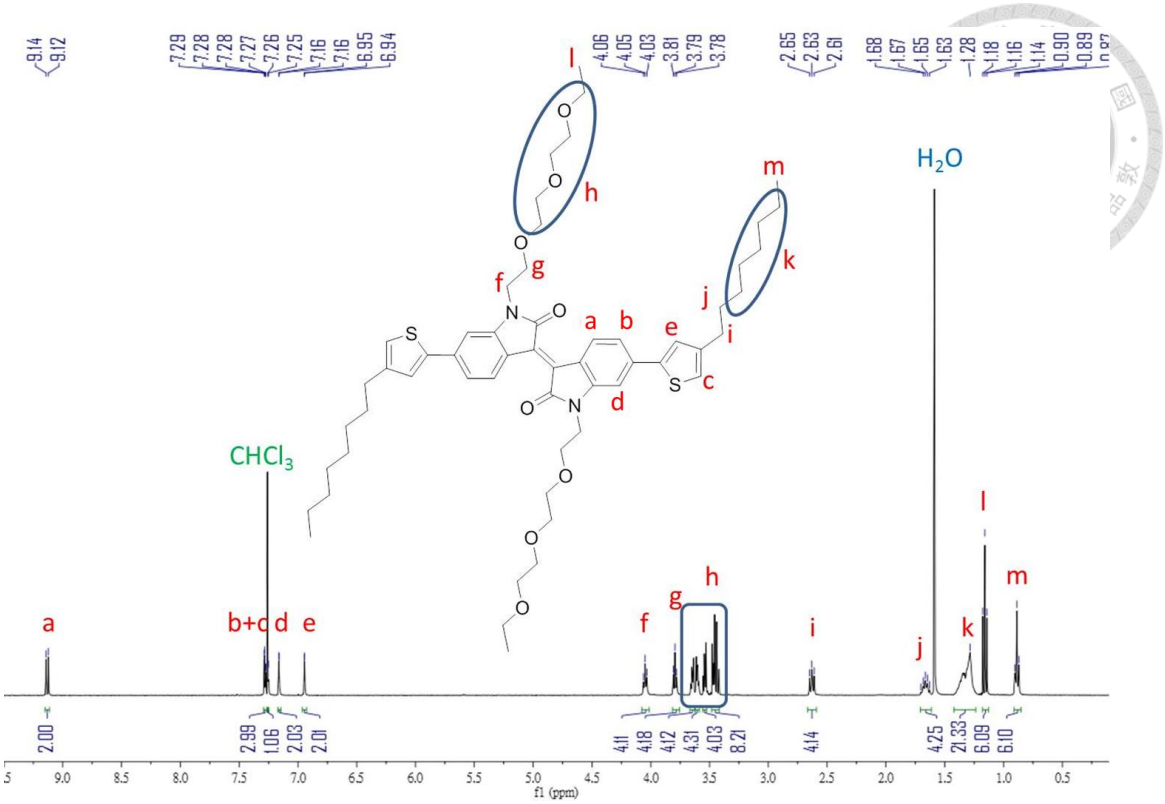

Figure 5.50. ^{1}H NMR of compound 21a

Synthesis of compound 21b

(E)-1,1'-bis(2-hexyldecyl)-6,6'-bis(4-octylthiophene-2-yl)-[3,3'-biindolinylidene]-2,2'-dione

Compound 20b (1.50 g, 1.73 mmole), compound 16 (1.86 g, 5.18 mmole), tris(dibenzylideneacetone)dipalladium(0) (79.0 mg, 0.08 mmole), and tri(o-tolyl)phosphine (52.5 mg, 0.17 mmole) were added to a 10ml microwave tube. After being capped with Teflon septum, the tube was vacuumed and refilled with nitrogen three times. Anhydrous tetrahydrofurane (3.5ml) was added to the tube via syringe. The parameter of microwave was set to be 90 ºC, 100 W and 15 minutes

doi:10.6342/NTU201904150

under standard mode. After the tube was cooled down, the mixture was concentrated and purified by silica gel column chromatography with solvent mixture hexane: dichloromethane = 2: 1 (v/v) as eluent. Solvents were then removed under reduced pressure, and the residue sticky product was recrystallized in methanol to obtain dark red solid, compound 21b (1.78 g, 94 %). ^{1}H NMR (400 MHz, $CDCl_3$) δ 9.15 (d, J = 8.4 Hz, 2H), 7.29 – 7.23 (m, 4H), 7.24 (s, 2H), 6.98 – 6.93 (m, 4H), 3.70 (d, J = 7.2 Hz, 4H), 2.63 (t, J = 7.7 Hz, 4H), 1.97 – 1.88 (m, 2H), 1.66 (quintet, J = 7.3 Hz, 4H), 1.44 – 1.18 (m, 68H), 0.91 – 0.82 (m, 18H). ^{13}C NMR (100 MHz, $CDCl_3$, δ): 169.00, 146.11, 145.04, 144.06, 138.31, 132.23, 130.47, 125.88, 121.28, 121.18, 119.37, 105.21, 44.77, 36.75, 32.24, 32.14, 30.83, 30.36, 30.02, 29.96, 29.81, 29.75, 29.65, 27.00, 23.02, 14.45.

doi:10.6342/NTU201904150

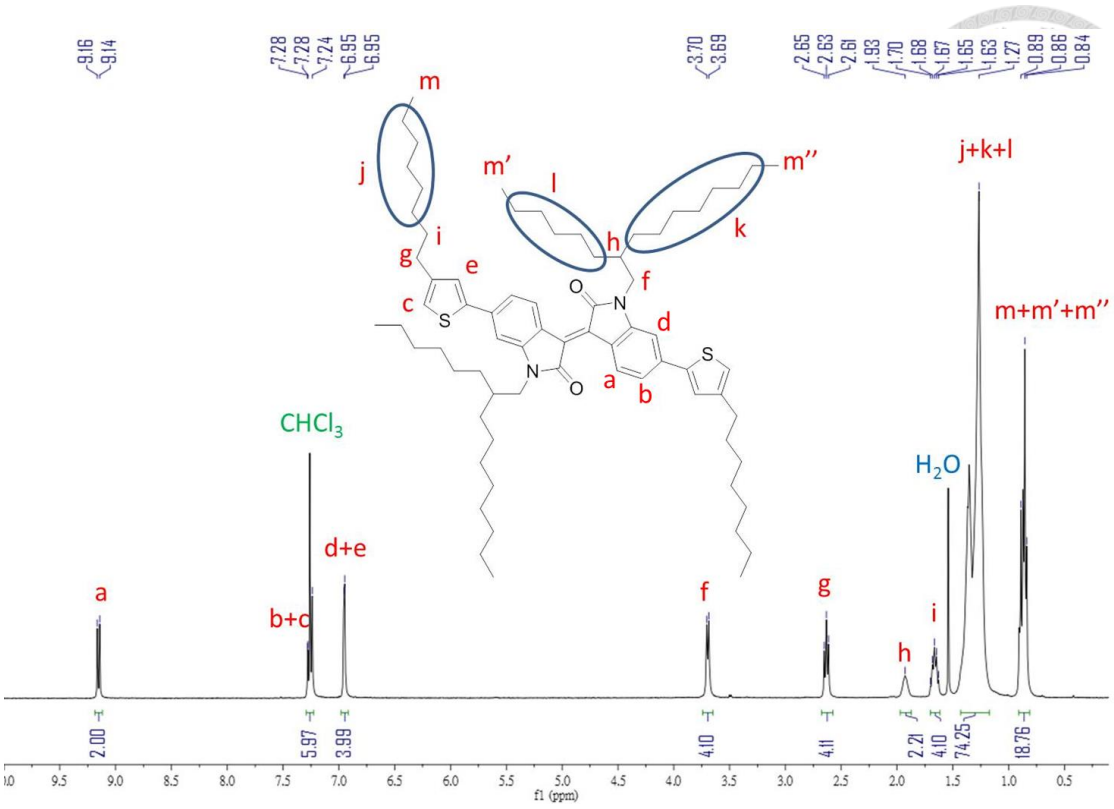

Figure 5.51. ^{1}H NMR of compound 21b

Synthesis of compound 22a

(E)-6,6'-bis(5-bromo-4-octylthiophene-2-yl)-1,1'-bis(2-(2-(2-ethoxyethoxy)ethoxy) ethyl)-[3,3'-biindolinylidene]-2,2'-dione

Compound 21a (3.00 g, 3.09 mmole) was dissolved in tetrahydrofurane (100ml), and the round bottom flask containing reaction mixture was wrapped by a layer of alumina foil to prevent light. 1-bromo-2,5-pyrrolidinedione (1.12 g, 6.33 mmole) was divided into 4 portions and each portion was added to the solution at an interval of 15 minutes. After being stirred in the dark for 12 hours to carry out the reaction, the solution was concentrated and then was purified by a flash column chromatography of

doi:10.6342/NTU201904150

silica gel with ether as eluent. Ether was then evaporated under reduced pressure, and the sticky residue was recrystallized in methanol. The dark purple solid, compound 22a (3.0 g, 88%) was obtained after filtration and dried in vacuum oven overnight. ^{1}H NMR (400 MHz, $CDCl_3$) δ 9.13 (d, *J* = 8.4 Hz, 2H), 7.17 (dd, *J* = 8.4, 1.8 Hz, 2H), 7.13 (s, 2H), 7.08 (d, *J* = 1.6 Hz, 2H), 4.03 (t, *J* = 5.6 Hz, 4H), 3.78 (t, *J* = 5.6 Hz, 4H), 3.66 – 3.62 (m, 4H), 3.62 – 3.58 (m, 4H), 3.56 – 3.52 (m, 4H), 3.49 – 3.42 (m, 8H), 2.58 (t, *J* = 7.8 Hz, 3H), 1.64 (quintet, *J* = 7.3Hz, 2H), 1.41 – 1.25 (m, 20H), 1.16 (t, *J* = 7.0 Hz, 6H), 0.89 (t, *J* = 6.9 Hz, 6H). ^{13}C NMR (100 MHz, $CDCl_3$, δ): 168.89, 147.81, 145.25, 144.06, 138.71, 133.62, 131.89, 127.13, 125.41, 121.37, 113.49, 71.46, 70.68, 66.84, 41.22, 32.24, 30.83, 30.02, 29.75, 15.65.

doi:10.6342/NTU201904150

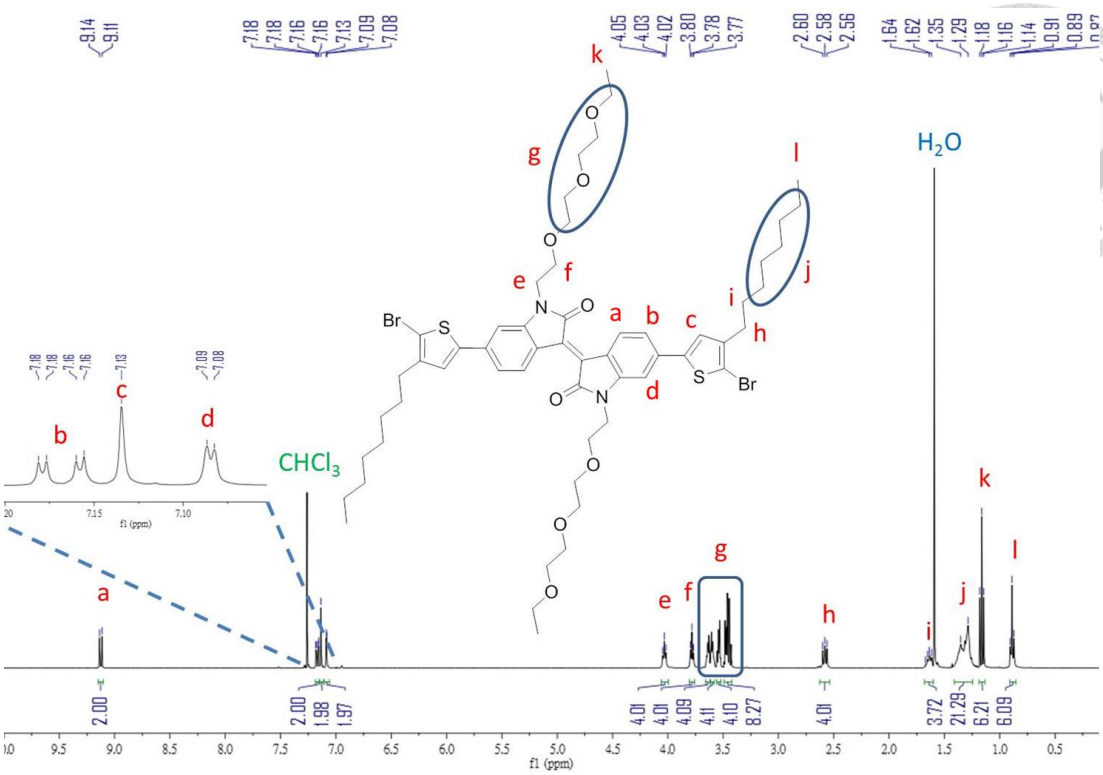

Figure 5.52. ^{1}H NMR of compound 22a

Synthesis of compound 22b

(E)-6,6'-bis(5-bromo-4-octylthiophene-2-yl)-1,1'-bis(2-hexyldecyl)-[3,3'-biindolinylidene]-2,2'-dione

Compound 21b (3.00 g, 2.38 mmole) was dissolved in tetrahydrofurane (150ml), and the round bottom flask was wrapped by a layer of alumina foil to prevent light. 1-bromo-2,5-pyrrolidinedione (0.87 g, 4.89 mmole) was divided into 4 portions and each portion was added to the solution at an interval of 15 minutes. After being stirred in the dark for 12 hours to carry out the reaction, the solution was concentrated and then it was purified by a flash column chromatography of silica gel with solvent

doi:10.6342/NTU201904150

mixture hexane: dichloromethane = 2: 1 (v/v) as eluent. Solvents were then evaporated under reduced pressure, and the sticky residue was recrystallized in methanol. The dark purple solid, compound 22b (3.0 g, 88%) was obtained after filtration and dried in vacuum oven overnight. ^{1}H NMR (400 MHz, $CDCl_3$) δ 9.15 (d, *J* = 8.4 Hz, 2H), 7.18 (dd, *J* = 8.4, 1.7 Hz, 2H), 7.08 (s, 2H), 6.85 (d, *J* = 1.6 Hz, 2H), 3.68 (d, *J* = 7.3 Hz, 4H), 2.58 (t, *J* = 7.6 Hz, 4H), 1.95 – 1.85 (m, 2H), 1.63 (quintet, *J* = 7.4 Hz, 4H), 1.45 – 1.16 (m, 68H), 0.91 – 0.84 (m, 18H). ^{13}C NMR (100 MHz, $CDCl_3$, δ): 168.79, 146.02, 143.93, 143.61, 137.28, 132.16, 130.66, 125.23, 121.50, 118.85, 110.24, 104.70, 44.73, 36.74, 32.24, 30.03, 29.75, 29.68, 29.63, 27.01, 23.02, 14.45.

doi:10.6342/NTU201904150

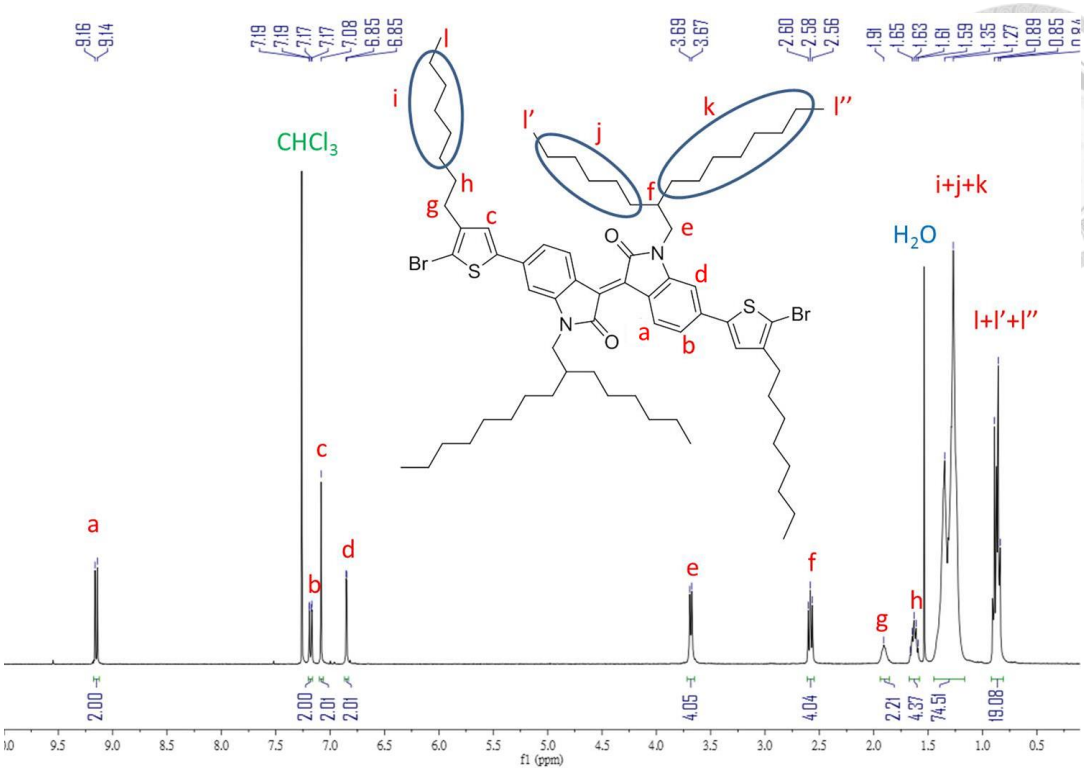

Figure 5.53. ^{1}H NMR of compound 22b

Synthesis of compound 23

2,5-bis(trimethylstannyl)thiophene

To the solution of thiophene (4.21 g, 0.05 mole) dissolved in anhydrous tetrahydrofurane (100ml), n-butyllithium (40 ml, 0.10 mole) was added dropwise via syringe. The mixture was reacted at -40℃ in dry ice/acetonitrile bath. Trimethyltin chloride (100 ml, 0.10 mol) was add to the solution, and the coolant was removed when the transfer finished. The solution was reacted at ambient temperature under stirring for 12 hours. The solution was concentrated and then extracted with hexane

doi:10.6342/NTU201904150

and distilled water several times. The combined organic layers were dried over anhydrous magnesium sulfate. After filtration, the solution was concentrated by rotary evaporator. The crude oil was recrystallized from cold methanol to obtain white solid, compound 23 (17.62 g, 86%). ^{1}H NMR (400 MHz, $CDCl_3$) δ 7.37 (s, 2H), 0.37 (s, 18H). ^{13}C NMR (100 MHz, $CDCl_3$, δ): 143.36, 136.16, -7.84

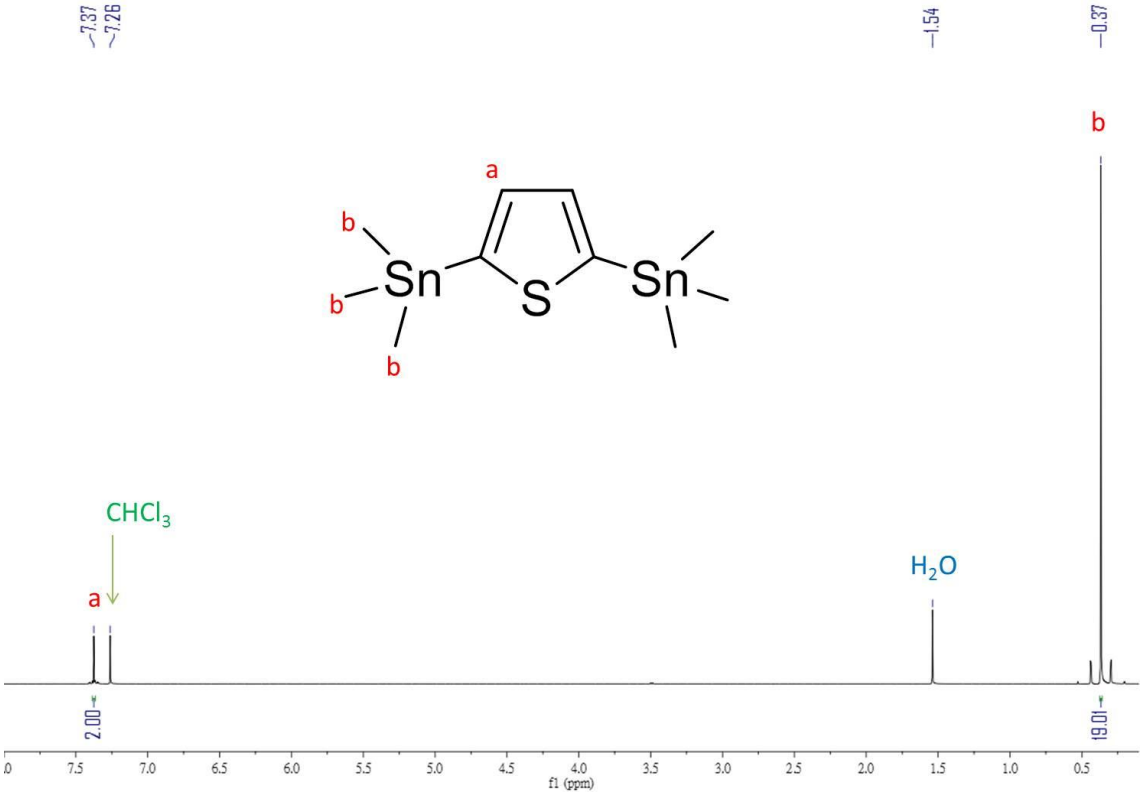

Figure 5.54. ^{1}H NMR of compound 23

doi:10.6342/NTU201904150

Synthesis of compound 24

5,5'-bis(trimethylstannyl)-2,2'-bithiophene

To a solution of 2,2'-bithiophene (8.31 g, 0.05 mole) in anhydrous tetrahydrofurane, n-butyllithium (40 ml, 0.10 mole) was added dropwise via syringe and the solution was cooled down by dry ice / acetonitrile bath. After the solution was reacted at -40℃ under stirring for 2 hours, trimethyltin chloride (100 ml, 0.10 mol) was added to the solution. Coolant was removed when the transfer finished, and the mixture was reacted at ambient temperature under stirring overnight. The solution was concentrated and extracted with hexane and distilled water several times. The combined organic layers were dried over anhydrous magnesium sulfate. Hexane was evaporated under reduced pressure. The yellow residue was recrystallized in methanol to obtain white solid, compound 24 (22.87 g, 93%). ^{1}H NMR (400 MHz, $CDCl_3$) δ 7.28 (d, *J* = 3.3 Hz, 2H), 7.09 (d, *J* = 3.3 Hz, 2H), 0.39 (s, 18H). ^{13}C NMR (100 MHz, $CDCl_3$, δ): 142.94, 136.97, 135.76, 124.76, -8.32.

doi:10.6342/NTU201904150

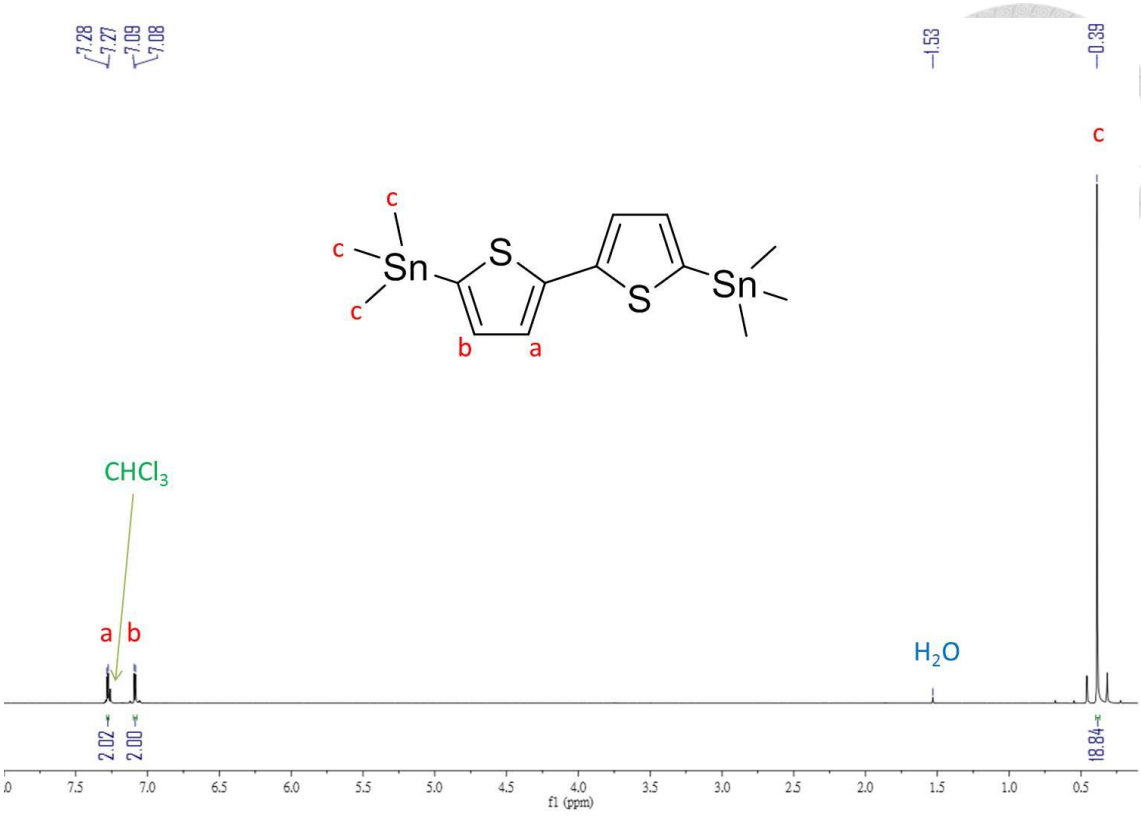

Figure 5.55. ^{1}H NMR of compound 24

Synthesis of compound 25

3-(bromomethyl)thiophene

A 250 ml round bottom flask was evacuated by vacuum system and refilled the nitrogen to remove the moisture in the flask. Next, thiophene-3-ylmethanol (5 g, 43.8 mmole) and 100 ml dry dichloromethane were placed into the flask. The flask was placed in an ice bath. Then phosphorus tribromide (4.14 ml, 44.0 mmole) was added into the flask over a 15 min period. The mixture was stirred under room temperature for 5 hours, then quenched with sodium bicarbonate solution. Then the mixture was extracted by hexane and distilled water. The organic layer was collected, dried by

doi:10.6342/NTU201904150

anhydrous magnesium sulfate, and filtered by filter paper. The filtrate was collected and the hexane was removed by rotary evaporator. After that, the condensed mixture passed through a plug of celite using dichloromethane as eluent. Finally, the mixture was purified by a plug of silica gel using hexane as eluent to obtain pale yellow oil, compound 25 (5.2 g, 65%). ^{1}H NMR (400 MHz, $CDCl_3$) δ 7.31 (m, 2H), 7.13 (dd, *J* = 4.9, 1.4 Hz, 1H), 4.53 (s, 2H). ^{13}C NMR (100 MHz, $CDCl_3$, δ): 137.51, 128.12, 126.15, 121.33, 28.54.

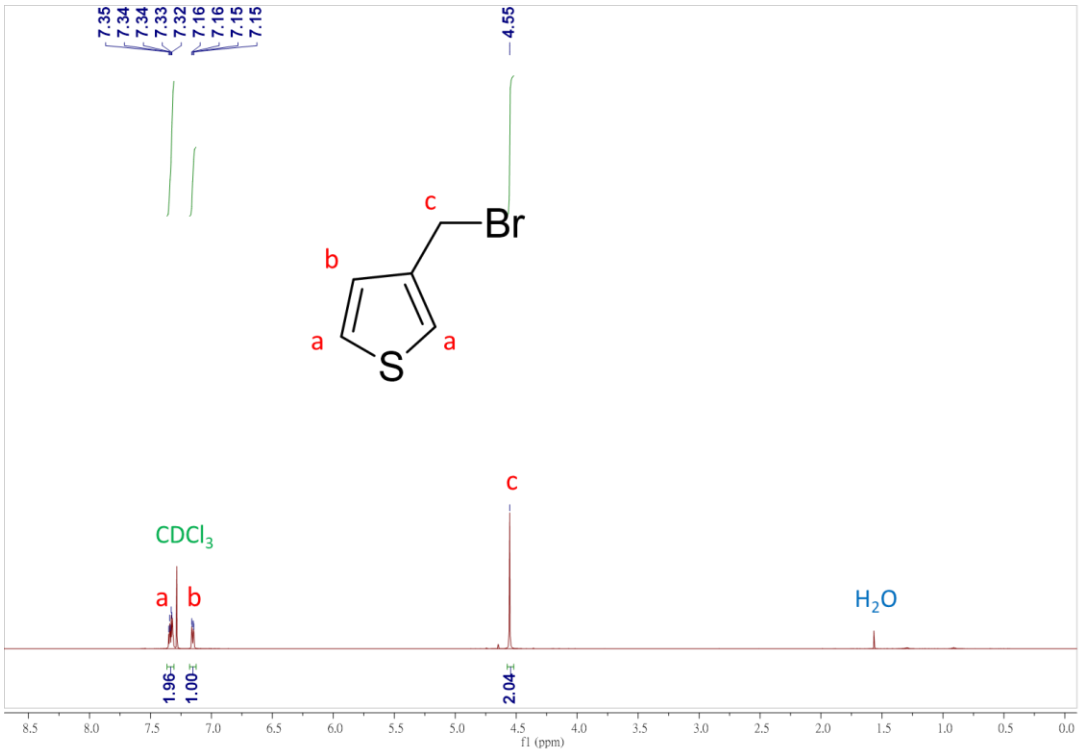

Figure 5.56. ^{1}H NMR of compound 25

doi:10.6342/NTU201904150

Synthesis of compound 26

1-(thiophene-3-yl)-2,5,8,11-tetraoxatridecane

A 250 ml round bottom flask was evacuated by vacuum system and refilled the nitrogen to remove the moisture in the flask. Next, 2-(2-(2-ethoxyethoxy)ethoxy)ethanol (5.00 g, 28.10 mmole) and 125 ml anhydrous tetrahydrofurane were placed in the flask. Then sodium hydride (0.80 g, 33 mmole) was added into the flask. After hydrogen gas evolution had ceased, compound 25 (4.80 g, 27.10 mmole) was added into the flask. The mixture was stirred under room temperature for 5 hours. The mixture was extracted by ethyl acetate and distilled water. The organic layer was collected, the ethyl acetate was removed by rotary evaporator. The condensed mixture was purified through column chromatography (ethyl acetate as eluent, silica gel) to obtain pale yellow oil, compound 26 (4.10 g, 55%). ^{1}H NMR (400 MHz, $CDCl_3$) δ 7.28 (dd, *J* = 4.9, 3.0 Hz, 1H), 7.21 (m, 1H), 4.57 (s, 2H), 3.56-3.70 (m, 12H), 3.50(q, *J* = 7.0 Hz, 2H), 1.2 (t, *J* = 7.0 Hz, 3H). ^{13}C NMR (100 MHz, $CDCl_3$, δ): 137.54, 128.14, 126.17, 121.35, 71.46, 70.68, 66.84, 15.25.

doi:10.6342/NTU201904150

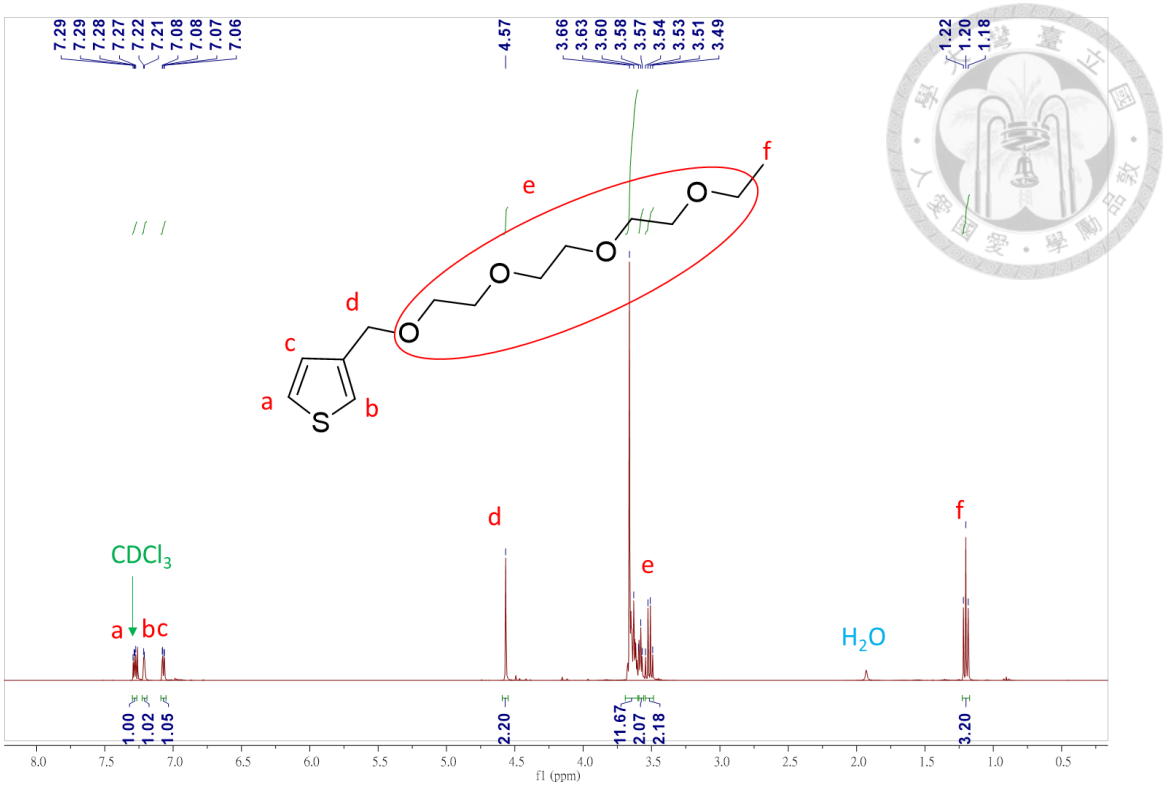

Figure 5.57. ^{1}H NMR of compound 26

Synthesis of compound 27

1-(2-bromothiophene-3-yl)-2,5,8,11-tetraoxatridecane

Compound 26 (3.00 g, 10.93 mmole) and 100 ml tetrahydrofuran was placed in a 250 ml round bottom flask, and the flask was put into ice bath. Next, 1-bromo-2,5-pyrrolidinedione (1.95 g, 10.93 mmole) was added into the flask. The mixture was stirred under 0 ^{o}C for 2 hours. After the reaction, the tetrahydrofuran was removed by rotary evaporator. The condensed mixture was purified through column chromatography (ethyl acetate as eluent, silica gel) to obtain yellow oil, compound 27 (3.28 g, 85%). ^{1}H NMR (400 MHz, $CDCl_3$) δ 7.23 (d, J = 5.6 Hz, 1H), 7.00 (d, J = 5.6

doi:10.6342/NTU201904150

Hz, 1H), 4.50 (s, 2H), 3.56-3.70 (m, 12H), 3.52(q, *J* = 7.0 Hz, 2H), 1.2 (t, *J* = 7.0 Hz, 3H). ^{13}C NMR (100 MHz, $CDCl_3$, δ): 147.10, 128.14, 126.17, 110.85, 71.46, 70.68, 66.84, 15.25.

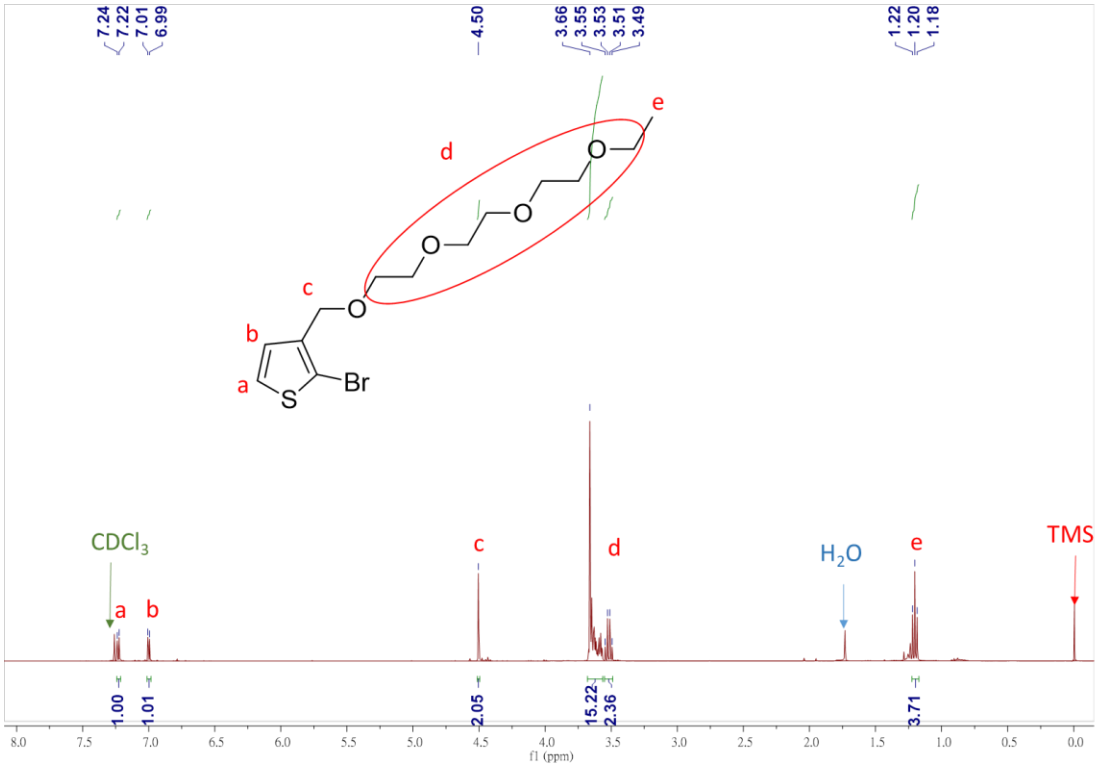

Figure 5.58. ^{1}H NMR of compound 27

Synthesis of compound 28

3,3''-di(2,5,8,11-tetraoxatridecyl)-2,2':5',2''-terthiophene

Compound 27 (1.00 g, 2.83 mmole), compound 23 (0.58 g, 1.42 mmole), tris(dibenzylideneacetone)dipalladium(0) (64.89 mg, 0.07 mmole), and tri(o-tolyl)phosphine (43.26 mg , 0.14 mmole), and 4 ml degassed tetrahydrofuran

doi:10.6342/NTU201904150

were placed in a 10ml microwave vessel then the vessel was put in the microwave reactor, and parameters for the reaction were set at 100 °C, 100 W, and 45 min. The mixture was purified through column chromatography (ethyl acetate as eluent, silica gel) to obtain yellow oil, compound 28 (714 mg, 80%). ^{1}H NMR (400 MHz, $CDCl_3$) δ 7.21 (d, *J* = 5.2 Hz, 2H), 7.16 (s, 2H), 7.14 (d, *J* = 5.1 Hz, 2H), 4.63 (s, 4H), 3.56-3.70 (m, 24H), 3.51(q, *J* = 7.0 Hz, 4H), 1.19 (t, *J* = 7.0 Hz, 6H). ^{13}C NMR (100 MHz, $CDCl_3$, δ):135.76, 135.36, 133.90, 130.25, 127.21, 124.16, 70.65, 69.81, 69.46, 66.87, 66.62, 15.15.

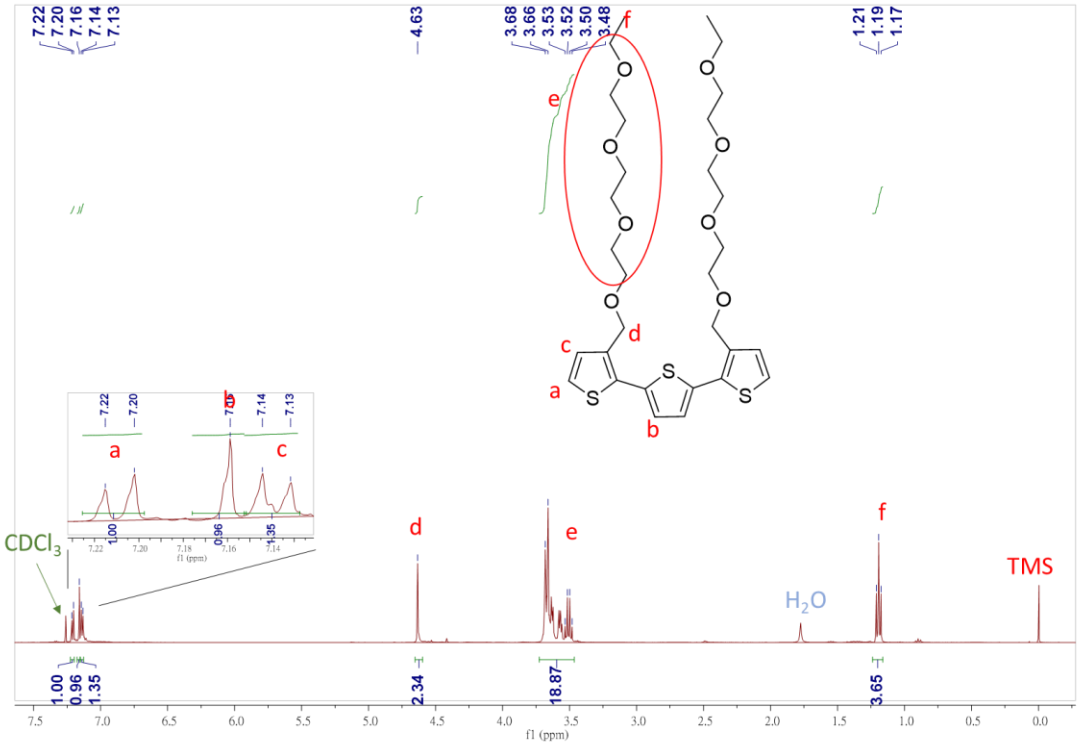

Figure 5.59. ^{1}H NMR of compound 28

doi:10.6342/NTU201904150

Synthesis of compound 29

3,3'''-di(2,5,8,11-tetraoxatridecyl)-2,2':5',2'':5'',2'''-quaterthiophene

Compound 27 (1.00 g, 2.83 mmole), compound 24 (0.70 g, 1.42 mmole), tris(dibenzylideneacetone)dipalladium(0) (64.89 mg, 0.07 mmole), and tri(o-tolyl)phosphine (43.26 mg , 0.14 mmole), and 4 ml degassed tetrahydrofuran were placed in a 10ml microwave vessel then the vessel was put in the microwave reactor, and parameters for the reaction were set at 100 ^{o}C, 100 W, and 45 min. The mixture was purified through column chromatography (ethyl acetate as eluent, silica gel) to obtain orange oil, compound 29 (828 mg, 82%). ^{1}H NMR (400 MHz, $CDCl_3$) δ 7.21 (d, *J* = 5.2 Hz, 2H), 7.14 (m, 6H), 4.64 (s, 4H), 3.56-3.70 (m, 24H), 3.51 (q, *J* = 7.0 Hz, 4H), 1.20 (t, *J* = 7.0 Hz, 6H). ^{13}C NMR (100 MHz, $CDCl_3$, δ):135.76, 135.36, 133.90, 130.25, 127.21, 124.16, 70.65, 69.81, 69.46, 66.87, 66.62, 15.15, -8.32.

doi:10.6342/NTU201904150

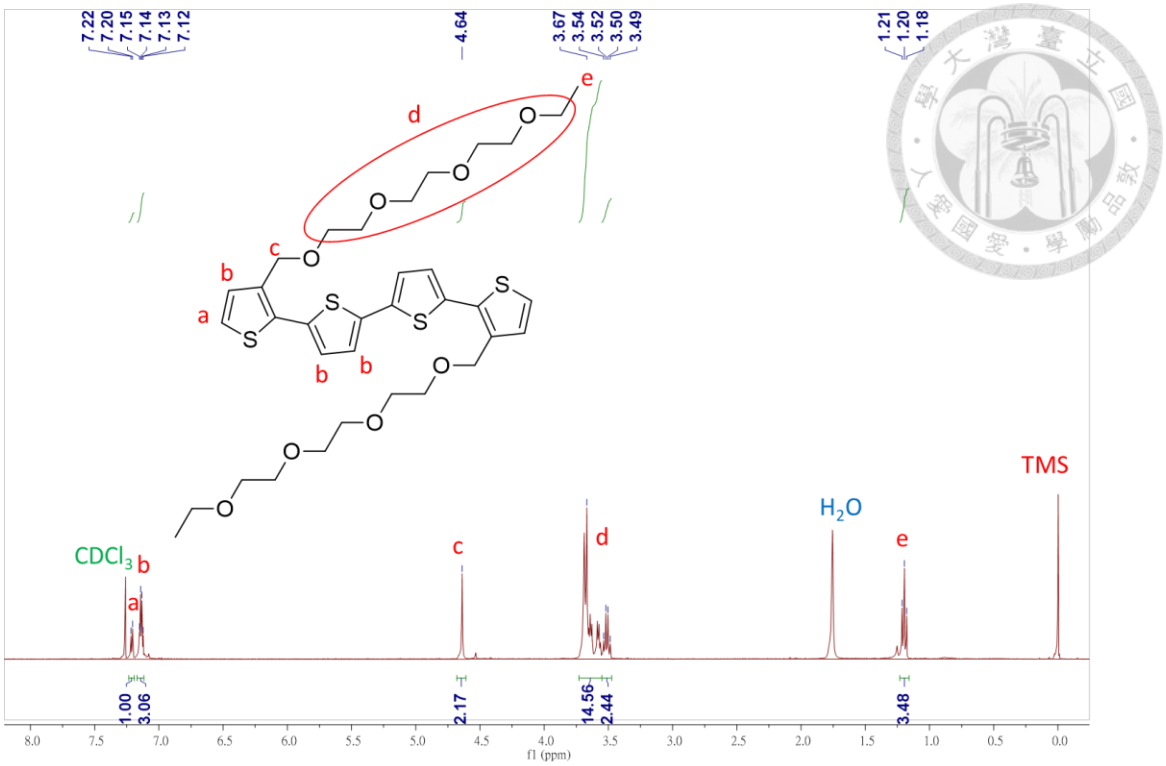

Figure 5.60. ^{1}H NMR of compound 29

Synthesis of compound 30

(3,3''-di(2,5,8,11-tetraoxatridecyl)-[2,2':5',2''-terthiophene]-5,5''-diyl)bis(trimethylstannane)

A 150 ml round bottom flask was evacuated by vacuum system and refilled the nitrogen to remove the moisture in the flask. Next, compound 28 (500 mg, 0.80 mmole) and 50 ml anhydrous tetrahydrofuran were placed in the flask. After that, the flask was put in -78^{o}C dry ice bath. Then, 0.64 ml 2.5M n-butyllithium in hexane solution (1.60 mmole) was added into the flask and the solution was stirred for 2 hours. The -78^{o}C dry ice bath was removed and the solution was stirred at room

doi:10.6342/NTU201904150

temperature for 1 hour. Then the flask was put in -78°C dry ice bath again and 1.60 ml 1M trimethyltin chloride in tetrahydrofuran solution (1.60 mmole) was added into the flask. After complete adding the trimethyltin chloride solution, the -78°C dry ice bath was removed and the solution was stirred at room temperature for 12 hours. The mixture was extracted by ethyl acetate and distilled water. The organic layer was collected, dried over anhydrous magnesium sulfate, and filtered by filter paper. The filtrate was collected and the ethyl acetate was removed by rotary evaporator. Finally, the condensed mixture can be further purified by column chromatography (ethyl acetate as eluent, celite gel) to obtain yellow oil, compound 30 (611 mg, 75%). ^{1}H NMR (400 MHz, $CDCl_3$) δ 7.19 (s, 2H), 7.14 (s, 2H), 4.64 (s, 4H), 3.56-3.70 (m, 24H), 3.51 (q, *J* = 7.0 Hz, 4H), 1.20 (t, *J* = 7.0 Hz, 6H), 0.38 (s, 18H). ^{13}C NMR (100 MHz, $CDCl_3$, δ):137.28, 135.25, 133.97, 130.25, 127.30, 124.29, 70.56, 69.72, 69.34, 66.75, 66.55, 15.05.

doi:10.6342/NTU201904150

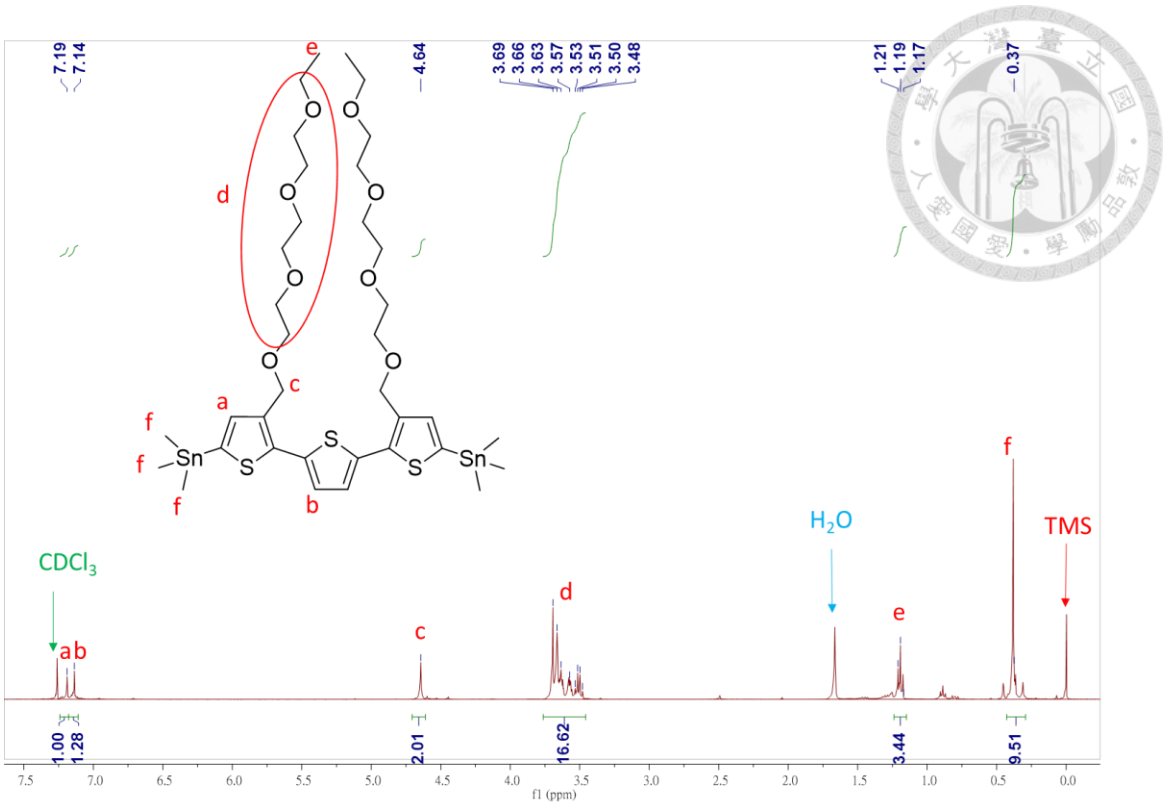

Figure 5.61. ^{1}H NMR of compound 30

Synthesis of compound 31

(3,3'''-di(2,5,8,11-tetraoxatridecyl)-[2,2':5',2'':5'',2'''-quaterthiophene]-5,5'''-diyl) bis(trimethylstannane)

Compound 29 (500 mg, 0.70 mmole), 0.56 ml 2.5M n-butyllithium in hexane solution (1.40 mmole), and 1.40 ml 1M trimethyltin chloride in tetrahydrofuran solution (1.40 mmole) were used to do the reaction. Following the synthetic procedure of compound 30, one obtained orange oil, compound 31 (508 mg, 70%). ^{1}H NMR (400 MHz, $CDCl_3$) δ 7.18 (s, 2H), 7.12 (dd, *J* = 8.8, 3.8 Hz, 4H), 4.64 (s, 4H), 3.56-3.70 (m, 24H), 3.51 (q, *J* = 7.0 Hz, 4H), 1.20 (t, *J* = 7.0 Hz, 6H), 0.38 (s, 18H). ^{13}C NMR (100 MHz,

doi:10.6342/NTU201904150

$CDCl_3$, δ):137.28, 135.25, 133.97, 130.25, 127.30, 124.29, 70.56, 69.72, 69.34, 66.75, 66.55, 15.05, -8.44.

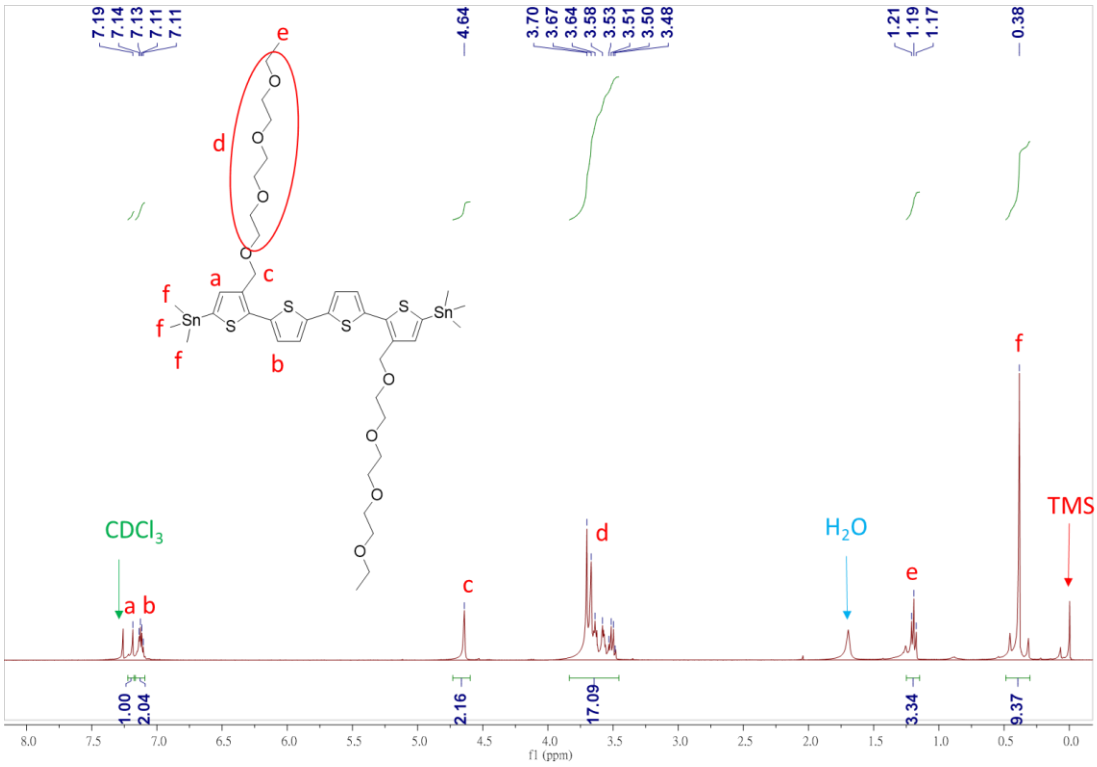

Figure 5.62. ^{1}H NMR of compound 31

General procedure for polymerization of oligothiophene-isoindigo based CPs.

The two monomers (0.2 mmole each), tris(dibenzylideneacetone)dipalladium(0) (10 mg, 0.01 mmole), **tris(*o*-tolyl)phosphine** (15 mg, 0.05 mmole) and 4 ml degassed tetrahydrofuran were placed in a 10ml microwave vessel to do the Still coupling polymerization by microwave reactor. The parameters for the reaction were set at 100 ^{o}C, 100 W, and 15 min. After polymerization, the polymers were precipitated in

doi:10.6342/NTU201904150

methanol then subjected to purification via Soxhlet extractions using a specific solvent sequence. For P3T(R_8)I(R_{b-16}) and P3T(R_8)I(E), the solvent sequence is methanol→hexane→chloroform. For P4T(R_8)I(R_{b-16}) and P4T(R_8)I(E), the solvent sequence is methanol→hexane→tetrahydrofurane→chloroform. For P3T(E)I(E), the solvent sequence is hexane→methanol→chloroform. For P4T(E)I(E), the solvent sequence is hexane→methanol→ethyl acetate→chloroform. Then we collected the chloroform solutions, removed the chloroform by rotary evaporator, and finally acquired pure polymers. The information of the monomers used in polymerization and the yield is shown in **Table 5.5.** The molecular weights of these polymers are measured by gel permeation chromatography (GPC) vs. polystyrene standards using chloroform as eluent. The molecular weight information of all synthesized isoindigo-based conjugated polymers is shown in **Table 5.6**.

doi:10.6342/NTU201904150

Table 5.5. Monomers used in polymerization and polymer yield

Polymers	Monomer 1	Monomer 2	Yield
P3T(R_8)I($R_{b\text{-}16}$)	22b	23	85%
P3T(R_8)I(E)	22a	23	82%
P3T(E)I(E)	30	20a	54%
P4T(R_8)I($R_{b\text{-}16}$)	22b	24	65%
P4T(R_8)I(E)	22a	24	62%
P4T(E)I(E)	31	20a	50%

Table 5.6. Summary of molecular weight of oligothiophene-isoindigo based CPs

Polymers	Mn(KDa)	Mw(KDa)	PDI
P3T(R_8)I($R_{b\text{-}16}$)	12.7	28.4	2.24
P3T(R_8)I(E)	19.7	42.5	2.16
P3T(E)I(E)	13.3	27.2	2.05
P4T(R_8)I($R_{b\text{-}16}$)	18.9	44.2	2.34
P4T(R_8)I(E)	12.2	30.9	2.54
P4T(E)I(E)	14.9	30.2	2.03

doi:10.6342/NTU201904150

5.3 Sample Preparation and Characterization

Gel permeation chromatography (GPC) The molecular weights of all synthesized polymers were measured by Waters GPC (Viscotek GPCMax) using chloroform as an eluent at 40℃. The instrument was equipped with two Waters Styragel columns (HR3 and HR4E), a refractive index detector (Waters 2414), and a dual-wavelength absorbance detector (Waters 2487). The wavelengths were set at 254 and 465 nm.

UV-Vis absorption spectra (UV-Vis) The UV-Vis spectra of all synthesized polymers were measured by Perkin Elmer UV-Vis instrument (Lambda 35). Scan range: 1000nm~300nm. Polymer solution for UV-Vis analysis: chloroform as solvent, concentration of 0.025 mg/ml. Polymer film for UV-Vis analysis: drawing 70 μl from 1 ml polymer solution (solvent: chloroform, concentration: 10 mg/ml) and dropping on the glass substrate (size: 1.25 cm*1.25 cm). After that, the glass substrate was spun (spin rate: 1000 rpm) by spin coater (Laurell Tec., WS-400A) to obtain the polymer film (thickness: ~100 nm). Annealed polymer film for UV-Vis analysis: spin-coated films were annealed at 200 ^{o}C for 1 hour.

Cyclic voltammetry spectra (CV) The CV spectra of all synthesized polymers were measured by CHI CV instrument (CHI611E). For analysis of redox potential of

doi:10.6342/NTU201904150

ferrocene: Electrolyte solution: 1M tetrabutylammonium perchlorate (TBAP) in acetonitrile. Working electrode: Platinum. Reference electrode: Ag/Ag^{+}. Auxiliary electrode: Platinum. Scan range: 0V~0.8V. For analysis of redox potential of the polymers: All setting is the same as the setting for analysis of ferrocene, except that the platinum is replaced with the polymer film as working electrode. Scan range: 0~1.4V (oxidation process), and 0~-1.4V (reduction process). Polymer film for CV analysis: drawing 100 μl from 1 ml polymer solution (solvent: chloroform, concentration: 10 mg/ml) and dropping on the ITO glass substrate (size: 1 cm*2 cm, Luminescence Technology Corp. 10Ω). After that, the ITO glass substrate was spun (spin rate: 1000 rpm) by spin coater to obtain the polymer film (thickness: ~100 nm).

Grazing-incidence wide-angle X-ray scattering (GIWAXS) The GIWAXS profile of all synthesized polymers were measured by GIWAXS instrument provided from Beam Line 13A and 17A in National Synchrotron Radiation Research Center (NSRRC). Incident angle: 0.2^{o} Annealed polymer film for GIWAXS analysis: drawing 60 μl from 1 ml polymer solution (solvent: chloroform, concentration: 10 mg/ml) and dropping on the silicon wafer (size: 1 cm*1 cm, Summit Tech corp., (100)±0.5°, P/boron). After that, the polymer film was annealed at 200 ^{o}C for 1 hour in nitrogen.

doi:10.6342/NTU201904150

Atomic force microscopy(AFM) The AFM images of all synthesized polymers were taken by Bruker AFM instrument (AS-12VLR). Annealed polymer film for AFM analysis is the same as for GIWAXS analysis.

Molecular orbital computation Molecular simulation was performed on Gaussian 09W package. B3LYP/6-31G** method was employed for all calculations. Due to limited computational resource, only one repeat unit was calculated.

Thermalgravimetric analysis (TGA). TGA experiment was performed by TA instrument (Q50). Sample weight loss was measured by heating the sample at a rate of 10 ºC/min from 25 ºC to 600 ºC.

Differential scanning calorimetry (DSC). DSC experiment was performed by TA instrument (Q200). For **oligothiophene-TPD based polymers**, the following procedure was set: (1) equilibrate at 0 ºC (2) isothermal for 5 min (3) heat from 0 ºC~ 300 ºC with heating rate of 10 ºC/min (4) isothermal for 5 min (5) cool from 300 ºC~0 ºC with cooling rate of 10 ºC/min (6) isothermal for 5 min (7) heat from 0 ºC~ 300 ºC with heating rate of 10 ºC/min. Only second heating round (step 7) profile was used to analyze the thermal property of the polymers. For **oligothiophene-isoindigo**

doi:10.6342/NTU201904150

based poymers, the following procedure was set: (1) equilibrate at 200 °C (2) isothermal for 1 hour (3) equilibrate at 0 °C (4) isothermal for 5 min (5) heat from 0 °C ~ 320 °C with heating rate of 10 °C/min for P3T(R_8)I($R_{b\text{-}16}$), P3T(R_8)I(E), P4T(R_8)I($R_{b\text{-}16}$), and P4T(R_8)I(E); heat from 0 °C~ 220 °C with heating rate of 10 °C/min for P3T(E)I(E), and P4T(E)I(E). Only heating round (step 5) profiles were used to analyze the thermal properties of the polymers.

doi:10.6342/NTU201904150

References

[1] Sun, J.; Zhang, Z.; Yin, X.; Zhou, J.; Yang, L.; Geng, R.; Zhang, F.; Zhu, R.; Yu, J.; Tang, W., High performance non-fullerene polymer solar cells based on PTB7-Th as the electron donor with 10.42% efficiency. *J. Mater. Chem. A* **2018,** *6* (6), 2549-2554.

[2] Fan, Q.; Wang, Y.; Zhang, M.; Wu, B.; Guo, X.; Jiang, Y.; Li, W.; Guo, B.; Ye, C.; Su, W.; Fang, J.; Ou, X.; Liu, F.; Wei, Z.; Sum, T. C.; Russell, T. P.; Li, Y., High-Performance As-Cast Nonfullerene Polymer Solar Cells with Thicker Active Layer and Large Area Exceeding 11% Power Conversion Efficiency. *Advanced Materials* **2018,** *30* (6), 1704546.

[3] Sun, C.; Pan, F.; Bin, H.; Zhang, J.; Xue, L.; Qiu, B.; Wei, Z.; Zhang, Z.-G.; Li, Y., A low cost and high performance polymer donor material for polymer solar cells. *Nature Communications* **2018,** *9* (1), 743.

[4] Liu, X.; Li, X.; Li, Y.; Song, C.; Zhu, L.; Zhang, W.; Wang, H.-Q.; Fang, J., High-Performance Polymer Solar Cells with PCE of 10.42% via Al-Doped ZnO Cathode Interlayer. *Advanced Materials* **2016,** *28* (34), 7405-7412.

[5] Li, S.; Ye, L.; Zhao, W.; Yan, H.; Yang, B.; Liu, D.; Li, W.; Ade, H.; Hou, J., A Wide Band Gap Polymer with a Deep Highest Occupied Molecular Orbital Level Enables 14.2% Efficiency in Polymer Solar Cells. *Journal of the American Chemical*

doi:10.6342/NTU201904150

Society **2018,** *140* (23), 7159-7167.

[6] Li, H.; Kim, F. S.; Ren, G.; Jenekhe, S. A., High-Mobility n-Type Conjugated Polymers Based on Electron-Deficient Tetraazabenzodifluoranthene Diimide for Organic Electronics. *Journal of the American Chemical Society* **2013,** *135* (40), 14920-14923.

[7] Nikolka, M.; Nasrallah, I.; Rose, B.; Ravva, M. K.; Broch, K.; Sadhanala, A.; Harkin, D.; Charmet, J.; Hurhangee, M.; Brown, A.; Illig, S.; Too, P.; Jongman, J.; McCulloch, I.; Bredas, J.-L.; Sirringhaus, H., High operational and environmental stability of high-mobility conjugated polymer field-effect transistors through the use of molecular additives. *Nature Materials* **2016,** *16*, 356.

[8] Luo, H.; Yu, C.; Liu, Z.; Zhang, G.; Geng, H.; Yi, Y.; Broch, K.; Hu, Y.; Sadhanala, A.; Jiang, L.; Qi, P.; Cai, Z.; Sirringhaus, H.; Zhang, D., Remarkable enhancement of charge carrier mobility of conjugated polymer field-effect transistors upon incorporating an ionic additive. *Science Advances* **2016,** *2* (5), e1600076.

[9] Kang, I.; Yun, H.-J.; Chung, D. S.; Kwon, S.-K.; Kim, Y.-H., Record High Hole Mobility in Polymer Semiconductors via Side-Chain Engineering. *Journal of the American Chemical Society* **2013,** *135* (40), 14896-14899.

[10] Lei, T.; Dou, J.-H.; Ma, Z.-J.; Yao, C.-H.; Liu, C.-J.; Wang, J.-Y.; Pei, J., Ambipolar Polymer Field-Effect Transistors Based on Fluorinated Isoindigo: High

doi:10.6342/NTU201904150

Performance and Improved Ambient Stability. *Journal of the American Chemical Society* **2012,** *134* (49), 20025-20028.

[11] Wang, Y.; Zhu, Y.; Lin, X.; Yang, Y.; Zhang, B.; Zhan, H.; Xie, Z.; Cheng, Y., Efficient non-doped yellow OLEDs based on thermally activated delayed fluorescence conjugated polymers with an acridine/carbazole donor backbone and triphenyltriazine acceptor pendant. *J. Mater. Chem. C* **2018,** *6* (3), 568-574.

[12] Crossley, D. L.; Urbano, L.; Neumann, R.; Bourke, S.; Jones, J.; Dailey, L. A.; Green, M.; Humphries, M. J.; King, S. M.; Turner, M. L.; Ingleson, M. J., Post-polymerization C–H Borylation of Donor–Acceptor Materials Gives Highly Efficient Solid State Near-Infrared Emitters for Near-IR-OLEDs and Effective Biological Imaging. *ACS Applied Materials & Interfaces* **2017,** *9* (34), 28243-28249.

[13] Jessop, I.; Díaz, F.; Terraza, C.; Tundidor-Camba, A.; Leiva, Á.; Cattin, L.; Bèrnede, J.-C., PANI Branches onto Donor-Acceptor Copolymers: Synthesis, Characterization and Electroluminescent Properties of New 2D-Materials. *Polymers* **2018,** *10* (5), 553.

[14] Di Nuzzo, D.; Kulkarni, C.; Zhao, B.; Smolinsky, E.; Tassinari, F.; Meskers, S. C. J.; Naaman, R.; Meijer, E. W.; Friend, R. H., High Circular Polarization of Electroluminescence Achieved via Self-Assembly of a Light-Emitting Chiral Conjugated Polymer into Multidomain Cholesteric Films. *ACS Nano* **2017,** *11* (12),

doi:10.6342/NTU201904150

12713-12722.

[15] Lu, C.-F.; Shih, C.-W.; Chen, C.-A.; Chin, A.; Su, W.-F., Tuning the Morphology of Isoindigo Donor–Acceptor Polymer Film for High Sensitivity Ammonia Sensor. *Adv. Funct. Mater.* **2018,** *28* (40), 1803145.

[16] Khim, D.; Ryu, G.-S.; Park, W.-T.; Kim, H.; Lee, M.; Noh, Y.-Y., Precisely Controlled Ultrathin Conjugated Polymer Films for Large Area Transparent Transistors and Highly Sensitive Chemical Sensors. *Advanced Materials* **2016,** *28* (14), 2752-2759.

[17] Yang, Y.; Zhang, G.; Luo, H.; Yao, J.; Liu, Z.; Zhang, D., Highly Sensitive Thin-Film Field-Effect Transistor Sensor for Ammonia with the DPP-Bithiophene Conjugated Polymer Entailing Thermally Cleavable tert-Butoxy Groups in the Side Chains. *ACS Applied Materials & Interfaces* **2016,** *8* (6), 3635-3643.

[18] Yang, T.; Liu, L.; Deng, Y.; Guo, Z.; Zhang, G.; Ge, Z.; Ke, H.; Chen, H., Ultrastable Near-Infrared Conjugated-Polymer Nanoparticles for Dually Photoactive Tumor Inhibition. *Advanced Materials* **2017,** *29* (31), 1700487.

[19] Li, D.-D.; Wang, J.-X.; Ma, Y.; Qian, H.-S.; Wang, D.; Wang, L.; Zhang, G.; Qiu, L.; Wang, Y.-C.; Yang, X.-Z., A Donor–Acceptor Conjugated Polymer with Alternating Isoindigo Derivative and Bithiophene Units for Near-Infrared Modulated Cancer Thermo-Chemotherapy. *ACS Applied Materials & Interfaces* **2016,** *8* (30),

doi:10.6342/NTU201904150

19312-19320.

[20] Subramaniyan, S.; Xin, H.; Kim, F. S.; Murari, N. M.; Courtright, B. A. E.; Jenekhe, S. A., Thiazolothiazole Donor–Acceptor Conjugated Polymer Semiconductors for Photovoltaic Applications. *Macromolecules* **2014,** *47* (13), 4199-4209.

[21] Yu, Z.; Zhang, Y.; Jiang, X.; Li, X.; Lai, J.; Hu, M.; Elawad, M.; Gurzadyan, G. G.; Yang, X.; Sun, L., High-efficiency perovskite solar cells employing a conjugated donor–acceptor co-polymer as a hole-transporting material. *RSC Adv.* **2017,** *7* (44), 27189-27197.

[22] Ullah, H.; Bibi, S.; Tahir, A. A.; Mallick, T. K., Donor-acceptor polymer for the design of All-Solid-State dye-sensitized solar cells. *Journal of Alloys and Compounds* **2017,** *696*, 914-922.

[23]Bin, H.; Gao, L.; Zhang, Z.-G.; Yang, Y.; Zhang, Y.; Zhang, C.; Chen, S.; Xue, L.; Yang, C.; Xiao, M.; Li, Y., 11.4% Efficiency non-fullerene polymer solar cells with trialkylsilyl substituted 2D-conjugated polymer as donor. *Nature Communications* **2016,** *7*, 13651.

[24] Kim, G.-W.; Lee, J.; Kang, G.; Kim, T.; Park, T., Donor–Acceptor Type Dopant-Free, Polymeric Hole Transport Material for Planar Perovskite Solar Cells (19.8%). *Advanced Energy Materials* **2018,** *8* (4), 1701935.

doi:10.6342/NTU201904150

[25] Ho, C.-C.; Chen, C.-A.; Chang, C.-Y.; Darling, S. B.; Su, W.-F., Isoindigo-based copolymers for polymer solar cells with efficiency over 7%. *J. Mater. Chem. A* **2014,** *2* (21), 8026-8032.

[26] Chen, F.; Jiang, Y.; Sui, Y.; Zhang, J.; Tian, H.; Han, Y.; Deng, Y.; Hu, W.; Geng, Y., Donor–Acceptor Conjugated Polymers Based on Bisisoindigo: Energy Level Modulation toward Unipolar n-Type Semiconductors. *Macromolecules* **2018,** *51* (21), 8652-8661.

[27] Gao, Y.; Deng, Y.; Tian, H.; Zhang, J.; Yan, D.; Geng, Y.; Wang, F., Multifluorination toward High-Mobility Ambipolar and Unipolar n-Type Donor–Acceptor Conjugated Polymers Based on Isoindigo. *Advanced Materials* **2017,** *29* (13), 1606217.

[28] Zhan, X.; Tan, Z. a.; Domercq, B.; An, Z.; Zhang, X.; Barlow, S.; Li, Y.; Zhu, D.; Kippelen, B.; Marder, S. R., A High-Mobility Electron-Transport Polymer with Broad Absorption and Its Use in Field-Effect Transistors and All-Polymer Solar Cells. *Journal of the American Chemical Society* **2007,** *129* (23), 7246-7247.

[29] Yan, Z.; Sun, B.; Li, Y., Novel stable (3E,7E)-3,7-bis(2-oxoindolin-3-ylidene)benzo[1,2-b:4,5-b′]difuran-2,6(3H,7H)-dione based donor–acceptor polymer semiconductors for n-type organic thin film transistors. *Chemical Communications* **2013,** *49* (36), 3790-3792.

doi:10.6342/NTU201904150

[30] Yuen, J. D.; Fan, J.; Seifter, J.; Lim, B.; Hufschmid, R.; Heeger, A. J.; Wudl, F., High Performance Weak Donor–Acceptor Polymers in Thin Film Transistors: Effect of the Acceptor on Electronic Properties, Ambipolar Conductivity, Mobility, and Thermal Stability. *Journal of the American Chemical Society* **2011,** *133* (51), 20799-20807.

[31] Kronemeijer, A. J.; Gili, E.; Shahid, M.; Rivnay, J.; Salleo, A.; Heeney, M.; Sirringhaus, H., A Selenophene-Based Low-Bandgap Donor–Acceptor Polymer Leading to Fast Ambipolar Logic. *Advanced Materials* **2012,** *24* (12), 1558-1565.

[32]Bijleveld, J. C.; Zoombelt, A. P.; Mathijssen, S. G. J.; Wienk, M. M.; Turbiez, M.; de Leeuw, D. M.; Janssen, R. A. J., Poly(diketopyrrolopyrrole−terthiophene) for Ambipolar Logic and Photovoltaics. *Journal of the American Chemical Society* **2009,** *131* (46), 16616-16617.

[33] Ashraf, R. S.; Kronemeijer, A. J.; James, D. I.; Sirringhaus, H.; McCulloch, I., A new thiophene substituted isoindigo based copolymer for high performance ambipolar transistors. *Chemical Communications* **2012,** *48* (33), 3939-3941.

[34] Ma, Z.; Sun, W.; Himmelberger, S.; Vandewal, K.; Tang, Z.; Bergqvist, J.; Salleo, A.; Andreasen, J. W.; Inganäs, O.; Andersson, M. R.; Müller, C.; Zhang, F.; Wang, E., Structure–property relationships of oligothiophene–isoindigo polymers for efficient bulk-heterojunction solar cells. *Energy. Environ. Sci.* **2014,** *7* (1), 361-369.

doi:10.6342/NTU201904150

[35] Li, Y.; Li, Z.; Wang, C.; Li, H.; Lu, H.; Xu, B.; Tian, W., Novel low-bandgap oligothiophene-based donor-acceptor alternating conjugated copolymers: Synthesis, properties, and photovoltaic applications. *J. Polym. Sci. A Polym. Chem.* **2010,** *48* (13), 2765-2776.

[36] Fu, B.; Baltazar, J.; Hu, Z.; Chien, A.-T.; Kumar, S.; Henderson, C. L.; Collard, D. M.; Reichmanis, E., High Charge Carrier Mobility, Low Band Gap Donor–Acceptor Benzothiadiazole-oligothiophene Based Polymeric Semiconductors. *Chemistry of Materials* **2012,** *24* (21), 4123-4133.

[37] Ichiro, I.; Hitoshi, S.; Yutaka, H., Fine-tuning of electronic properties in donor–acceptor conjugated polymers based on oligothiophenes. *Japanese Journal of Applied Physics* **2018,** *57* (3S2), 03EJ01.

[38] Ye, L.; Zhang, S.; Zhao, W.; Yao, H.; Hou, J., Highly Efficient 2D-Conjugated Benzodithiophene-Based Photovoltaic Polymer with Linear Alkylthio Side Chain. *Chemistry of Materials* **2014,** *26* (12), 3603-3605.

[39] Zhang, M.; Gu, Y.; Guo, X.; Liu, F.; Zhang, S.; Huo, L.; Russell, T. P.; Hou, J., Efficient Polymer Solar Cells Based on Benzothiadiazole and Alkylphenyl Substituted Benzodithiophene with a Power Conversion Efficiency over 8%. *Advanced Materials* **2013,** *25* (35), 4944-4949.

[40] Zhang, Y.; Hau, S. K.; Yip, H.-L.; Sun, Y.; Acton, O.; Jen, A. K. Y., Efficient

doi:10.6342/NTU201904150

Polymer Solar Cells Based on the Copolymers of Benzodithiophene and Thienopyrroledione. *Chemistry of Materials* **2010,** *22* (9), 2696-2698.

[41] Moulé, A. J.; Tsami, A.; Bünnagel, T. W.; Forster, M.; Kronenberg, N. M.; Scharber, M.; Koppe, M.; Morana, M.; Brabec, C. J.; Meerholz, K.; Scherf, U., Two Novel Cyclopentadithiophene-Based Alternating Copolymers as Potential Donor Components for High-Efficiency Bulk-Heterojunction-Type Solar Cells. *Chemistry of Materials* **2008,** *20* (12), 4045-4050.

[42] Ho, C.-C.; Chang, S.-Y.; Huang, T.-C.; Chen, C.-A.; Liao, H.-C.; Chen, Y.-F.; Su, W.-F., Synthesis, characterization and photovoltaic properties of poly(cyclopentadithiophene-alt-isoindigo). *Polymer Chemistry* **2013,** *4* (20), 5351-5360.

[43] Li, M.; An, C.; Pisula, W.; Müllen, K., Cyclopentadithiophene–Benzothiadiazole Donor–Acceptor Polymers as Prototypical Semiconductors for High-Performance Field-Effect Transistors. *Accounts of Chemical Research* **2018,** *51* (5), 1196-1205.

[44] Lin, H.-W.; Lee, W.-Y.; Chen, W.-C., Selenophene-DPP donor–acceptor conjugated polymer for high performance ambipolar field effect transistor and nonvolatile memory applications. *J. Mater. Chem.* **2012,** *22* (5), 2120-2128.

[45] Lee, W.-H.; Son, S. K.; Kim, K.; Lee, S. K.; Shin, W. S.; Moon, S.-J.; Kang, I.-N., Synthesis and Characterization of New Selenophene-Based Donor–Acceptor

doi:10.6342/NTU201904150

Low-Bandgap Polymers for Organic Photovoltaic Cells. *Macromolecules* **2012,** *45* (3), 1303-1312.

[46] Alghamdi, A. A. B.; Watters, D. C.; Yi, H.; Al-Faifi, S.; Almeataq, M. S.; Coles, D.; Kingsley, J.; Lidzey, D. G.; Iraqi, A., Selenophene vs. thiophene in benzothiadiazole-based low energy gap donor–acceptor polymers for photovoltaic applications. *J. Mater. Chem. A* **2013,** *1* (16), 5165-5171.

[47] Jenekhe, S. A.; Lu, L.; Alam, M. M., New Conjugated Polymers with Donor−Acceptor Architectures: Synthesis and Photophysics of Carbazole−Quinoline and Phenothiazine−Quinoline Copolymers and Oligomers Exhibiting Large Intramolecular Charge Transfer. *Macromolecules* **2001,** *34* (21), 7315-7324.

[48] Duan, C.; Chen, K.-S.; Huang, F.; Yip, H.-L.; Liu, S.; Zhang, J.; Jen, A. K. Y.; Cao, Y., Synthesis, Characterization, and Photovoltaic Properties of Carbazole-Based Two-Dimensional Conjugated Polymers with Donor-π-Bridge-Acceptor Side Chains. *Chemistry of Materials* **2010,** *22* (23), 6444-6452.

[49] Lai, M.-H.; Tsai, J.-H.; Chueh, C.-C.; Wang, C.-F.; Chen, W.-C., Syntheses of New 3,6-Carbazole-Based Donor/Acceptor Conjugated Copolymers for Optoelectronic Device Applications. *Macromolecular Chemistry and Physics* **2010,** *211* (18), 2017-2025.

[50] Zhou, H.; Yang, L.; Stuart, A. C.; Price, S. C.; Liu, S.; You, W., Development of

doi:10.6342/NTU201904150

Fluorinated Benzothiadiazole as a Structural Unit for a Polymer Solar Cell of 7 % Efficiency. *Angewandte Chemie International Edition* **2011,** *50* (13), 2995-2998.

[51] Wang, X.; Wang, M., Synthesis of donor–acceptor conjugated polymers based on benzo[1,2-b:4,5-b′]dithiophene and 2,1,3-benzothiadiazole via direct arylation polycondensation: towards efficient C–H activation in nonpolar solvents. *Polymer Chemistry* **2014,** *5* (19), 5784-5792.

[52] Wang, N.; Chen, Z.; Wei, W.; Jiang, Z., Fluorinated Benzothiadiazole-Based Conjugated Polymers for High-Performance Polymer Solar Cells without Any Processing Additives or Post-treatments. *Journal of the American Chemical Society* **2013,** *135* (45), 17060-17068.

[53] Lei, T.; Cao, Y.; Fan, Y.; Liu, C.-J.; Yuan, S.-C.; Pei, J., High-Performance Air-Stable Organic Field-Effect Transistors: Isoindigo-Based Conjugated Polymers. *Journal of the American Chemical Society* **2011,** *133* (16), 6099-6101.

[54] Lei, T.; Wang, J.-Y.; Pei, J., Design, Synthesis, and Structure–Property Relationships of Isoindigo-Based Conjugated Polymers. *Accounts of Chemical Research* **2014,** *47* (4), 1117-1126.

[55] Zhang, G.; Fu, Y.; Xie, Z.; Zhang, Q., Synthesis and Photovoltaic Properties of New Low Bandgap Isoindigo-Based Conjugated Polymers. *Macromolecules* **2011,** *44* (6), 1414-1420.

doi:10.6342/NTU201904150

[56] Wang, E.; Ma, Z.; Zhang, Z.; Vandewal, K.; Henriksson, P.; Inganäs, O.; Zhang, F.; Andersson, M. R., An Easily Accessible Isoindigo-Based Polymer for High-Performance Polymer Solar Cells. *Journal of the American Chemical Society* **2011,** *133* (36), 14244-14247.

[57] Ha, J. S.; Kim, K. H.; Choi, D. H., 2,5-Bis(2-octyldodecyl)pyrrolo[3,4-c]pyrrole-1,4-(2H,5H)-dione-Based Donor–Acceptor Alternating Copolymer Bearing 5,5′-Di(thiophen-2-yl)-2,2′-biselenophene Exhibiting 1.5 cm2·V–1·s–1 Hole Mobility in Thin-Film Transistors. *Journal of the American Chemical Society* **2011,** *133* (27), 10364-10367.

[58] Huo, L.; Hou, J.; Chen, H.-Y.; Zhang, S.; Jiang, Y.; Chen, T. L.; Yang, Y., Bandgap and Molecular Level Control of the Low-Bandgap Polymers Based on 3,6-Dithiophen-2-yl-2,5-dihydropyrrolo[3,4-c]pyrrole-1,4-dione toward Highly Efficient Polymer Solar Cells. *Macromolecules* **2009,** *42* (17), 6564-6571.

[59] Zhu, Y.; Rabindranath, A. R.; Beyerlein, T.; Tieke, B., Highly Luminescent 1,4-Diketo-3,6-diphenylpyrrolo[3,4-c]pyrrole- (DPP-) Based Conjugated Polymers Prepared Upon Suzuki Coupling. *Macromolecules* **2007,** *40* (19), 6981-6989.

[60] Piliego, C.; Holcombe, T. W.; Douglas, J. D.; Woo, C. H.; Beaujuge, P. M.; Fréchet, J. M. J., Synthetic Control of Structural Order in

doi:10.6342/NTU201904150

N-Alkylthieno[3,4-c]pyrrole-4,6-dione-Based Polymers for Efficient Solar Cells. *Journal of the American Chemical Society* **2010,** *132* (22), 7595-7597.

[61] Zou, Y.; Najari, A.; Berrouard, P.; Beaupré, S.; Réda Aïch, B.; Tao, Y.; Leclerc, M., A Thieno[3,4-c]pyrrole-4,6-dione-Based Copolymer for Efficient Solar Cells. *Journal of the American Chemical Society* **2010,** *132* (15), 5330-5331.

[62] Guo, X.; Ortiz, R. P.; Zheng, Y.; Kim, M.-G.; Zhang, S.; Hu, Y.; Lu, G.; Facchetti, A.; Marks, T. J., Thieno[3,4-c]pyrrole-4,6-dione-Based Polymer Semiconductors: Toward High-Performance, Air-Stable Organic Thin-Film Transistors. *Journal of the American Chemical Society* **2011,** *133* (34), 13685-13697.

[63] Berrouard, P.; Najari, A.; Pron, A.; Gendron, D.; Morin, P.-O.; Pouliot, J.-R.; Veilleux, J.; Leclerc, M., Synthesis of 5-Alkyl[3,4-c]thienopyrrole-4,6-dione-Based Polymers by Direct Heteroarylation. *Angewandte Chemie International Edition* **2012,** *51* (9), 2068-2071.

[64] Berrouard, P.; Dufresne, S.; Pron, A.; Veilleux, J.; Leclerc, M., Low-Cost Synthesis and Physical Characterization of Thieno[3,4-c]pyrrole-4,6-dione-Based Polymers. *The Journal of Organic Chemistry* **2012,** *77* (18), 8167-8173.

[65] Dong, Y.; Hu, X.; Duan, C.; Liu, P.; Liu, S.; Lan, L.; Chen, D.; Ying, L.; Su, S.; Gong, X.; Huang, F.; Cao, Y., A Series of New Medium-Bandgap Conjugated Polymers Based on Naphtho[1,2-c:5,6-c]bis(2-octyl-[1,2,3]triazole) for

doi:10.6342/NTU201904150

High-Performance Polymer Solar Cells. *Advanced Materials* **2013,** *25* (27), 3683-3688.

[66] Li, W.; Yan, L.; Zhou, H.; You, W., A General Approach toward Electron Deficient Triazole Units to Construct Conjugated Polymers for Solar Cells. *Chemistry of Materials* **2015,** *27* (18), 6470-6476.

[67] Yasuda, T.; Imase, T.; Sasaki, S.; Yamamoto, T., Synthesis, Solid Structure, and Optical Properties of New Thiophene-Based Alternating π-Conjugated Copolymers Containing 4-Alkyl-1,2,4-triazole or 1,3,4-Thiadiazole Unit as the Partner Unit. *Macromolecules* **2005,** *38* (4), 1500-1503.

[68] Chu, T.-Y.; Lu, J.; Beaupré, S.; Zhang, Y.; Pouliot, J.-R.; Wakim, S.; Zhou, J.; Leclerc, M.; Li, Z.; Ding, J.; Tao, Y., Bulk Heterojunction Solar Cells Using Thieno[3,4-c]pyrrole-4,6-dione and Dithieno[3,2-b:2′,3′-d]silole Copolymer with a Power Conversion Efficiency of 7.3%. *Journal of the American Chemical Society* **2011,** *133* (12), 4250-4253.

[69] Zhou, N.; Guo, X.; Ortiz, R. P.; Harschneck, T.; Manley, E. F.; Lou, S. J.; Hartnett, P. E.; Yu, X.; Horwitz, N. E.; Burrezo, P. M.; Aldrich, T. J.; López Navarrete, J. T.; Wasielewski, M. R.; Chen, L. X.; Chang, R. P. H.; Facchetti, A.; Marks, T. J., Marked Consequences of Systematic Oligothiophene Catenation in Thieno[3,4-c]pyrrole-4,6-dione and Bithiopheneimide Photovoltaic Copolymers.

doi:10.6342/NTU201904150

Journal of the American Chemical Society **2015,** *137* (39), 12565-12579.

[70] Liu, S.; Bao, X.; Li, W.; Wu, K.; Xie, G.; Yang, R.; Yang, C., Benzo[1,2-b:4,5-b′]dithiophene and Thieno[3,4-c]pyrrole-4,6-dione Based Donor-π-Acceptor Conjugated Polymers for High Performance Solar Cells by Rational Structure Modulation. *Macromolecules* **2015,** *48* (9), 2948-2957.

[71] Zhu, L.; Wang, M.; Li, B.; Jiang, C.; Li, Q., High efficiency organic photovoltaic devices based on isoindigo conjugated polymers with a thieno[3,2-b]thiophene π-bridge. *J. Mater. Chem. A* **2016,** *4* (41), 16064-16072.

[72] Su, Y.-W.; Lin, Y.-C.; Wei, K.-H., Evolving molecular architectures of donor–acceptor conjugated polymers for photovoltaic applications: from one-dimensional to branched to two-dimensional structures. *J. Mater. Chem. A* **2017,** *5* (46), 24051-24075.

[73] Yao, Y.; Dong, H.; Hu, W., Ordering of conjugated polymer molecules: recent advances and perspectives. *Polymer Chemistry* **2013,** *4* (20), 5197-5205.

[74] Zhu, J.; Han, Y.; Kumar, R.; He, Y.; Hong, K.; Bonnesen, P. V.; Sumpter, B. G.; Smith, S. C.; Smith, G. S.; Ivanov, I. N.; Do, C., Controlling molecular ordering in solution-state conjugated polymers. *Nanoscale* **2015,** *7* (37), 15134-15141.

[75] Holland, E. R.; Bloor, D.; Monkman, A. P.; Brown, A.; Leeuw, D. D.; Bouman, M. M.; Meijer, E. W., Effects of order and disorder on field-effect mobilities measured

doi:10.6342/NTU201904150

in conjugated polymer thin-film transistors. *Journal of Applied Physics* **1994,** *75* (12), 7954-7957.

[76] Jeon, G. G.; Lee, M.; Nam, J.; Park, W.; Yang, M.; Choi, J.-H.; Yoon, D. K.; Lee, E.; Kim, B.; Kim, J. H., Simple Solvent Engineering for High-Mobility and Thermally Robust Conjugated Polymer Nanowire Field-Effect Transistors. *ACS Applied Materials & Interfaces* **2018,** *10* (35), 29824-29830.

[77] Savikhin, V.; Jagadamma, L. K.; Purvis, L. J.; Robertson, I.; Oosterhout, S. D.; Douglas, C. J.; Samuel, I. D. W.; Toney, M. F., Morphological, Chemical, and Electronic Changes of the Conjugated Polymer PTB7 with Thermal Annealing. *iScience* **2018,** *2*, 182-192.

[78] Verploegen, E.; Mondal, R.; Bettinger, C. J.; Sok, S.; Toney, M. F.; Bao, Z., Effects of Thermal Annealing Upon the Morphology of Polymer–Fullerene Blends. *Adv. Funct. Mater.* **2010,** *20* (20), 3519-3529.

[79] Intemann, J. J.; Yao, K.; Yip, H.-L.; Xu, Y.-X.; Li, Y.-X.; Liang, P.-W.; Ding, F.-Z.; Li, X.; Jen, A. K. Y., Molecular Weight Effect on the Absorption, Charge Carrier Mobility, and Photovoltaic Performance of an Indacenodiselenophene-Based Ladder-Type Polymer. *Chemistry of Materials* **2013,** *25* (15), 3188-3195.

[80] Kang, H.; Uddin, M. A.; Lee, C.; Kim, K.-H.; Nguyen, T. L.; Lee, W.; Li, Y.; Wang, C.; Woo, H. Y.; Kim, B. J., Determining the Role of Polymer Molecular Weight

doi:10.6342/NTU201904150

for High-Performance All-Polymer Solar Cells: Its Effect on Polymer Aggregation and Phase Separation. *Journal of the American Chemical Society* **2015,** *137* (6), 2359-2365.

[81] Mei, J.; Bao, Z., Side Chain Engineering in Solution-Processable Conjugated Polymers. *Chemistry of Materials* **2014,** *26* (1), 604-615.

[82] Hwang, Y.-J.; Earmme, T.; Subramaniyan, S.; Jenekhe, S. A., Side chain engineering of n-type conjugated polymer enhances photocurrent and efficiency of all-polymer solar cells. *Chemical Communications* **2014,** *50* (74), 10801-10804.

[83] Zhang, Z.-G.; Li, Y., Side-chain engineering of high-efficiency conjugated polymer photovoltaic materials. *Science China Chemistry* **2015,** *58* (2), 192-209.

[84] Sun, Y.; Zhang, C.; Dai, B.; Lin, B.; Yang, H.; Zhang, X.; Guo, L.; Liu, Y., Side chain engineering and conjugation enhancement of benzodithiophene and phenanthrenequnioxaline based conjugated polymers for photovoltaic devices. *J. Polym. Sci. A Polym. Chem.* **2015,** *53* (16), 1915-1926.

[85] Lei, T.; Cao, Y.; Zhou, X.; Peng, Y.; Bian, J.; Pei, J., Systematic Investigation of Isoindigo-Based Polymeric Field-Effect Transistors: Design Strategy and Impact of Polymer Symmetry and Backbone Curvature. *Chemistry of Materials* **2012,** *24* (10), 1762-1770.

[86] Guo, X.; Puniredd, S. R.; Baumgarten, M.; Pisula, W.; Müllen, K.,

doi:10.6342/NTU201904150

Benzotrithiophene-Based Donor–Acceptor Copolymers with Distinct Supramolecular Organizations. *Journal of the American Chemical Society* **2012,** *134* (20), 8404-8407.

[87] Zhu, L.; Jiang, C.; Chen, G.; Zhou, Z.; Li, Q., Side chain engineering: The effect on the properties of isoindigo-based conjugated polymers contain different length and structure alkyl chains on nitrogen atom. *Organic Electronics* **2017,** *49*, 278-285.

[88] Duan, C.; Willems, R. E. M.; van Franeker, J. J.; Bruijnaers, B. J.; Wienk, M. M.; Janssen, R. A. J., Effect of side chain length on the charge transport, morphology, and photovoltaic performance of conjugated polymers in bulk heterojunction solar cells. *J. Mater. Chem. A* **2016,** *4* (5), 1855-1866.

[89] Osaka, I.; Saito, M.; Koganezawa, T.; Takimiya, K., Thiophene–Thiazolothiazole Copolymers: Significant Impact of Side Chain Composition on Backbone Orientation and Solar Cell Performances. *Advanced Materials* **2014,** *26* (2), 331-338.

[90] Song, K. W.; Song, H. J.; Lee, T. H.; Heo, S. W.; Moon, D. K., An effect on the side chain position of D–π–A-type conjugated polymers with sp2-hybridized orbitals for organic photovoltaics. *Polymer Chemistry* **2013,** *4* (11), 3225-3235.

[91] Akkuratov, A. V.; Susarova, D. K.; Moskvin, Y. L.; Anokhin, D. V.; Chernyak, A. V.; Prudnov, F. A.; Novikov, D. V.; Babenko, S. D.; Troshin, P. A., A strong influence of the positions of solubilizing alkyl side chains on optoelectronic and photovoltaic properties of TTBTBTT-based conjugated polymers. *J. Mater. Chem. C* **2015,** *3* (7),

doi:10.6342/NTU201904150

1497-1506.

[92] Yang, S.-F.; Liu, Z.-T.; Cai, Z.-X.; Dyson, M. J.; Stingelin, N.; Chen, W.; Ju, H.-J.; Zhang, G.-X.; Zhang, D.-Q., Diketopyrrolopyrrole-Based Conjugated Polymer Entailing Triethylene Glycols as Side Chains with High Thin-Film Charge Mobility without Post-Treatments. *Advanced Science* **2017,** *4* (8), 1700048.

[93] Meng, B.; Song, H.; Chen, X.; Xie, Z.; Liu, J.; Wang, L., Replacing Alkyl with Oligo(ethylene glycol) as Side Chains of Conjugated Polymers for Close π–π Stacking. *Macromolecules* **2015,** *48* (13), 4357-4363.

[94] Mei, J.; Kim, D. H.; Ayzner, A. L.; Toney, M. F.; Bao, Z., Siloxane-Terminated Solubilizing Side Chains: Bringing Conjugated Polymer Backbones Closer and Boosting Hole Mobilities in Thin-Film Transistors. *Journal of the American Chemical Society* **2011,** *133* (50), 20130-20133.

[95] Tsumura, A.; Koezuka, H.; Ando, T., Macromolecular electronic device: Field-effect transistor with a polythiophene thin film. *Applied Physics Letters* **1986,** *49* (18), 1210-1212.

[96] Babel, A.; Jenekhe, S. A., Alkyl chain length dependence of the field-effect carrier mobility in regioregular poly(3-alkylthiophene)s. *Synthetic Metals* **2005,** *148* (2), 169-173.

[97] Marrocchi, A.; Lanari, D.; Facchetti, A.; Vaccaro, L., Poly(3-hexylthiophene):

doi:10.6342/NTU201904150

synthetic methodologies and properties in bulk heterojunction solar cells. *Energy. Environ. Sci.* **2012,** *5* (9), 8457-8474.

[98] McCullough, R. D.; Lowe, R. D., Enhanced electrical conductivity in regioselectively synthesized poly(3-alkylthiophenes). *Journal of the Chemical Society, Chemical Communications* **1992,** (1), 70-72.

[99] Shi, C.; Yao, Y.; Yang; Pei, Q., Regioregular Copolymers of 3-Alkoxythiophene and Their Photovoltaic Application. *Journal of the American Chemical Society* **2006,** *128* (27), 8980-8986.

[100] Guo, X.; Quinn, J.; Chen, Z.; Usta, H.; Zheng, Y.; Xia, Y.; Hennek, J. W.; Ortiz, R. P.; Marks, T. J.; Facchetti, A., Dialkoxybithiazole: A New Building Block for Head-to-Head Polymer Semiconductors. *Journal of the American Chemical Society* **2013,** *135* (5), 1986-1996.

[101] Seo, J. H.; Gutacker, A.; Walker, B.; Cho, S.; Garcia, A.; Yang, R.; Nguyen, T.-Q.; Heeger, A. J.; Bazan, G. C., Improved Injection in n-Type Organic Transistors with Conjugated Polyelectrolytes. *Journal of the American Chemical Society* **2009,** *131* (51), 18220-18221.

[102] Duarte, A.; Pu, K.-Y.; Liu, B.; Bazan, G. C., Recent Advances in Conjugated Polyelectrolytes for Emerging Optoelectronic Applications. *Chemistry of Materials* **2011,** *23* (3), 501-515.

doi:10.6342/NTU201904150

[103] Lee, M.-H.; Kang, M.; Jeong, H.-G.; Park, J.-J.; Hwang, K.; Kim, D.-Y., Effect of Semi-Fluorinated Alkyl Side Chains on Conjugated Polymers with Planar Backbone in Organic Field-Effect Transistors. *Macromol. Rapid. Commun.* **2018,** *39* (23), 1800431.

[104] Kim, H. J.; Han, A. R.; Cho, C.-H.; Kang, H.; Cho, H.-H.; Lee, M. Y.; Fréchet, J. M. J.; Oh, J. H.; Kim, B. J., Solvent-Resistant Organic Transistors and Thermally Stable Organic Photovoltaics Based on Cross-linkable Conjugated Polymers. *Chemistry of Materials* **2012,** *24* (1), 215-221.

[105] Chen, X.; Zhang, Z.; Liu, J.; Wang, L., A polymer electron donor based on isoindigo units bearing branched oligo(ethylene glycol) side chains for polymer solar cells. *Polymer Chemistry* **2017,** *8* (36), 5496-5503.

[106] Chen, X.; Zhang, Z.; Ding, Z.; Liu, J.; Wang, L., Diketopyrrolopyrrole-based Conjugated Polymers Bearing Branched Oligo(Ethylene Glycol) Side Chains for Photovoltaic Devices. *Angewandte Chemie International Edition* **2016,** *55* (35), 10376-10380.

[107] Kanimozhi, C.; Yaacobi-Gross, N.; Burnett, E. K.; Briseno, A. L.; Anthopoulos, T. D.; Salzner, U.; Patil, S., Use of side-chain for rational design of n-type diketopyrrolopyrrole-based conjugated polymers: what did we find out? *Physical Chemistry Chemical Physics* **2014,** *16* (32), 17253-17265.

doi:10.6342/NTU201904150

[108] Zhao, X.; Xue, G.; Qu, G.; Singhania, V.; Zhao, Y.; Butrouna, K.; Gumyusenge, A.; Diao, Y.; Graham, K. R.; Li, H.; Mei, J., Complementary Semiconducting Polymer Blends: Influence of Side Chains of Matrix Polymers. *Macromolecules* **2017,** *50* (16), 6202-6209.

[109] Zhang, S.; Gao, J.; Wang, W.; Zhan, C.; Xiao, S.; Shi, Z.; You, W., Effect of Replacing Alkyl Side Chains with Triethylene Glycols on Photovoltaic Properties of Easily Accessible Fluorene-Based Non-Fullerene Molecular Acceptors: Improve or Deteriorate? *ACS Applied Energy Materials* **2018,** *1* (3), 1276-1285.

[110] Liao, H.-C.; Hsu, C.-P.; Wu, M.-C.; Lu, C.-F.; Su, W.-F., Conjugated Polymer/Nanoparticles Nanocomposites for High Efficient and Real-Time Volatile Organic Compounds Sensors. *Analytical Chemistry* **2013,** *85* (19), 9305-9311.

[111] Elsawy, W.; Lee, C.-L.; Cho, S.; Oh, S.-H.; Moon, S.-H.; Elbarbary, A.; Lee, J.-S., Isoindigo-based small molecules for high-performance solution-processed organic photovoltaic devices: the electron donating effect of the donor group on photo-physical properties and device performance. *Physical Chemistry Chemical Physics* **2013,** *15* (36), 15193-15203.

[112] Kline, R. J.; McGehee, M. D.; Kadnikova, E. N.; Liu, J.; Fréchet, J. M. J.; Toney, M. F., Dependence of Regioregular Poly(3-hexylthiophene) Film Morphology and Field-Effect Mobility on Molecular Weight. *Macromolecules* **2005,** *38* (8),

doi:10.6342/NTU201904150

3312-3319.

[113] Ren, Y.; Hiszpanski, A. M.; Whittaker-Brooks, L.; Loo, Y.-L., Structure–Property Relationship Study of Substitution Effects on Isoindigo-Based Model Compounds as Electron Donors in Organic Solar Cells. *ACS Applied Materials & Interfaces* **2014,** *6* (16), 14533-14542.

[114] Osaka, I.; Takimiya, K., Backbone orientation in semiconducting polymers. *Polymer* **2015,** *59*, A1-A15.

[115] Lee, E.; Hammer, B.; Kim, J.-K.; Page, Z.; Emrick, T.; Hayward, R. C., Hierarchical Helical Assembly of Conjugated Poly(3-hexylthiophene)-block-poly(3-triethylene glycol thiophene) Diblock Copolymers. *Journal of the American Chemical Society* **2011,** *133* (27), 10390-10393.

[116] Choo, Y.; Majewski, P. W.; Fukuto, M.; Osuji, C. O.; Yager, K. G., Pathway-engineering for highly-aligned block copolymer arrays. *Nanoscale* **2018,** *10* (1), 416-427.

doi:10.6342/NTU201904150